

STATUS OF THESIS

Title of thesis **Comparative Studies of Titanium Silicate as Heavy Metal Removal Adsorbent Synthesized through Conventional and Hybrid Surfactant Template Techniques**

I **ALIMI BINTI OTHMAN** hereby allow my thesis to be placed at the Information Resource Center (IRC) of Universiti Teknologi PETRONAS (UTP) with the following conditions:

1. The thesis becomes the property of UTP
2. The IRC of UTP may make copies of the thesis for academic purposes only
3. This thesis classified as

Confidential

Non-confidential

If the thesis is confidential, please state the reason:

The contents of the thesis will remain confidential for _____ years.

Remarks on disclosure:

Endorsed by

Signature of Author

No 1, Jln PJS 6/1A,
Kampung Lindungan 46000
Petaling Jaya, Selangor

Date: _____

Signature of Supervisor

Department of Chemical Engineering
Universiti Teknologi PETRONAS
Malaysia

Date: _____

APPROVAL PAGE

UNIVERSITI TEKNOLOGI PETRONAS

Approval by Supervisors

The Undersigned certify that they have read, and recommend to The Postgraduate Studies Programme for acceptance, a thesis entitled “**Comparative Studies of Titanium Silicate as Heavy Metal Removal Adsorbent Synthesized through Conventional and Hybrid Surfactant Template Techniques**” for the fulfillment of the requirements for the degree of Master of Science in Chemical Engineering.

Date

Signature : _____

Main supervisor : _____

Date : _____

UNIVERSITI TEKNOLOGI PETRONAS

Comparative Studies of Titanium Silicate as Heavy Metal Removal Adsorbent
Synthesized through Conventional and Hybrid Surfactant Template Techniques

By

Alimi Binti Othman

A THESIS

AS A REQUIREMENT FOR THE DEGREE OF MASTER OF SCIENCE

IN CHEMICAL ENGINEERING PROGRAMME

BANDAR SERI ISKANDAR

PERAK

JANUARY 2009

DECLARATION

I hereby declare that the thesis is based on my original work except for quotations and citations which have been duly acknowledged. I also declare that it has not been previously or concurrently submitted for any other degree at UTP or other institutions.

Signature: _____

Name : ALIMI BINTI OTHMAN

Date : _____

ACKNOWLEDGMENTS

(In the name of Allah, the most Beneficent, and the most Merciful)

Firstly, thanks for Allah, for giving me the strength and persistence to keep going without lost hope to keep going in scientific research even during the most difficult moment. May Allah accept this work, counts it as good deed and make it useful.

Secondly, nothing is sufficient to express my deep regards and sincere gratitude to my research supervisor, AP Dr. Isa Md. Tan for his constant encouragement and inspiration throughout the course of this work I am getting till today. To me, he is very helpful, always think positively, passionate, and full of creative ideas. Also thanks to Dr. Azmi and Dr. Chandra for his guide in my data analysis.

Third, I'm thankful UTP lab technicians (En. Jai, En Fauzi, En. Yusuf, Firdaus, Asnizam, En. Feisal, En Anwar, Fizan, KakLong and Zimah) and PETRONAS Research Scientific Services (PRSS) personnel (especially Puan Shamsina and En. Zaimi) for their assistance and co-operation during experimental period.

Fourth, I am indebted to the Chemical Engineering Department and Postgraduate Studies Program; Universiti Teknologi PETRONAS have each provided me necessary means of support. Thanks to postgraduate office staffs, especially Kak Norma, Pn. Kamaliah, Pn. Has, and En. Fadhil.

Fifth, I consider myself lucky to have understanding colleague which simply means that I learned a lot from them, not only academically but also in administration part of my personality. My special thanks to Epul who always give his opinion, Shahidah, Zai, Ari, Mar, Lyn, Ana, Leong, Kiki and Aisyah, who always give support.

Last but not least, I would like to express my love and thank to my family members, my sibling, family in law. Specially thanks to my husband and both my parents, who give unconditionally love, great supports and help in their own way, have patiently prayed day and night for my success especially during all my difficulties.

ABSTRACT

Titanium silicate-1 (TS-1) has attracted much attention during the last decade because of its interesting catalytic and adsorption properties. Most of TS-1 synthesis methods require the use of a comparatively copious amount of a costly template such as tetra propyl ammonium hydroxide (TPAOH). Thus, an attempt to reduce the cost of TS-1 synthesis by an alternatively or at least lessen the concentration of TPAOH. Two reactants to precipitate TS in the template involving tetra-n-butyl titanate (TNBT) as titanium source and tetra ethyl ortho silicate (TEOS) as silica source were used as precursors. The results were compared with the TS sample prepared without sodium dodecyl sulphate (SDS) and with sample prepared with different Si/Ti ratios. Si/Ti ratio of 33:1 was chosen to prepare titanosilicate (TS) samples synthesized by the conventional method using TPAOH as surfactant and TS samples synthesized using SDS and TPAOH as hybrid surfactant. Characterization of TS samples has been achieved by using a Fourier transform infra-red (FTIR) spectroscope, x-ray diffraction (XRD) and scanning electron microscope (SEM) to show the degree of crystallinity, while UV-VISIBLE spectroscopy was used to confirm whether the Ti present in the TS is in the tetrahedral position or in the form of extra framework. It shows the presence of the characteristic band for TS at 960cm^{-1} , confirming Si-O-Ti linkages present in all samples. Surface area and pore size distribution of TS samples were measured by nitrogen adsorption analysis. It was revealed that all TS produced by hybrid surfactant generated a higher surface area compared to conventional method. The nitrogen adsorption analysis shows that TS-hybrid synthesized using a mild condition i.e. crystallized at room temperature and atmosphere pressure possesses a bimodal with fairly narrow pore size distribution. Batch experiment investigations utilizing Cu(II) and Pb(II) ions were conducted to examine the heavy metal removal capabilities of TS. The results showed that almost all of the TS produced by hybrid surfactant generated a higher metal ions uptake Q_t , compared to conventional method. TS templated using hybrid surfactant offers a less costlier and less time-consuming route compared conventional methods.

ABSTRAK

Semenjak sedekad yang lalu, Titanium silicate-1 (TS-1) telah menarik banyak perhatian penyelidik kerana keberkesanannya sebagai pemangkin dan penyerap. Walaubagaimapun, kebanyakan kaedah sintesis TS-1 memerlukan penggunaan acuan yang mahal seperti tetra propil ammonium hidroksida (TPAOH). Oleh itu, beberapa cubaan dilakukan untuk mengurangkan kos dalam kaedah sintesis TS-1 dengan mengurangkan penggunaan TPAOH atau menggantikan dengan sodium dodecyl sulfate (SDS). Dua reaktan yang digunakan ialah tetra-n-butyl titanate (TNBT) sebagai sumber titanium dan tetra ethyl ortho silicate (TEOS) sebagai sumber silica. Keputusan yang diperolehi dibandingkan dengan sampel titanosilicate (TS) yang disediakan dengan/atau menggunakan SDS dan juga dibandingkan dengan sampel disediakan dengan nisbah Si/Ti yang berbeza. Nisbah Si:Ti pada 33:1 telah dipilih bagi menghasilkan TS secara konvensional dan TS yang dihasilkan dengan menggunakan penghibridan dua surfaktan (SDS/TPAOH). Pencirian TS dilakukan menggunakan spektroskopi Fourier transform infra-red (FTIR), penyerakan sinar-X (XRD) dan mikroskopi pengimbas elektron (SEM) bagi mengenalpasti tahap penghabluran kristal, manakala spektroskopi cahaya nampak UV (UV-Visible) digunakan untuk mengenalpasti kehadiran titanium dalam kedudukan tetrahedral. Luas permukaan dan serakan saiz liang butiran bagi semua sampel dianalisis menggunakan analisis penyerapan nitrogen. Keputusan yang diperolehi menunjukkan sampel yang dihasilkan secara penghibridan surfaktan menghasilkan luas permukaan yang lebih tinggi berbanding sampel yang dihasilkan secara konvensional. Analisis penyerapan nitrogen tersebut juga menunjukkan sampel TS-hybrid yang dihablurkan pada suhu bilik serta tekanan atmosfera mempunyai serakan saiz ling roma pada dua julat (mikro dan meso). Eksperimen penyerapan ion logam berat secara berperingkat menggunakan ion Cu(II) dan Pb(II) ions telah dilakukan bagi mengesan keberkesanan sampel TS terhadap penyingkiran logam berat. Keputusan menunjukkan hampir semua TS dihasilkan secara penghibridan surfaktan menjana pengambilan ion logam berat yang lebih tinggi berbanding sampel yang dihasilkan secara konvensional. TS menggunakan acuan penghibridan surfaktan menetengahkan kaedah yang lebih murah dan mudah.

TABLE OF CONTENT

DECLARATION.....	ii
ACKNOWLEDGMENTS	iii
ABSTRACT	iv
ABSTRAK.....	v
TABLE OF CONTENT.....	vi
LIST OF TABLE	x
LIST OF FIGURE.....	xi
LIST OF ABBREVIATIONS.....	xiv
CHAPTER 1 INTRODUCTION.....	1
1.1 PROBLEM STATEMENT	1
1.1.1 Heavy Metal as Pollution Substances.....	1
1.1.2 Wastewater Treatment.....	2
1.1.3 Adsorbent For Heavy Metal Removal.....	4
1.2 PROBLEM SOLUTION; AN ATTEMPT TO FIND NEW ADSORBENT	5
1.2.1 From Microscale to Nanoscale.....	6
1.2.2 The Era of Zeolites	6
1.2.3 From Microporous to Mesoporous.....	7
1.2.4 Bimodal Pores; Micro-Mesoporous	9
1.2.5 Titanosilicate as Adsorbent.....	9
1.3 OBJECTIVES OF THE PROJECT	10
1.4 SCOPE OF STUDY.....	11
CHAPTER 2 LITERATURE REVIEW	12
2.0 PREFACE	12
2.1 DEFINITION AND CLASSIFICATION OF ZEOLITES:	12
2.1.1 Metallo-silicates:	13
2.1.2 Titanosilicates:	13
2.2 FACTORS AFFECT IN SYNTHESIS OF TITANOSILICATE:.....	14
2.2.1 Effect of Self Assembly Molecules (SAM):.....	15
2.2.2 Effect of Alkalinity:.....	16
2.2.3 Effect of Temperature and Time:	16

2.2.4 Effect of Dilution:	17
2.2.5 Effect of Inorganic Cation:	17
2.3 SYNTHESIS METHODS OF TITANOSILICATE.....	18
2.3.1 Methods to Produce Metal-Incorporated Zeolites.....	18
2.3.2 Additional Methods to Produce Metal Nanoparticles/Mesoporous System via Sol Gel Method.....	23
2.4 MICROEMULSION TECHNIQUE.....	26
2.4.1 Emulsions.....	26
2.4.2 Surface Active Agents (Surfactants) and Cosurfactants.....	27
2.4.3 Micellar Structure and Properties.....	30
2.4.4 Microemulsion	30
2.4.5 Literature Reviews of Microemulsion Technique.....	34
2.4.6 Microemulsion as Template Media In Synthesis	36
2.5 CHALLENGES IN TITANOSILICATE SYNTHESIS	41
2.5.1 Application of Titanosilicates and Its Challenge	49
2.6 PHYSICO-CHEMICAL CHARACTERIZATION.....	56
2.6.1 Powder X-ray Diffraction (PXRD)	56
2.6.2 Infrared Spectroscopy (IR)	57
2.6.3 UV- Vis Spectroscopy.....	57
2.6.4 Scanning Electron Microscopy (SEM).....	58
2.6.5 Adsorption Measurement.....	58
CHAPTER 3 THEORY	60
3.1 PREFACE	60
3.2 THE CLASSIFICATION OF ADSORPTION MECHANISM	60
3.3 FACTORS AFFECTING THE RATE OF PHYSISORPTION.....	61
3.4 ADSORPTION SYSTEMS.....	62
3.5 ADSORPTION EQUILIBRIUM.....	62
3.5.1 Freundlich isotherm.....	63
3.5.2 Langmuir Isotherm	63
3.6 LINEAR METHOD.....	64
3.7 ADSORPTION KINETICS	65

CHAPTER 4	RESEARCH METHODOLOGY	67
4.1	INTRODUCTION	67
4.2	MATERIALS	68
4.3	DETERMINATION OF PHASE DIAGRAM	69
4.4	TITANIUM SILICATE PREPARATION.....	69
4.4.1	Synthesis of adsorbent TS-X (X=1, 2; Si/Ti =33, X=3, 4; Si/Ti =10)	69
4.4.2	Synthesis of adsorbent TS-A and TS-E.....	70
4.4.3	Synthesis of adsorbent TS-X (X=B,C,D,F,G,H).....	71
4.5	CHARACTERIZATION OF ADSORBENT.....	75
4.5.1	X-ray diffraction:.....	75
4.5.2	UV-Vis Spectroscopy:.....	75
4.5.3	IR Spectroscopy:	75
4.5.4	Scanning Electron Micrograph (SEM) Analysis:.....	76
4.5.5	Nitrogen Adsorption Analysis	76
4.5.6	Thermogravimetry (TG) Analysis.....	77
4.6	ADSORPTION STUDY	78
4.6.1	Stock and Working Solution of Metal Ions	78
4.6.2	Effect of Adsorbent Dosages on Metal Ion Adsorption	78
4.6.3	Adsorption Equilibrium	78
4.6.4	Kinetics of Metal Ions Adsorption	78
4.6.5	Isotherms of Metal Ions Adsorption.....	79
4.6.6	Calculation of Q_t	79
4.6.7	Calculation of K_d	80
4.6.8	Calculation of Adsorption Kinetics Parameter	80
4.6.9	Calculation of Adsorption Isotherms Parameter	80
CHAPTER 5	RESULTS AND DISCUSSION	81
5.1	INTRODUCTION	81
5.1.1	Formation Mechanism	81
5.1.2	Process for The Preparation.....	82
5.2	TOPOLOGY OF TERNARY PHASE DIAGRAM	84
5.3	X-RAY DIFFRACTION (XRD)	85

5.4	SCANNING ELECTRON MICROGRAPHS (SEM)	89
5.5	UV-VISIBLE SPECTRAL ANALYSIS.....	92
5.6	FT-IR ANALYSIS.....	95
5.7	THERMOGRAVIMETRY (TG) ANALYSIS.....	102
5.8	POROSITY CHARACTERISTICS OF ADSORBENTS	105
5.9	PRODUCT UTILIZATION STUDIES	120
	5.9.1 Adsorption Characteristics of Adsorbents In Metal Solutions.....	120
	5.9.2 Equilibrium Time Study	123
	5.9.3 Adsorption Kinetics.....	125
CHAPTER 6 CONCLUSION AND RECOMMENDATION.....		135
6.1	CONCLUSION.....	135
6.2	CONCLUSION FOR PRODUCT UTILIZATION	138
6.3	RECOMMENDATION	139
PUBLICATIONS		140
REFERENCES.....		141
APPENDIX A.....		164
APPENDIX B		166
APPENDIX C		172
APPENDIX D.....		180
APPENDIX E		185
APPENDIX F		186

LIST OF TABLE

Table 1.1-1 Comparison of main physico-chemical treatments of heavy metal (HM) removal techniques.....	2
Table 2.4-1 Classification and characteristics of emulsion system.....	26
Table 2.4-2 Type and Characteristics of Surfactants.....	29
Table 2.4-3 Summary of the Literature on Synthesis Zeolites in SAM	38
Table 2.5-1 Summary of the Literature on Synthesis TS.....	42
Table 2.5-2 Treatment of different heavy metal (HM) by adsorption.....	51
Table 2.5-3 Treatment of different HM on Titanium Silicate by adsorption.....	55
Table 3.2-1 Typical Characteristics of Adsorption Processes (Source from ref. 134).....	61
Table 4.4-1 Molar Gel Composition Of Different Synthesis Mixture.....	70
Table 4.4-2 Molar Gel Composition Of Different Synthesis Mixture.....	71
Table 5.4-1 Gel Ratio and Product Ratio Of Samples.....	89
Table 5.4-2 Gel Ratio and Product Ratio Of Samples.....	92
Table 5.5-1 Summary of UV-Vis Result	93
Table 5.6-1 Molar composition and relative intensity of TS samples.....	97
Table 5.6-2 Band Assignments in IR spectra of samples	101
Table 5.8-1 Structure properties of TS-X (X=A,B,C,D,E,F,G,H)	105
Table 5.9-1 Cu ²⁺ Adsorption on all adsorbents.....	121
Table 5.9-2 Pb ²⁺ Adsorption on three Adsorbents	121
Table 5.9-3 Some Physical Parameters of Heavy Metal Ions in Solution (source from references 10 and references therein).....	122
Table 5.9-4 Langergren First-Order, Pseudo Second-Order And Langergren Second Order Constants and Correction Coefficient	129
Table 5.9-5 Isotherm Parameters Obtained By Using Linear Method (qm: mg/g; K _a : L/mg; K _F : mg/g).....	134

LIST OF FIGURE

Figure 1.2-1 (a) MCM-41 (b) MCM-48 (source from 178)	8
Figure 2.1-1 Framework structure of TS-1 (source from ref. 57).....	14
Figure 2.2-1 Stabilization energy for TAA ⁺ cations occluded in ZSM-5 and ZSM-11 at an occupancy of four cations per unit cell. All energies are in kcal per unit cell (source from ref. 58).....	16
Figure 2.3-1 Sol-gel process [source from ref. 64]	20
Figure 2.3-2 Boron replacement by titanium in borosilicate. [source from ref. 42]	23
Figure 2.4-1 Size ranges of the disperse phase in liquid-liquid dispersions. (Source from ref. 95)	27
Figure 2.4-2 Schematic diagram of surface active molecule.....	28
Figure 2.4-3 A spherical micelle. The packing of amphiphilic molecules is controlled by the effective cross-sectional area ₁ of the head group, n and the hydrophobic chain of length, l and volume, V. (source from ref. 54)	30
Figure 2.4-4 A schematic diagram of spherical micelle (w/o microemulsion) and reverse micelle (o/w microemulsion) (source from ref. 50 and 103).....	31
Figure 2.4-5 water/SDS/1-butanol ternary phase diagram. The black area, L represent microemulsion [source from ref. 88].....	32
Figure 2.4-6 Synthesis of nanoscale particles in micelles; (a) two microemulsions; (b) microemulsion plus second reactant (source from ref. 41).....	35
Figure 2.6-1 The six IUPAC standard adsorption isotherms.....	59
Figure 3.6-1 Isotherms and their linear form (Source from ref. 38)	64
Figure 4.3-1 a) Emulsion (turbid liquid) and b) Microemulsion (transparent).....	69
Figure 4.4-1 Flowchart of synthesis adsorbent TS-X (X=1,2;Si/Ti =33, X=3,4;Si/Ti =10)	72
Figure 4.4-2 Flowchart of synthesis adsorbent TS-X [X=A(0h), B(18h), C(24h), D(48h)]	73
Figure 4.4-3 Flowchart of synthesis adsorbent TS-X [X= E(0h), F(18h), G(24h), H(48h)]	74
Figure 4.5-1 IR Spectroscopy	75
Figure 4.5-2 Scanning Electron Micrograph (SEM) Spectroscopy	76

Figure 4.5-3 Thermogravimetry (TG) Analyzer	77
Figure 5.1-1 Formation mechanism of mesoporous titanosilicates	82
Figure 5.2-1 water/SDS/1-butanol ternary phase diagram. The grey area represents microemulsion.....	84
Figure 5.3-1 XRD pattern of calcined samples with different Si/Ti ratio [TS-1(Si/Ti: 33), TS-2(Si/Ti: 33), TS-3(Si/Ti: 10), and TS-4(Si/Ti: 33)] and different crystallization time [Si/Ti: 33;TS-E (0hr), TS-F (18hrs), TS-G (24hrs) and TS-H (48hrs)]	85
Figure 5.3-2 XRD pattern of calcined samples with different crystallization time [TS-A (0hr), TS-D (48hrs)]	86
Figure 5.3-3 Correlation between pure titanium dioxide and samples TS-A	87
Figure 5.4-1 SEM/EDX of Calcined TS-1 and TS-2 Samples Prepared At Si/Ti Ratio 33 In Presence Of SDS (EHT = 15 KV, Mag. = 2 KX).....	90
Figure 5.4-2 SEM/EDX Of Calcined TS-1 and TS-2 Samples Prepared At Si/Ti Ratio 33 In Absence of SDS (EHT = 15 KV, Mag. = 2 KX).....	90
Figure 5.4-3 SEM/EDX Of Calcined Samples TS-A prepared in Hybrid surfactant (EHT = 15 KV, Mag. = 4 KX).	91
Figure 5.4-4 SEM/EDX Of Calcined Samples TS-E prepared in TPAOH (EHT = 15 KV, Mag. = 5 KX).....	91
Figure 5.5-1 UV-Vis spectra of calcined powders synthesized with the molar composition $2.82\text{butanol} \cdot x\text{TiO}_2 \cdot 1\text{SiO}_2 \cdot y\text{SDS} \cdot 15.6\text{IPA} \cdot 27.78\text{H}_2\text{O}$ where $x = 0.03$ (1), 0.03 (2), 0.1 (3), 0.1 (4) and $y = 0.72$ (1 and 3), 0 (2 and 4).	94
Figure 5.5-2 UV-Vis spectra of calcined samples of TS-A, TS-B, TS-C, TS-D, TS-E, TS-F, TS-G and TS-H.	94
Figure 5.6-1 IR spectra of calcined powders synthesized with the molar composition $2.82\text{butanol} \cdot x\text{TiO}_2 \cdot 1\text{SiO}_2 \cdot y\text{SDS} \cdot 15.6\text{IPA} \cdot 27.78\text{H}_2\text{O}$ where $x = 0.03$ (TS-1), 0.03 (TS-2), 0.1 (TS-3), 0.1 (TS-4) and $y = 0.72$ (1 and 3), 0 (2 and 4).....	96
Figure 5.6-2 IR Spectra of as-synthesized samples prepared by hybrid surfactant with different crystallization time TS-A (0hr), TS-B (18hrs), TS-C (24hrs) and TS-D (48hrs)	98
Figure 5.6-3 IR Spectra of calcined samples prepared by hybrid surfactant with different crystallization time TS-A (0hr), TS-B (18hrs), TS-C (24hrs) and TS-D (48hrs)	99

Figure 5.6-4 IR spectra of calcineds sample prepared with different crystallization time TS-E (0hr), TS-F (18hrs), TS-G (24hrs) and TS-H (48hrs)	100
Figure 5.7-1 TGA curve of as-synthesized a) TS-1 (prepared with SDS) b) TS-A (prepared with SDS and TPAOH) and c) TS-E (prepared with TPAOH).....	103
Figure 5.8-1 Nitrogen sorption isotherms of sample.....	106
Figure 5.8-2 Pore size distribution (PSD) of the material (BJH analysis of the adsorption branch of the isotherm).....	110
Figure 5.8-3 Pore size distribution (PSD) of the material (BJH analysis of the adsorption branch of the isotherm).....	111
Figure 5.8-4 Nitrogen isotherm and PSD of double-mesopore silica prepare by Wang et al. [Source from ref. 176]	112
Figure 5.8-5 t-Plots of mesoporous, nonporous solids, microporous and micro- and mesoporous solids (References 22).....	114
Figure 5.8-6 t-Plot of sample TS-A.....	114
Figure 5.8-7 t-Plots of sample TS-B and TS-C.....	115
Figure 5.8-8 t-Plots of sample TS-D and TS-E.....	116
Figure 5.8-9 t-Plots of sample TS-F and TS-G.....	117
Figure 5.8-10 t-Plots of sample TS-H	118
Figure 5.8-11 Illustrations for different type IV isotherms and their interpretation. The isotherm in A was observed for samples TS-E and TS-D, while the isotherm in B was observed for samples TS-A and TS-B. (Images copied from Ref. 62)	119
Figure 5.9-1 Contact Time Study for Metals Adsorption on Adsorbent A and Adsorbent H.....	123
Figure 5.9-2 Possible adsorption mechanisms in adsorbent	124
Figure 5.9-3 (A) First-Order Lagergren, (B) Pseudo Second-Order And (C) Lagergren Second Order Plots For Heavy Metals Adsorption On Adsorbent A And Adsorbent D	128
Figure 5.9-4 a) Langmuir-2 plots for Cu (II) adsorption on adsorbent A and H b) Langmuir-2 plots for Pb II adsorption on adsorbent A and H.....	132
Figure 5.9-5 c) Freundlich plots for Cu (II) adsorption on adsorbent A and H, d) Freundlich plots for Pb (II) adsorption on adsorbent A and H	133

LIST OF ABBREVIATIONS

TS - titanium silicate
IUPAC - International union of pure and applied chemistry
HM - heavy metal
SA - surface area
Ref. - reference
PSD - pore size distribution
SAM - Self Assembly Molecules
SDS - sodium dodecyl sulphate
TAA - tetra alkyl ammonium
TMA - tetra methyl ammonium
TPA - tetra propyl ammonium
TBA - tetra buthyl ammonium
TPAOH - tetra propyl ammonium hydroxide
TNBT - tetra N- butyl titanate
TEOS - tetra ethyl ortho silicate
IPA - isopropyl alcohol
XRD - X-ray diffraction
EDX - energy dispersion X-ray
SEM - scanning electron microscopy
TGA - thermogravimetry analysis
AAS- atomic adsorption apectroscopy
BET - Brunauer-Emmet-Teller
BJH - Barrett-Joyner-Halenda
IR – infrared
U- Vis - ultraviolet visible
FT-IR - Fourier transformed infrared

CHAPTER 1 INTRODUCTION

1.1 PROBLEM STATEMENT

1.1.1 Heavy Metal as Pollution Substances

Heavy metals (HM) are a general collective term applied to the group of metals and metalloids with an atomic density greater than 6 g/cm^3 [1]. HM ions including Pb and Cu are not only undesirable as they create odor, bad taste, unsightly color, foaming, etc but the major concern is related with their toxicity, mutagenic and carcinogenic tendencies even at very low levels [2,3,4]. Once these metals have entered the environment they remain there indefinitely circulating, and will inevitably end up in the human food chain. [4]. The US Environmental Protection Agency has strict limits on the allowable concentration of lead in drinking water from the original 0.05 ppm to 0.005 ppm.

The Department of Environment (DOE), Malaysia reported that almost all the samples collected from the coastal waters of the country had values of lead, copper and cadmium exceeding the proposed standards of 0.05 mg/litres, 0.01 mg/litre and 0.005 mg/litre respectively [5]. This limitation has meant that some industries are unable to meet the new and more stringent requirements [6-14]. Thus, it is essential to restrict the levels of HM released in industrial effluent waters to safe levels before they enter the environment. An effort to solve such challenging wastewaters pollution is achieved by innovating a low-cost and effective method for the removal of HM from wastewaters.

1.1.2 Wastewater Treatment

There are many benefits obtained by using physico-chemical treatment over the biological treatment to uptake toxic metals from aqueous waste streams. Compared to biological treatment, physico-chemical treatment can be readily controlled and used fairly rapidly without any adverse effects [15]. The major physico-chemical treatments are compared in **Table 1.1-1**.

Table 1.1-1 Comparison of main physico-chemical treatments of heavy metal (HM) removal techniques

Treatment Technologies	Advantages	Disadvantages
i) Oxidation/precipitation		
Chemical Precipitation	Simple, low cost [16] are well suited to automatic control and performed at ambient conditions [17]	Huge generation of sludge that needs extra disposal [20], tend to be effective on a narrower range of contaminants [17]
-Sulfide precipitation	allows for the precipitation of metals when chelating agents are present [18], remove Cd, Cr (VI), Co, Cu, Fe, Hg, Mn, Ni, Pb, Zn effectively [19]	Very sensitive quality control instrumentation and need special safety equipment, generation of highly toxic and odorous hydrogen sulfide gas [18,19]
Air oxidation	Relatively simple, low-cost, <i>in-situ</i> HM removal, oxidize other inorganic and organic constituents in water[16]	slow process, efficient control of the pH and oxidation step is needed[16]
Chemical oxidation	Oxidizes other impurities and kill microbes; relatively simple and rapid process; minimum residual mass[16, 17]	efficient control of the pH and oxidation step is needed[16], may generate toxic chlorinated organic compounds [17]
ii) coagulation/coprecipitation/electrocoagulation		
Alum coagulation	Durable powder chemicals are available; relatively low cost and easy handling; effective over a wider range of pH [16]	Produces toxic sludges; low removal of HM; pre-oxidation may required [16]
Iron coagulation	more efficient than alum coagulation on weigh basis	Medium removal of HM; need sedimentation and filtration
Lime softening	Chemicals are available commercially [16]	Readjustment of pH is required [16], high cost, potential air pollution problem with recalcining furnace [21], should be followed by a biological treatment as a polishing treatment after HM removal [19]

Continue Table 1.1-1

Treatment Technologies	Advantages	Disadvantages
iii) membrane		
Nanofiltration	Well-defined and high removal efficiency, also removes BOD and phosphorus associated with suspended materials [21]	Very high capital and running cost, preconditioning; high water rejection [16,21]
Reverse osmosis, Electro dialysis	No toxic solid waste is produced [16], simple to design and operate, have low maintenance requirements, Capable of removal of other contaminants [22]	High tech operation and maintenance, toxic wastewater produced [16], Fouling of the membrane reduces the membrane flux; reduces the efficiency of the water purification system [23]
iv) adsorption and ion-exchange (details are summarized in table 2.5)		
Synthetic Zeolites -ordered mesoporous silica [24,25,26], zeolites of A, P, X, Y types [24,27-31].	High selectivity adsorbents due to large surface area, fast adsorption kinetics ,controllable pore size and pore arrangement , able to remove from both ion exchange and sorption mechanism	Less suitable for column methods; due to smaller particle sizes
Natural zeolites -Al ₂ O [11], clay [7,12,32-35], rice husk [36]	Cheap, non-toxic nature, available abundantly	Not standardized, depending on the impurity and deposit of zeolitic minerals
Metallic oxide -nanosized Sn ₂ O ₂ [37]	High capacity due to large surface area; high number of adsorption site	For conventional metal oxide; Low capacity, efficient control of pH and temperature is needed. These problem are overcome by nanosized metal oxide [37] but only involve sorption mechanism
Activated carbon	Hydrophobic, favors organics over water [38], remove organic material instead of biological treatment	i) Difficult to regenerate [38]; ii) though can generate, the regeneration, capital, operation and management costs is expensive; [21,39], iii) adsorption properties may be correlated with the chemical nature of the carbon surface rather than the surface area and the porosity [16], iv) regenerate on furnace – potential air pollution problem [21], v) low adsorption of some constituent if competing constituent that are amenable to activated carbon adsorption are presented [17]
6. Activated alumina	Relatively well known and commercially available [16]	Needs replacement after 4-5 times regeneration, trace removal not effective [16]

Continue Table 1.1-1

Treatment Technologies	Advantages	Disadvantages
iv) adsorption and ion-exchange (details are summarized in table 2.5)		
Ion exchange resin	Well-defined medium and capacity; pH independent [16], the metal contaminant can be recovered and reuse, provides effective and selective removal of these metals from highly contaminated wastewater [18]	The resins may be fouled by some organic substances [23], high cost medium; high tech operation and maintenance; regeneration creates a sludge disposal problem [16]
Biosorbents -algae [39], graft copolymer of cellulosic materials [9]	Have high affinity for divalent cation, chemical resistance radiation stability and low-cost of production over conventional ion-exchange [16]	Produce secondary pollutant, usually need physical and chemical pretreatment, [16] can regenerate for two times only [9, 39]
Iron coated sand, sodium iron titanate [20]	Cheap, no regeneration is required [16]	Not standardized, produce toxic waste [16]

From the review as shown in **Table 1.1-1**, we can conclude that most of them deal with cost, secondary product and regeneration of sorbent as limiting factors. Currently, among the methods listed, adsorption technology is one of the most popular, widely used and has gained much attention in industrial application because it is more efficient and economically feasible as a wastewater treatment process compared to other methods [6,8,40]. Sorption is considered more efficient and economically feasible as a wastewater treatment process because it is clean and energy efficient method, high selectivity for certain ions even in solutions of low concentration of the target ions, high treatment capacity, high removal efficiency and can also be utilized in metal recovery and water reuse. However, as mention earlier, the cost of sorbent is of its limiting factors and, thus, it is of concern to research new materials to replace commonly used activated carbons and resins. Focus is now directed towards finding a suitable adsorbent for heavy metal removal.

1.1.3 Adsorbent for Heavy Metal Removal

Fine adsorbents suitable for metal removal from water are synthetic and natural zeolite, metallic oxide, activated carbon, ion exchange resin, biosorbent [41].

The natural zeolites, though cheap, have some limitations. The contents and composition of natural zeolites vary over a wide range, depending on the impurity and the deposits of zeolitic minerals in a given country [27]. Their exchange capacities usually depend on the surface area of the zeolite in the natural rock which is usually comparable low and on the composition property of the compound present in the natural material which is usually are of lower Si/Al ratio [24,27,42]. As example, natural zeolite, erionite (ERI) has toxicity comparable or even worse than some of the most potent asbestos [42]. For that reason, synthetic zeolites have been used widely instead of the naturally occurring zeolites as the former allows for a high degree of customization (similar properties in every single particle of same type zeolites; in term of porosity, crystallinity, content and surface area). While the process of ion removal using zeolites has been the subject of a number of investigations, the emphasis has invariably been placed firmly on the synthesis of efficient zeolite based catalysts. Zeolites have been applied in the removal of ammonium ions from municipal wastewater, in water softening, and, to a limited extent, in the treatment of radioactive water containing cesium and strontium [6]. However, the application of zeolites in environmental pollution control in terms of HM from aqueous media has received limited attention. The lack of literature on the use of zeolites for HM cleanup is possibly due to the low solution pH that is often necessary (particularly in the case of iron) to ensure that adsorbent is stoichiometric; due to zeolites can suffer structural breakdown even under weakly acidic conditions and prevent metal hydroxide precipitation; due to lower hydrophobicity and hydrothermal stability [38].

1.2 PROBLEM SOLUTION; AN ATTEMPT TO FIND NEW ADSORBENT

Based on the review under section 1.1.3 in this thesis, synthetic zeolites possess both ion exchange and adsorption capabilities. Hence, nanostructured zeolites consisting of nanoparticles of metal oxides in their pores are increasingly finding applications as improved adsorbents compared with conventional adsorbents [6-11,31,39,40,41]. The nanostructured zeolites serve as effective adsorbents due to the following reasons [39]:

- (1) They possess high surface areas and have a large surface-to-bulk ratio (due to smaller size) compared with conventional oxides;
- (2) They have unusual shape and high number of reactive edges, corners, and defect sites that impart a higher surface reactivity;
- (3) Properties such as Lewis acidity and Lewis basicity can be tailored for a specific application; and
- (4) Nanostructured zeolites can be palletized while maintaining the high surface area of the fine powders.

It is clear that, nanostructured zeolites represent a new family of porous inorganic sorbents that exhibit unusual adsorption properties [40]. These benefits are exploited further in this research. Synthetic zeolites are first synthesized and later used for HM removal. In this research, more emphasized into zeolite synthesis and characterization.

1.2.1 From Microscale to Nanoscale

Nowadays, nanoscale technologies have replaced those in the microscale. Nanoscale materials belong to a unique family of compounds which are considered as materials that form a bridge between molecular and condensed matter [32]. They fall in the regime where neither quantum chemistry nor the classic theory of physics can be applied [42]. Nanoparticles consist of tiny particles with size ranging from 1 to 1000nm, and it could be amorphous, crystalline, or even an aggregate of small crystallites. Nanophase, nanoscale, or nanostructured material all refer to a solid that has nanometer size in either one (wire) or two (film) or three dimensions (particle) [40]. The trend of using smaller and more precise structure through miniaturization is not only well known and applied in nano-electronic industry but it has a wide application in the environment, energy and chemical sectors. The goal is not just to get smaller devices but to access low-energy, low-cost and a more effective device.

1.2.2 The Era of Zeolites

Among the smaller and precise structure devices, zeolites is a group of minerals that represents a family of natural and synthetic microporous crystalline oxides materials.

There are two properties of zeolite molecular sieves that make them commercially viable as adsorbents; they are selective and strong adsorbers and they are selective ion exchanger [32]. Today, zeolites impact a diverse range of industries. Nearly every step in the refining of petroleum involves the use of a zeolite as a catalyst, catalyst support or adsorbent. Several zeolites are effective in removing ammonia and objectionable smells from the environment. [32,40,42].

1.2.3 From Microporous to Mesoporous

International Union of Pure and Applied Chemistry (IUPAC) classifies porous materials into three categories - microporous with pores of less than 2 nm in diameter, mesoporous having pores between 2 and 50 nm, and macroporous with pores greater than 50 nm [32]. The term nanoporous materials have been used for those porous materials with pore diameters of less than 100 nm. [43]

Titanium could be inserted into molecular sieve structure, many researchers focused on the synthesis of Ti containing molecular sieves. Known as titanosilicate these molecular sieves such as TS-1 (substitution of Si^{4+} by Ti^{4+} in the silicalite-1, siliceous analog of ZSM-5), TS-2 (substitution of Si^{4+} by Ti^{4+} in the silicalite-2, siliceous analog of ZSM-11) and TS-beta (titano-alumino-silicate analog of zeolite beta) have all been synthesized hence broadening the scope of molecular sieves [44-47]. All the above mentioned materials are microporous with an average pore radius less than 1.0nm [44], thereby providing diffusional limitations for the reactant and product molecules accessibility to the active sites.

Owing to the limitation associated with microporosity, there has been a new and growing demand for well-defined mesoporous materials. This is due to their prominent features such as high surface area, narrow pore size distribution and highly ordered mesopore architecture [46]. Lyotropic system, i.e. microemulsion, reverse micelles and bilayer lamellar can be used as microreaction matrices to produce mesoporous silica possessing a tunnel like structure [40]. Intensive research in the synthesis of mesoporous titanosilicate (TS) by templating it using self lyotropic system or self assembly molecules (SAM) relies

on the phases in lyotropic system which act as a host to generate inorganic barrier for controlled size and morphology. Manipulation of SAM to overcome the severe limitations of microporous materials lead to the discovery of MS41 family of silicate amorphous mesoporous materials by Mobil Oil scientists in 1992. Their most known and extensively studied material is MCM-41 mesoporous silicate possessing one-dimensional hexagonal arrangement pores (**Figure 1.2-1a**). The cubic MCM-48 material exhibits three-dimensional pore system that is more resistant to pore blocking and allows for a faster diffusion of reactants than a one-dimensional array of pores (**Figure 1.2-1b**).

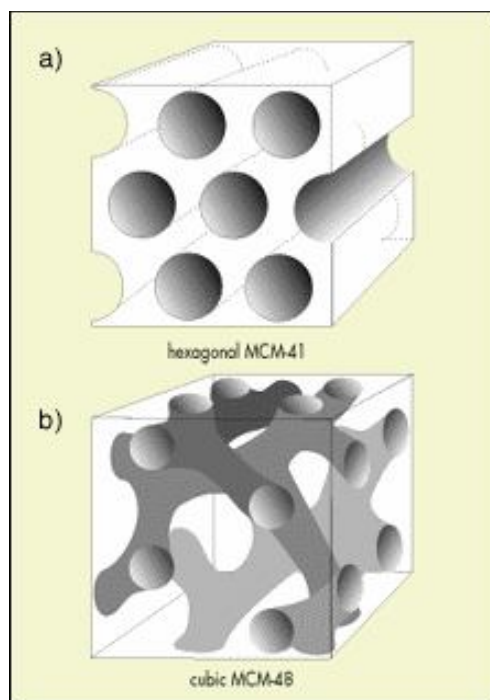


Figure 1.2-1 (a) MCM-41 (b) MCM-48 (source from 178)

Most of the silica- and phosphate-based mesoporous materials related to MCM-41 do not possess high acidity, high activity and hydrothermal stability compared with the microporous analogues [40,43]. Other than limitations of the MCM-type mesoporous materials is associated with inability to survive harsh conditions such as high temperatures and pressures [40]. Being a microporous material a constraint is placed on the size of the accessible molecules. Mesoporous materials can overcome this drawback.

The race is now on to produce nanoscale metal oxide with bimodal pores to overcome drawbacks of microporous materials as seen in zeolites and to further develop mesoporous materials using zeolites that are mediated by surfactants.

1.2.4 Bimodal Pores; Micro-Mesoporous

Very recently, there is a new demand on material having a bimodal pore structure which is suitable for carrying a range of chemical reactions which require, on the one hand, large pores and, at the same time, small pores. This kind of materials can be applied for reactions where large molecules can easily enter the system via the mesopores and are then reacted on or undergo conversion in the micropores [46]. This may result in selective reaction. The material intrinsically has a high surface area in combination with large pores that result in high accessibility and consequently high intrinsic volumetric activity. Another advantage of creating ordered microdomains in the walls of the mesopore structure is the possibility of introducing catalytic sites with higher acid strength than what can be achieved in a purely mesoporous material.

1.2.5 Titanosilicate as Adsorbent

Recently, the application of synthetic zeolites of titanosilicate ETS-10 [10,25,27,32,33,48], functionalized amorphous silica gel [49] and mesoporous silica [6,32,49] has been reported. However, the application of amorphous titanosilicate TS-1 in wastewater treatment is yet to be explored. Either crystalline or amorphous TS-1, has only been recently reported for selective oxidation reactions such as aromatic hydroxylation, epoxidation of alkenes, ammoximation of cyclohexanone and oxidation of alkanes, and alcohols using hydrogen peroxide as the oxidant [50]. A composite TS adsorbent, prepared by sol-gel method, involving SiO₂-TiO₂ nanostructured has been shown to remove elemental mercury vapor effectively [51].

Many researchers have prepared TS-1 by using different methods. However, their methods require the use of a relatively large amount of expensive template; tetra propyl ammonium hydroxide (TPAOH) and is accompanied by a long crystallization time at high temperatures and pressures. This makes TS-1 costly. It is thus desirable to find an

alternative method, which will help lower the TPAOH concentration and eliminate the tedious crystallization procedures; therefore lowering the cost of TS-1. It is known that the addition of TPAOH induces the hydrolysis reaction in the system. [42]. consequently, decreasing the concentration of TPAOH leads to non uniform particles. The particle sizes are larger with a lower catalytic performance. It is also very difficult to avoid the precipitation of TiO_2 during the preparation of precursor mixture or during the crystallization of precursor gel leading to the presence of extraframework titanium [50].

In searching for an alternative route, Khomane [50] managed to synthesise TS-1 at low template concentration in micellar media containing nonionic surfactant. However, there is no report on the synthesis of TS at low template concentration in microemulsion media containing anionic surfactant. The anionic surfactant is thought to avoid the precipitation step of TiO_2 (extra framework of TiO_2). Crystalline TS-1 demonstrating accessibilities to molecules larger than the pore size still remains peculiar. Kesharavaja et al. has overcome this paradox by developing bimodal microporous mesoporous amorphous titanosilicate (MMATS) which possess both the advantageous features of a crystalline and an amorphous titanosilicate at the same time. Motivated by the work of Khomane and Keshavaraja et al. a method for the preparation of an amorphous bimodal pore titanium silicalite-1 in the presence of SDS and TPAOH is now explored in this work. The synthesized amorphous bimodal titanium silicate-1 is then used for HM removal.

1.3 OBJECTIVES OF THE PROJECT

The main objectives of the project are:

1. To synthesize a microporous or/and mesoporous titanosilicate (TS)
2. To synthesize smaller size titanosilicate
3. Investigate the use of bimodal amorphous TS (further explanation in section 2.5.1) as adsorbent for the removal of toxic heavy metal from aqueous solutions
4. Investigate the kinetics and adsorption isotherms of Cu(II) and Pb(II) ions adsorption on synthesized TS

Most researchers in this field have synthesized either crystalline TS-1 or amorphous TS-1 by using a large amount of a costly template - tetra propyl ammonium hydroxide (TPAOH) surfactant. It requires a long crystallization time at high temperatures and pressures. Hence the present study aims to synthesis amorphous TS more cost effectively and energy efficient. This research focus on the synthesis and characterization of synthesized TS. The capability of these amorphous TS as heavy metal removal adsorbent was further evaluated only as minor research in order to see the sorption properties; either it can be utilize as adsorbent or only can be utilized as catalyst. The author hopes that the finding will be useful as a foundation for further work in field other than wastewater treatment, maybe in catalysis studies.

1.4 SCOPE OF STUDY

Microemulsion phase area of a system containing 3 components; sodium dodecyl sulphate (SDS) as surfactant/water/1-butanol is investigated in order to select the best composition of the 3 components needed for a successful templating of titanosilicate (TS). Synthesis of TS is investigated by comparing the effect of variables such as with and without the presence of surfactant SDS, different Si/Ti ratios, in the presence of small amounts of cosurfactant tetra propyl ammonium hydroxide (TPAOH), in the presence of sodium dodecyl sulphate (SDS) and TPAOH as hybrid surfactant-templated, and crystallization time. Investigation on TS synthesis parameters and TS-synthesized characterizations were the core hands on experiment and finding in this research.

In this study, TS growth in hybrid surfactant- template (TS-A) and TS synthesized by conventional method (TS-H) was chosen as solid adsorbents and compared for subsequent adsorption characteristic of copper and lead solutions. The best adsorbent was chosen based on percentage of removal, distribution ratio and uptake. Kinetic and adsorption isotherms are employed to study the adsorption activity of the selected adsorbent intended for heavy metal (HM) removal. As mention earlier, HM removal utilization studies onto synthesized adsorbent only as minor research. Hence, no sorption mechanisms of synthesized adsorbent were discussed here.

CHAPTER 2 LITERATURE REVIEW

2.0 PREFACE

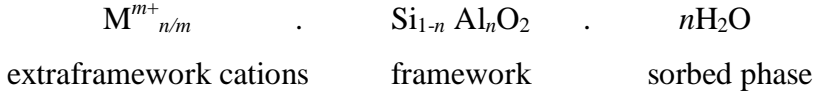
Porous materials when appropriately selected should meet certain characteristic, such as high surface area, narrow pore size distribution and selective pore size readily tuneable over a wide range. As mention in section 1.2, although porous adsorbents in micropore range (<2nm) and mesopore range (2-50nm) are high demand due to their certain advantage, they also have certain shortcomings. Hence, new and better adsorbents that meet a persistent demand for both microporous and well defined mesoporous materials are required to meet the challenges. Amorphous bimodal micro-mesoporous titanasilicate are expected to play a prominent role as effective adsorbents of large size molecules pollutants. Unfortunately, preparation method of titanasilicate is complicated and highly critical. To overcome this, fundamental of synthesis must be deeply understood and better synthesis route must be chosen to utilize both surface area and pores size controls. This chapter briefly explains;

- 1) Definition of zeolites, metallosilicate, and titanasilicate,
- 2) Various factors that affect the synthesis of a particular phase in order to optimize their crystallizing mixtures and products,
- 3) Synthesis method,
- 4) Challenge and review of some literatures.

2.1 DEFINITION AND CLASSIFICATION OF ZEOLITES:

A zeolite is a crystalline microporous aluminosilicate with a framework based on an extensive three-dimensional network of oxygen ions. Situated within the tetrahedral sites formed by the oxygen can be either a Si^{4+} or an Al^{3+} ion [32,52,53]. Upon incorporation of Al into the silica framework, the +3 valence number on the Al makes the framework negatively charged, and requires the presence of extraframework cations (inorganic and organic cations can satisfy this requirement) within the structure to keep the overall

framework neutral. The trivalent Al ion in the zeolite can either partly or completely be replaced by other trivalent ions like Ga^{+3} , B^{+3} , Fe^{+3} , etc or by tetravalent ions such as Ti^{+4} , Zr^{+4} , Sn^{+4} , etc. [52,53]. The general representative empirical formula of any zeolite written in oxide form would appear as:



where M is the cation from group I or II of valence or organic cations [4]. The extraframework cation is counter ions to these materials. The amount of Al within the framework can vary over a wide range of Si/Al ratio = 1 to ∞ , the completely siliceous form being polymorphs of SiO_2 [32,52,53]. Typically, in as-synthesized zeolites, water present during the synthesis occupies the internal voids of the zeolites. The sorbed phase and organic non-framework cations can be removed by thermal treatment/oxidation, making the intracrystalline space available. The fact that zeolites retain their structural integrity upon loss of water makes them different from other porous hydrates such as CaSO_4 [32].

2.1.1 Metallo-silicates:

Various metal ions have been successfully incorporated in framework structures of different morphologies and the resultant molecular sieves are termed as metallo-silicates. Commercial applications of some of the metal silicates, such as the borosilicates AMS-(MFI) and the titanosilicate TS-1(MFI), have motivated further interest in parts of the periodic table beyond silicon, aluminium and oxygen [54,55].

2.1.2 Titanosilicates:

Few decades ago, Barrer [57] predicted that theoretically titanium could substitute into molecular sieves structures. Now it is established that Ti^{4+} can and does substitute into silicate framework to crystallize titanium silicalite molecular sieve analogs of the

silicates. [54,55]. When the substitution is carried out in the silicalite -1, pure siliceous analog of ZSM-5, the resultant titanosilicate is termed as TS-1. When the substitution is carried out on silicalite -2, pure siliceous analog of ZSM-11, the resultant titanosilicate is known as TS -2. Similarly titanosilicates from other morphologies such as TS-48 (the titanium analog of ZSM-48), TS-Beta (titano-alumina-silicate analog of zeolite beta), Ti-MCM-41, etc are also known. Among all the titanosilicates, TS -1 and TS-2 have been used extensively in the catalytic reactions because of their unique pore architecture and higher catalytic activity. TS-1 contains only Si and Ti in the tetrahedral structure, without any Al as shown in **Figure 2.1-1**. Consequently, the framework of TS-1 has no charge, no Brønsted acidity and has hydrophobic properties. [56].

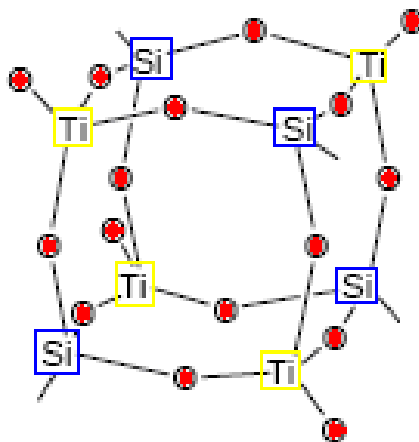


Figure 2.1-1 Framework structure of TS-1 (source from ref. 57)

2.2 FACTORS AFFECT IN SYNTHESIS OF ZEOLITES / TITANOSILICATE:

Generally, the difficulty in the synthesis of metallo-silicates arises because of the formation of stable insoluble metal oxide / hydroxide precipitate, either during preparation of gel or during the crystallization of the metallo silicate [54]. Commonly, the use of high purity tetra ethyl ortho silicate (TEOS) and tetra ethyl ortho titanate (TEOT) and tetra propyl ammonium hydroxide (TPAOH) is necessary to provide the active phase. Other silicates such as tetramethyl ortho silicate (TMOS) have been used but the rate of hydrolysis is more rapid and unbalanced [54]. More over, the normal pHs of the gels for the synthesis of the metallo silicates are around 9-13. Under such alkaline conditions, Ti^{+4} has a strong tendency to form insoluble amorphous TiO_2 species, unlike

silicates or aluminates which dissolve under alkaline conditions. The presence of extra-framework Ti-species has a strong influence in its catalytic activity. It may promote extensive homolytic side reactions including decomposition of hydrogen peroxide. [52]. Besides the general knowledge that high quality titanosilicate were crystallized under alkaline condition, there is a lot of other factors that must be considered in titanosilicate synthesis methodology such as the role of template, temperature, crystallization time; t, Si, Al, inorganic and organic species, OH⁻, water organic solvents and seeded growth.

2.2.1 Effect of Self Assembly Molecules (SAM):

Generally, surfactant or organic molecules such as, amines or quaternary ammonium salts are usually known as SAM as well as space filler. The role of organic molecules in the synthesis of zeolites can be in various forms; space filler, SAM, and template. Most the organic molecules can be considered to be space filler except for tetrapropylammonium cation (TPA). TPA cation can be thought to be as SAM, since it promotes the synthesis of MFI over a wide range of composition and is also entrapped in the channel of zeolites. [58]. TPA cation in the form of hydroxide is the most commonly employed template for the synthesis of TS.

The roles TPA cation in stabilizing the zeolite structure has been the subject of many studies. This is due to a combination of several factors such as charge, hydrophobicity, and geometry which lead to energetically favorable associations between silicate anions and TPA promote and promote nuclei formation. Even a simple substitution of one the propyl groups by -H and -CH₂OH is enough to disrupt the favorable interactions for nuclei formation and limits the composition under which MFI can be made. Altering the length of the alkyl chain, making it smaller (as in TEA) or longer (as in TBA), disrupts the nucleation. Energy calculations have been carried out by few researchers [59-61] to explain the stabilization achieved by the occlusion of tetraalkylammonium (TAA) in ZSM-5 and ZSM-11 as shown and compared in **Figure 2.2-1**. Calculations show that at a level of 1 TAA⁺ per unit cell the stabilizing energy increases monotonically with the C/N ratio of the cation. For four TAA⁺ cations per unit cell, the stabilization energy increases to a maximum for TPA and then declines in progressing to TBA. In TEA, the stabilizing

effects of the organic aluminosilicate interactions are less than TPA, whereas in TBA, the chains are too long and lead to repulsive interaction between adjacent TBA molecules, thereby disrupting nucleation [60]. In conclusion, increase in organic-zeolite nonbonded interaction favors zeolites stabilization [58].

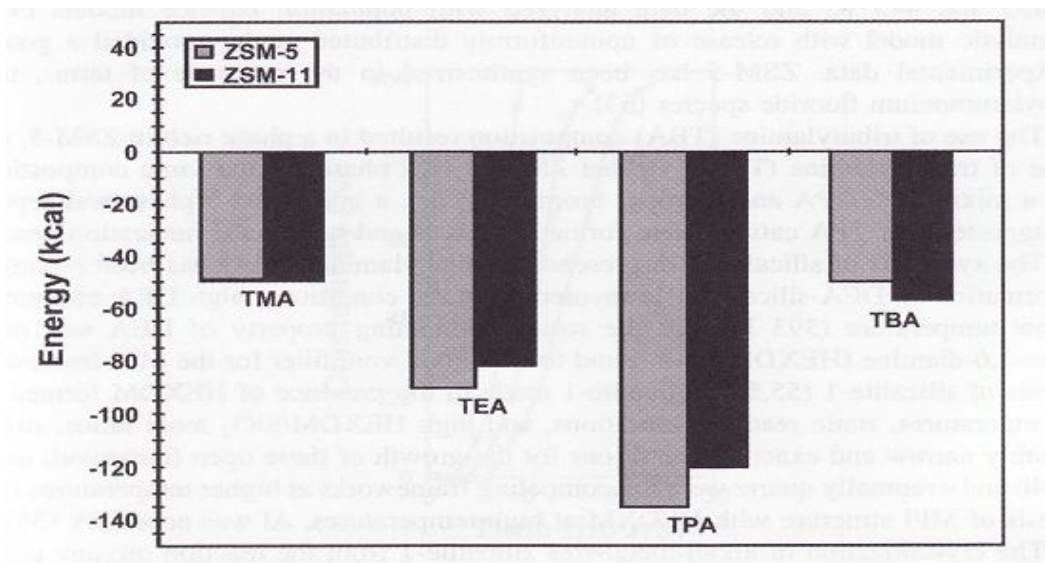


Figure 2.2-1 Stabilization energy for TAA^+ cations occluded in ZSM-5 and ZSM-11 at an occupancy of four cations per unit cell. All energies are in kcal per unit cell (source from ref. 58)

2.2.2 Effect of Alkalinity:

Alkalinity of the solution plays a key role in the hydrothermal synthesis of zeolites. This is known as mineralizer or mobilizing agent. It solubilizes both silicon and aluminium sources and brings them in a homogeneous solution with sufficient number of soluble precursors for the zeolite synthesis. However, the alkalinity of the solution has a marked influence on the crystal size as well as the solid yield of the TS -1. At high OH-concentration multiple nucleation takes place which leads to the formation of irregularly shaped crystals. [52].

2.2.3 Effect of Temperature and Time:

The rate of nucleation increases with an increase in the temperature of crystallization in zeolite synthesis. It can again determine the type of products that will crystallize from

the solution. At high temperatures, the water molecules, which normally fill up the pores of the porous solids, will be evaporated and a dense packed structure is expected. Similarly if the pores are filled up with a high boiling liquid, then even at elevated temperatures an open porous structure is usually formed. [52].

TS-1 synthesis also follows the general rules that with time, the crystallinity of the sample is increased. However, it has both a lower limit and an upper limit. Beyond these limiting values the formation of extra-framework titanium species is facilitated. [52].

2.2.4 Effect of Dilution:

Dilution has an effect in the nucleation and crystallization process in the synthesis of TS-1. Increase in the water content leads to the dilution of the reactive zeolite precursors. Therefore, increased dilution prevents supersaturation and retards nucleation. Besides, increase in dilution forms a thicker sphere of hydration around both the silicate / titanosilicate species. Before these reactive species condense, they have to strip off their hydration sphere. So increased dilution may lead to an increase in nucleation time and may retard crystallization. [52].

2.2.5 Effect of Inorganic Cation:

The presence of inorganic cations (Na^+ , K^+ , Cs^+ , etc) has a tremendous role in the synthesis of TS -1. In general, inorganic cations (Na^+ , K^+ , Cs^+ , etc) as well as organic (TME^+ , TEA^+ , TPA^+ , etc) strongly perturb the hydrogen bonding among the water molecules and orient them in a particular pattern around them. The smaller the size of the cation, the greater is the charge density, and the perturbation of the hydrogen bonded water molecules. Depending on whether these cations can organize the water molecules or not, they are defined as structure breaking and structure making. The small cations such as Li^+ , Na^+ , K^+ , etc, are called structure making as they can reorganize the water molecules. Large cations like Cs^+ , NH_4^+ , etc are called structure breaking, as because of their low charge density they are not able to reorganize the water molecules. [52,58]. Structure breaking cations favored the formation of large (15-25 μm) single crystals or twins, whereas structure making cation produced Si-rich crystallites distributed within 5 to

15 μ m range. [58]. However, alkali and alkaline earth metals have a negative effect on the synthesis of TS -1. The presence of alkali cation prevents the incorporation of the Ti⁴⁺ in the silicalite lattice and favors the formation of extra-framework titanium species. [52]. Crystallization of MFI structure zeolites is possible only in a very limited range with Na⁺, to some extent with K⁺, but not at all with Li⁺. However, synthesis is possible for bicationic systems with Na⁺ as one of the ions.

2.3 SYNTHESIS METHODS OF TITANOSILICATE

In the patent of Taramasso et al., two methods are described for the synthesis of TS-1. The first method involved mixed alkoxide or sol-gel technique which is obtained by controlled hydrolysis of tetraethoxy titanium (IV) and tetraethoxysilane [42]. In the second method; dissolved titanium method, the precursor obtained by mixing colloidal silica and a solution containing TPAOH, hydrolyzed titanium alkoxide and H₂O₂ [42]. In both methods, the titanium has been slowly added into the silicate solution, either through slow hydrolysis of alkyltitanate or through slow coprecipitation of alkylsilicate with an alkyltitanate because of their potential for irreversible formation of titanium dioxide phase, [55]. Therefore, one could expect that the synthesis of materials containing isolated tetrahedral titanium sites to be rather difficult (was explained in part 2.2, and also in part 2.3 and 2.5 later on).

2.3.1 Methods to Produce Metal-Incorporated Zeolites

2.3.1.1. Direct hydrothermal treatment (Sol-gel technique)

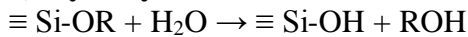
Sol gel processing refers to room temperature formation of solid inorganic materials from molecular precursor in liquid solution [39]. It is based on the addition of inorganic compounds (metal salts or alkoxides) in aqueous or organic solvents to form polymeric or particulate sols. These sols are then condensed to various types of gels [39]. The sol-gel process is a versatile solution process extensively utilized to design and synthesize inorganic-organic hybrid materials with nanometer-scale architecture [62]. It involves the transition of a system from a liquid “sol” into a solid “gel” phase [24,27-

29,31,34,41,49,62-74]. In this method the metal atoms will be introduced in the mesoporous materials body, and at high metal loading, nanoparticles/particles will form (but not necessarily placed in the pores). One of the promising features of sol-gel technique is;

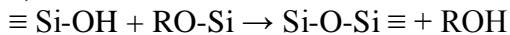
- 1) can control surface chemistry, compositions and microstructure by varying the processing parameter
- 2) room temperature synthesis
- 3) varying product forms; powder, film, fiber, monolith
- 4) because the process begins with a relatively homogenous mixture, the resulting product is a uniform, ultra-fine porous powder
- 5) can be scaled up to accommodate industrial scale production

The sol-gel process is usually divided into the following steps: forming a solution, gelation, aging, drying, and densification. There are 3 basic equations involved in sol-gel process:

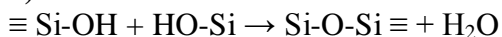
1) Hydrolysis reaction



2) Alcohol condensation



3) Water condensation



There are several parameters which influence the hydrolysis and condensation reactions (sol-gel process), including the reactivity of metal alkoxide, water/alkoxide ratio, solution pH, temperature, and nature of the solvent and additives [64] (the parameter is same as for synthesis titanosilicate as explained in section 2.2). As the hydrolysis and condensation reactions continue, viscosity increases until the “sol” ceases to flow and forms a “gel”. When the "sol" is cast into a mold, a wet "gel" will form. With further drying and heat-treatment, the "gel" is converted into a dense ceramic or glass particles. If the liquid in a wet "gel" is removed under supercritical conditions, a highly porous and

extremely low density material called "aerogel" is obtained. As the viscosity of a "sol" is adjusted into a proper viscosity range, ceramic fibres can be drawn from the "sol". Ultra-fine and uniform ceramic powders are formed by precipitation, spray pyrolysis/ chemical vapor deposition, or emulsion techniques [64]. The various processing options in the sol gel procedure are illustrated in **Figure 2.3-1**.

Sol-gel materials synthesized without the addition of templates often are microporous materials when dried in air (denoted as xerogels) [12]. When sol-gel processes are used to prepare mesoporous materials, charged cationic/anionic species or neutral surfactants are employed as templates. They direct the mesophase formation based on electrostatic interaction and hydrogen-bonding interactions, respectively [64].

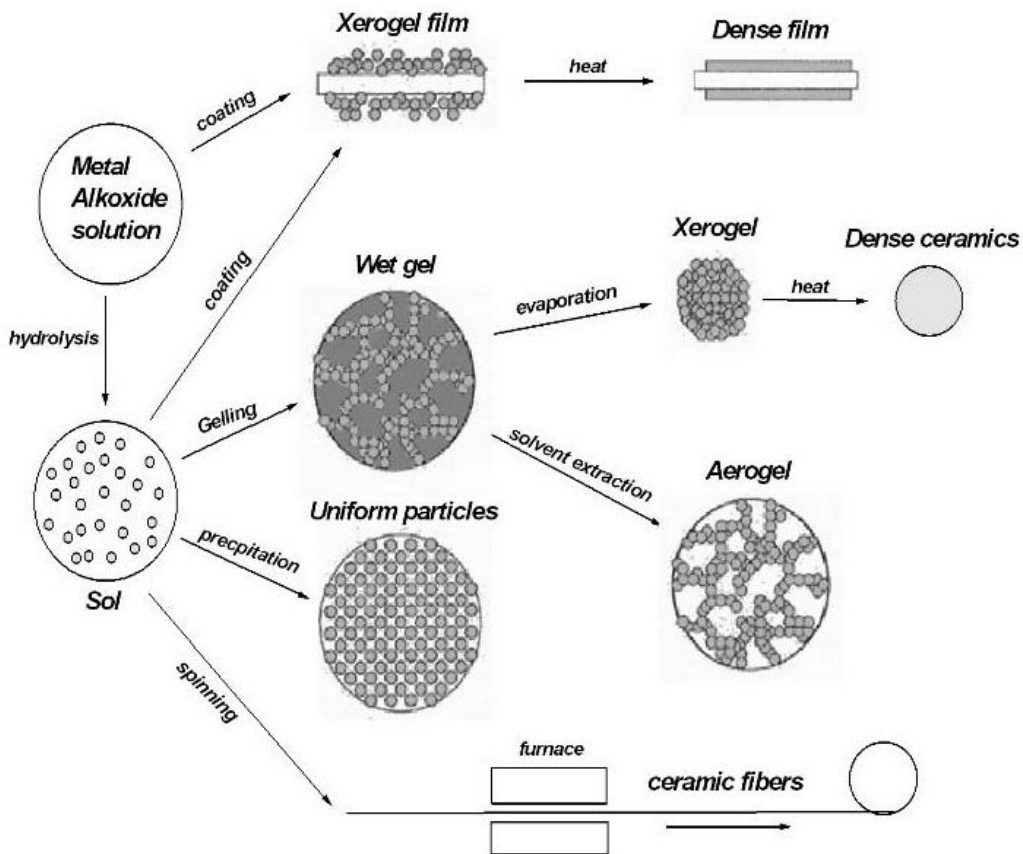


Figure 2.3-1 Sol-gel process [source from ref. 64]

2.3.1.2. *Impregnation with metal compounds*

An alternative 'dry' procedure to synthesize TS-1 by impregnating silica with a titanium precursor dissolved in aqueous TPAOH was developed by Padovan et al. Later, modification of this method employed $\text{TiO}_2/\text{SiO}_2$ cogels [42]. Impregnation is extensively used in the preparation of metal-functionalized mesoporous materials. The process includes direct impregnation of preformed mesoporous solids with solutions of the desired metal compound. The process is normally followed by subsequent reduction, thermal decomposition, UV-irradiation, or ultrasonic treatment. The formed metal atoms are randomly distributed over the mesoporous surface, and /or particles are formed in the pores, without any structural order. To form the nano-particle by wet impregnation, several authors used consecutive impregnations (four to five times), drying the material in between, to ensure that the mesopores are completely filled with metal precursor. In this case, the amount of precursor is fixed and determined by the pore size and volume; the recipe is well reproducible as the final particle size is controlled by the precursor amount and in some cases by the pore size. Normally, impregnation provides efficient incorporation of metal compounds inside the pores, but the particle growth is not controlled (particle size distribution is broad and particles are located statistically) if no special conditions are applied. On the other hand, particle size is often restricted by the pore size [62]. A.S Hamdy [62] has applied impregnation method to synthesis mesoporous amorphous TUD-1 (ultra large titanium silicate). However though he had proved that the mesoporous embedded with nanoparticle TiO_2 , the particles are bigger, not uniform in size and the porous is only in one size region (macroporous). Moreover, the desired product only can be achieved at higher metal loading and higher crystallizing/treatment time. The pore size distribution is broad for low metal loading and is non-porous in nature as the N_2 sorption analysis show no hysteresis loops. The catalytic properties of the TUD-1 produces is less active compared to TiO_2 .

Padovan et al. had tried synthesis of TS-1 by wetness impregnation method of $\text{SiO}_2\text{-TiO}_2$ coprecipitate. The dried $\text{SiO}_2\text{-TiO}_2$ co-precipitate is impregnated with a required quantity of TPAOH solution similar to the pore volume of the solid and the subsequent treatment leads to the formation of TS-1 without the formation of TiO_2 species. Uguina et al. has

successfully synthesized TS-1 from SiO₂-TiO₂ co gel using modified Padovan's method. Gao et al. synthesized TS -1 using aq. solution of TiCl₃ as the titanium source and thereby avoiding the precipitation of TiO₂. However all synthesis route above will only produce titanosilicate without any trace of extra-framework titanium species after more than 2-5 days autoclave treatment at high temperature [52,62,64,65,74,75,77-87; refer to summary in **Table 2.5-1**].

2.3.1.3. Template ion exchange with transition metal cations

Another interesting method of introducing inorganic functionality into mesoporous solids is based on the replacement of the surfactant by transition metal cations. In this case, the metal cations are located at the interior pore surface, replacing the cationic surfactant. The ion-exchange reaction is normally driven by replacement of monovalent cations (surfactant) with divalent (or trivalent) metal cations, and thus entropy is responsible for an efficient ion exchange. A unique feature of this ion-exchange technique is that the metal ions are transported solely inside the pores, while the external surface can be capped with inert hydrophobic groups. This method seems to be superior to direct impregnation or chemical vapour deposition methods, as no precipitation on outer surface takes place (if the outer surface is capped). Its use has been very limited (only a few papers have been published so far) [62]. Rigutto et al.[42] prepared aluminium-free zeolite beta containing framework titanium by reacting with TiCl₄ as depicted in **Figure 2.3-2** Kraushaar et al. have introduced atom planting method and successfully shown that the incorporation of Ti⁴⁺ in the crystal lattice of silicalite occurs when dealuminated ZSM-5 are treated with TiCl₄ vapor at a high temperature. Motivated by works of Kraushaar et al, Carati et al. have respected the experiment using deborated borosilicalite. Though these materials exhibit some catalytic properties, they are not as good as TS-1 in catalytic performance as most of the Ti incorporation occurs at the external lattice. Other than chlorides, Popa et al. have described the synthesis of TS-1 in the presence of fluoride ions. Lopez et al. have shown that extraframework Ti⁴⁺ is formed when fluorides are used. Their method however requires more templates to hydrolyze the silica precursor. [50].

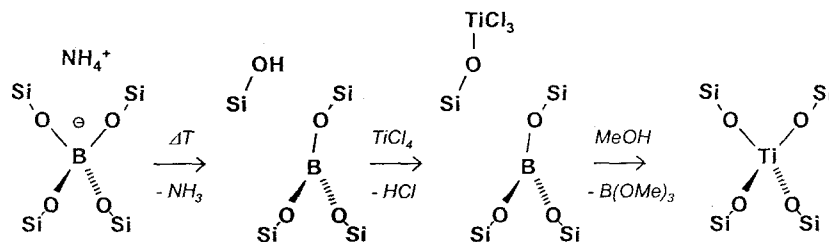


Figure 2.3-2 Boron replacement by titanium in borosilicate. [source from ref. 42]

2.3.2 Additional Methods to Produce Metal Nanoparticles/Mesoporous System via Sol Gel Method

2.3.2.1 Precipitation

One conventional method to prepare nanoparticles of metal oxide is the precipitation method. This process involves dissolving a salt precursor to make metal oxide. The corresponding metal hydroxides usually form and precipitate in water by adding a basic solution such as sodium hydroxide or ammonium hydroxide to the solution. The resulting hydroxide is calcined and after filtration and washing, the final powder is obtained. This method is useful in preparing composites of different oxides by coprecipitation of the corresponding hydroxide in the same solution. One of the disadvantages of this method is the difficulty to control the particle size and size distribution. Very often, fast uncontrolled precipitation takes place resulting in large particles. [64].

2.3.2.2 Chemical vapour deposition

Another way to control the nano-particle growth and particle spreading is through chemical vapour deposition (CVD) method [64]. CVD is a general term applied to the deposition of solids materials from chemical precursors in the vapor phase [39]. However, this method is restricted to thin films or small particles (not suitable for e.g. monolithic samples) to prevent uneven distribution of the metal compounds within the material. Another limitation of CVD is that under many conditions too large particles are formed. Nevertheless, the lack of specific interactions between the silica pore walls and the volatile compounds does not always exclude growth outside the pores [64]. In a number of cases it has been reported that particle sizes exceed the pore diameter (ca. 3-4

nm) and the exact particle location and particle size distribution remain unclear [39]. Unlike growth by physical deposition, this method is very complex and needs numerous test runs to reach suitable growth parameters [39]. The method is highly complex as [15, 88]:

- 1) it generally includes multicomponent species in the chemical reactions.
- 2) the chemical reactions generally produce intermediate products
- 3) the growth has numerous independent variables
- 4) the growth includes more consecutive steps than in physical methods

A. Ungureanu et al. [89] has used this method of synthesis route to prepare two different kinds of titanosilicate zeolite molecular sieves. Although they claimed this material is bimodal meso-microporous titanosilicate by reporting the decrease in micropore volume, no proves were shown through either hysteresis loops or BJH pore size distribution. They also reported that Ti in the samples is not active

2.3.2.3 Chemical interaction of metal compounds with functional groups of the mesoporous surface

Here, functionality of the mesoporous walls is necessary, and chemical interaction should be the driving force for the incorporation of metal species on the surface of the pores. This interaction can be realized in two ways, e.g. for Si-compounds (i) during sol-gel reaction when one of the silica precursors bears such groups and (ii) as a post-synthesis via interaction of various compounds with silanol groups (dissolution/recrystallization of the mesoporous phase) [43]. As functional groups for interaction with inorganic compounds, thiol and amine are frequently used. In this procedure, the functional groups can play a dual role (i) being an anchor for metal compounds and/or (ii) reacting with the surface of the growing nano-particle. In several cases silanol groups of silica walls can be used for direct functionality incorporation along with inorganic compounds followed by the corresponding treatment (reduction, calcination, interaction with H₂S, etc.) [90]. This procedure avoids the growth of nano-particles in the outer pore space which is a major drawback of the impregnation/calcination method. In addition, the metal particle size is not influenced by the type of reducing agent, and in fact a very efficient

mechanism of size restriction is observed. Presumably the metal nano-particles are forced to nucleate in the mesopore entries, but restricted to grow beyond their cavity [62].

R.V. Grieken et al. [91], has prepared titanium containing mesoporous silica by silylation of mixed oxides obtained via sol-gel method. They have shown that this treatment not only allows the synthesis of materials with large BET area, pore sizes and pore volumes in the range of aerogels, but it also allowed the modification of their surface from hydrophilic to hydrophobic. However this can only be done at high Si/Ti ratio and no confirmation of TS-1 fingerprint was done in their research. Moreover, the efficiency of the silylation treatment depends on the nature of the agent used in similar reaction conditions.

Xiao and co-workers [92] have reported the synthesis of mesoporous MTS-9 by the assembly of TS-1 nanoclusters with triblockcopolymers in strongly acidic media. Unfortunately, the calcinations of as-synthesized MTS-9 at 500°C for several hours resulted in significant reduction of its catalytic activity [150].

Wang et al. [93] had obtained hollow crystal TS-1 with large intra-crystalline voids by a post synthesis treatment of the calcined zeolite with highly alkaline TPAOH solutions. Z. Yuan et al. [94] had successfully formed bimodal mesoporous silica by mild temperature post-synthesis hydrothermal treatment. D.T. On et al. also managed to form bimodal meso-micro-porous UL-TS-1 by post-synthesis hydrothermal treatment. The treatment has proved to be particularly attractive in the case of zeolites containing extraframework Ti oxide species; part of these contaminating species are dissolved and incorporated to the zeolite framework upon recrystallization [93]. However these involve multiple steps which require more energy, more time and more costly TPAOH. If the crystallization reaction for the 1st step itself will need more than 3 days while the post treatment will need another 2 days, one can conclude that this preparation is complex and time consuming.

An alternative approach was by templating in micelles/microemulsion as described in the following section. A clear advantage of this method is the opportunity to use well-developed procedures to control particle size and particle size distribution of the nanoparticles.

2.4 MICROEMULSION TECHNIQUE

2.4.1 Emulsions

An emulsion is a thermodynamically unstable dispersion of two mutually immiscible liquids, such as water and oil [95]. Emulsions are colloidal systems [96]. A classification of emulsion systems is based on size, macroscopic appearance and thermodynamic stability as is given in **Table 2.4-1** and **Figure 2.4-1** [95,96]. Disperse phase formation is not a spontaneous process ($\Delta G < 0$) and requires the supply of an external energy, such as mechanical energy (i.e. stirring). However, the process of droplet dispersion is associated with an increase of the surface/volume ratio and therefore there is a requirement of large surface energy in order to achieve a long term stability. Therefore, emulsions are generally thermodynamically unstable unless emulsifying agents are added. These agents are surfactants (tensides)- amphiphilic molecules which reduce the surface tension between the two phases. [54,95,96].

Table 2.4-1 Classification and characteristics of emulsion system

	Characteristics		
	Optical appearance	Particle sizes (nm)	Thermodynamic stability
Coarse Macroemulsion	Milky opaque	>1000	No
Fine Macroemulsion	Blue-white	100-200	approaching
Micro/nanoemulsion	Transparent or translucent	10-100	Yes
Micellar solution	Translucent	2-10	No

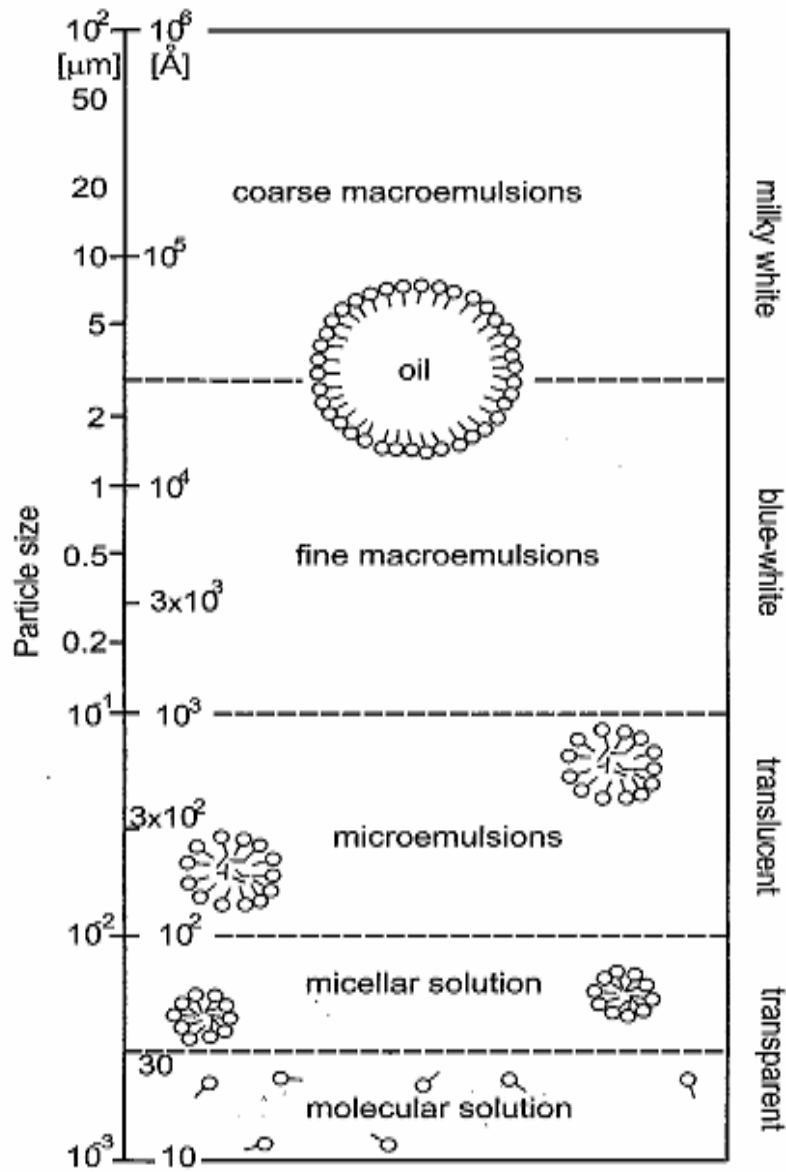


Figure 2.4-1 Size ranges of the disperse phase in liquid-liquid dispersions. (Source from ref. 95)

2.4.2 Surface Active Agents (Surfactants) and Cosurfactants

The word surfactant originates from surface-active agent [54,95]. It was called as such because of their main properties; tendency to segregate to an air-water interface and consequently to lower the surface tension compared to pure water. [54]. A surfactant

molecule such as phospholipids and soaps is a self-assemble molecule in a certain solution such as water or salt solution [97]. It consists of two different groups with different solubilities even though it is chemically bonded together [98]. The head group has a hydrophilic (water-loving) region of the molecule and it is generally depicted as a circle. The tail group contains hydrophobic (water-hating) species and it is generally depicted either as a straight line or a wavy tail. The tail group consists of one or more hydrocarbon chains. **Figure 2.4-2** illustrates the schematic diagram of a surfactant generally. Surfactant not only stabilize complex liquid system but also important in controlling droplets size [99]. They can change the interfacial energy and lowers the interfacial tension [50,54].

Surfactants are divided into four categories i) cationic, ii) zwitterionic, iii) nonionic and, iv) anionic [50,54]. **Table 2.4-2** lists the representative class of surfactants and its characteristic. Surfactants stabilized micelle, lamellar and microemulsion system by forming an interface film which separates oil and water, usually participate the co-surfactant [99]. This cosurfactant or also known as amphiphilic additives are often a medium chain-length alcohol. n-Alcohols ranging from 1-butanol to 1-heptanol were already studied as amphiphilic additives, or co-surfactant, to sodium dodecyl sulfate (SDS) [100]. When microemulsions are formed without cosurfactant, the resulting ternary system is a simple model for phase behaviour. [54].

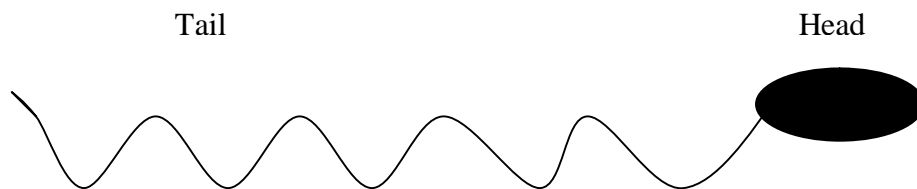


Figure 2.4-2 Schematic diagram of surface active molecule.

Table 2.4-2 Type and Characteristics of Surfactants

TYPE	Characteristic	Chemical name	Molecular Formula	Abbreviations
Anionic	<ul style="list-style-type: none"> the anionic surfactant dissociates in aqueous solution, giving an anion carrying the amphiphilic properties and an inactive cation (e.g. Na⁺ or K⁺) -most widely produced 	<ul style="list-style-type: none"> Sodium dodecylsulfate Sodium p-odecylbenzenesulfonate Sodium bis (2-ethylhexyl) 	<ul style="list-style-type: none"> C₁₂H₂₅O-SO₃-Na p-C₁₂H₂₅(C₆H₄)SO₃Na C₂₀H₃₇O₇ 	<ul style="list-style-type: none"> SDS SDBS AOT
Cat-ionic	<ul style="list-style-type: none"> In aqueous solutions, cationic surfactants are ionized in a cation carrying the amphiphilic properties, and an inactive anion, such as Cl⁻ or Br⁻ The cationic group is most often a quaternary ammonium and amines group 	<ul style="list-style-type: none"> Cetyltrimethylammonium bromide Didodecyl dimethyl ammonium bromide Dodecyltrimethylammonium bromide Cetylpyreneium 	<ul style="list-style-type: none"> C₁₆H₃₃N(CH₃)₃Br (C₁₂H₂₅)₂N-(CH₃)₂Br C₁₆H₃₃PyBr 	<ul style="list-style-type: none"> CTAB DDAB DTAB
Zwitter ionic	<ul style="list-style-type: none"> - containing both positive and negative charges on the head group - the positive charge is often associated with an ammonium group and the negative charge is often a carboxylate - non-toxic and easy to dissolve - used in cosmetic product since they have found to be non- 	<ul style="list-style-type: none"> Tetradecyl-dimethylamine Hexadecylsulfobetaine N-Dodecyl-N,N-dimethyl 	<ul style="list-style-type: none"> C₁₄H₂₉-N⁺ (CH₃)₂O-C₁₆H₃₃-N⁺Me₂(CH₂)₃SO₃⁻ 	<ul style="list-style-type: none"> TDMAD SB3-16
Non-ionic	<ul style="list-style-type: none"> -do not give ions in solution. -The hydrophilic part of their molecule is usually a polyether chain, and more rarely polyhydroxyl chain. -The hydrophobic tail is an alkyl chain -not sensitive to hard water 	<ul style="list-style-type: none"> Sorbitan monolaurate Polyoxyethylene (23)-dodecyl ether 	<ul style="list-style-type: none"> C₁₁H₂₃CO-OCH₂CHOH-(C₄H₅O)-(OH)₂ CH₃(CH₂)₁₁-(OCH₂CH₂)_n OH N~23 	<ul style="list-style-type: none"> Span 20 Brij-35

2.4.3 Micellar Structure and Properties

The thermodynamic properties of amphiphiles in solution are controlled by the tendency for the hydrophobic region to avoid contact with the water, a phenomenon termed as the hydrophobic effect. This leads to the association of molecules into micelles, which are spherical or elongated structures in which the hydrophobic inner core is shielded from water by the surrounding corona formed for the hydrophilic ends of the molecules. These aggregates form by spontaneous self-assembly at sufficiently high concentrations of surfactant [50,54,95,101]. A schematic two-dimensional representation with different regions of micelle/ microdroplet is shown in figure 2.4.3.

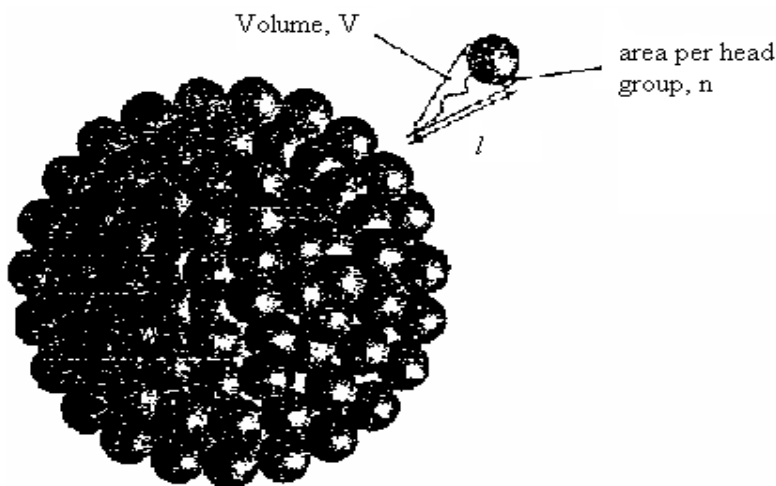


Figure 2.4-3 A spherical micelle. The packing of amphiphilic molecules is controlled by the effective cross-sectional area of the head group, n and the hydrophobic chain of length, l and volume, V . (source from ref. 54)

2.4.4 Microemulsion

Microemulsion is originally introduced by Schulman and Hoar at 1943 [95]. Firstly, he proposed few techniques to produce negative Newtonian interfacial tension, which ultimately formed microemulsion. Few years later, a lot of features in this system are explored and in 1955, this system is called swollen micellar solution or transparent emulsion [102]. They are usually of the oil-in-water type [54]. During microemulsion

formation, a phase is broken into numerous droplets which are invisible to the eye as they possess diameters 100-1000 Å (**Figure 2.4-1**).

Microemulsion is defined as two different liquids with different thermodynamically stable phases, optically isotropic (but not kinetically stable) and consists of surfactants or surfactant and certain co-surfactant. Microemulsion is formed spontaneously, their properties are independent of the manner in which they were produced, and they are thermodynamically stable. Ordinary emulsions, in contrast, require mechanical or chemical work for their production, so that at best they are kinetically stable i.e. the droplets are protected from coalescence. Theoretically, microemulsion are only thermodynamically stable if their interfacial tension is approaching zero or less ($< 10^{-2}$ dyne/cm). At their simplest, microemulsions are a special case of emulsions; colloidal solutions of normal or inverted, swollen micelles [95]. It spontaneously dissolves in an oil in water (o/w) system and water in oil (w/o) system (**Figure 2.4-4**.) through surfactant which differentiate between microemulsion from emulsion (turbid milky-like). A microemulsion can self order and determine its nano-structure by minimize its free energy.

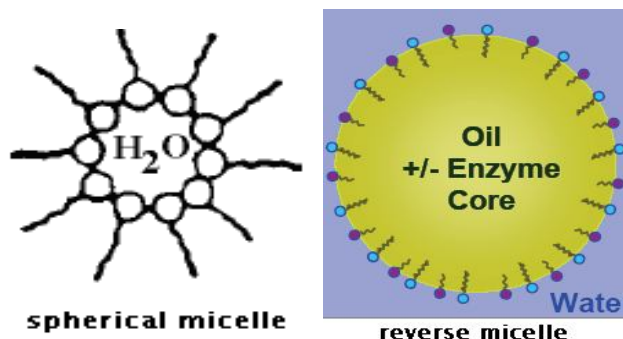


Figure 2.4-4 A schematic diagram of spherical micelle (w/o microemulsion) and reverse micelle (o/w microemulsion) (source from ref. 50 and 103)

2.4.4.1 Phase Diagram and Microemulsions

A phase may be defined as a region of component space homogeneously filled with matter. A phase diagram provides a compact graphical representation of phase

boundaries of any feasible system (uni- or multicomponent). Isothermal phase equilibrium of a ternary system can be described with the cross-section of the phase prism (triangular phase diagram) as schematically shown in **Figure 2.4-5**. To form microemulsion solution in 1-butanol/SDS/H₂O solution, the required percentage of composition should be the L region. If the percentage composition is outside the border of the L region, the formed mixture is turbid. Hence, it is not a microemulsion.

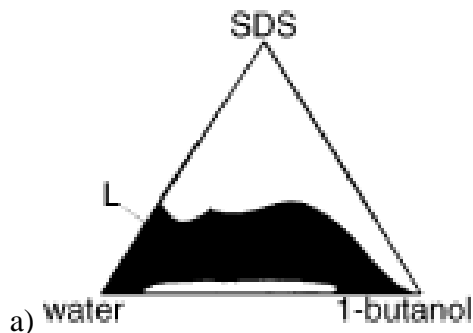


Figure 2.4-5 water/SDS/1-butanol ternary phase diagram. The black area, L represent microemulsion [source from ref. 88]

2.4.4.2 Application of micelles and microemulsions

In the last two decades, there has been a revolution in the utilization of microemulsion systems in a variety of chemical and industrial processes such as; i) petroleum fields; as fuels, lubricant and cutting oil ii) pharmaceuticals, iii) cosmetics iv)corrosion inhibitor, v)coating and textile finishing, vi)detergency, vii)agrochemicals, viii)food, x)biotechnology, xi)in analytical application, xii)as liquid membrane xiii) as media for synthesis nanoparticles, xiv) microemulsion in remediation and detoxification xv) synthesis microporous media by microemulsion gel technique. It is a long list to demonstrate their significance and potential use in various sectors. Hence, only a few among the processes and applications is presented briefly here.

2.4.4.2.1 Enhanced Oil Recovery

A lot of researchers attempted to understand the mechanism involved in an enhanced oil recovery (eor) using surfactant and microemulsion flooding brought about by the low

interfacial tension and good wetting properties of microemulsion [60,61,90,104-114]. Roughly 20 % of the otherwise unrecoverable underground oil can be obtained by an enhanced oil recovery process. The oil remains trapped in the capillary of the rocks of the reservoir because of the high interfacial tension (about 20-25 mN/m) between the crude oil and reservoir brine. So, microemulsion is used to push the oil out of the capillaries in order to achieve 80-90% recovery. If the interfacial tension can be reduced to around 3-10 mN/m, a substantial fraction of the residual oil in the porous media in which it is trapped can be mobilized. Low interfacial viscosity of the system is also advantageous [60].

Apart from enhanced oil recovery, other potential applications of microemulsion in petroleum industry will include [50,112,115,116];

- i) dispersion of water droplets in different kinds of fuel in order to curtail exhaust pollution by CO and NO_x
- ii) manufacturing of cutting oil or laminating emulsion for metal working
- iii) formulation of oil based drilling fluids which benefited from a high viscosity as a result of a small amount of tiny water droplets

2.4.4.2.2 Pharmaceuticals and cosmetics

Thermodynamic stability, higher degree of homogeneity and solubilization capacity give rise to the various applications of microemulsions (particularly gel or liquid crystalline phases) in pharmaceuticals and cosmetics [60]. The easy of formation, remarkable environment independent stability, excellent solubilization capacity, transparency, etc. favour microemulsions as a better proposition over other compartmentalized systems [117]. Microemulsion is interesting for the cosmetics industry not only for their thermodynamic stability but also because of their transparency. Moreover, the small particle size (100-500nm) means that they penetrate into the skin rapidly faster. Gel, sunscreen, perfume gels, skin cleansing and skincare gels are all built on this base [95], [60,118]. However, toxicity, bioincompatibility of surfactants and cosurfactants, requirement of high concentrations for formulations and other relevant factors such as maintenance of thermodynamic stability in the temperature range between 0° and 40°C,

salinity, constant pressure during storage, low solubilizing capacity for high molecular weight drug (and oil), etc. limit the uses of microemulsions in the pharmaceutical and medicinal fields [118].

2.4.5 Literature Reviews of Microemulsion Technique

A literature survey depicts that the ultra-fine nanoparticles in the size range between 2 and 50 nm can be easily prepared by this method. This technique uses either an inorganic phase in w/o microemulsions or o/w microemulsion (reverse micelles) with an approach based on the formation of micro/nano reaction vessel for the preparation of nanoparticles. A very important aspect in microemulsion technique involves the ability to control the size through an appropriate selection of surfactant beforehand. The ability of controlling lies under a dynamic nanodroplet structure which can act as a medium for a chemical reaction. When reactants react with each other, microemulsion functions as nanoreactor because it can generate nanoparticles and act as a cage hence inhibiting the growth of particles and agglomeration when particle size near to nanodroplet size is accomplished [59].

Water in oil microemulsions are used to form nanoparticles by nano-reactors from the micro-water droplets. There are two typical methods in this technique as shown in **Figure 2.4-6**. A typical method for the preparation of metal oxide nanoparticles within micelles consists of two microemulsions (two microemulsion method), one with the metal salt of interest and the other with the reducing or oxide containing agent and mixing them together. When two different reactants mix, the interchange of the reactants takes place due to the collision with water microdroplets. The reaction (reduction, nucleation, and growth) takes place inside the droplet, which control the final size of the particles. The interchange of nuclei between two microdroplets does not take place due to restrictions from the emulsifier. Once the particle inside the droplets attains its full size, the surfactant molecules attach to the metal surface, thus stabilizing and preventing further growth.

In microemulsion plus second reactant method, a microemulsion or macroemulsion and aqueous solutions carry the appropriate reactant to obtain the desired particles. The interchange of the reactants takes place during the collision of the water droplets in microemulsion. The interchange of the reactant is very fast so that for the most commonly used microemulsions, it occurs just during the mixing process. The reduction, nucleation, and growth occurring inside the droplet controls the final particle size. The chemical reaction within the droplet is very fast, so the rate determining step will be the initial communication step of the microdroplets with different droplets. The rate of both nucleation and growth are determined by the probabilities of the collisions between several atoms, between one atom and a nucleus and between two or more nuclei. Once a nucleus forms with the minimum number of atoms, the growth process starts. For the formation of monodisperse particles, all nuclei must form at the same time and grow simultaneously and with the same rate. Reverse micelles are used to prepare nanoparticles by using an aqueous solution of reactive precursors that can be converted to insoluble particles. Nanoparticle synthesis inside the micelles can be achieved by hydrolysis of reactive precursors such as alkoxides, and precipitation reactions of metal salts. Solvent removal and calcinations lead to the final product. The advantages of using this method include the ability to prepare of very small particles and the ability to control the particle size.

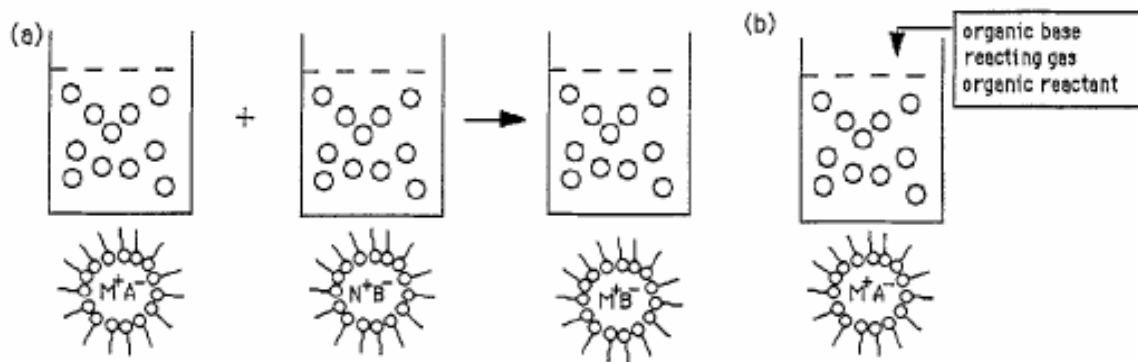


Figure 2.4-6 Synthesis of nanoscale particles in micelles; (a) two microemulsions; (b) microemulsion plus second reactant (source from ref. 41)

2.4.6 Microemulsion as Template Media In Synthesis

The self assembly of molecules (SAM) or surfactant can be exploited to template inorganic minerals such as silica, alumina and titania. The resulting structures resemble those of zeolites, except that the pore size is larger for the surfactant-templated materials than those that result from channels between atoms in classical zeolite structures [50,54,119,115]. In conventional zeolites, the pore size is typically up to 1nm, whereas using amphiphile solutions it is possible to prepare an inorganic material with pores up to the mesoporous range [2-50nm]. They are of immense interest due to their potential applications as catalysts and molecular sieves. Thus, just as the channels in conventional zeolites have the correct size for the catalytic conversion on methanol to petroleum, the pore-size in surfactant-templated materials could catalyse reactions involving larger molecules. It was initially believed that templating process simply consisted of the formation of an inorganic 'cast' of a microemulsion phase. In other words, pre-formed surfactant aggregates were envisaged to act as nucleation and growth sites for materials. However, it now appears that the inorganic material plays an important role and that the structuring occurs via a cooperative organization of inorganic and organic material. Considering, for example, the templating of silica, a common method is to mix a tetraalkoxysilane and surfactant in an aqueous solution [54]. Based on this knowledge, a lot of researchers use microemulsion as confined space or nanoreactors for zeolite growth, as has been shown to be very successful in the synthesis of metal, metal oxide and metal sulfide nanoparticles. This area has experienced considerable growth since the initial report by Dutta and co-workers of zeolite A and zincophosphate FAU analogue growth in microemulsions [120]. Since then few researcher attempt to use SAM to synthesise crystalline microporous molecular sieves such as zeolites [7,63]. Avelino et al. has proved in their research that it was possible to synthesise stable amorphous microporous molecular sieves with pore dimensions pre-defined by the size and shape of the SAM. A type of thermally and hydrothermally stable amorphous microporous molecular sieves, with pore dimensions and micropore volume determined by the size and the shape of SAM can be obtain by controlling the synthesis condition [8]. Kyoko Aikawa et al. also had synthesise porous silica by the hydrolysis of TEOS in bicontinuous microemulsion containing polyoxyethylene (POE) dodecylether, isooctane and water [9].

Yates and colleagues have reported microemulsion mediated growth schemes to form $\text{AlPO}_4\text{-5}$ and silicalite-1 materials at high temperatures, and yan'slab has recently reported the synthesis of zeolite nanocrystals in cationic microemulsion using microwave heating [120, ref. Therein]. Lee [120] et al's lab has been actively involved in this area studying silicalite-1 at low and high temperatures, as well as growth of zeolite in nonionic microemulsions. Lee et al's view of this synthetic approach was that there are two balancing or competing factors in this approach. On one hand, the microemulsion constitutes a confined space that will potentially modulate nucleation and growth (nanoreactor). On the other hand, the surfactant will coordinate to the crystallographic spaces of the growing crystal and affect the growth rates depending on the crystallographic orientation of the surface and the strength of the inorganic-organic interactions. [120]. The latter effect can be achieved by changing the chemical nature of the surfactant. An important argument in determining the formation and growth of microporous materials in microemulsions is the nature and strength of the interactions between the surfactants forming the microemulsion and the zeolite particles or silicates precursors. Lee's results support this hypothesis, as they suggest that it is the strength and nature of the surfactant-silicate interactions, not the confined space afforded by the microemulsion, that determine the size and morphology of the zeolite crystals obtained. In Lee et al. current reports, they have successfully synthesized silicalite-1 at low temperatures (368k) in the presence of anionic emulsion. They obtained coffin, disklike, spherical, and twinned nanocrystals under different experimental conditions. In this work, they showed that surfactant identity, TPAOH content, existence of salts and cosurfactant affect the crystallinity and morphology of silicalite-1. Their work also demonstrated that the crystal size and shape is different in all cases that those synthesized in the absence of the microemulsion. Their work shows that the crystal morphology can be tuned by adjusting the interaction between surfactant and zeolitic surface [120]. Some of researcher works in this area that I have explained above have been summarized in **Table 2.4-3**.

Table 2.4-3 Summary of the Literature on Synthesis Zeolites in SAM

Table 2.4-3 Summary of the Literature on Synthesis Zeolites in SAM									
Researcher	Year	Method of Synthesis	Templating SAM	Parameter studied	Characterization	Advantage/Achievement	Remarks/disadvantage	Reaction Temperature/crystallization time	Calcination temperature/time
Boonamn uayvitaya et al.[121]	2006	Surfactant-mediated Sol-gel	CTAB SDS Brij 56	surfactant identity	TGA, BET, FTIR, SEM,	Different surfactant able to template at different particle	Very low surface area and pore volume for sample template in SDS	Room temperature / 4-7d	600 °C / 4h
Jang & Bae [122]	2006	gel	Pluronic P123, Pluronic 25R4	Phase behavior of polymer & silica in hybrid	FTIR, TEM, BET, AFM	Nearly monodisperse pore obtained	Not mention	Not mention/ 3h	-
Lee et al.[120]	2005		TPA/ SDS, CTAB, AOT	1)presence and absence of microemulsion 2)microemulsion composition 3) surfactant identity	TGA, BET, TEM, XRD, FESEM	1)Different uniform shape (synthesized in microemulsion) 2) irregular shape (no microemulsion)	1) Zeolites cannot be formed in microemulsion at 368K. 2) surfactant/TPA ratio < 10 is needed to form silicalite-1	198°C / 96h	450 °C / 8h

Continue Table 2.4-3 Summary of the Literature on Synthesis Zeolites in SAM									
Researcher	Year	Method of Synthesis	Template cation/ SAM	Parameter studied	Characterization	Advantage/Achievement	Remarks/disadvantage	Reaction Temperature/ crystallization time	Calcination temperature/ time
Sharma et al. [123]	2005	Surfactant-mediated Sol-gel	TPA ⁺ / Fluorinated surfactant/ hydrophobic polymer oil	Presence and absence of fluorinated surfactant /polymer oil surfactant	BET, TEM, SAXS	In presence of fluorinated surfactant give higher surface area	The fluorinated surfactant disrupt the original mesostructured	-	-
Corma. & Di'az-Cabanas [124]	2005		TPAOH/ MSPTOH M ₆ BQOH MBTMOH TEAOH	Effect of different SAM	XRD, BET, NMR, FTIR	Thermally and hydrothermal stable upon calcinations	XRD show material are amorphous and have no order at short or long range	150°C / 6-168h	550 °C / 3h

Continue Table 2.4-3 Summary of the Literature on Synthesis Porous Silica in SAM									
Researcher	Year	Method of Synthesis	Template cation/surfactant	Parameter studied	Characterization	Advantage/achievement	Remarks/disadvantage	Reaction Temperature/crystallization time	Calcination temperature / time
Lee & Shantz [125]	2004		TPA ⁺ / SDS	1) synthesis temperature	XRD, TEM, SEM, BET	Non-ionic microemulsion able to template the shaped and size of silicalite-1	Use high ratio of TPAOH,	-	550 °C / 20h
			AOT	2) micro-emulsion					
Ko. et al [126]	1997	Surfactant-mediated Sol-gel	TPABr, hydroxyl-functionalized surfactant, gemini surfactant	3) surfactant identity	XRD, Fe-SEM,			80-135°C/96h	450°C / 8h
			HTMACl, HTEABr,	1) Synthesis temperature 2) surfactant identity		Continuous shifts of the pore size distribution to a larger size as the alkyl chain length of surfactant increased	Hydrothermally not stable even at low temperature	0-80°C / 4h	550°C / not mention
Ryoo et al. [53]	1999								

2.5 CHALLENGES IN TITANOSILICATE SYNTHESIS

The factors that influence the synthesis of titanosilicate and several routes to synthesize TS-1 with no extra- framework titanium species has been elaborated briefly in sections 2.2 and 2.3. More recent work in this area have been summarized in **Table 2.5-1**. The various methods as described, require the use of a relatively large amount of the expensive template (TPAOH), and/or reaction at high temperature and high pressure with special vessel (autoclave) hence making TS-1 costly. It is known that decreasing the reaction temperature, reaction pressure and concentration of TPAOH leads to non-uniform particles and larger particle sizes. It is also very difficult to avoid the formation of stable insoluble TiO₂ precipitate, either during the preparation of gel or during the crystallization of the titanosilicate leading to presence of extraframework of titanium. Larger, non-uniform particles and presence of extraframework Ti-species have a strong influence in its catalytic activity. However, due to limited research on heavy metal (HM) removal capability onto amorphous TS-1, among factors written above, only particle sizes and uniformity give significance effect to their HM removal capability. Van der pol et al. has studied the effects of various reaction parameters on the synthesis of TS-1 and had shown that those smaller crystallites are much more active than the larger crystallites. It may also promote extensive homolytic side reactions including decomposition of hydrogen peroxide [52,50]. So, many attempts have been made to synthesize TS-1 with smaller crystallite which is one of the objectives of our research.

Table 2.5-1 Summary of the Literature on Synthesis TS

Table 2.5-1 Summary of the Literature on Synthesis TS									
Re-searcher	Year	Method of Synthesis	Template cation/surfactant	Parameter studied	Characterization	Advantage/achievement	Remarks/disadvantage	Crystallization Temperature/ time	Calcination temperature/ time
N. Venkatarthi [75]	2004	formation of anatase in ethylene glycol solutions of titanium ions as a function of the solution composition	Hexamethyl-eneimine	in the absence and in the presence of Si ⁴⁺ dopant ions	XRD, SEM, TGA, DTA, FT-IR, ESR, UVVis, XPS, NMR	Incorporation of titanium in the framework, -Uniform morphology	Low surface area ~ 140 m ² /g	200°C/360h in autoclave	Dried at 100°C for 5h in static air.
R. Wang et al. [76]	2005	synthesis from assembly titanosilicate precursor under alkaline condition	CTAB	-	UVVis, XRD, BET, FTIR	hydrothermally stable than Ti-MCM-41. smaller micropore volume and pore size, incorporation of titanium in TS	FTIR show that the samples are amorphous	200°C/ 72h	Heat at 100°C /6h

Continue table 2.5-1 Summary of the Literature on Synthesis TS									
Researcher	Year	Method of Synthesis	Template cation/surfactant	Parameter Studied	Characterization	Advantage/achievement	Remarks/disadvantage	Crystallization Temperature/time	Calcination temperature / time
K.A. Genov [64]	2004	Sol Gel	TEA ⁺	Incorporation of different metal	XRD, UV-Vis, SEM, Raman, BET	Possess tetrahedral coordination, no non-framework anatase	amorphous. Extra-framework titanium, non-crystallined mesostructured material, particles do not have any well-defined morphology	200°C/ 24h in auto-clave (static condition)	Dried at room temperature
M.S. Hamdy [62]	2005	Sol gel and Wetness impregnation	TEA ⁺	1) cogel preparation in methods 2) Ti and Al content in raw xerogel	UV-Vis, NMR, Raman, BET	Surface area more than 500 m ² /g for Si/Ti ratio~10	do not have any well-defined morphology	178°C/ 86h in autoclave (under stirring)	
G. Ovejero et al. [77]	1998	Sol-gel and Template ion exchange with Al	TPA ⁺		XRF, XRD, XPS, FTIR, SEM,	Incorporation of titanium in the zeolites	- amount of TPAOH must be increased to obtain zeolites with high crystallinity	170°C/ 24h in autoclave	550°C/ 7h

Continue table 2.5-1 Summary of the Literature on Synthesis TS									
Researcher	Year	Method of Synthesis	Template cation/surfactant	Parameter studied	Characterization	Advantage/achievement	Remarks/disadvantage	Crystallization Temperature/time	Calcination temperature / time
R.B Khomane et al. [78]	2002	Prepare in micellar media In small amount of TPAOH and nonionic surfactant	Tween 20	1) presence and absence of surfactant	XRD, UV-Vis, FTIR SEM,	-Absence of extra-framework TiO ₂ - Highly crystalline uniform particles -reduced cost	-Still require extreme energy, pressure and long reaction time	160°C/ 18h in autoclave	550°C/ 15h
C.X. Hui et al. [79]	2004		Tween 20, tween 40, tween 60, tween 80	-	TGA, XRD, FTIR, BET, UV-Vis, SEM	- incorporation of Ti in zeolites -the crystal size of the TS-1 zeolite was more uniform			
H. Liu et al. [80]	2005		Tween 20, 60, Span 60, Span 80 or TX-100		XRD, FT-IR, UV-vis, XPS, SEM, BET	No anatase TiO ₂ , crystal size smaller, increase amount of Ti incorporated and surface area			

Continue table 2.5-1 Summary of the Literature on Synthesis TS									
Researcher	Year	Method of Synthesis	Template cation/surfactant	Parameter Studied	Characterization	Advantage/achievement	Remarks/disadvantage	Crystallization Temperature/ time	Calcination on temperature / time
M. Nandi & A. Bhaumik [81]	2006	using Phosphoric acid as promoter	Octadecyl trimethylammonium chloride	1) effect of promoter 2) different Si/Ti ratio	XRD, BET, FTIR, UV-VIS	Uniform mesopore materials with high titanium loading obtained	Presence of extraframework for high titanium content samples	70°C / 24h in autoclave	500°C / 8h
P. Murkhejee [52]	2000		TPA ⁺	1) effect of promoter 2) reaction time -	UV-Vis, FTIR, SEM, XRD	-Leads to formation of smaller crystals with almost uniform particle size -Absence of anatase TiO ₂	Bigger particles size obtained for samples synthesized at 1)low temperature, 2)under reflux condition, atmospheric pressure	105-260 °C / 36h in autoclave, 110 °C/48h under reflux cond., atm. pressure	540°C / 16h

Continue table 2.5-1 Summary of the Literature on Synthesis TS									
Researcher	Year	Method of Synthesis	Template cation/surfactant	Parameter studied	Characterization	Advantage/achievement	Remarks/disadvantage	Crystallization Temperature/ time	Calcination temperature / time
Hongbin Du et al. [82]	1996	Direct hydrothermal	TPABr TMA ⁺	1) Si / Ti ratio 2) OH ⁻ /SiO ₂ ratio -	XRD, FTIR, SEM, TGA, NMR	-Synthesis TS having zorite structure titanium incorporation into framework, -single platelet and smaller zorite (TMA) - twin aggregate zorites TPABr	-Si / Ti ratio > 0.5, the crystallinity decreased, Si / Ti ratio < 0.7, zorite accompanied with other unknown phase were obtained -OH ⁻ /SiO ₂ ratio beyond 3.4, -no crystallite produced -not stable above 300°C	180°C/ 72-120h in autoclave (under stirring)	Dried at ambient temperature

Continue table 2.5-1 Summary of the Literature on Synthesis TS									
Researcher	Year	Method of Synthesis	Template cation/surfactant	Parameter Studied	Characterization	Advantage/achievement	Remarks/disadvantage	Crystallization Temperature/ time	Calcination temperature / time
A.Tuel & Y. B. Taarit [83]	1995	Direct hydrothermal	TMPA ⁺	1) crystallization time 2) Si/Ti ratio	XRD, UV-Vis, SEM, TGA	Incorporation of titanium in the framework, smaller crystals (0.5-1µm)	-Require large amount of TMPA, Si/Ti ratio < 25 produce poor crystalline sample extraframework species were detected for titanium content ~ 1 wt% Ti. extraframework Ti species even for low Ti content	170°C/ 24h in autoclave (static condition)	600°C/ 10h in air flow
Madhusudan [84]	1994		Hexamethonium ions	-		Synthesized TS-1 with ZSM-48		180°C/ 86h in autoclave (under stirring)	550°C/ 7h
Serrano et al. [85]	1992		Diamino - alkanes			Synthesized the first TS-1 with ZSM-48 structure			

Continue table 2.5-1 Summary of the Literature on Synthesis TS									
Researcher	Year	Method of Synthesis	Template cation/surfactant	Parameter Studied	Characterization	Advantage/achievement	Remarks/disadvantage	Crystallization Temperature/time	Calcination temperature
N.A. Turta et al. [86]	2007	using ammonium halides as template - sol-gel method	CTAB-Br	1) temperature 2) different Si/Ti ratio	XRD, SEM, FTIR, UV-VIs	Crystalline materials, titanium, absence of anatase TiO ₂	Produces larger aggregated crystals	105-260 °C / 36h in autoclave,	550°C / 18h
Q.H. Xia & Z. Gao [87]	1997		TEACl TBACl	1) temperature 2) reaction time 3) Si/Ti, TEA/Si, H ₂ O/Si, NH ₃ /Si ratio On the crystallizaion kinetic	UV-Vis, FTIR, SEM, XRD		The mean crystal size of the products of the system is slightly bigger than the products of TPAOH systems	105-260 °C / 36h in autoclave, 110 °C/48h under reflux cond., atm. pressure	540°C / 16h

2.5.1 Application of Titanosilicates and Its Challenge

Titanium silicates, is known to be useful as catalyst in many oxidation reactions. Application in this field can be broadly classified into 2 categories based on their structure, namely (1) amorphous and (2) crystalline titanium silicates. Both amorphous and crystalline titanium silicates have been used as catalyst in selective oxidation of hydrocarbons and their derivatives. The amorphous titanium silicates are known to catalyse oxidation of hydrocarbons on their derivatives using organic hydroperoxides as the oxidizing agents. Tanev et al [127] have described the use of an amorphous titanium silicate as a catalyst to epoxidise propylene to propylene oxide using organic hydroperoxides such as tertiary butyl hydroperoxide or ethylbenzene hydroperoxide as the oxidizing agents. On the other hand, crystalline titanium silicates such as TS-1 [128, 129], are known to catalyse the oxidation of hydrocarbons or their derivatives, when H₂O₂ rather than organic hydroperoxides are used [130]. P.J. Kooyman [131] studied the oxidation of phenol over an amorphous titanium silicate using H₂O₂ as the oxidizing agent but found only a low selectivity towards the hydroxylation products at high conversion levels on the phenol [130]. However, we always ignore that crystalline titanium silicates, such as TS-1, has one drawback; while they are highly active and selective in catalytic reactions involving small molecules, they are inactive when the dimensions of the reactant molecules are larger than the pore size of the crystalline titanium silicates thereby excluding the reactants from access to the internal pores of the crystalline material wherein practically all the active sites needed for the catalytic conversion are located [130]. Such challenge should be overcome as many of the oxidation processes in the fine chemicals industry involve the selective oxidations of bulky hydrocarbons or their derivatives. Hence, Keshavaraja et al. [130,131] developed titanium silicates which possess the advantageous features of both the amorphous and crystalline titanium silicates. Such a material would, ideally, possess; (i) a bimodal pore size distribution with one characteristic pore width in the region of micropores, namely less than 10 Å and a second characteristic pore width in the region of mesopores, namely between 10 and 100 Å, thereby enabling the oxidation of bulky organic molecules [130] and, (ii) contains the titanium ions in a structural environment similar to that prevalent in crystalline titanium silicate, TS-1, so that oxidation of hydrocarbons can be accomplished

using the more convenient and common hydrogen peroxide rather than being confined to the use of organic hydroperoxides [130]

His invention relates to a novel family of stable synthetic micro-meso porous amorphous titanosilicates, identified as MMATS, and possessing specific characteristic which distinguished them from other titanosilicates of prior art. [44,130]. They have successfully described his invention is able to utilize aqueous H₂O₂ in oxidation reactions.

Motivated by his work, Shan et al. [132] also have conducted a few researchs employing amorphous titanosilicate in selective oxidation processes such as: (i) epoxidation of alkanes to produce epoxides, (ii) partial oxidation of alkanes to produce ketonic or alcoholic derivatives, (iii) partial oxidation of alcohols, (iv) hydroxylation of aromatic compounds to add hydroxyl group to the aromatic ring structure, and (v) ammoximation of ketones with ammonia and hydrogen peroxide or nitrogen oxide to produce corresponding oximes

Due to the same reason; relatively small average diameter of the channel system in the case of zeolites will present problems for the oxidation of bulk molecules, both R.V Grieken [91] et al. and F. Figueras et al. [93] have achieved epoxidation of styrene with *tert*-butyl hydroperoxide and olefins respectively using amorphous titanosilicates. However, their invention showed low selectivity as catalyst comparable to other commercial zeolites.

It has now been discovered that certain amorphous titanium silicate demonstrate remarkable rates of uptake for heavy metal such as lead, cadmium, zinc, chromium, mercury and copper which are in the order of magnitude greater than that of prior art absorbent or ion exchangers under the conditions tested which include the presence of competing ions such as calcium and magnesium [143]. Up to now, to my knowledge, only G.W. Dodwell et al. [143] from Engerhald Corporation has attempted to utilize amorphous titanium silicate as heavy metal removal. **Table 2.5-2** provides a review of several potential low cost adsorbents to remove the various HM from the effluents. From

the review in **Table 2.5-2**, we can conclude that most of modified or treated natural adsorbents and synthetic adsorbents can achieve more than 90% removal of heavy metals compare to natural adsorbent. Thus, it gain interest of many researcher to explore the potential value of those adsorbents. **Table 2.5-3** provides a review of adsorption treatment of HM by various kind of titanium silicates. Based on summary review in **Table 2.5-2** and **Table 2.5-3**, we can conclude that most of data fitted to Langmuir and Pseudo 2nd Order kinetic model. Thus, the author believes both models are useful to describe data obtained in utilization studies which had be explain in section 5.9.

Table 2.5-2 Treatment of different heavy metal (HM) by adsorption

Year	Authors	Adsorbent / Adsorbate ions	Variables Studied	Remarks
1998	Bala-subramanim et al. [134,135]	Lignite / Cr ²⁺ .	Adsorbent dosage	Kinetic showed the applicability or Lagergren model. The datas' fit well first order rate kinetics.
1999	T.N.C. Dantas et al. [65]	Diatomited treated with microemulsion (DTM) / Ni ²⁺ ,Cu ²⁺ ,Cr ²⁺	Batch adsorption and column adsorption experiment	Experimental data show best fit to Langmuir isotherm.
2000	S. Wu & J. P. Chen [66]	Modified commercial activated carbon Filtrasorb 200 / Cu ²⁺	Effect of initial conc. and pH. Ads. modification procedures	Modification by citric acid increases the copper ion ads. capacity more than 90%. Freundlich model best fit the experimental results.
2000	Kapadia et al. [134 & ref. therein]	Fly ash / Cu ²⁺	Initial conc.and pH. Adsorbent dosage.	Maximum efficiency was at the pH of 6.0. The fly ash treatment raises the pH of effluent.
2001	T.N.C. Dantas et al. [67]	Diatomited treated with microemulsion (DTM) / Cr ²⁺	Influence of DTM drying time versus size, pH, HM cation retention by DTM	The desorption study show that 100% of Cr ²⁺ can be easily eluted by HCl. Langmuir isotherm showed a better fit to the process.
2001	Rao et al. [134 & ref. therein]	Bagasse, Fly ash / Cu ²⁺ & Pb ²⁺	Particle size, Adsorbent dosage, Initial conc., pH.	Ads. capacity for the removal of Cu ²⁺ decrease in the order Fly ash > Bagasse> PAC and for removal of Pb ²⁺ ; PAC > Bagasse>Fly ash

Continue **Table 2.5-2**

Year	Authors	Adsorbent / Adsorbate ions	Variables Studied	Remarks
2003	R. Sublet et al. [68]	Chabazite, resins, activated carbon, manganese oxide, cellulose powder/Pb ²⁺	Ads. batch experiments. Closed loop micro-column test	Only 3 media; ZAC (powder activated carbon coated with synthetic zeolite-SZ1) , natural chabazite and natural manganese oxide turn out to be potentially able to remove lead in dynamic condition
2004	Viswanathan et al. [ref. In 134]	Chitin, Saw dust, Clay, Fly ash/ Zn ²⁺ & Ni ²⁺ ions	pH, Particle size, Initial conc., Calcium ion.	Chitin has the maximum adsorbent potential compared to other adsorbents. Nickel shows more preference for adsorption sites of chitin than Zinc.
2004	R. Qadeer & S. Akhtar [69]	Activated carbon/ Pb ²⁺	Ads. isotherm. Ads. kinetics	The rate determining step was found to be film diffusion
2004	P.X. Sheng et al. [70]	Marine algal biomass/ Pb ²⁺ , Cu ²⁺ , Cd ²⁺ , Zn ²⁺ , Ni ²⁺	Effect of PH Determination of equilibrium time, ads.	Up to 90% removal within 60min. all experiments data best fit to langmuir ads.
2004	A. Lagashetty & A. Venkataraman [71]	Nanosized SnO ₂ / Pb ²⁺	Adsorption study	Up to 40 % removal from initial 285ppm metal concentration
2004	E. Erdem et al. [72]	Clinoptilolite / Mn ²⁺ , Cu ²⁺ , Co ²⁺ , Zn ²⁺	Adsorption of various metals at 303K. Isotherm model.	Ads. isotherms data match to Langmuir, Freundlich and Dubinin-Kagane-Reduschlevich (DKR). Maximal exchange levels attained: 19.84% (Mn ²⁺), 66.10% (Cu ²⁺), 77.96% (Co ²⁺), 45.96% (Zn ²⁺)
2005	F. E. Okieimen et al. [9]	Cellulose graft copolymers modified with acrylic acid / Cu ²⁺ , Cd ²⁺	Sorption capacity and distribution ratio	Recovery of over 90% of metal ions
2005	M. H. Mustafa [73]	Modified kaolin + low grade ninivite / Pb ²⁺ , Hg ²⁺ , Cd ²⁺ ,	Adsorption isotherm and kinetic	Removal efficiencies were up to 85%, 90% and 95% for Cd ²⁺ , Pb ²⁺ , Hg ²⁺ respectively.
2006	K.G. Bhattacharyya, S. S. Gupta [7]	Kaolinite, montmorillonite and modified derivatives / Cu ²⁺	Surface area. Cation exchange capacity (CEC)	The ads. data follow Langmuir isotherm and better represent by second order kinetic.

Continue **Table 2.5-2**

Year	Authors	Adsorbent / Adsorbate ions	Variables Studied	Remarks
2006	H. N. Bhatti et al. [74]	Modified <i>Moringa oleifera</i> Lam. (horseradish tree) biomass / Zn ²⁺	Effect of PH, dosage, particle size of adsorbent, initial conc.	85.2% metal removal for biomass treated with NaOH compared than non-treated biomass (74%). Both Langmuir and Freundlich bes fit experimental data. Ads. process best described by pseudo 2 nd order kinetic model
2006	M. Sprynskyy et al. [34]	Clinoptilolite/ Pb ²⁺ , Cu ²⁺ , Cd ²⁺ , Ni ²⁺	Ads. study. Sorption modelling	Up to 40% (Cu ²⁺ , Cd ²⁺) and up to 90% (Ni ²⁺), are sorbed during the first stage on the microcrystals surface. Langmuir is the best for low initial conc.
2007	O. Demirbas et al. [63]	Hazelnut shell / Cu ²⁺	Effect of particle size, pH, temperature thermodynamic	Langmuir isotherm fit well the isotherm data and 2 nd order kinetic model
2007	M. Puanngam & F. Unob [8]	Modified MCM-41 and silica gel / Hg ²⁺	Effect of pH, , ionic strength, interfering ions, competing cation – anion	Uptake up to 80%. MCM-41 fit well Langmuir isotherm only. Modified silica gel fit well both Langmuir and Freundlich model
2007	A. El Sikaily et al. [136]	activated carbon developed from green alga <i>Ulva lactuca</i> / Cr ²⁺	Effect of pH, time, dosage, initial conc. Ads. isotherm Ads. kinetic	Up to 90% removal of Cr ²⁺ . Best fit is obtained using Langmuir-1 and Langmuir-2. poor fit with pseudo first order kinetic, best fit with pseudo 2 nd order kinetic.
2007	D. Karamanis, P.A. Assimakopoulos [12]	Aluminium pillared layered montmorillonites (PILMs) / Cs ²⁺ , Cu ²⁺	Effect of pH. Cu ²⁺ sorption of different PILMs. Ads isotherm. Ads kinetics	Up to 80% removal of Cs ²⁺ , up to 99.7% removal of Cu ²⁺ . PILMs sample with a solution to solid ratio (v/m) of 1L/g, removed 95.7% of ab initial 32 mg/L in natural mineral water.
2007	A. Gunay et al. [137]	Pretreated clinoptilolite / Pb ²⁺	Effect of initial conc. and pH. Ads isotherm. Ads kinetic	Removal efficiency of pretreated clay is 1.5 times higher than natural clay. Pseudo 1st order kinetic and the Temkin isotherm best described the adsorption data.

Continue **Table 2.5-2**

Year	Authors	Adsorbent / Adsorbate ions	Variables Studied	Remarks
2007	D. Tiwari et al. [13]	Sericite / Cu^{2+} and Pb^{2+}	Effect of pH, ionic strength, time and initial conc.	Equilibrium attain within 10 min for Cu^{2+} and 90 min for Pb^{2+}
2007	M. N. Khan & M. F. Wahab [138]	Chemically modified corncobs / Pb^{2+} , Cu^{2+} , Cr^{2+} , Zn^{2+} , Ni^{2+}	Effect of pH, competing cation and anion, competitive removal of Cu^{2+} in binary metal systems	Batch experimental studies show up to 94% removal. 57% removal of Cu^{2+} ion for 256 mg/L of Cu^{2+} ion and Zn^{2+} ion in industrial effluent sample of 500ml. 51.07% and 73.49% removal for different two real industrial effluent samples namely A12 and B12 respectively
2007	M.N. Akie et al. [139]	NaFeTiO_4 , $\text{Na}_2\text{Fe}_2\text{Ti}_6\text{O}_{16}$, iron-doped $\text{Na}_2\text{Fe}_2\text{Ti}_6\text{O}_{16}$ / Ni^{2+}	Ion-exchange studies	Both of adsorbent show up to 99% removal efficiency of Nickel.
2007	N. L. Dias Filho et al. [140]	Polyhedral oligomer silsequioxane functionalized with organic base / Cu^{2+}	Adsorption isotherms.	Experimental data fitted Langmuir isotherm. Retention capacities were not affected after several retention/elution cycles during 6 month of continuous use.
2007	W. Shaobin & E. Ariyanto [141]	Clinoptilolite / malachite green (MG) and Pb ions	Dynamic ads in single and binary component systems. Ads isotherm	Pb^{2+} follow Freundlich isotherm and up to 90% removal. In binary system, Pb^{2+} exhibits relative higher affinity and selectivity. Dynamic ads. of MG and Pb^{2+} followed the 1 st order kinetics.
2007	H. Yang et al. [26]	surfactant templated mesoporous silica / Pb^{2+} , Cu^{2+} , Mn^{2+} , Zn^{2+} , Fe^{2+} , Ag^{2+}	Ads. characteristics Ads. Kinetics Ads. Isotherm Regeneration of adsorbent	Up to 99.3% removal of, Cu^{2+} and 99.4% removal of Pb^{2+} . Adsorption were maintained at a level more than 0.19 mmol/g with an uptake ratio more than 94% in the 1st 3 cycles. After 8th cycles, it reduced to 90.4%
2008	T.K. Sen & M.V. Sarzali [11]	Aluminium oxide / Cd^{2+}	Effect of pH, dosage and temperature. Ads. isotherm. Ads. kinetic.	Experimental data fitted to Langmuir-2 and Freundlich. Amount of metal ion adsorb increased with initial metal ion conc., pH, but decreases with adsorbent dosage.

Table 2.5-3 Treatment of different HM on Titanium Silicate by adsorption

Year	Authors	Adsorbent / Adsorbate ions	Variables Studied	Remarks
1997	E.A. Behrens & A. Clearfield [49]	$M_3HTi_4O_4(SiO_4)_3 \cdot 4H_2O$ (M=Na ⁺ , K ⁺) / Sr ²⁺ and Cs ²⁺	General adsorption measurement, adsorption measurement in groundwater stimulant and in nuclear waste type condition	Exchange capacity is 52% and 63% of theoretical unit for both Sr ⁺ and Cs ²⁺ respectively. Sodium form of exchanger produced a higher K _d . Percentage removal values are almost identical both exchanger (97-98%)
1998	Xu, Y. M. et al. [6]	Mesoporous Ti-MCM-41 / Pb ²⁺ , Cd ²⁺ , Hg ²⁺ , Zn ²⁺ , Cu ²⁺ , Mg ²⁺ , Na ²⁺	Surface characters, adsorption isotherms, kinetic and thermodynamic	Between 1.5-1.7 protons are released, on the average, per Pb ²⁺ , ion adsorbed. More than 80% HM removal within 15minutes..
2002	X.S. Zhao et al. [25]	ETS-10 / Pb ²⁺	Adsorption isotherms and kinetics	Less than 10s required to attain equilibrium. Experimental data best fitted to pseudo 2 nd order kinetic and Langmuir isotherm. Each Pb ²⁺ ion can replace 1.5Na ⁺ and 0.5K ⁺ ions
2004	L. Lv et al. [10]	Micro-porous ETS – 10 / Pb ²⁺ , Cd ²⁺ , Zn ²⁺ , Cu ²⁺ ,	Effect of pH, electrolyte, and initial ionic concentration	In addition to the ion exchange mechanism, other mechanism such as adsorption or complexation may be involved in the uptake process of the HM ions on ETS-10 particularly for Pb ²⁺
2006	J.H. Choi et al. [27]	ETS-10 and ETS-10/ Pb ²⁺ , Cd ²⁺ ,	Equilibrium capacity and isotherm study	Uptake of HM influenced by particle size of zeolites. Uptake reaches maximum beyond 2000ppm.

Continue **Table 2.5-3**

Year	Authors	Adsorbent / Adsorbate ions	Variables Studied	Remarks
2006	J.H. Choi et al. [33]	Nano-sized ETS-10 and Al-substituted-ETS-10/ Cu ²⁺ , Zn ²⁺ , Mn ²⁺ , Co ²⁺	Effect of temperature and concentration. sorption isotherms and kinetics	The uptake of HM ions influenced by particles size of zeolites. The uptake rates for both HM were extremely rapid and well represented by pseudo 2 nd order model.
2007	L.F. Su & X.S. Zhao [142]	ETS-10, ETS -10, ETS-10, ETS-10 / Pb ²⁺	Adsorption behavior of different element incorporated in ETS-10	Experimental data best fitted to pseudo 2 nd order kinetics and Langmuir model. ETBS-10 (11%), ETAS-10 (16.9%), ETGS-10 (12.5%) higher maximum ads. capacities than ETS-10
2007	C.B. Lopes et al. [51]	ETS-4 / Hg ²⁺	Batch experiment using Nernst Planck. Equilibrium isotherm. Pseudo second-order kinetic model	Large ion exchange capacity. 75-95% uptake of Hg ²⁺ . Freundlich isotherm fitted equilibrium data accurately. Only 27.83% uptake obtained by the data fitted to pseudo second-order kinetic model

2.6 PHYSICO-CHEMICAL CHARACTERIZATION

Significant evidence for titanium incorporation has been compiled. Three primary methods of identification specific titanium incorporation have been defined and are routinely used [55]; (i) The increased in the unit cell parameter of the material relative to silicalite(MFI), (ii) the presence of an infrared band at 960cm⁻¹ and (iii) lack of anatase (nonframework TiO₂) absorption in UV-Visible spectra. That identification will be done by several techniques for the characterization of different zeolites. Each technique provides important information about the structure of a particular zeolite.

2.6.1 Powder X-ray Diffraction (PXRD)

When a solid is isolated from a synthesis mixture, it is first analyzed by PXRD. PXRD is an important method for the qualitative & quantitative characterization of zeolites. The technique is routinely used as a means of qualitative identifications of zeolites because

the XRD pattern of a particular zeolite can be considered as its fingerprint. It also provides information on the phase purity & changes in lattice parameters with changing compositions in order to evaluate crystallinity and unit cell effects [144]. The normal scan range in zeolite and microporous molecular sieves is in $(50 - 400) 2\theta$ as most important peaks are obtained in this range. Comparing with the standard PXRD pattern, the material can be identified. But for mesoporous solids, the scan angle is between $(10 - 100) 2\theta$ as most intense peaks are obtained in this range.

2.6.2 Infrared Spectroscopy (IR)

This experimental technique offers structural details of zeolite structure through different vibrational modes. Besides, it is helpful in measuring the acidity of the materials as well as for the detection of isomorphous substitution in the framework. There are several techniques for recording IR spectra such as dilution with KBr, nujol mull, and self supported wafer. The KBr dilution method is the most commonly employed method. The lattice vibrations of zeolites, normally, occur in the range $300-1300\text{ cm}^{-1}$. Acid strength of zeolites can also be determined by FTIR spectroscopy in the absorption range $3600-3700\text{ cm}^{-1}$ (Brönstead acid sites. Incorporation of metals also can be determined as an additional band at 960 cm^{-1} appears because of M-O-Si linkages (M = Metal).

In the case of TS-1, it has two important regions in the IR spectrum. One the OH region and the other below 1000 cm^{-1} . In region below 1000 cm^{-1} lattice structure bands appears at 805 and 555 cm^{-1} . All the titanium silicates exhibit one common feature; a band at about $960-970\text{ cm}^{-1}$ [55]. Though there are a lot of discrepancies regarding the assignment of this band, but it is generally accepted that this band is due to stretching vibration of Si-O bond perturbed by a neighboring Ti (IV) in the lattices position. [52].

2.6.3 UV- Vis Spectroscopy

This is particularly useful for metal incorporated zeolites i.e., metallosilicates. The absorption in the UV-Vis range arises because of the ligand to metal charge transfer. It helps to determine the co-ordination number of the metal in the zeolite. Thus for TS-1, the absorption at 215 nm is due to the transfer of charge from O^{2-} to tetrahedrally

coordinated Ti^{+4} . By increase in co-ordination number, the charge-transfer band shifted to longer wave length. TS-1 exhibits a charge transfer band at 205-220 nm due to the presence of isolated $[\text{TiO}_4]$ or $[\text{TiO}_3\text{OH}]$ moieties. This occurs due to electron transfer from ligand oxygen to the vacant orbital of titanium ions in the framework. Therefore, it is directly related with the titanium incorporation in the framework position. So a change in the band position is directly related with the change in coordination state of Ti (IV) in the framework. Hence the presence of the band at ca. 210 nm is accepted as evidence for the presence of isolated Ti (IV) species whereas the band at 280-330 nm, if present, is taken as the presence of extra-framework titanium species. [52].

2.6.4 Scanning Electron Microscopy (SEM)

This is another important tool for characterization of the zeolite catalyst. The micrograph shows the morphology of the particle formed (e.g., cubic, circular, etc) as well as the presence of amorphous phase in the samples. [52].

2.6.5 Adsorption Measurement

To determine the pore size distribution, pore volume and surface area, the adsorption of nitrogen is usually carried out over zeolites and related molecular sieves at low pressure (10^{-6} Torr) and low temperature (77K). The sieving property of a zeolite depends on its pore size, pore volume as well as surface area. The analysis of adsorption isotherm helps in determining the micropore volume and pore size distribution of the molecular sieves. [145]. The six IUPAC standard adsorption isotherms are shown in **Figure 2.6-1**. They differ because the systems demonstrate different gas/solid interactions.

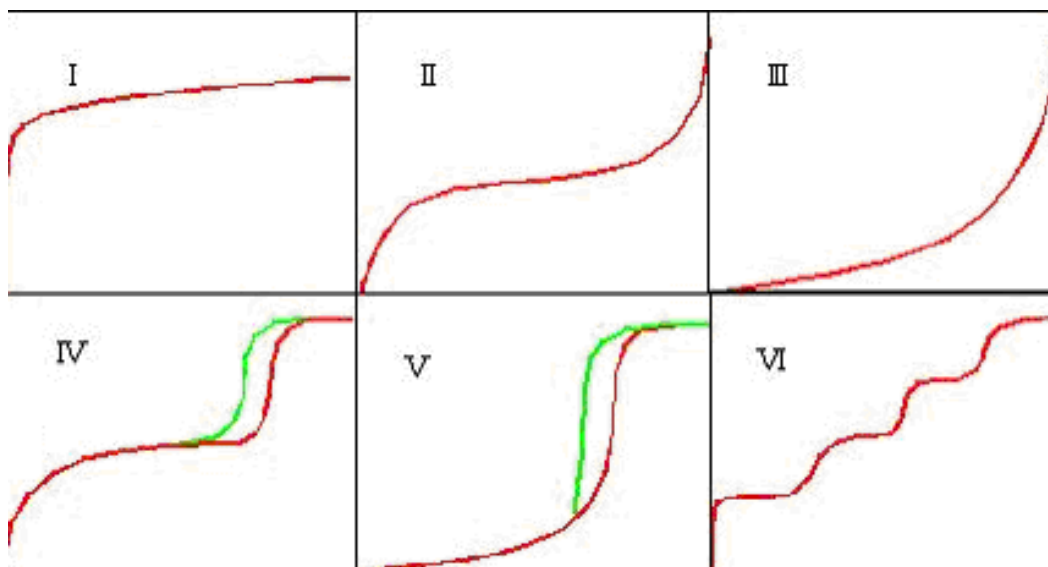


Figure 2.6-1 The six IUPAC standard adsorption isotherms

The Type I isotherm is typical of microporous solids and chemisorption isotherms. Type II is shown by finely divided non-porous solids. Type III and type V are typical of vapor adsorption (i.e. water vapor on hydrophobic materials). Type VI and V feature a hysteresis loop generated by the capillary condensation of the adsorbate in the mesopores of the solid. Finally, the rare type VI step-like isotherm is shown by nitrogen adsorbed on special carbon. Once the isotherm is obtained, a number of calculation models can be applied to different regions of the adsorption isotherm to evaluate the specific surface area (i.e. BET, Dubinin, Langmuir, etc.) or the [micro and mesopore volume and size distributions](#) (i.e. BJH, DH, H&K, S&F, etc.) [145].

CHAPTER 3 THEORY

3.1 PREFACE

Among the unit operations in water and wastewater treatment, adsorption is probably the main method use widely by the industry. Adsorption has been found to be an effective and economic method with high potential for the removal, recovery and recycling of heavy metals from wastewater [7]. In a general adsorption process, the adsorbed solutes are referred to as adsorbate & the adsorbing agent is the adsorbent [66]. This chapter briefly presents the theory utilize in equilibrium, kinetic and isotherm adsorption study in this research.

3.2 THE CLASSIFICATION OF ADSORPTION MECHANISM

The selectivity of an adsorbent is strongly connected to its microcrystalline structure [130]. It consists of microcrystallites linked together by surface functional group [147]. Based on the position of these functional organics group, adsorption phenomena can be classified as physisorption and chemisorption. In physisorption, weak Van der Waals - type forces and physical bonds are produced and the process is reversible [146,134,148]. There is no electron transfer involved in either the molecule or at the substrate surface and it is a nonspecific process [134]. On the other hand, chemisorption is a highly specific process that involves ionic or covalent bond formation which requires a high energy, and is irreversible [148]. The important classification between chemisorption and physisorption is shown in **Table 3.2-1**

Table 3.2-1 Typical Characteristics of Adsorption Processes (Source from ref. 134)

Characteristics	Physical Adsorption	Chemical Adsorption
Binding force	Due to physical force of attraction, thus this process is also called as Vanderwaal's adsorption	Due to chemical forces or bonding, thus this process is also called as activated adsorption.
Saturation uptake	Multilayer phenomena	Single layer phenomena
Activation Energy	No activation energy involved	May be involved
Temperature Range (over which adsorption occurs)	Adsorption is appreciable at lower temperature below boiling point of adsorbate	Adsorption can take place even at higher temperature
Nature of sorbate	Amount of adsorbate removed depends more on adsorbate than on adsorbent	Depends on both adsorbent and adsorbate
Crystallographic specificity	Virtually independent of surface atomic geometry	Marked variation between crystal planes
Heat of adsorption	1 Kcal/mole	50 - 100 Kcal/mole

3.3 FACTORS AFFECTING THE RATE OF PHYSISORPTION

Since the complexity of chemisorption mechanism, this work only concern the major factors affects the physisorption rate as summarized [134,146];

Surface area of the adsorbent:

- The rate of adsorption increases with increase in surface area of the adsorbent
- Rate of adsorption $\approx 1/\text{Diameter of adsorbent}$ for powdered adsorbent

Pore structure of the adsorbent:

- Pore diameters determine accesibility of selected ions participating in the adsorption process.

Nature of solute (adsorbate):

- Solubility of solute: Adsorption $\approx (1/\text{Solubility of solute in solvent})$
- Molecular size of solute: Increase in molecular size of solute enhances adsorption
- Generally, the adsorption of organic solute out of an organic solvent is lesser than its adsorption through an aqueous solution. Since the solvent use in through out this experimental studies is water, need not consider further solvents effect.

3.4 ADSORPTION SYSTEMS

Designating adsorption systems as a method of wastewater treatment, it is important to consider the modes of contacting solid adsorbent and wastewater. The contact between solid adsorbent and the liquid can be made by at least six systems: batch contact, fixed bed (up flow or down flow), pulsed bed, steady state moving bed fluidized bed and moving mat filters [146,148]. Conventionally, batch contact and fixed bed systems are used for lab-scale research studies. Batch systems preferably used if the volume of wastewater to be treated or adsorbent is less [38].

3.5 ADSORPTION EQUILIBRIUM

Generally adsorption process proceeds through varied mechanisms such as external mass transfer of solute onto sorbent followed by intraparticle diffusion [134,38]. Thus, we need extensive experimental data concerning the specific adsorption application to determine the rate-controlling step. Commonly, empirical design procedures based on adsorption equilibrium conditions are employed to predict adsorber performance. When a quantity of adsorbent is contacted with a given volume of a liquid containing an adsorbate solute, the adsorption process starts. Once the process starts, it occurs until equilibrium is achieved. The concept of 'equilibrium' implies such that the rate at which molecules are adsorbing the surface is equal to the rate at which molecules are leaving the surface. The physical chemistry involved in such process may be complex and up to now, no single theory of adsorption has been put forward to explain all the systems [38]. However, engineer requires only the data at equilibrium conditions. Untill now, the oldest theories were still used to predict the sorption process eventhough the assumption on which those models lie were found to be not entirely valid in later years. [134,38].

Adsorption isotherm is a curve which relates the amount of adsorbate adsorbed per unit mass of adsorbent to the amount of unadsorbed adsorbate remaining in solution at equilibrium [36]. Numerous models have been developed to describe and understand the adsorption system behaviors. Among them, the most widely used equilibrium models to understand the adsorption systems were Freundlich and Langmuir isotherm equations.

3.5.1 Freundlich isotherm

Herbert Max Finley Freundlich, a German physical chemist, presented an empirical adsorption isotherm for non ideal sorption on heterogeneous surfaces as well as multilayer sorption and is expressed by the equation [38,149]:

$$\ln q_e = \ln K_f + 1/n(\ln C_e) \quad (2)$$

where q_e is the amount of adsorbate ions adsorbed at equilibrium time, C_e is equilibrium concentration of adsorbate ions in solution. K_f and n are isotherm constants which indicate the capacity and the intensity of the adsorption, respectively and can be calculated from the intercept and slope of plot between $\ln q_e$ and $\ln C_e$ [146,38].

3.5.2 Langmuir Isotherm

The Langmuir [150] isotherm model has been successfully applied to many pollutant adsorption processes and it is most commonly used adsorption isotherm for the adsorption of a solute from a liquid solution [150].

According to Hall et al. [151] the essential features of the Langmuir isotherm can be expressed in terms of a dimensionless constant separation factor or equilibrium parameter KL which is defined by the following relationship:

$$KL = 1/(1 + K_a C_o) \quad (4)$$

Where KL is a dimensionless separation factor, C_o the initial concentration (mg/l), K_a the Langmuir constant (l/mg). The parameter KL indicates the shape of the isotherm and nature of the adsorption process [KL > 1: Unfavorable; KL = 1: Linear; 0 < KL < 1: Favorable; KL = 0: Irreversible]. The value of KL obtained were in the between 0 and 1 indicate the favorable adsorption [36].

3.6 LINEAR METHOD

The most appropriate method in designing the adsorption systems and assessing the performance of the adsorption systems is to have an idea on adsorption isotherms [134, 38]. Throughout the years, linear regression was frequently used to determine the most fitted isotherm model and the linear least-squares method to the linearly transformed isotherm equations. It has been widely used for finding the parameters of the model to determine the coefficient. The linear regression analysis was the most commonly used technique to determine the best-fit isotherm and the method of least squares has been used for finding the parameters of the isotherms.

The isotherms; Freundlich, Langmuir and their corresponding linearized forms are shown in **Figure 3.6-1**. From **Figure 3.6-1**, it was observed that the Langmuir isotherm can be linearized to at least four different types and simple linear regression will result in different parameter estimates [38]. Out of the four different types of linearized Langmuir isotherm equations, Langmuir-1 and Langmuir-2 are the most commonly used by several researchers because of the minimized deviations from the fitted equation resulting in the best error distribution [9,38,152]. The q_m , and K_a values for Langmuir-1, Langmuir-2, Langmuir-3, and Langmuir-4 were predicted from the plot between C_e/q_e versus C_e , $1/q_e$ versus $1/C_e$, q_e versus q_e/C_e , and q_e/C_e versus q_e , respectively. [38,153].

Isotherms and their linear forms (q_m : mg/g; K_a : L/mg; K_F : (mg/g) ^{1/n})		
Isotherm	Linear form	Plot
Freundlich $q_e = K_F C_e^{1/n}$	$\log(q_e) = \log(K_F) + \frac{1}{n} \log(C_e)$	$\log(q_e)$ vs. $\log(C_e)$
Langmuir-1	$\frac{C_e}{q_e} = \frac{1}{q_m} C_e + \frac{1}{K_a q_m}$	$\frac{C_e}{q_e}$ vs. C_e
Langmuir-2 $q_e = \frac{q_m K_a C_e}{1 + K_a C_e}$	$\frac{1}{q_e} = \left(\frac{1}{K_a q_m} \right) \frac{1}{C_e} + \frac{1}{q_m}$	$\frac{1}{q_e}$ vs. $\frac{1}{C_e}$
Langmuir-3	$q_e = q_m - \left(\frac{1}{K_a} \right) \frac{q_e}{C_e}$	q_e vs. $\frac{q_e}{C_e}$
Langmuir-4	$\frac{q_e}{C_e} = K_a q_m - K_a q_e$	$\frac{q_e}{C_e}$ vs. q_e

Figure 3.6-1 Isotherms and their linear form (Source from ref. 38)

Langmuir isotherms can be linearized to at least four different types and simple linear regression will result in different parameter estimates. Out of four different type of linearized Langmuir isotherm equations, Langmuir-1 and Langmuir-2 are most commonly used by several reseachers because of the minimized deviations from the fitted equation resulting in the best error distribution [38,152]. In comparative analysis of Langmuir Linear method, Kumar¹¹ have showed that Langmuir-2 best fitted for adsorption at room temperature. The linearized form of Langmuir-2 can be written as [8, 11,13]

$$1/q_e = 1/(K_a q_m)(1/C_e) + 1/q_m \quad (6)$$

The Langmuir constants, q_m (maximum adsorption capacity) and K_a (values for Langmuir-2) are predicted from the plot between $1/q_e$ versus $1/C_e$.

3.7 ADSORPTION KINETICS

In order to select an optimum operating condition for full-scale batch experiments in metal removal process, information on the kinetics of metal uptake is required. Mathematical models that can describe the transient behaviour of a batch sorption process operated under different experiment conditions are very useful for scale-up studies or process optimization [154]. A number of models with varying degrees of complexity have been developed to describe the kinetics of metal sorption in batch system [151]. Among numerous available kinetic model, Lagergren's kinetics equation has been most widely used for the adsorption of an adsorbate from an aqueous solution [155].

In order to distinguish kinetics equation based on adsorption capacity of solid from concentration of solution, Lagergren's [156] first order rate equation has been called pseudo-first order since 1998 [152]. The second-order kinetic expression for the adsorption systems of divalent metal ions has been reported by Ho [157]. Again to distinguish kinetics equation based on adsorption capacity of solid from concentration of solution. Ho's second-order rate equation has been called pseudo-second order. The earlier application of the pseudo-second order equation to the kinetic studies of

competitive heavy metal adsorption by sphagnum moss peat was undertaken by Ho et al. [158].

Lagergren first-order, Lagergren second order and pseudo second-order kinetic models as shown below:

Lagergren first-order model [156]:

$$\log (q_e - q_t) = \log q_e - K_{ad}t/2.303 \quad (5)$$

Lagergren second order model [156]:

$$1/(q_e - q_t) = 1/q_e + K_t t \quad (6)$$

Pseudo second-order model [152, 157]:

$$t/q_t = 1/(K'q_e^2) + t/q_e \quad (7)$$

Where q_t is the amount of heavy metal adsorbed per unit mass of adsorbent (mg/g) at time t (min), q_e the amount of heavy metal adsorbed per unit mass of adsorbent (mg/g) at equilibrium, K_{ad} the Lagergren rate constant (1/min), K' the pseudo second-order rate constant (g/mg.min) and K the Lagergren second order rate constant (g/mg min).

CHAPTER 4 RESEARCH METHODOLOGY

4.1 INTRODUCTION

The research methodology in the work reported in this thesis can be divided into 4 sections. The first section is the preparation and determination of phase diagram. The objective of this section is to prepare ternary system containing 3 components; sodium dodecyl sulphate (SDS) surfactant/water/1-butanol and investigate the microemulsion phase area on the system. The outcome of this investigation is used in second part of this work.

In the second section, base on the phase area in the system investigated in the first section, titanosilicate (TS) was synthesized in the microemulsion area. The microemulsion acted as a template or as self-assembly molecules. The results are compared with the TS sample prepared without surfactant and also compared with sample prepared with different Si/Ti ratios. Characterization of TS has been carried out by using x-ray diffraction spectrometer, FTIR (Fourier Transform Infra-red) spectroscopy, and UV-VISIBLE spectroscopy.

In the third part of this work, which is also an improvement from second part, tetra propyl ammonium hydroxide (TPAOH) is introduced in the synthesis preparation and Si/Ti ratio: 33 were chosen. Hence, titanosilicate TS - derived adsorbents E, F, G, and H were synthesized by conventional method in the presence of small amounts of tetra propyl ammonium hydroxide (TPAOH). Along with these adsorbents A, B, C, and D were also synthesized using sodium dodecyl sulphate (SDS) and TPAOH as hybrid surfactant templates in butanol. Adsorbents B, C, D, F, G, and H were crystallized under high pressure and temperature while adsorbents A and E were preserved at room temperature. During the synthesis, TPAOH acted as a subsidiary structure-directing agent. FTIR and UV-Vis spectroscopy have been utilized out to confirm framework of titanium. Surface

area and pore size distribution of all the TS were measured by nitrogen adsorption analysis.

In the fourth section of this work, adsorbents A and H which exhibited a higher BET surface area ($459.5 \text{ m}^2/\text{g}$ and $277.5 \text{ m}^2/\text{g}$ respectively) were selected as solid adsorbents for subsequent adsorption behavior investigations utilizing Cu (II) and Pb (II) ions to evaluate whether they possess heavy metal removal capabilities. In this work, the adsorption isotherm and kinetic behaviour of the adsorbent were studied via batch experiment. The data that was obtained were analyzed utilizing atomic adsorption spectrometer (AAS).

4.2 MATERIALS

For synthesis, the following chemicals were used: Tetraethyl ortho silicate 20% aqueous (TEOS, Aldrich), tetra n-butyl titanate (TNBT, Aldrich), sodium dodecyl sulfate (SDS, s.d. FINE-CHEM, Ltd.), isopropyl alcohol (IPA, s.d. FINE-CHEM, Ltd.) and Tetrapropyl ammonium hydroxide solution (20 % wt aq., Aldrich), 1-butanol (s.d. FINE-CHEM, Ltd.). Demineralised water was used throughout the experiment.

For adsorption studies, nitrates of copper and lead were used to prepare metal ion solutions. No further pH adjustment of these solutions was made since hydrolysis of metals prevented the precipitation of the corresponding metal hydroxides.

4.3 DETERMINATION OF PHASE DIAGRAM

Various amounts of components were weighed according to the ratio as depicted by the ternary diagram and are sealed in ampoules. Then, the samples were mixed using a vortex mixer and centrifuged to attain homogeneity. The samples were left in a temperature-controlled bath at 25 °C for 72 hours to bring the system at equilibrium.

A very convenient method for the preparation of a microemulsion and construction of planar triangular phase diagram is accomplished by titration. A surfactant is dissolved in aqueous (or organic) medium and is titrated with an organic (or aqueous) phase. The transition points (turbid and transparent) are noted (as shown in **Figure 4.3-1**). The single-phased, optically transparent domains correspond to the microemulsions whereas turbid zones are for multiphase systems [50]. Repeating the same procedure for different concentration of surfactant solution will enable me to determine almost all transition points. Thus, a triangular phase diagram can easily be drawn (**Figure 5.2-1**).

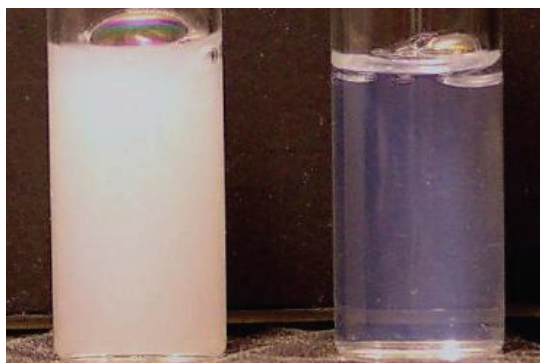


Figure 4.3-1 a) Emulsion (turbid liquid) and b) Microemulsion (transparent)

4.4 TITANIUM SILICATE PREPARATION

4.4.1 Synthesis of adsorbent **TS-X (X=1, 2; Si/Ti =33, X=3, 4; Si/Ti =10)**

Four samples with different Si/Ti molar ratios (sample 1 and 2, [Si /Ti = 33], sample 3 and 4, [Si /Ti = 10] were synthesized hydrothermally at high temperature (160°C). This Si/Ti ratio value was chosen based on research and experimental result onto different Si/Ti ratio parameter done by several researchers; P. Mukherjee [52], A. Kesharavaja [44], and K.A. Genov [64]. Taking sample TS-1 synthesis as an example, 10 g of SDS

was dissolved in 24 g of distilled water. This surfactant solution was added to 10 g of 1-butanol with mild stirring, resulting in the formation of a clear transparent solution. To the above micellar solution 10 g of tetraethyl orthosilicate (TEOS) was added dropwise into the surfactant solution with vigorous stirring. The stirring was continued for another one hour. To this clear solution 0.5g of tetra n-butyl titanate (TNBT) in 4.5 g of isopropyl alcohol (IPA) was added dropwise with vigorous stirring. Stirring was continued for another one hour. The mixture was then crystallized at 160°C for 1h under autogeneous pressure. The product was recovered by centrifugation, washed with distilled water and dried (110°C, 12h). For sample 2 the procedure was replicated except that the anionic surfactant (SDS) was not used. For each sample 3 and 4, 1.67g TNBT in 4.5 g IPA was used instead of the 0.5g TNBT in 4.5g IPA for sample 1 and 2. Sample 4 does not contain SDS. The calcination was carried out on all samples in a conventional furnace 550°C for 15 h with an initial rate of temperature increment of 2°/min. The starting mixture has a molar composition as shown in **Table 4.4-1**

Table 4.4-1 Molar Gel Composition of Different Synthesis Mixture

Sample	Molar gel composition
1	0.03 TiO ₂ : 1 SiO ₂ : 0.72 SDS: 1.56 IPA: 27.78 H ₂ O: 2.82 butanol
2	0.03 TiO ₂ : 1 SiO ₂ : 0 SDS: 1.56 IPA: 27.78 H ₂ O: 2.82 butanol
3	0.1 TiO ₂ : 1 SiO ₂ : 0.72 SDS: 1.56 IPA: 27.78 H ₂ O: 2.82 butanol
4	0.1 TiO ₂ : 1 SiO ₂ : 0 SDS: 1.56 IPA: 27.78 H ₂ O: 2.82 butanol

4.4.2 Synthesis of adsorbent TS-A and TS-E

In a typical synthesis of adsorbent TS-A, 0.5 g of TPAOH and 10 g of SDS was dissolved in 24 g of distilled water. This surfactant solution was added to 10 g of 1-butanol with mild stirring, resulting in the formation of a clear transparent solution. To the above micellar solution 10 g of tetraethyl orthosilicate (TEOS) was added in a dropwise fashion with vigorous stirring. The stirring was continued for another one hour. To this clear solution 0.5g of tetra n-butyl titanate (TNBT) in 4.5 g of isopropyl alcohol (IPA) was

added dropwise under vigorous stirring. Stirring was continued for another one hour producing a turbid suspension. The mixture was then preserved at room temperature for 48h. The product was recovered by centrifugation, washed with distilled water, dried (110°C, 12h). For sample TS-E the procedure was the same as explained above except that the anionic surfactant (SDS) was not used. The calcination was carried out for all samples in a furnace with a flow of air at 550°C for 15 h with an initial rate of temperature increment of 2°/min.

4.4.3 Synthesis of adsorbent TS-X (X=B,C,D,F,G,H)

A procedure similar to which was described above was followed, except that after precipitation, the mixture was crystallized at 433K at 18 hours (sample TS-B and TS-G), 24 hours (sample TS-C and TS-F), and 48 hours (sample D and H) in a parr autoclave under autogenous pressure. Nitrogen gas was flow through inlet of the autoclave until it reach stable pressure (30-40 barr) in order to give pressure in the autoclave. The picture and diagram of the parr autoclave was included in **Appendix F**. The starting mixture has a molar composition as shown in **Table 4.4-2**

Table 4.4-2 Molar Gel Composition Of Different Synthesis Mixture

Sample	Molar gel composition
TS-X (X=A,B,C,D)*	0.03 TiO ₂ : 1 SiO ₂ : 0.72 SDS: 0.01TPAOH:1.56 IPA: 27.78 H ₂ O: 2.82 butanol
TS-X (X=E,F,G,H)*	0.03 TiO ₂ : 1 SiO ₂ : 0 SDS: 0.01TPAOH:1.56 IPA: 27.78 H ₂ O: 2.82 butanol

*TS-X (crystallization temperature); X = A(0h), B(18h), C(24h), D(48h), E(0h), F(18h), G(24h), H(48h)

Figure 4.4-1 Flowchart of synthesis adsorbent TS-X ($X=1,2;Si/Ti =33$, $X=3,4;Si/Ti =10$)

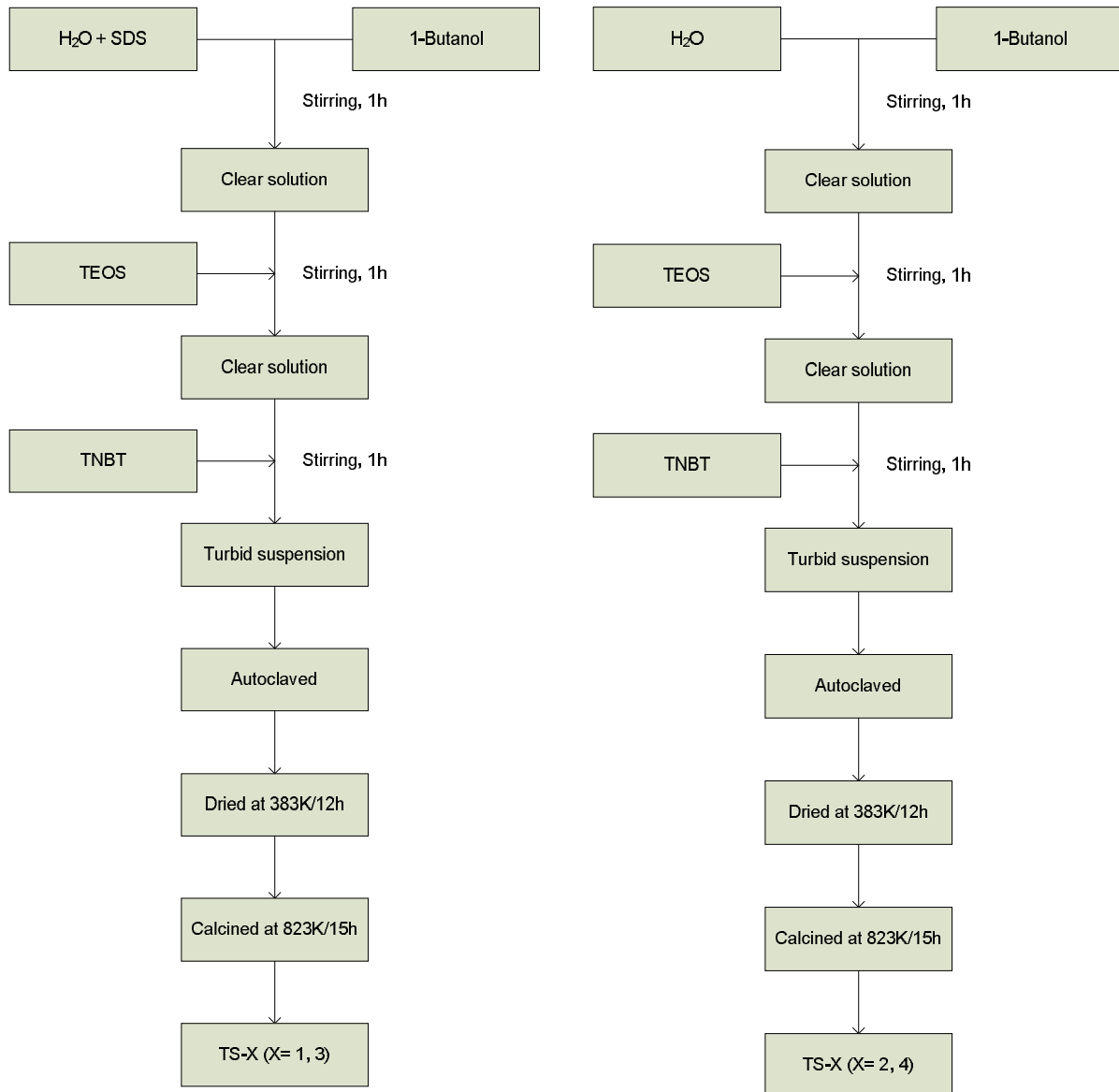


Figure 4.4-2 Flowchart of synthesis adsorbent TS-X [X= A(0h), B(18h), C(24h), D(48h)]

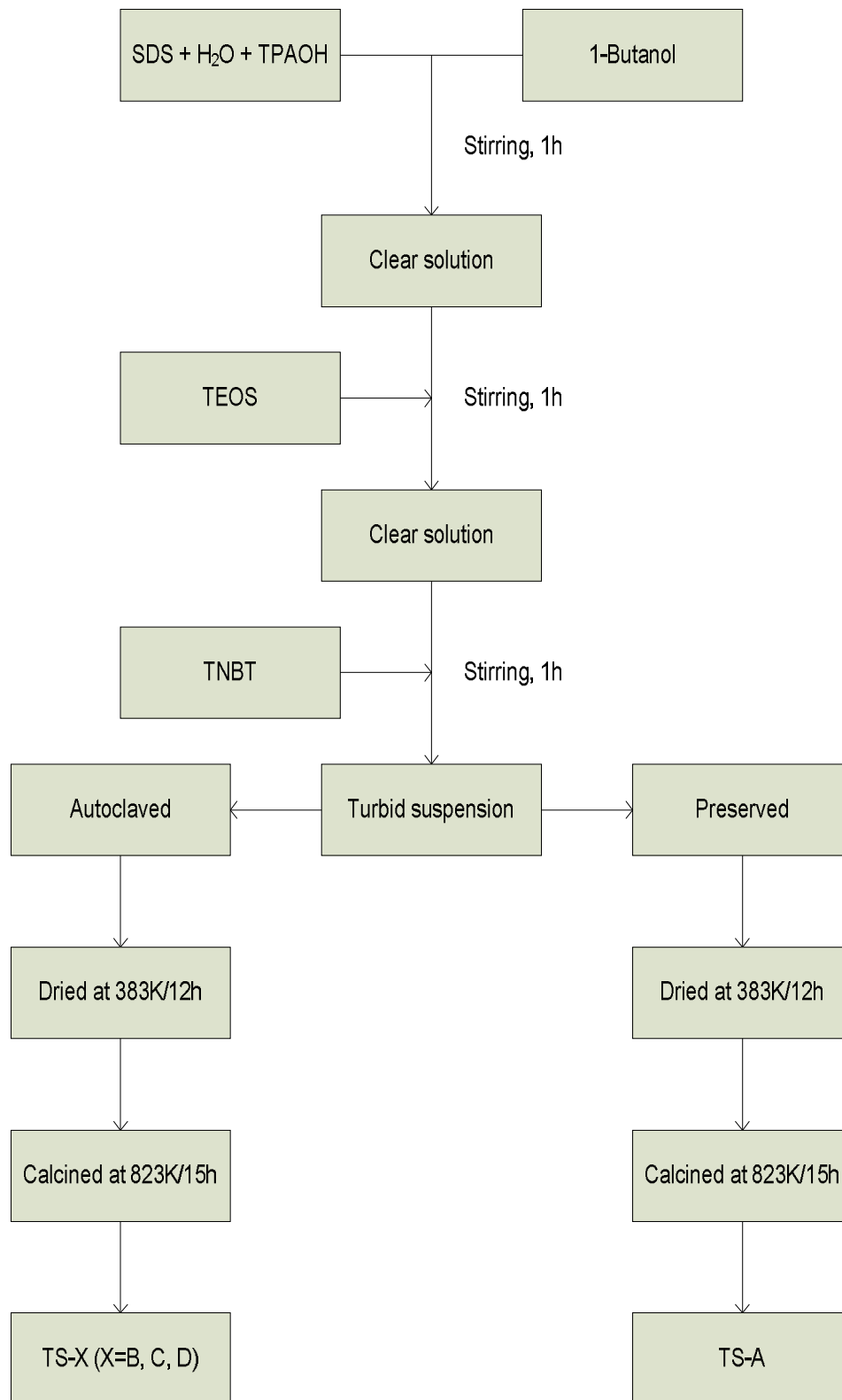
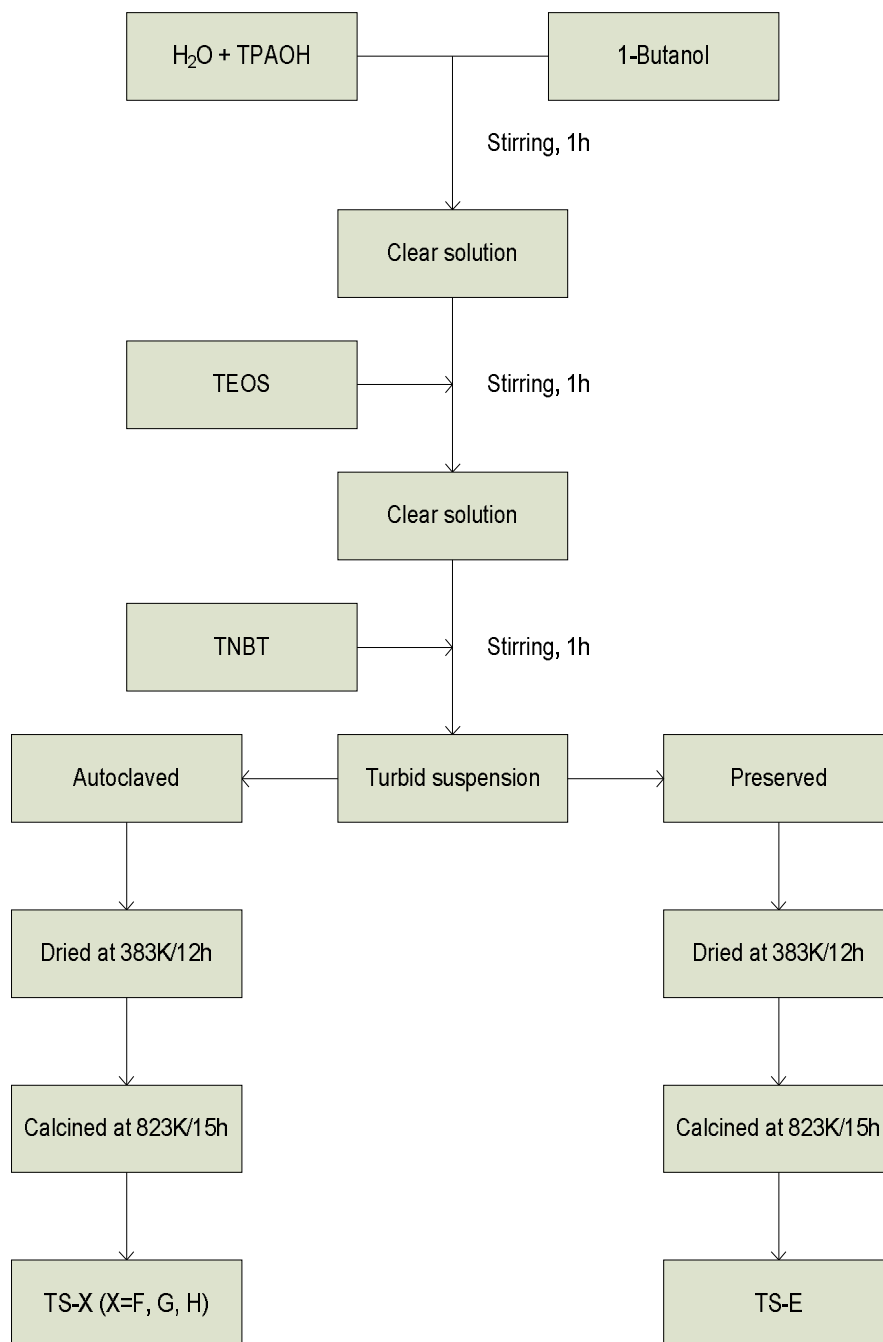


Figure 4.4-3 Flowchart of synthesis adsorbent TS-X [X= E(0h), F(18h), G(24h), H(48h)]



4.5 CHARACTERIZATION OF ADSORBENT

All samples synthesized were characterized by conventional techniques such as XRD, UV-VIS, SEM, Nitrogen adsorption analysis and FTIR.

4.5.1 X-ray diffraction:

X-ray powder diffraction (XRD) analysis is a method for determining the type of species present in the catalyst as well as the degree of crystallinity. XRD analyses were performed using a Bruker A&S D8 Advanced Diffractometer instrument equipped with a $\text{CuK}\alpha$ radiation source, at 40 kV and 30 m², in the scanning angle (2θ) range of 2–40° at a scanning speed of 1.2°/min.

4.5.2 UV-Vis Spectroscopy:

UV-Vis spectra were recorded in a Shimadzu UV-VIS spectrometer (UV - 3900 PC). The base line correction was made using barium sulphate as the standard. All the spectra were recorded in the range 190-600 nm.

4.5.3 IR Spectroscopy:



Figure 4.5-1 IR Spectroscopy

IR spectra were recorded with a FTIR spectrometer (Perkin Elmer Series 1600) and analyses by Spectrum One software in the range 400 - 4000 cm⁻¹ using KBr pellet.

4.5.4 Scanning Electron Micrograph (SEM) Analysis:



Figure 4.5-2 Scanning Electron Micrograph (SEM) Spectroscopy

The samples were first coated with gold-palladium to avoid surface charge build-up. The SEM analyses were recorded using an Oxford Instruments INCA-sight (model LEO 1430 VP), operated at 15 kV. Samples were loaded on a stub and coated with gold-palladium film before scanning to avoid charge build-up. This SEM had been utilized by using ZAF quantitative method at an accelerating voltage of 20kV and spot size of 3 to perform energy dispersion X-ray (EDX) on the sample to quantify the calcined species.

4.5.5 Nitrogen Adsorption Analysis

Nitrogen adsorption tests were performed to obtain BET surface area(SA) and pore size distribution of the adsorbent using a Micrometrics ASAP 2000 gas analyzer. This test was performed in Petronas Research and Services Centre, PRSB, Bangi. A sample consisting of 0.15 g of each adsorbent were loaded in turn into blank sample tube. The sample was degassed at 150°C and evacuated to 500µmHg for 12 hours before analysis to remove impurities and moisture. While the samples were degassed and evacuated,

liquid nitrogen was connected to the cold trap dewar flask to trap impurities in the manifold. After degassing overnight, the sample were allowed to cool at ambient temperature under vacuum and subsequently the tube was backfilled with nitrogen gas before it can be removed safely. The sample tube was reweighed. The actual sample mass was keyed into the software. Then, it was placed into the analysis port. The sample cell was immersed in liquid nitrogen in a dewar flask during analysis. The sample information was then fed into the software to start the analysis. The nitrogen adsorption-desorption measurements were conducted for 56 points. The surface area and pore volume were calculated using the Brunauer-Emmett-Teller (BET) method, while the pore size distribution was determined from the desorption branch of the adsorption isotherm by the Barrett-Joyner-Halenda (BJH).

4.5.6 Thermogravimetry (TG) Analysis



Figure 4.5-3 Thermogravimetry (TG) Analyzer

The thermal analysis was measured using Pyris 1 Thermalgravimetric Analyzer with temperature precision of ± 2 °C. 3-5 mg of the samples was loaded in an aluminum crucible. The scanning rate was 20 °C/min. The measurement was carried out under N₂ atmosphere with gas flow rate of 20 ± 1 mL/min.

4.6 ADSORPTION STUDY

For adsorption study, following general steps were taken;

4.6.1 Stock and Working Solution of Metal Ions

200 ppm stock solution of copper and lead were prepared by dissolving known amount of salt of the respective metal into distilled water and was then diluted in volumetric flasks. Working solutions of metal ions ranging from 20-100 ppm were prepared by diluting the stock solution to the required concentrations.

4.6.2 Effect of Adsorbent Dosages on Metal Ion Adsorption

This study was conducted to determine the best percentage loading of adsorbent that produced the highest amount of metal ion adsorbed for the subsequent adsorption study. 10mL of metal ion solution of initial concentration of 20 ppm (mg/L) was contacted with different weight amounts of 10 mg, 30 mg, 60mg and 100 mg of adsorbent A and adsorbent H. A rotary shaker at 30 °C for 24 h at a constant speed of 80 rpm was used. The resulting mixture was filtered and concentrations of heavy metal were determined using AAS-7000 (Shimadzu).

4.6.3 Adsorption Equilibrium

This study was conducted to determine the equilibrium time and adsorption capacity required for the adsorption of Cu (II) and Pb (II) on adsorbent A and H. For equilibrium time study, 0.01 g of adsorbents was mixed with 10 ml of heavy metal solutions in plastic bottles. The plastic bottles were placed on a shaker at a constant speed of 80 rpm. At each time interval, the resulting mixture was filtered and the concentrations of heavy metal were determined using AAS-7000 (Shimadzu).

4.6.4 Kinetics of Metal Ions Adsorption

For adsorption kinetic test, 0.01 milligrams of adsorbent A and H were put in 10mL of metal ions solution in plastic bottles. Both solutions were agitated on a shaker for 5, 10, 15, 20, 25, 30, 35, 40 min at room temperature. The resulting mixture was filtered and the concentrations of heavy metal determined using AAS-7000 (Shimadzu).

4.6.5 Isotherms of Metal Ions Adsorption

For adsorption isotherm test, metal nitrates were dissolved in deionized water to prepare an initial metal ion solution with concentrations of 10 mg/L, 20 mg/L, 30 mg/L, 40 mg/L, 50 mg/L, 60 mg/L, 70 mg/L, 80 mg/L, 90 mg/L, and 100 mg/L. Adsorbent A and H (0.01 g each) were put in 10 mL of metal ion solution and placed in plastic bottles and agitated on a shaker for 40 min at room temperature. The resulting mixture was filtered and the concentrations of heavy metal determined using AAS-7000 (Shimadzu).

4.6.6 Calculation of Q_t

The amount of metal ion adsorbed on the adsorbent or uptake of ions adsorb in a single reaction in batch experiment was calculate as followed;

$$Q_t = (C_o - C_e) \quad (1)$$

Q_t = the amount of metal ion on the adsorbents (mmol/g)

C_o (mmol/L) = initial concentrations of the given ion in solution.

C_e (mmol/L) = final concentrations of the given ion in solution.

4.6.7 Calculation of K_d

The ability of adsorbents to remove a metal ion from aqueous solution can be expressed in terms of the amount of metal ions on the adsorbents (Q) and the distribution ratio (K_d). They can be calculated according to Eqs. (2) and (3):

$$Q_t = (C_o - C_e) \times V/W \quad (2)$$

$$K_d = 10^3 Q/C_e \quad (3)$$

Q_t = the amount of metal ion on the adsorbents (mmol/g)

K_d = the distribution ratio of the metal (mL/g)

V = the volume of the aqueous solution (L)

W = the weight of the adsorbent (g),

C_o (mmol/L) = initial concentrations of the given ion in solution.

C_e (mmol/L) = final concentrations of the given ion in solution.

4.6.8 Calculation of Adsorption Kinetics Parameter

As explained in 3.7.

4.6.9 Calculation of Adsorption Isotherms Parameter

As explained in 3.5, 3.5.1 and 3.5.2

CHAPTER 5 RESULTS AND DISCUSSION

5.1 INTRODUCTION

In this chapter, the author discussed the results and compared with previous researches. Before proceeding with the results and discussion, the author will present the mechanism of the formation of the titanosilicates and the process of preparation as digest from reports done by K. Kosuge & P. Singh [45] and Shan et al. [46] respectively. Thus mechanism and process of preparation were reported here because the author believed these elements are very important in order to get the required product.

5.1.1 Formation Mechanism

A digestion as reported by K. Kosuge & P. Singh [45];

By adding a mixture of a surfactant (SDS and/or TPAOH), co-surfactant (1-butanol) with water (forming micelles) to a mixture of a silicon oxide with a titanium oxide, a soft mesostructured assembly of the micelles composed of water molecules and surfactant with silicon and titanium alkoxide species is formed as shown in **Figure 5.1-1(a)**. The soft mesostructured assembly then solidifies to form a transparent gel containing aggregates having a mesostructure matrix of inorganic species organized around surfactant molecules each serving as a template, for the formation of a porous array inside the matrix (**Figure 5.1-1(b)**). When the gel is aged, dried and calcined, the organic templates and water are removed to form a Ti porous silica possessing a high surface area (**Figure 5.1-1(c)**).

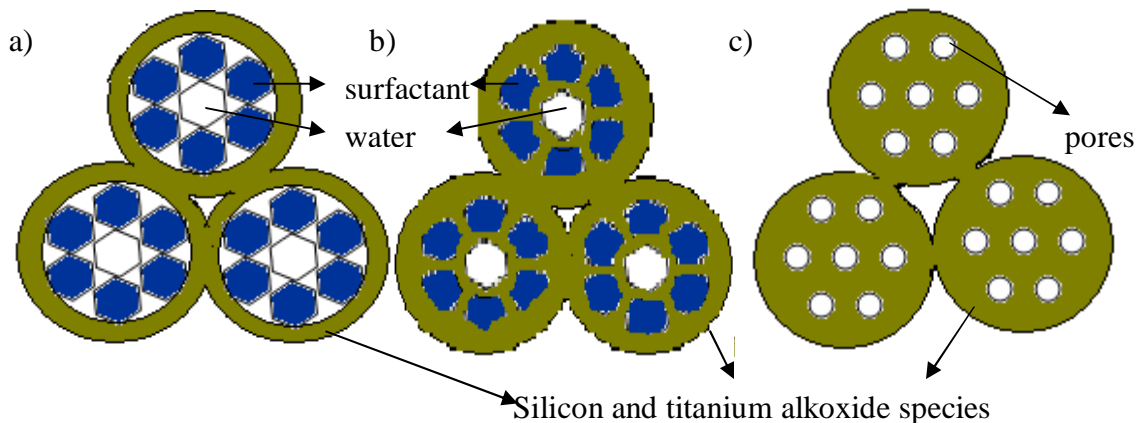


Figure 5.1-1 Formation mechanism of mesoporous titanosilicates

5.1.2 Process for The Preparation

A digestion as explained by Shan et al.[146];

The starting material is generally an amorphous material and may comprise of inorganic oxides such as silicon oxide (silica source: TEOS). The additional metals (titanium source: TNBT) may be incorporated into the material to initiate the process of producing a structure that contains micropores and mesopores or the metal may be added to the preparation to produce inorganic oxide that contains both mesopores and micropores. In present preparation, TNBT is mixed with dry IPA before mixing in TEOS to avoid instantaneous hydrolysis [87].

The template or micropore forming agent that utilized TPAOH generally used for producing molecular sieves and zeolites from silicates, SDS generally used to template nanosize molecules with larger pores either mesoporous or macroporous. If micropores are to be introduced into the mesoporous phase, a micropore forming agent (TPAOH) is preferentially added for producing micropores in zeolite production. TPAOH was a good mineralizer so as to accelerate aeolotropy during the formation of mesostructure and further pore size and uniform distribution of organic groups [76,166]. The organic

compounds (TPAOH/SDS) interact with the inorganic oxide (silicon oxide and titanium oxide) by hydrogen bonding.

In many cases, the resulting inorganic oxide that includes both micropores and mesopores is a pseudo crystalline material that includes an ordered or regular structure in a three dimensional pattern without it being crystalline.

To achieve good mixing between the inorganic oxide precursor solution and the aqueous template mixture, drop-wise addition of the template solution into the inorganic oxide phase is performed. The synthesis mixture is preserved at room temperature (for sample TS-A and sample TS-E), for a period of time to expel any organic compounds from the inorganic source (such as ethanol generated from TEOS). Thereby the water and inorganic components generated from the inorganic oxide source (such as methanol or ethanol) evaporate. The size of the mesopores and the volume of micropores in the final product are influenced by the length and temperature of the hydrothermal step. Generally observed, the percentage of mesopores of the final product increases while the percentage of micropores decreases with increasing temperature and increasing duration of the hydrothermal treatment. In order, to maintain micropore volume, the crystallization step is avoided. It is also possible to extend the hydrothermal treatment such that micropore volume becomes negligible and the material contains essentially only mesopores. The material is then gradually heated to about the boiling point of water. After the drying stage to remove water, the materials still contains traces of surfactants (TPAOH/SDS). The mixture is heated at calcinations temperature preferably at least 400°C and maintained at such temperature. To prevent hot spots, the heating rate should be sufficiently low and the height of the sample bed should be limited. During the calcinations, the structure of the material is finally formed as organic molecules are concomitantly mainly expelled from the sample.

5.2 TOPOLOGY OF TERNARY PHASE DIAGRAM

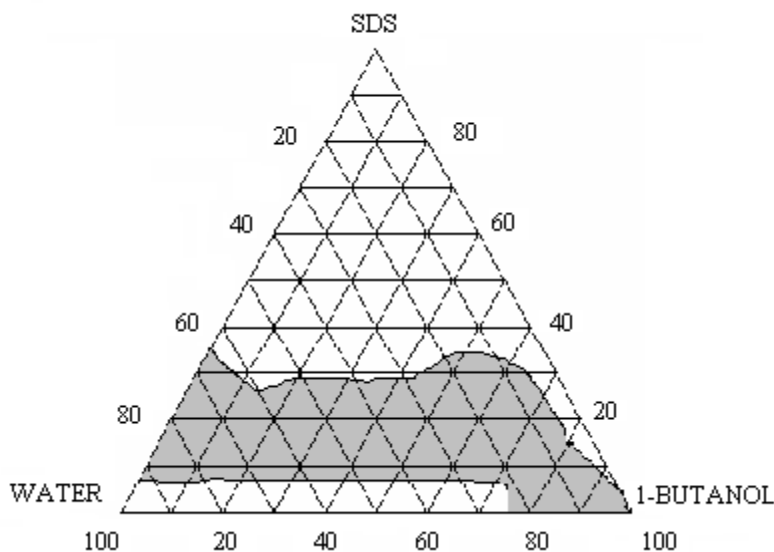


Figure 5.2-1 Water/SDS/1-butanol ternary phase diagram. The grey area represents microemulsion.

The ternary SDS/water/1-butanol system has been plotted and used to determine microemulsion phase area on the system. The temperature was kept constant at $25 \pm 0.1^\circ\text{C}$, while the total weight fractions of surfactant, water and 1-butanol, was varied. Microemulsion phase determination was performed using a visual inspection in transmitted light. Base on this experiment, microemulsion only exists at ratios of the weight fraction of surfactant lower than 0.5. If the weight ration proceeds 0.5, a lyotropic liquid crystalline phase is formed. Weight fraction within the grey area were selected and used to template TEOS (silica source) and TNBT (titanium source). This finding was almost same as K. Aikawa et al. [88] findings.

5.3 X-RAY DIFFRACTION (XRD)

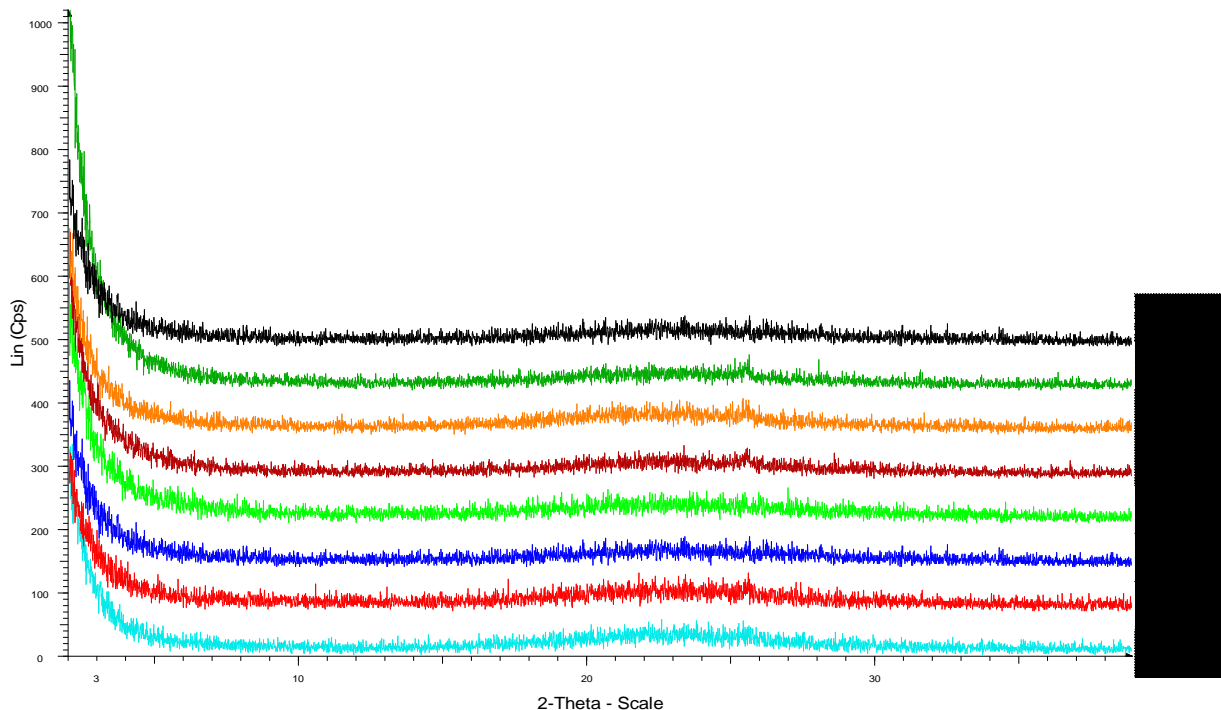


Figure 5.3-1 XRD pattern of calcined samples with different Si/Ti ratio [TS-1(Si/Ti: 33), TS-2(Si/Ti: 33), TS-3(Si/Ti: 10), and TS-4(Si/Ti: 33)] and different crystallization time [Si/Ti: 33;TS-E (0hr), TS-F (18hrs), TS-G (24hrs) and TS-H (48hrs)]

Figure 5.3-1 shows the X-ray diffraction patterns of all samples did not exhibit any sharp reflections but instead a broad diffuse band similar to that of amorphous silica is demonstrated. A completely amorphous structure without any long range order is evident in the materials. XRD could not pick up smaller zeolitic nucleus that maybe present in crystalline form [124 and references therein]. The minimum 2θ range in available XRD machine here is only up to 3° as can be seen in short range order of XRD in **Figure 5.3-1**, while mostly single diffraction peaks for titanium silicate assigned to mesostructure was between $2.1-2.7^\circ$ [47,59,64,92,132,159,160,161]. However it seems (as in **Figure 5.3-1**) that there would be a single diffuse peak if it was extrapolated until 0° . This single peak

may be assigned to a regular structure, which has been described as characteristic of the 3D “wormhole” structured or MCM-41 hexagonal structure.

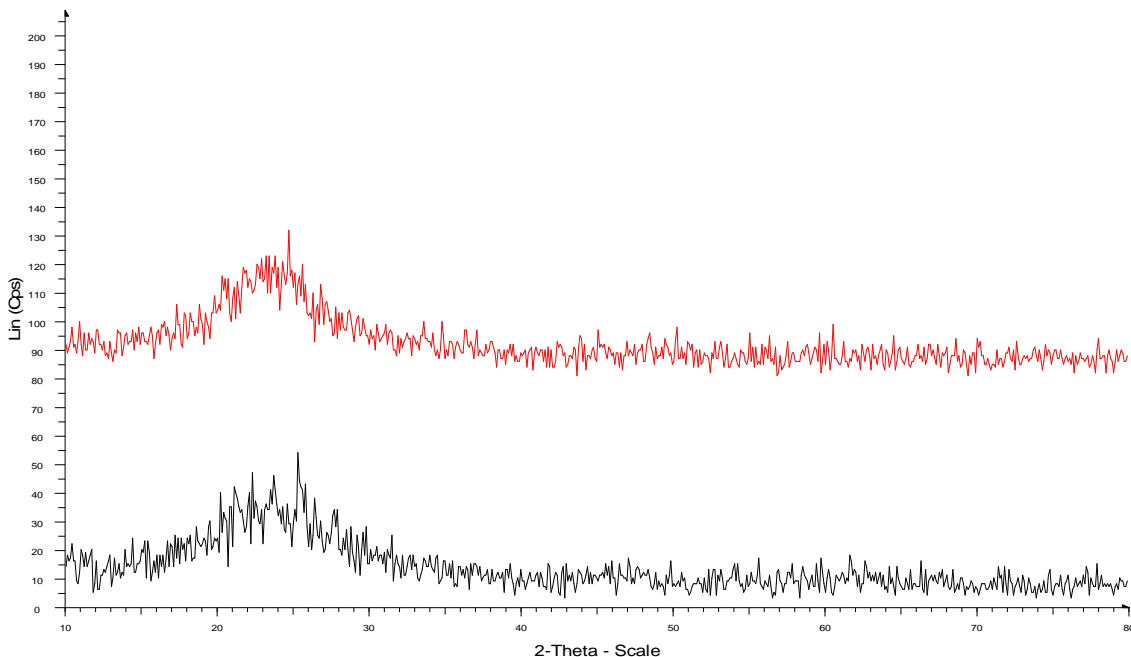


Figure 5.3-2 XRD pattern of calcined samples with different crystallization time [TS-A (0hr), TS-D (48hrs)]

Zeolites Y, ZSM-5 and zeolite precursors having crystal size below 8 nm appear amorphous to XRD. [124 and references there in]. Similar finding was reported by A. Corma & M.J. Diaz Cabanas. [124], A. Khesaravaja et al. [44], and Shan et al. [46,132,162,163]. A. Kesharavaja et al. [44] have reported that their sample was not only XRD amorphous but also did not indicate the presence of crystalline TiO_2 in TEM images and electron diffraction analysis. They claim that it does not necessarily mean that regions with short range order similar to that crystalline TiO_2 are absent in their samples as very fine crystalline particles could be present even in samples which are apparently amorphous to XRD, electron diffraction, and TEM imaging. For sample prepared in hybrid surfactant (as shown in **Figure 5.3-2**), seem to suggest semi-amorphous features. As we can see in **Figure 5.3-3**, there is no separate crystalline phase

TiO₂ (like anatase) that could be correlated to crystalline standard anatase titanium dioxide.

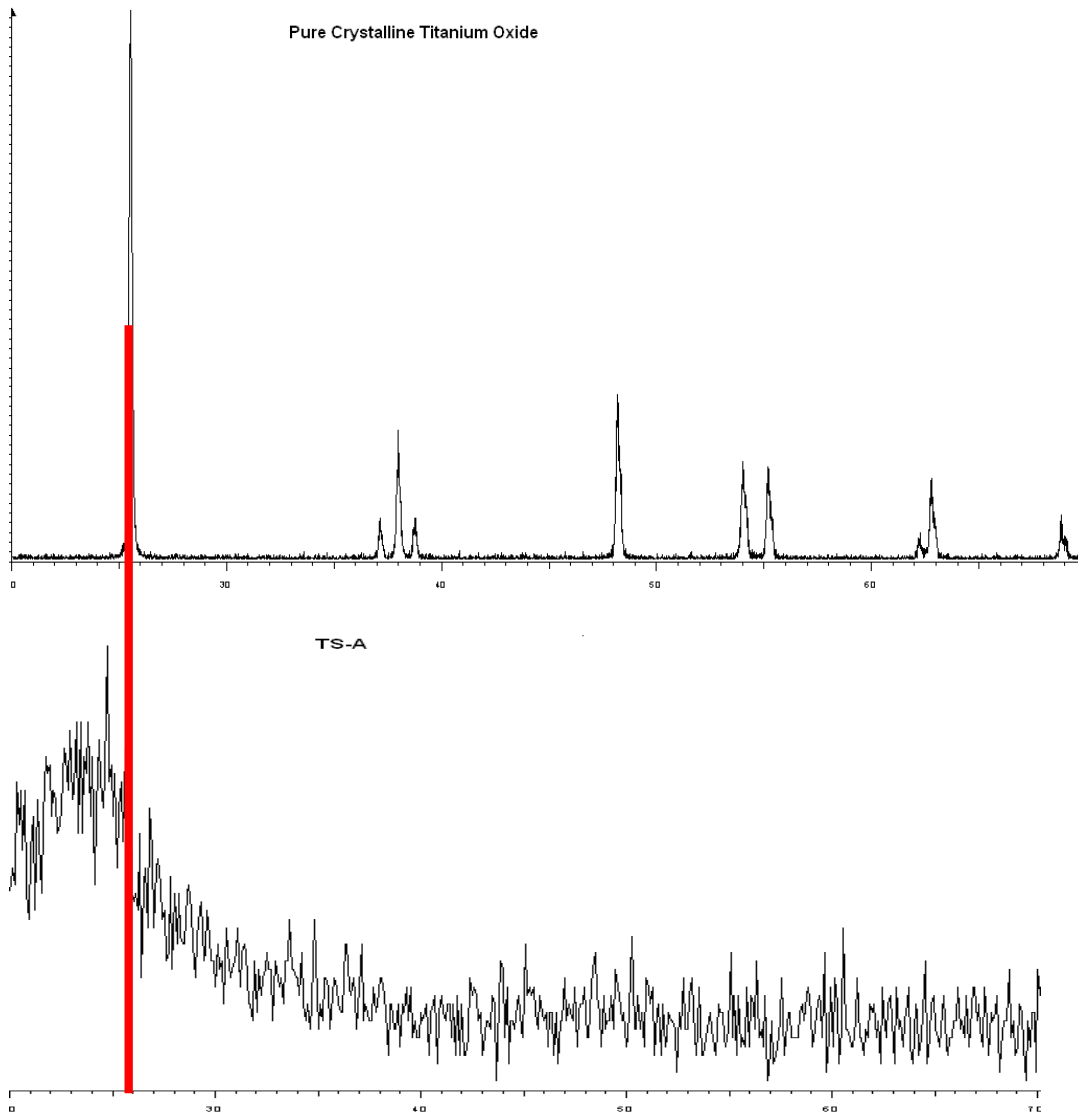


Figure 5.3-3 Correlation between pure titanium dioxide and sample TS-A

Despite the limitation to detect peaks at low 2θ values, the amorphous nature of the material can be related to the fact that SDS amount is relatively low and 1-butanol amount is large [92]. A large amount of solvent/ co-surfactant can dissolve a surfactant and in the same time limit the formation of micelles. If this prevails, the ordered

mesostructured will not form. By increasing titanium content, the rates of nucleation and crystal growth increase, leading to the formation of more nuclei responsible for nucleation and subsequent crystallization. Hong bin et al. [82] had reported that the effect of Ti/Si ratio is not significant above a Ti/Si ratio of 0.24 but when Ti/Si ratio exceed 0.5, the crystallinity decreases and impurity products were predominantly synthesized. Similar finding was reported by Caixia Qi et al. [164] and K.A. Genov [76]. At low Titanium content, the rates of nucleation and crystallization were very low and large crystallites could be produced [82]. At low OH-/Si ratio amorphous materials is predominant.

Crystallization temperature and crystallization time also play an important role in order to produce high crystalline materials. Data gained by D. Trong On et al. [165] showed that amorphous mesoporous titanasilicate are progressively transformed into crystalline materials after 10 days crystallization. While experiments performed by A. Eimer et al. [161] showed that at least 100°C and 2 days would be needed to produce crystalline TS-1. Their results also showed that even a precursor solution aged at room temperature during 7 days, does not exhibit zeolite crystals. The results reflect the complex influence of some processing parameters on the nature of the final solid. This result was totally different with the finding by Yuan et al. [94] which produced crystalline MCM-41 hexagonal structure for untreated and uncalcined structured while amorphous XRD results for sample crystallize at 100°C for 5 days and calcined at 540°C for 5h. However, the amorphous sample was shown to process bimodal pore size distribution. Similar finding (amorphous XRD and bimodal pore size distribution) is found for sample A in our experiments. The finding by Hongbin Du et al. [82] also showed that titanium silicate sample began to lose its crystallinity at 300°C and became an amorphous phase when held at 550°C for 3h. Similar finding was found by C. Rizzo et al. [166] and K. Kosuge & P.S. Singh [45] which observed amorphous phase at 500°C. K. Kosuge & P.S. Singh [45] found that framework titanium species are quite stable up to 700°C while samples calcined at 1000°C indicate the transformation of framework titanium species into a crystalline titania phase.

5.4 SCANNING ELECTRON MICROGRAPHS (SEM)

The SEM photographs and EDX of TS samples prepared in the presence of (TS-1) and absence (TS-2) of SDS are shown in **Figure 5.4-1** and **Figure 5.4-2** respectively. The crystallites in the product obtained in the presence of SDS surfactant are smaller and generally not uniformly sized. In the absence of SDS, the particles seem to form larger aggregates. The non-uniformly sized aggregate crystals is thought to be associated with the absence of TPAOH. TPAOH is an important organic cation to stabilize MFI structure [50].

EDX analysis indicates the presence of TiO_2 and SiO_2 in the calcined samples. **Table 5.4-1** shows the gel and product ratio of samples based on EDX findings. As reported by A. Tuel & Y.Ben Taarit [83], the Si/Ti ratio in calcined zeolites is lower than originally found in the precursor gel. This indicates that not all the silicon and titanium was involved in the crystallization [83]. The absence of a transition at 330nm in the UV-vis spectrum (**Figure 5.5-1**) indicate the samples contained no extraframework titanium species.

Table 5.4-1 Gel Ratio and Product Ratio of Samples

Sample	Gel Si/Ti ratio	Gel Ti/Si ratio	Product Si/Ti ratio*	Product Ti/Si ratio
TS-1	33	0.03	27	0.04
TS-2	33	0.03	27	0.04
TS-3	10	0.10	9	0.11
TS-4	10	0.10	9	0.11

* calculated from EDX analysis

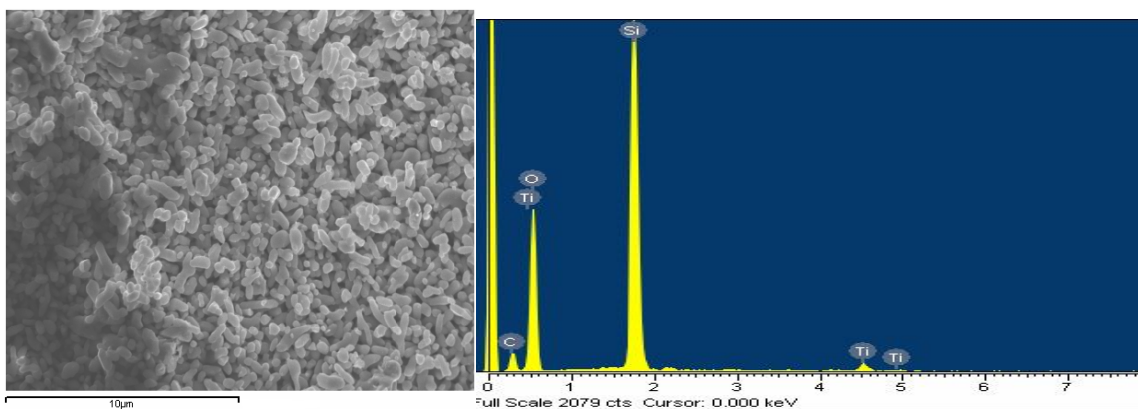


Figure 5.4-1 SEM/EDX of Calcined TS-1 and TS-2 Samples Prepared At Si/Ti Ratio 33 In Presence Of SDS (EHT = 15 KV, Mag. = 2 KX).

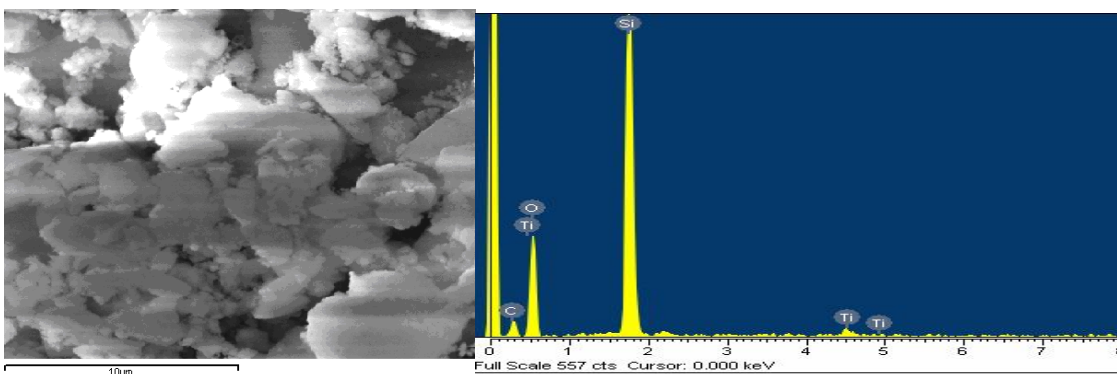


Figure 5.4-2 SEM/EDX of Calcined TS-1 and TS-2 Samples Prepared At Si/Ti Ratio 33 In Absence of SDS (EHT = 15 KV, Mag. = 2 KX).

The SEM photographs and EDX of TS samples prepared in hybrid surfactant (SDS/TPAOH) (TS-A) and template in only TPAOH (TS-E) are shown in **Figure 5.4-3** and **Figure 5.4-4** respectively. The crystallites in the product obtained in hybrid surfactant (TS-A) are generally uniformly sized (spherical to hexagonal like morphology) and no aggregates compared to those produced by conventional method (TS-E) – template in TPAOH. Both products produced hexagonal structures between 1-3 μ m. Sample TS-E also have some aggregates probably due to this product is preserved and no crystallization step forming regular structure [50]. The combination of hybrid surfactant was able to give a regular structure due to a cooperative behavior between surfactant SDS

and TPAOH at the time of crystallization. The shape is so different and more regular compared than TS-1 (twin aggregate and dumbbell structure) prepared in SDS alone.

EDX analysis indicates the presence of TiO_2 and SiO_2 in the calcined samples. **Table 5.4-2** shows the gel and product ratio of samples based on EDX findings. Si/Ti ratio in calcined zeolites of TS-A is almost similar with the original gel precursor. This indicates that all the originally introduced Ti and Si are involved in the crystallization [83]. However, the Si/Ti ratio in calcined zeolites of TS-E is lower than the gel precursor. This is confirmed by the absence and presence of 330nm transition in the UV-vis spectrum (**Figure 5.5-2**) of TS-A and TS-E respectively associated with extraframework titanium.

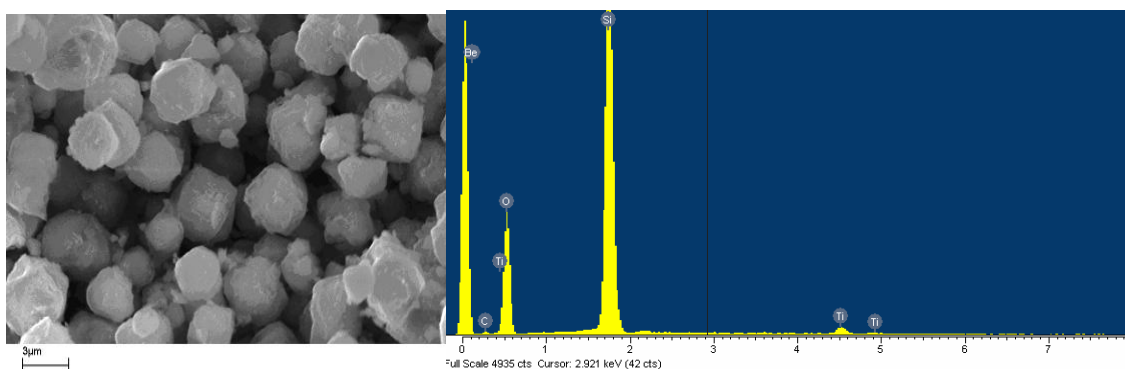


Figure 5.4-3 SEM/EDX of Calcined Samples TS-A prepared in Hybrid surfactant (EHT = 15 KV, Mag. = 4 KX).

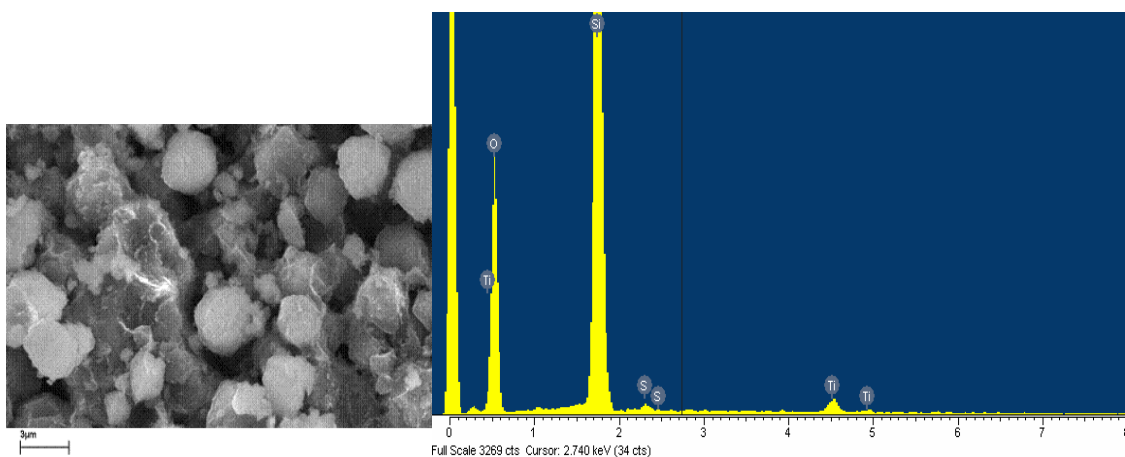


Figure 5.4-4 SEM/EDX of Calcined Samples TS-E prepared in TPAOH (EHT = 15 KV, Mag. = 5 KX).

Table 5.4-2 Gel Ratio and Product Ratio Of Samples

Sample	Gel Si/Ti ratio	Gel Ti/Si ratio	Product Si/Ti ratio*	Product Ti/Si ratio
TS-A	33.00	0.03	33.40	0.03
TS-E	33.00	0.03	29.60	0.03

* calculated from EDX analysis

5.5 UV-VISIBLE SPECTRAL ANALYSIS

Generally, UV-VISIBLE spectroscopy is used to confirm whether the Ti present in the product is in the tetrahedral position or in the form of extra framework TiO₂. Figure 5.6.1 shows a charge transfer band at 210-230nm, which is characteristic of an isolated framework Ti⁴⁺ [77,83,93]. Table 5.6 simplified the results interpretation. The absence of absorption in the 280-330nm region suggests the absence of extra framework TiO₂ [83,93,167,168].

As shown in UV-Vis spectrum (**Figure 5.5-1**), the band intensity was seen to increase monotonically with the increase in Si/Ti ratio [169]. The broader bands (220-350 nm) for sample TS-4 (Si/Ti: 10) in the absence of SDS indicate that there are distorted titanium tetrahedrons [170]. The broad bands at 201-235 nm for sample TS-3 represent the absorptions at the different angles of the distortions [170]. Both samples TS-2 and TS-4 which prepared in absence of SDS generate bands at a lower intensity. This is due to the amorphous structure of the sample [166]. They also show the presence of a broad band around 280-310 nm which indicate the presence of anatase TiO₂. The bands near 310nm represent blue shift from the 350nm band for anatase TiO₂. Such a blue shift has also been reported by Luan et al and G. Li et al. [169,170,171]. TS-4 also shows the presence of a broad band near 270 nm which is attributed to highly dispersed high coordinated penta or octahedral titanium ions [64,85,89]. Sample prepared in the presence of SDS (sample TS-1) show sharp bands at 210 nm. This indicates that titanium is tetrahedrally coordinated with the zeolite framework and titanium atoms are

located on the lattice positions of the zeolite [50]. TS-2 on the other hand only shows weak bands at 210 nm with a lower intensity.

Table 5.5-1 Summary of UV-Vis Result

Sample TS-	Preparation			Results			Interpretation
	Surfactant	Si/Ti ratio	Crystallization time	Broad band (~nm)	Weak band (~nm)	Strong band (~nm)	
1	SDS	33	15 hours			210	Isolated framework Ti ⁴⁺
2	-	33	15 hours	280-330	210		Extraframework TiO ₂
3	SDS	10	15 hours	201-235	210		Distorted titanium tetrahedron
4	-	10	15 hours	220-350 ^{a)}	270 ^{b)}		a) Extraframework TiO ₂ , b) highly dispersed titanium ions
A	SDS/TPAOH	33	0 hours			230	Isolated framework Ti ⁴⁺
B	SDS/TPAOH	33	18 hours	199-240	215		titanium species in T _d coordination
C	SDS/TPAOH	33	24 hours			~230	titanium species in the amorphous state
D	SDS/TPAOH	33	48 hours			~230	
E	TPAOH	33	0 hours		230 ^{a)}	330 ^{b)}	a) titanium species in the amorphous state b) Extraframework TiO ₂
F	TPAOH	33	18 hours	199-240, 310-330	215 ^{a)} , 310 ^{b)}		a) titanium species in T _d coordination b) Extraframework TiO ₂
G	TPAOH	33	24 hours	Shoulder at 280 ^{a)}	230 ^{b)}		a) isolated tetrahedral Ti species b) titanium species in the amorphous state
H	TPAOH	33	48 hours	Shoulder at 280 ^{a)}	230 ^{b)}		a) isolated tetrahedral Ti species b) titanium species in the amorphous state

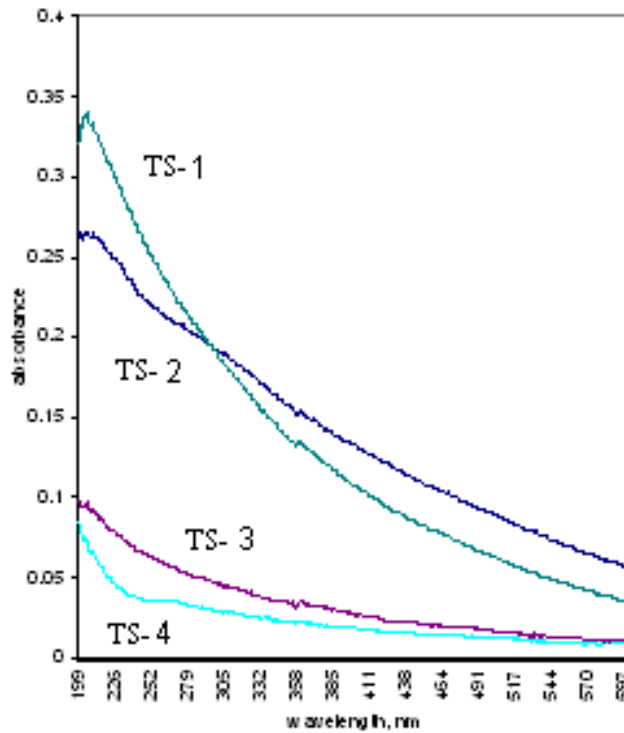


Figure 5.5-1 UV-Vis spectra of calcined powders synthesized with the molar composition $2.82\text{butanol} \cdot x\text{TiO}_2 \cdot 1\text{SiO}_2 \cdot y\text{SDS} \cdot 15.6\text{IPA} \cdot 27.78\text{H}_2\text{O}$ where $x = 0.03$ (1), 0.03 (2), 0.1 (3), 0.1 (4) and $y = 0.72$ (1 and 3), 0 (2 and 4).

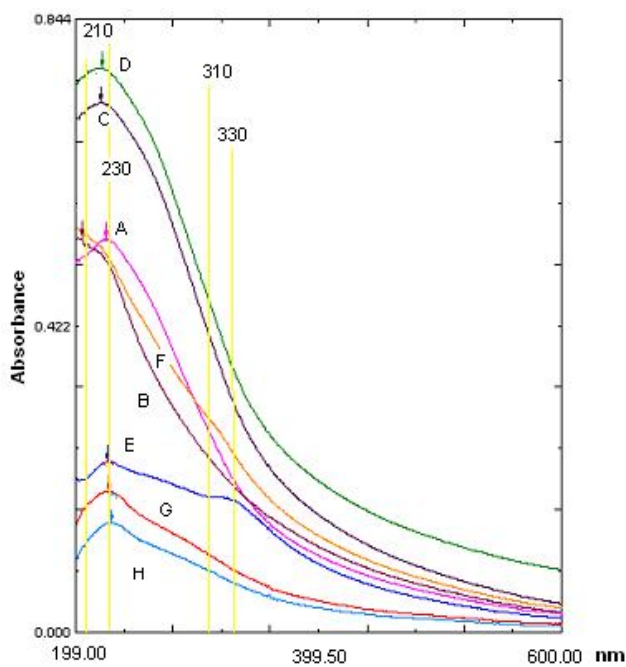


Figure 5.5-2 UV-Vis spectra of calcined samples of TS-A, TS-B, TS-C, TS-D, TS-E, TS-F, TS-G and TS-H.

The UV-Vis spectra of the calcined sample (**Figure 5.5-2**) show a strong (210-230nm) band for samples prepared in hybrid surfactant and weaker band for samples prepared by conventional method. This is attributed to the isolated, tetraordinated position of Ti (VI) on zeolite framework positions [26,50,52,64,75-77,82,83,92,142,166]. The band originates from the charge transfer of the $p\pi-d\pi$ transition between titanium and oxygen of the framework Ti-O-Si species [64]. The band at near 215nm (observed only in sample TS-B and TS-F) assigned to titanium species in T_d coordination [64,81,93,172] and the band centred at 230nm (observed for all samples other than samples TS-B and TS-F), is assigned to the titanium species in the amorphous state with coordination numbers between 4 and 6 [64]. Besides the strong adsorption at 210nm which is characteristic of Ti^{4+} in tetrahedral symmetry, there is also significant absorption in the region 210-300nm, suggesting that compared to TS-1 (which has a sharp absorption band at 210nm), the coordination in this samples is more heterogeneous [131]. Similar finding has been reported by A. Keshavaraja et al. [131]. The lack of the band at $\lambda > 300$ nm in spectra of all samples except for sample TS-E and TS-F, confirms that there is an absence of an extraframework of anatase TiO_2 [24,26,50,52,64,76,82,83,89,93]. This would suggest that for conventional synthesis of titanosilicate, 18h of crystallization is required to prevent the formation of anatase TiO_2 . Spectrum of sample TS-E has shown obvious band at 330nm which results from extraframework of octahedrally coordinated titanium [64,165,173]. The presence of shoulder at 280nm observed in spectra of sample TS-G and TS-H, suggesting the presence of isolated tetrahedral Ti species [75].

5.6 FT-IR ANALYSIS

FTIR spectroscopy is used to characterize the titano-silica mesoporous materials. The important spectral assignments pertaining to FTIR have been explained in section 2.6.2 in this thesis. The band at 960 cm^{-1} supports the incorporation of the tetrahedral titanium into the zeolite lattice. This band is contributed by the valence vibration of a SiO_4 -tetrahedron with a titanium atom [77,83,142].

Based on **Figure 5.6-1**, all the samples generate broad band at 960 cm^{-1} assignable to amorphous nature of Si-O-Ti structures [75,82,89,142,166,173]. No band at 550 cm^{-1} was

observed except in sample TS-1. Several researchers have assigned the 550cm^{-1} band to the asymmetric stretching mode of the five membered ring present in ZSM-5 which should therefore be an indication of the presence of the MFI structure of TS-1 in the region of $400\text{-}600\text{cm}^{-1}$ [76,142,165 and reference therein]. The presence of a shoulder in the region of zeolites structure vibrations could indicate that in TS-1 samples, in spite of their amorphous nature; form some regular secondary building units. A broad band was observed at $1250\text{-}1020$ correspond to Si-O-Si vibration for all the samples [173]. There is a slight band around 800cm^{-1} assignable to Si-OC₂H₅ stretching. The Si-OC₂H₅ functional groups indicate that the hydrolysis and condensation reaction of TEOS was only partial [121]. Moreover, the spectra confirm the fact that the surfactant templates were completely removed as there were no bands representing the functional group of surfactant template were found [76,121]. However, the vibrational band of isopropanol ($\sim 1320\text{cm}^{-1}$ –deformation vibrations of isopropyl group) have been observed on the spectrum. It shows that isopropanol alcohols is not completely removed at the calcinations temperature.

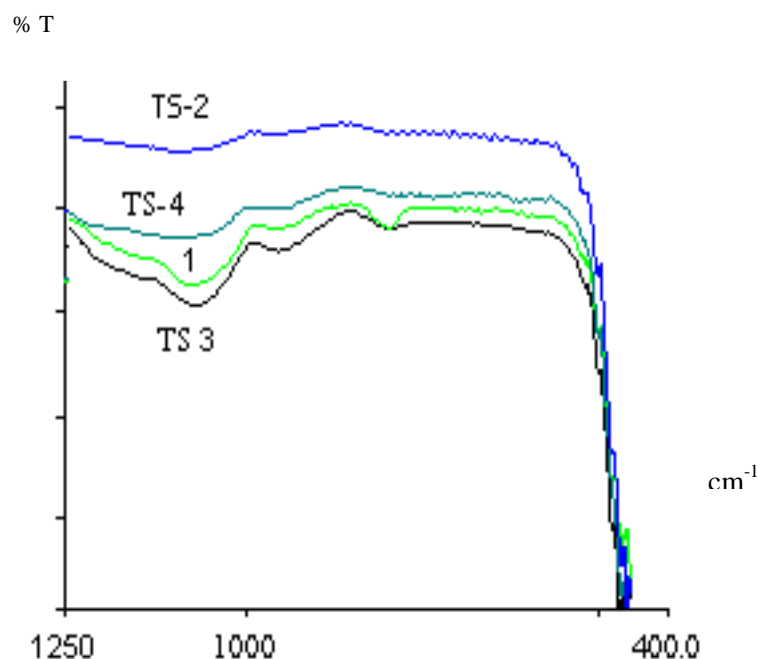


Figure 5.6-1 IR spectra of calcined powders synthesized with the molar composition 2.82 butanol $\cdot x$ TiO₂ $\cdot 1$ SiO₂ $\cdot y$ SDS $\cdot 15.6$ IPA $\cdot 27.78$ H₂O where $x = 0.03$ (TS-1), 0.03 (TS-2), 0.1 (TS-3), 0.1 (TS-4) and $y = 0.72$ (1 and 3), 0 (2 and 4).

The growing intensities of the 960 cm⁻¹ band correlated well with the increasing amounts of titanium that is being incrementally incorporated in the structure [89,142]. Possibly the decrease of intensity of the band may be part of titanium that represents lost framework positions during calcinations. In the presence of SDS as in samples TS-1 and TS-3, the intensities of the 960 cm⁻¹ band decreased compared to the samples prepared in the absence of SDS. The decrease in the intensity of peak at 960 cm⁻¹ is believed to be due to the presence of Ti vacancies in the Ti-O-Ti chains, leading to the decrease in Ti-O stretching of TS-1 [142]. A qualitative correlation between the intensities of 960 cm⁻¹ and titanium content has been observed at the first synthesis of TS-1 [77]. As shown in **Table 5.6-1**, the relative intensity of these band peaks increased linearly as titanium loading increased. This confirms the incorporation of Ti⁺⁴ in the framework position in the TS-1 samples. Similar finding has been reported by Didik [56] and G. Li & S. Zhao [169]. It is also observed that the relative intensity of similar titanium loading is very similar for all samples which suggest at first sight, a similar degree of Ti incorporation into the crystalline structure [77].

Table 5.6-1 Molar composition and relative intensity of TS samples

Sample	Molar composition ratio of TiO ₂	I_{960}/I_{800} ^a
1	0.03	0.97
2	0.03	0.96
3	0.1	1.01
4	0.1	1.02

^aratio between the intensities, in absorbance units, of the 960 and 800 cm⁻¹ IR bands.

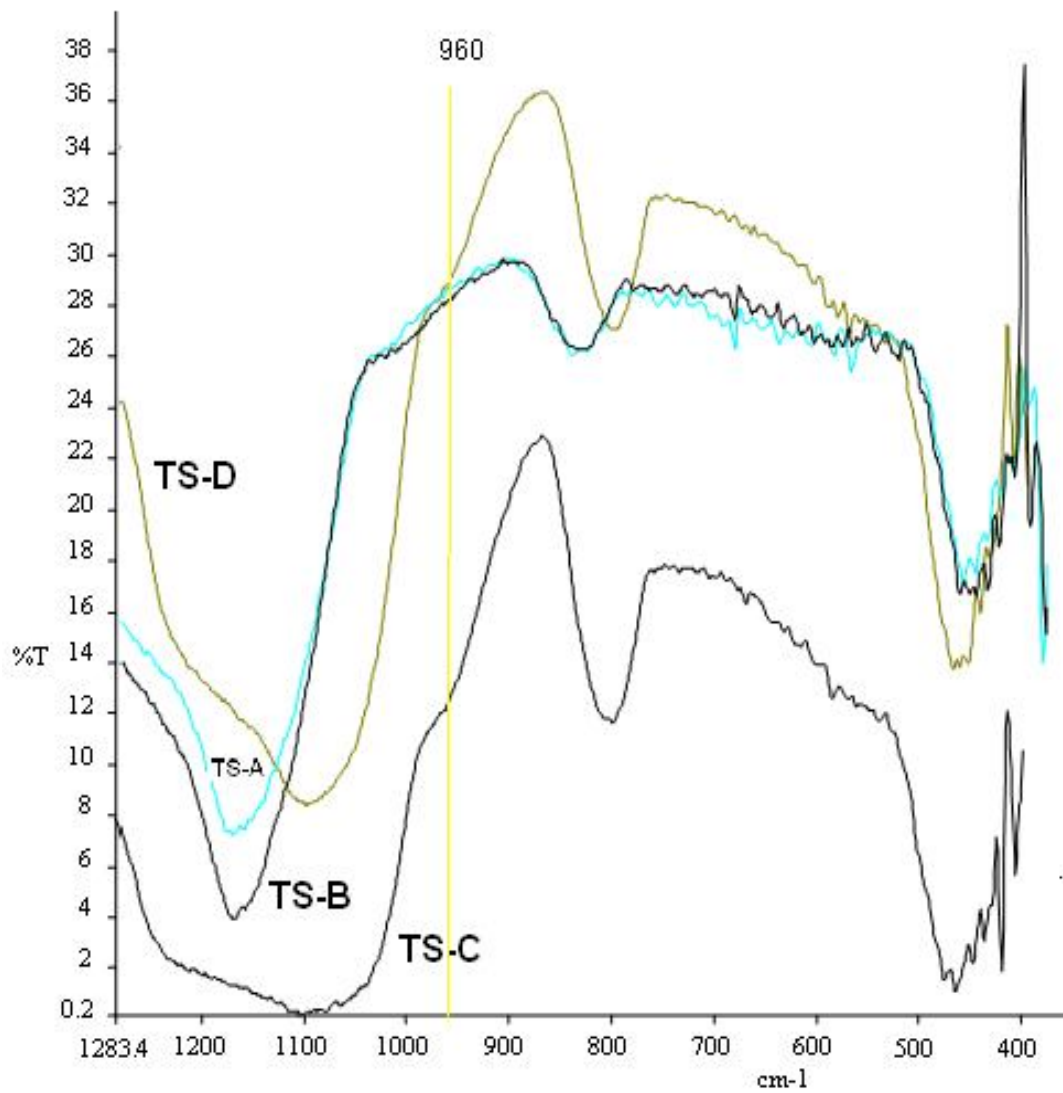


Figure 5.6-2 IR Spectra of as-synthesized samples prepared by hybrid surfactant with different crystallization time TS-A (0hr), TS-B (18hrs), TS-C (24hrs) and TS-D (48hrs)

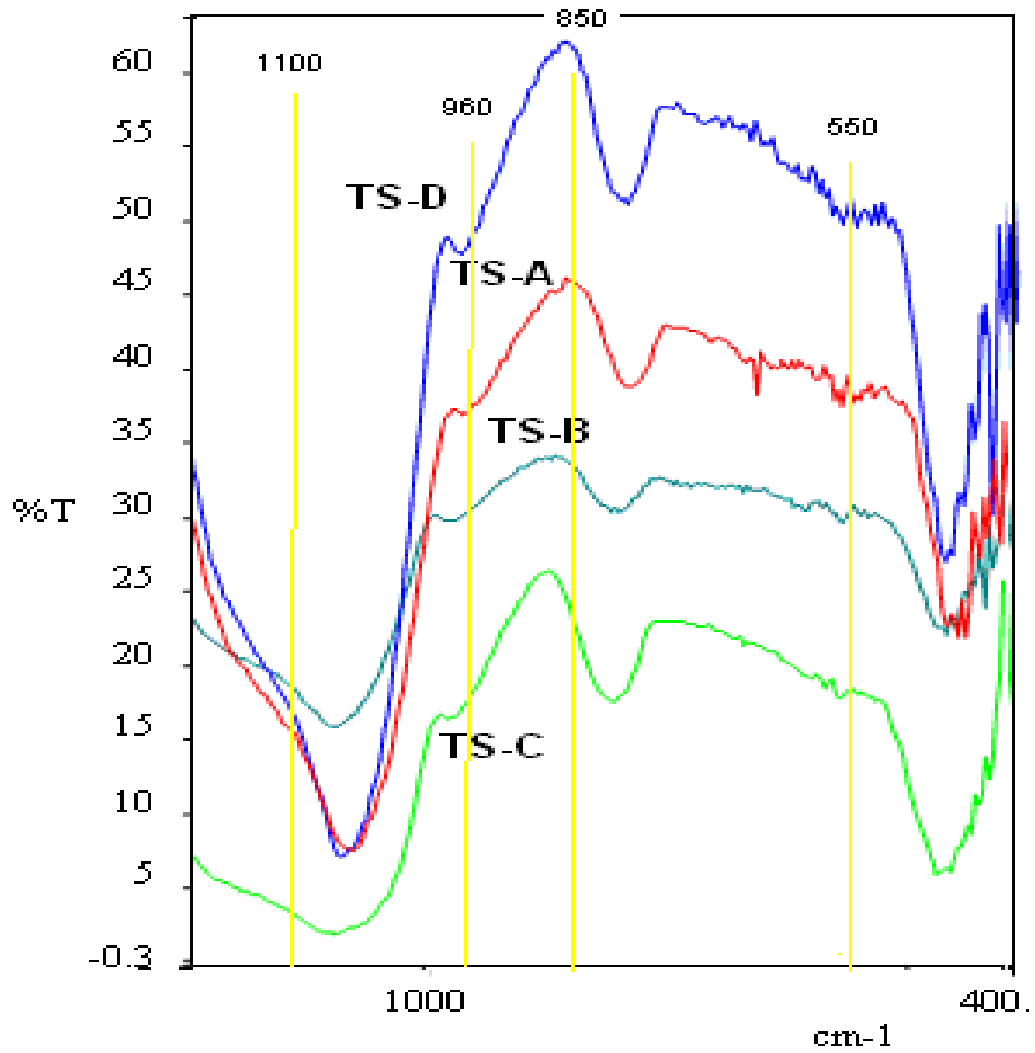


Figure 5.6-3 IR Spectra of calcined samples prepared by hybrid surfactant with different crystallization time TS-A (0hr), TS-B (18hrs), TS-C (24hrs) and TS-D (48hrs)

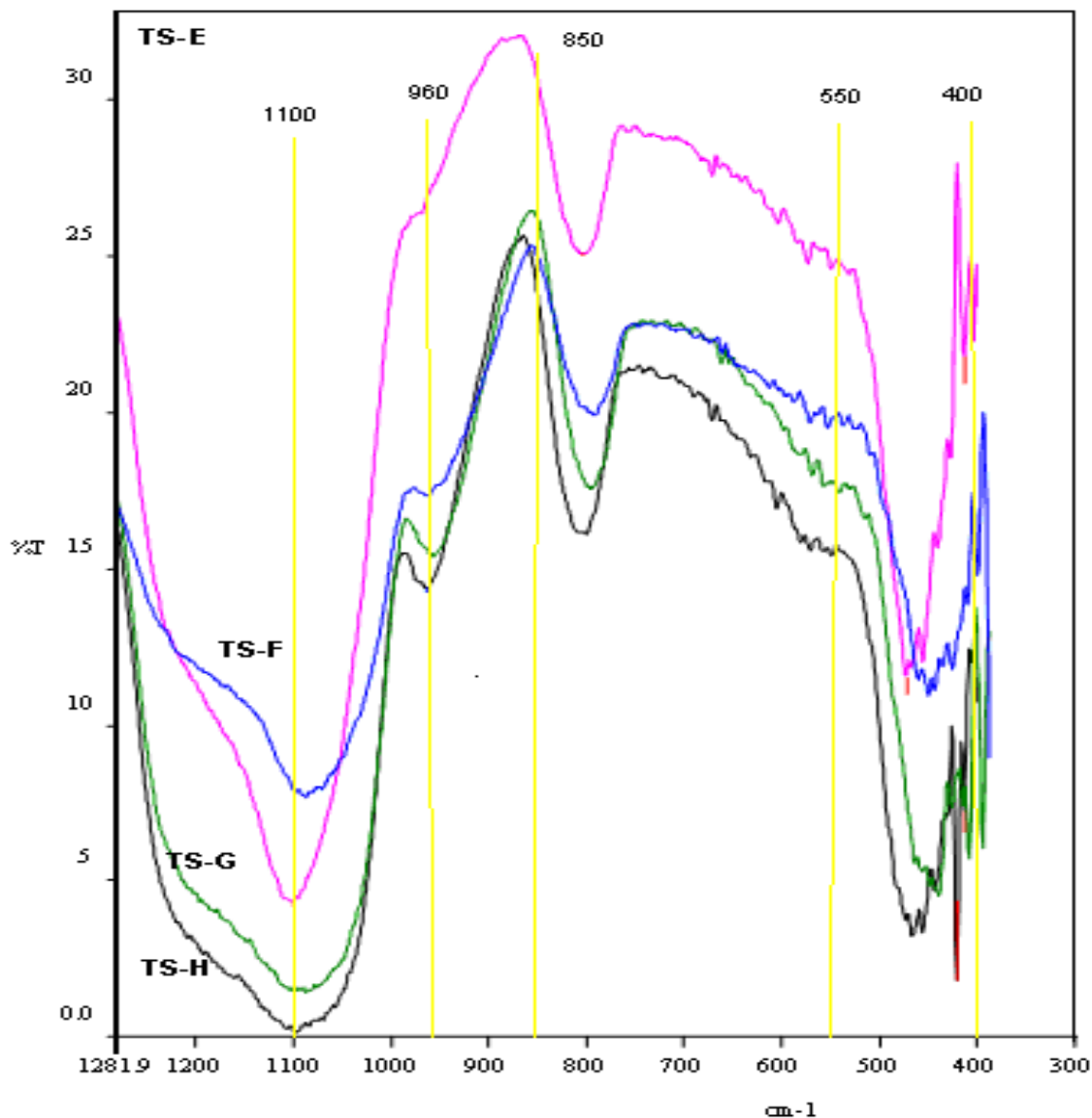


Figure 5.6-4 IR spectra of calcineds sample prepared with different crystallization time TS-E (0hr), TS-F (18hrs), TS-G (24hrs) and TS-H (48hrs)

As we can see in **Figure 5.6-2**, **Figure 5.6-3** and **Figure 5.6-4**, the spectrum look similar and as explained in section 2.6.2 and literature [26,50,52,64,74-76,78,82,83], the data are typical for MFI type zeolites [**Table 5.6-2**]. The most concern fingerprint in IR-spectroscopy of titanium containing zeolites, however is the vibrational band at 960cm^{-1} . In as-synthesized samples (**Figure 5.6-3**), such band is not observed probably because the

Ti center is possibly perturbed by the presence of the template molecules [50,52,56,75,142]. It is well known that the IR-spectra of zeolites containing titanium on framework sites such as TS-1, TS-2 and Ti-beta but not in IR-spectra of the pure silicalite-1, only aluminium containing zeolites, titanium oxides and even ETS-10 which contains Ti in octahedral coordination. So, it is clear that this important fingerprint is associated with the incorporation of titanium species with tetrahedral oxygen coordination.

Table 5.6-2 Band Assignments in IR spectra of samples

Bands [cm^{-1}]	Assignment
300-400	External vibrations caused by breathing motions of 8, 10 or 12-ring apertures
420-500	Si-O/ Ti-O bending mode
550	Five-membered rings of Si-O-T (T=Si or Ti) in microporous zeolites
580-610	Double ring. External vibrations in the double six-membered and four membered rings
680-850	Symmetric stretching of SiO_4 tetrahedron bonds. The external vibration at $700\text{-}780\text{cm}^{-1}$
800-900	Normal modes including the ν_{as} (SiO_3) and γ (Ti-O) vibrations
960	Stretching vibrations of SiO_4 tetrahedron bound to Ti atoms as Si-O-Ti linkages
1000-1250	-Si-O-Si- asymmetric stretching

Based on **Figure 5.6-3** and **Figure 5.6-4**, the presence of a band at 960 cm^{-1} is observed in all the calcined samples which is an indication of Ti^{+4} incorporation in the silicalite framework [50,52,602,75,76,78,82,142]. In all the cases, the ratio of the band at 550 cm^{-1} and 450 cm^{-1} is approximately more than 1.3, indicating the presence of a crystalline material in spite of its lack of evidence provided by XRD studies. Thus, by considering the fact that IR spectra of all calcined samples in the skeleton vibration region, we cannot reject the amorphous nature of the samples. Similar findings has been reported by Mukherjee [52] and A. Corma and M.J. Diaz-Cabanás [124].

It is also observed that the higher crystallization time, the intensity of the 960 cm^{-1} band and 550 cm^{-1} also increase which is in concordance with findings reported by A. Corma and M.J. Diaz-Cabanas [124], D. Trong On et al. [165], and A. Ungureanu et al. [124]. All samples show a sharp band near 460 cm^{-1} in the region of $400\text{-}600\text{ cm}^{-1}$, which is similar to those of amorphous materials. However, all the samples exhibit a small band at 550 cm^{-1} in addition to the the band near 460 cm^{-1} . The band near 550 cm^{-1} is similar to that of a five-membered ring of Si-O-T (T=Si or Ti) in microporous zeolites such as ZSM-5 or TS-1. Thus, it suggests that all samples have MFI structure of TS-1 which is consistent with those reported in the literature [92,165]. The FTIR spectra of all calcined samples in **Figure 5.6-3** and **Figure 5.6-4** show the splitting of the band at $\sim 550\text{ cm}^{-1}$ (except for sample TS-C and TS- G) and obvious band at $\sim 960\text{ cm}^{-1}$ (except for TS-E), which are characteristic of nanocrystals and titanium framework, respectively [94,174 and reference therein]. Such a splitting was recently reported for silicalites with small particle sizes ($<100\text{nm}$) and ultra large TS-1 (prepared by D. Trong et al. [165] and A. Ungureanu et al. [89]). The presence of splitting at 550cm^{-1} was assigned to the high concentration of defect sites and crystallite strain along the a crystallographic direction [89].

5.7 THERMOGRAVIMETRY (TG) AND DIFFERENTIAL THERMAL ANALYSIS

Figure 5.7-1a) shows the decomposition run of as-synthesized titanosilicate samples (TS-1) having $\text{SiO}_2/\text{TiO}_2$ molar ratio of 33 using an anionic surfactant (SDS). The mass of the TS-1 decreased with temperature. The TGA curve shows three regimes of weight losses attributed to: (i) elimination of water molecules adsorbed on the crystal surface ($\sim 87.5\text{ wt.}\%$, $T_{\text{max}}= 98\text{ }^\circ\text{C}$), (ii) decomposition of organic ions (SDS) trapped within the pores ($\sim 84\text{ wt.}\%$, $T_{\text{max}}= 230\text{ }^\circ\text{C}$) in concordance with values reported for decomposition of SDS from mesoporous silica networks [121], and (iii) oxidative decomposition of the occluded 1-butanol at $\sim 425\text{-}550^\circ\text{C}$ ($\sim 62.5\text{ wt.}\%$). [78,166]. There are no major changes or transformations observed in the temperature range between $\sim 650\text{-}750^\circ\text{C}$ which essentially provides the high thermal stability of TS synthesized in the presence of surfactant system [78].

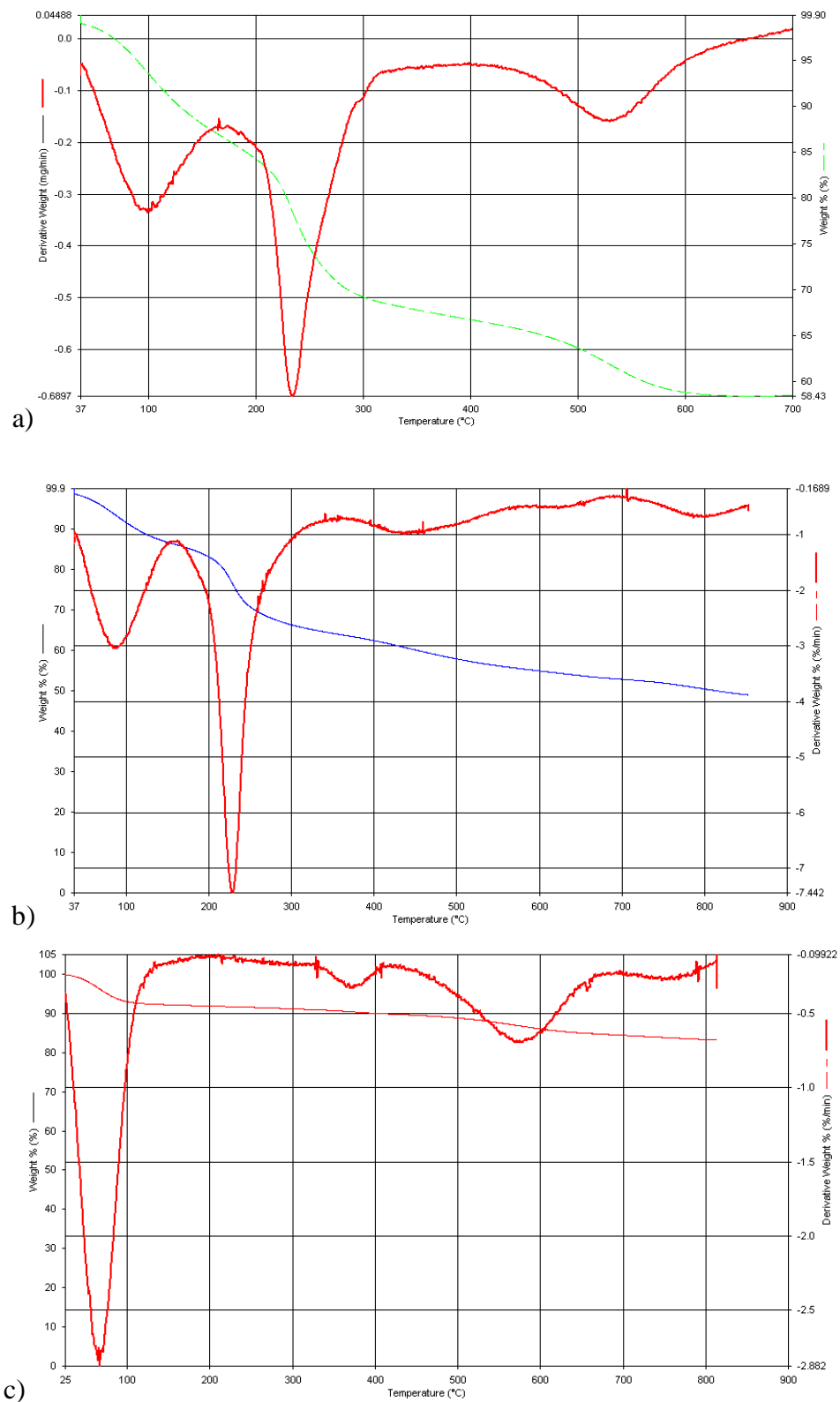


Figure 5.7-1 TGA curve of as-synthesized a) TS-1 (prepared with SDS) b) TS-A (prepared with SDS and TPAOH) and c) TS-E (prepared with TPAOH)

From **Figure 5.7-1b**), a similar trend was observed for as-synthesized titanosilicate samples (TS-A) having SiO₂/TiO₂ molar ratio of 33 in the presence of hybrid surfactant (TPAOH and SDS) with an additional regime corresponding to the decomposition of organic ions (TPA⁺) trapped within the pore spaces; (~62 wt.%, T_{max}= 420 °C). As we can see in **Figure 5.7-1c**), the 3 major steps are distinguished; dehydration of water (~92 wt.%, T_{max}= 80 °C), decomposition of TPA⁺ (~92 wt.%, T_{max}= 390 °C) and 1-butanol(~84 wt.%, T_{max}= 550 °C).

It was clearly observed for sample TS-A, the total weight loss at 700°C is approximately 48% in agreement with the values reported for mesoporous materials [78]. Whereas, sample TS-1 loses approximately 43% of its weight, indicate of the decomposition of organic template in microporous crystals of silicalites and titanosilicates [161 and reference therein]. Thus, this difference of ~5% could be associated to the combination of surfactant molecules initially occluded in the voids formed by zeolite nanocrystals agglomeration [161 and reference therein]. Finally, there are no major changes or transformations observed for sample TS-1 in the temperature range between 650-750°C which essentially provides evidence of the high thermal stability of TS-1 whereas for sample TS-A, there are only slight changes in the temperature range between 650-800 °C which show the instability of titanosilicate prepared in hybrid surfactant [78,167]. Based on these results, we consider that the calcinations temperature 550°C can completely remove all templates titanosilicates samples investigated.

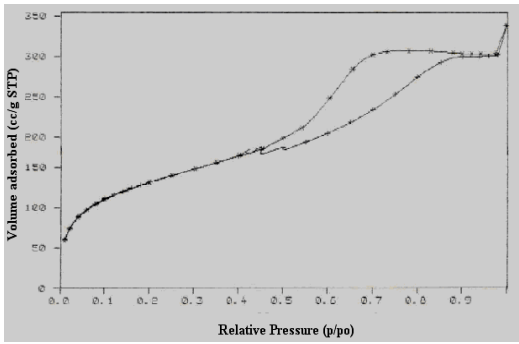
5.8 POROSITY CHARACTERISTICS OF ADSORBENTS

Gas adsorption measurements are a typical method for studying the properties of porous materials. Adsorption and desorption isotherm phenomena by an adsorbate (normally nitrogen at 77K) used to determine the surface area and mesopore size distribution. The nitrogen and adsorption data can be obtained by using instruments capable to produce a plot of the derivative of pore volume as a function of pore diameter. Micropores are defined as pores having a diameter of less than about 20Å. Mesopores are defined as pores having a diameter from about 20Å to about 500Å [132]. In the mesopore range, such a plot may be used by applying BET adsorption theory and Barrett, Joyner and Halenda (BJH) method.

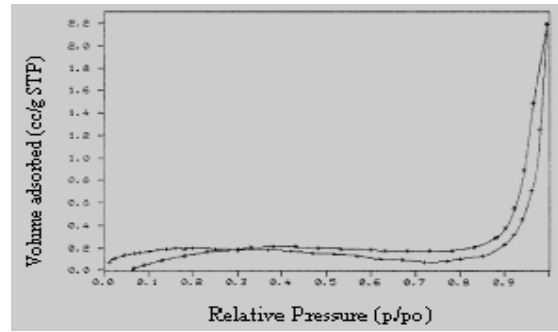
Sample TS-X (X= A-H) were analyzed, as described in section 4.5.5. The BET measurement and N₂ adsorption-desorption isotherms at 77 K of all eight samples are shown in **Table 5.8-1** and **Figure 5.8-1** respectively.

Table 5.8-1 Structure properties of TS-X (X=A, B, C, D, E, F, G, H)

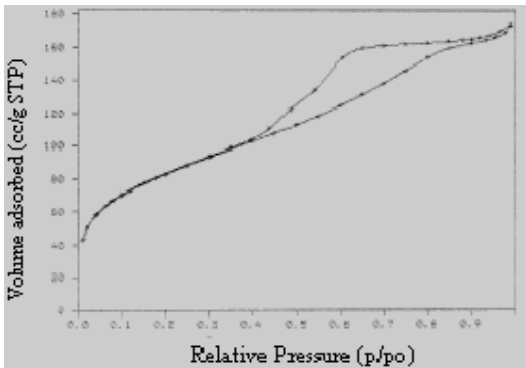
Crystallization time	Adsorbent	BET surface area (m ² /g)	BET pore diameter (Å)	BJH Average pore diameter (4v/A) (Å)	Micropore volume (cc/g)
0h	A	459.48	45.6	49.7	0.034
18h	B	282.51	38.2	40.6	0.021
24h	C	158.67	8.1	8.9	0.003
48h	D	47.83	8.7	9.4	0.015
0h	E	0.73	186.6	216.3	0.000
18h	F	3.12	221.5	237.4	0.001
24h	G	240.52	120.8	130.1	0.011
48h	H	277.55	183.1	196.8	0.016



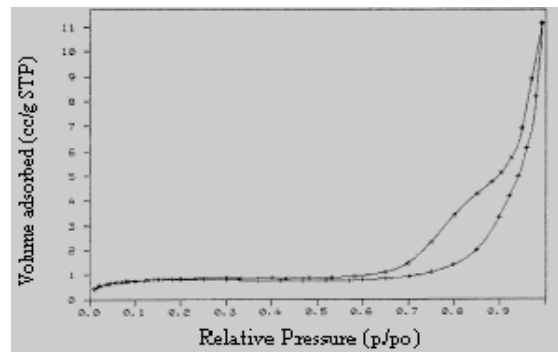
TS-A



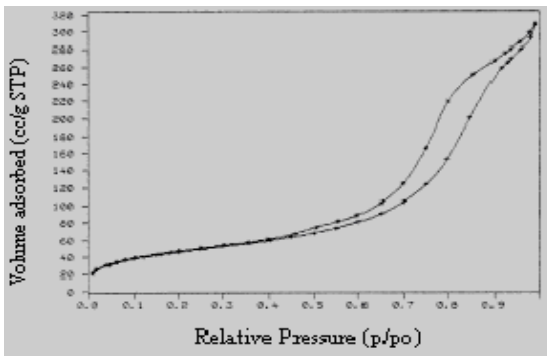
TS-E



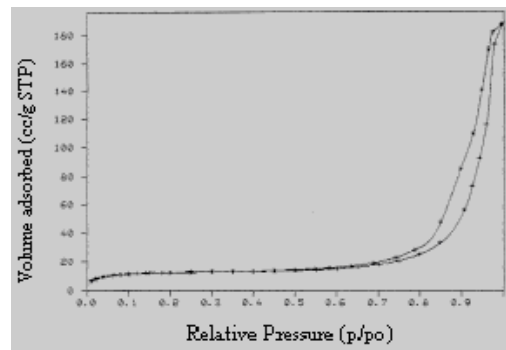
TS-B



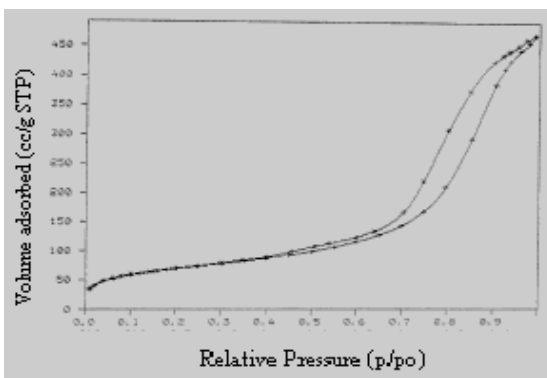
TS-F



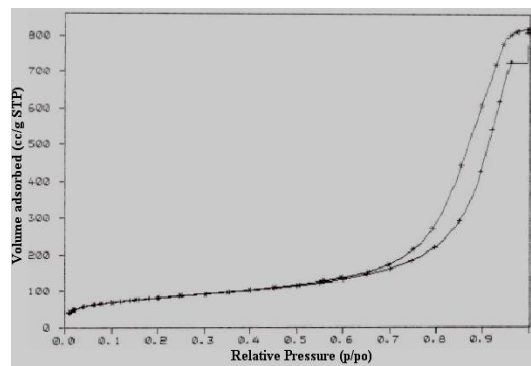
TSC



TS-G



TS-D



TS-H

Figure 5.8-1 Nitrogen sorption isotherms of sample

Samples TS-A, TS-B, TS-C, and TS-D which were synthesized with SDS and TPAOH as hybrid surfactant templates (TS-hybrid), exhibited small pore diameters (from **Table 5.8-1**). The average pore diameter trend decreases because in the presence of SDS, it will adhere together as a mass. Similar findings were reported by Boonamnuayvita et al. [121] and reference therein. Also as expected from the influence of duration of crystallization, the micropore volume tends to decrease by crystallization time. Micropore volume decrease according to following order: TS-A > TS-B > TS-D > TS-C. However, similar trend is not observed for sample synthesized in only TPAOH. Micropore volume increase in the following order: TS-E < TS-F < TS-G < TS-H. Adsorbent E, F, G and H synthesized using TPAOH have a lower surface area and lower pore volume. Sample TS-A has highest surface area, highest micropore volume and yet not too small nor too big pore diameter. In comparison with sample TS-E which also preserved at room temperature, TS-A has higher surface area, higher pore volume but lower pore diameter. TS-A also has a comparable surface area with others titanosilicate [64,93,113,161,173]. This economic adsorbent show that micelles can template titanosilicate without need any extend energy.

From **Table 5.8-1**, it can be seen that for TS-hybrid, crystallization time for 18h is enough resulting microporous titanosilicate. Titanosilicate synthesis in TPAOH only (TS-conventional; TS-E, TS-F, TS-G and TS-H), the higher crystallization temperatures, produced products with greater surface area while in TS-hybrid, the reverse relationship is found. The result is significant to the mechanism of commonly porous silica synthesized by surfactant such as MCM-41; where a large ionic radius TPA^+ , is thought to react with the hydroxyl group of hydrolyzed silicates. Since the interaction of the silicate precursor with surfactant were stronger than with TPA^+ , the ion pair diffused to the surfactant interface and the silicate precursor interacted with surfactant head groups. Then the silicates are able to progress to the condensation and polymerization stages within the surfactant micelles. Thus, TPAOH is suspected to modify the strength of the electrostatic interaction between silicates and the anionic surfactant micelles to enhance pore properties [175]. TPAOH helped to accelerate the condensation of silicates and strengthen the physical structure of adsorbents [26].

From **Figure 5.8-1**, generally a typical type IV adsorption isotherm is observed for all samples. It also can be seen that the isotherms presented in this figure show that the total sorption uptake increase with increasing crystallization time for all samples of amorphous TS except for sample TS-A which show quite high sorption uptake despite a room temperature ageing process [176]. According to IUPAC [45] classification, the hysteresis loop was said to be a characteristic feature of a type IV isotherm. Broad hysteresis loop of *H2* according to IUPAC [45] classification can be seen in both TS-A and TS-B. The broad hysteresis loops in the isotherms reflect long mesopores with no pore blocking effect which will otherwise limit the emptying and filling of the accessible pore space. In nitrogen isotherm of TS-A, at relative pressure $p/p_o \approx 0.4-0.9$ the loop is slightly broad, the desorption branch slightly steeper than the adsorption branch. The *H2* hysteresis loop consistent with a narrow pore size distribution. A similar hysteresis loop was observed in mesoporous organosilica template in cationic surfactant [177], template in triblock copolymer [92], and using aqueous ammonia as catalyst [176], and amorphous titanosilicate prepared by silylation of mixed oxides obtained via a two step sol-gel method [91]. *H2* hysteresis loop in the isotherm curve is typical of 3D wormhole structured MSU-type (siliceous mesostructured cellular foam with three dimensional (3D) wormhole structure) materials [92].

Interestingly in TS-A nitrogen sorption curve, two separates hysteresis is observed. A *H2* hysteresis loop is immediately followed by a flat curve, corresponding to the filling of microporous belonging to zeolitic structure [89]. The flat curve was then immediately followed by another hysteresis expressed *H1* hysteresis loop as defined by IUPAC [45]. The same observation of two separates hysteresis in one isotherm was also observed by Wang et al. [176] which reveal two mesopore sizes in their material (**Figure 5.8-4**). It is thought that both microporous and mesoporous sizes were generated. This is confirmed through pore size distribution calculated by BJH desorption cumulative volume (**Figure 5.8-2**). A steep increase in the Langmuir type adsorption isotherm at a relative pressure below 0.1 indicates the existence of micropore structure. At $p/p_o \approx 9.5-10.0$, there is a noticeable absence of a steep region of desorption branch which is characteristic of microporous and may imply that a change in the texture has occurred on the mesoporous

framework of the products [178]. This curve looks like type I isotherm which is consistent with microporous sample and similar observation was reported for titanosilicate prepared in cationic fluorinated surfactant [16] and Ti-MCM-41 prepared from assembly of preformed TS precursors with CTAB micelle in both acidic and alcohol media [92].

Generally, the typical N₂ adsorption isotherm, which plays a significant role in characterization of the new mesoporous materials such as MCM-41 materials shows a type IV behavior with a sharp inflection characteristics of capillary condensation within uniform mesopores at p/p_o *ca.* 0.2-0.5 [176]. There is an additional hysteresis loop in the p/p_o *ca.* of 0.8-1.0 [32,50,176] region. The hysteresis loop at $p/p_o > 0.8$ is now acknowledged to originate from interparticle capillary condensation or from the structure collapse of portions of the MCM-41 structure during the hydrothermal treatment or calcination [77,93,176]. Recently reports on the synthesis of amorphous micro-mesoporous titanosilicate and mesoporous silica by Kesharavaja et al. [131] and Yuan et al. [94] respectively have shown a sharp lefting-up hysteresis loop at $p/p_o > 0.8$ and dual peak in pore size distribution. However, there is no trace inflection in the region of $p/p_o = 0.35$ on the nitrogen sorption isotherms that would otherwise indicate the existence of smaller mesopores.

The illuminating information one can gain from the analysis of the materials TS-A is that even though it is amorphous, it possesses a bimodal with fairly narrow pore size distribution. It was synthesized in the mildest condition i.e. absence of any nitrogenate organic base under room temperature and atmosphere pressure. To my knowledge, the lowest temperature to synthesize bimodal titanosilicate at atmosphere pressure without nitrogenate organic base is 70°C [44]. The same nitrogen sorption and bimodal pore size distribution observation was reported in [44], [94] and [174]. If generally, when a material is prepared by sol-gel method under basic pH, the rate of hydrolysis is faster than the rate of condensation and the resulting material is essentially microporous [177], while under mild conditions, the rate of condensation is faster than the rate of hydrolysis generating mesoporous materials. A neutral pH leads to bimodal micro-mesoporous

material. This observation was reported by A. Keshavaraja et al. [131] by maintaining almost neutral pH in producing bimodal structure material. However, in this present research, there is no pH analyses performed to confirm that. It must be said that TPAOH and isopropyl alcohol (which is basic) used through out in the preparation of synthesis all samples.

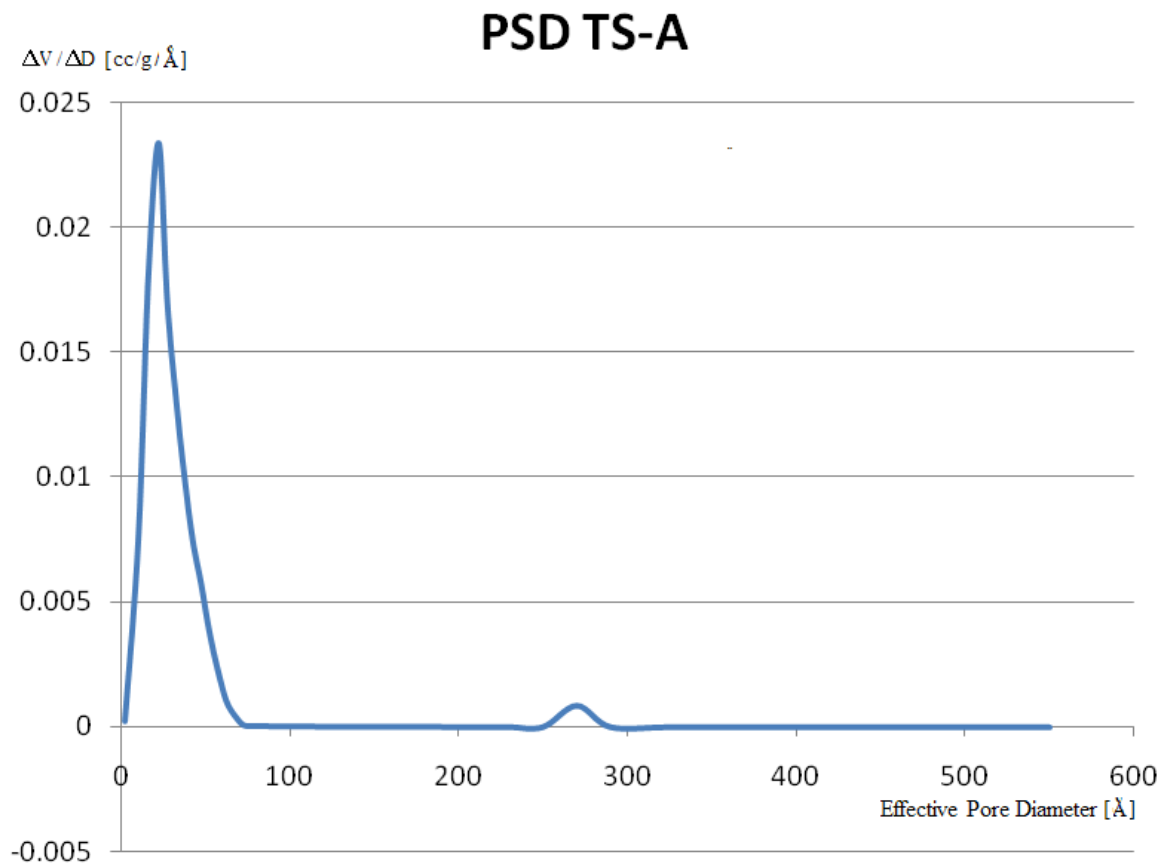


Figure 5.8-2 Pore size distribution (PSD) of the material (BJH analysis of the adsorption branch of the isotherm)

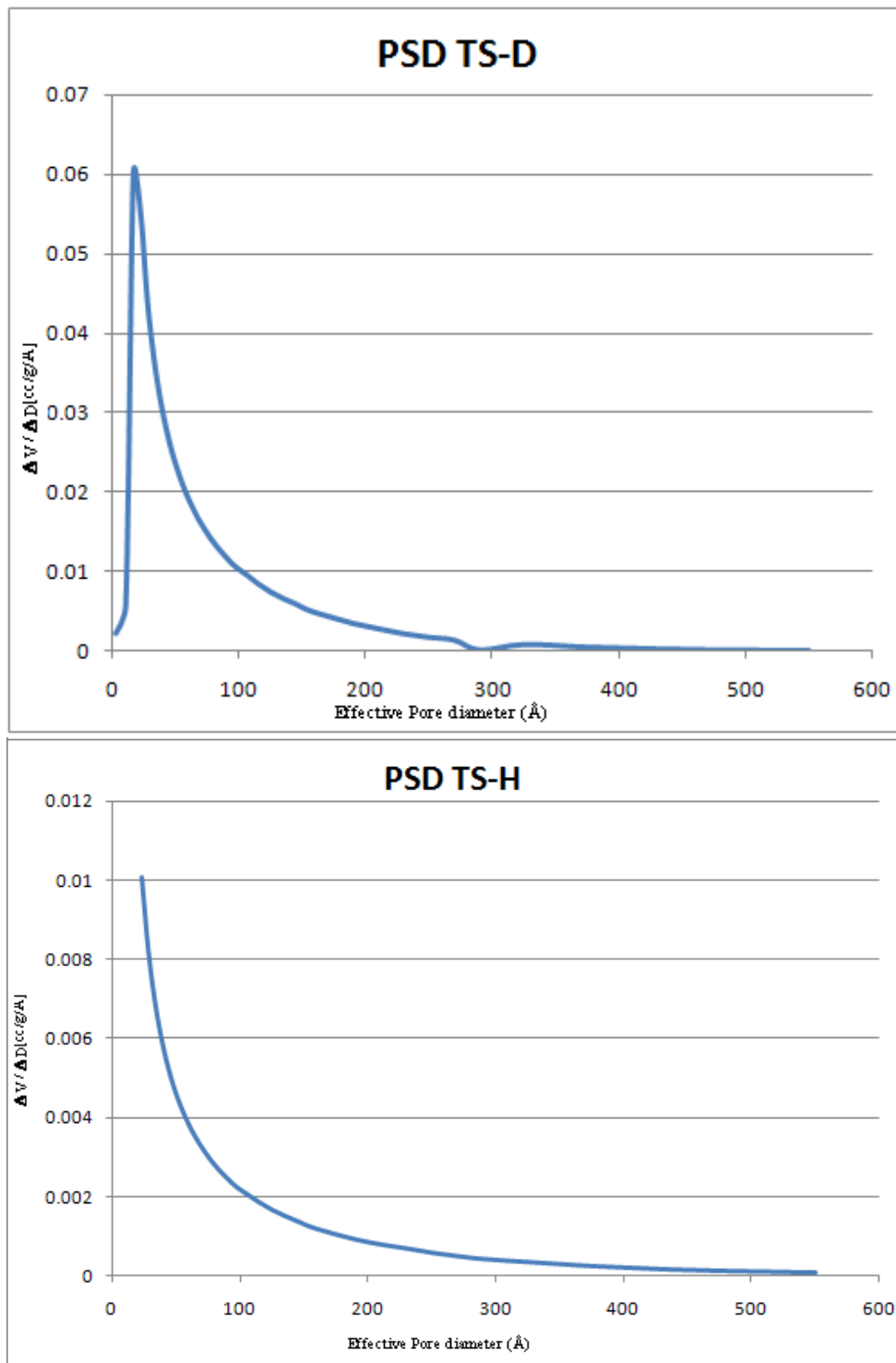


Figure 5.8-3 Pore size distribution (PSD) of the material (BJH analysis of the adsorption branch of the isotherm)

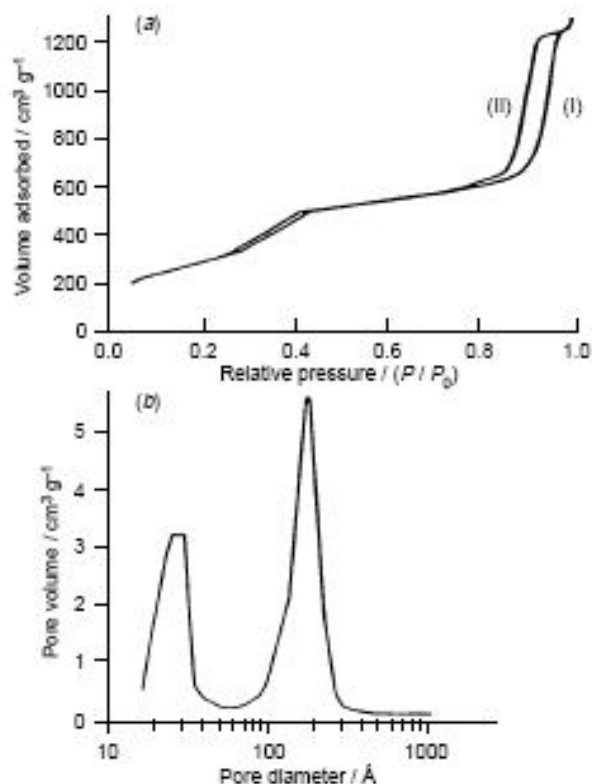


Fig. 2 (a) N_2 adsorption (I)–desorption (II) isotherms on the calcined sample and (b) the pore size distribution of the material

Figure 5.8-4 Nitrogen isotherm and PSD of double-mesopore silica prepare by Wang et al. [Source from ref. 176]

From **Figure 5.8-1**, it can be seen that nitrogen sorption curve on both TS-C and TS-D show hysteresis loop of combination *H2*- *H3* types. The same observation was reported by A.Corma and J. Diaz Cabanas [124] which also use self directing agent to prepare amorphous microporous molecular sieves. *H2* hysteresis loop commonly indicate well disordered pores [21] tend to be made up of interconnected networks of pores of different size and shape because of pore blocking and percolation phenomena [21,124]. Type *H3* hysteresis loop is usually exhibited by the non-rigid aggregates of platy particles or adsorbents containing slit-shaped pores. TS-D has a small surface area but a broad distribution of large mesopores indicates by capillary condensation at high p/p_0 . This was consistent with a narrow pore size distribution (PSD) of TS-D possessing a maxima at

190Å. It has a broad PSD compared to TS-H. The latter has a maxima at 27.5Å (**Figure 5.8-2** and **Figure 5.8-3**).

From **Table 5.8-1** and **Figure 5.8-1**, it could be seen that for TS-hybrid, the higher crystallization time generated products with reduced surface area and pores (except for sample D). The pores are not uniformly. The uniformity of the pore is indicated by a large hysteresis loop. This is associated with the sensitivity of the micelles template to temperatures which can disrupt the template formation.

For sample synthesized by conventional method in TPAOH (TS-E, TS-F, TS-G and TS-H), based on nitrogen sorption isotherm, all of them display hysteresis loop of combination *H1-H3* types indicating mesoporosity. Similar hysteresis loop was observed in mesostructured titanosilicates [76] and UL-TS-1 [124]. Sample TS-E has a type III adsorption curve consistent with a hydrophobic adsorbent [173]. Both the adsorption and desorption branches is very steep suggesting that the pores remain open at saturation pressure but until only to close at the lowest pressure. This phenomenon still could not be explained. While in TS-H nitrogen sorption isotherm, it can be seen that the hysteresis loop does not close at high relative pressure due to an artifact caused by the small surface area of the sample [177].

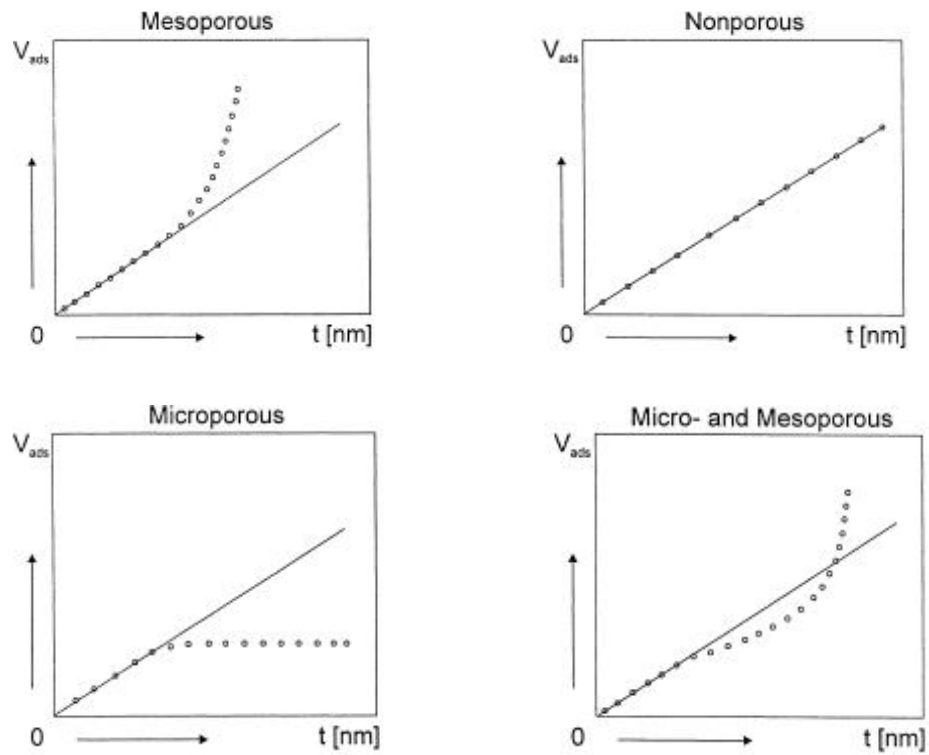


Figure 5.8-5 t-Plots of mesoporous, nonporous solids, microporous and micro- and mesoporous solids (References 22)

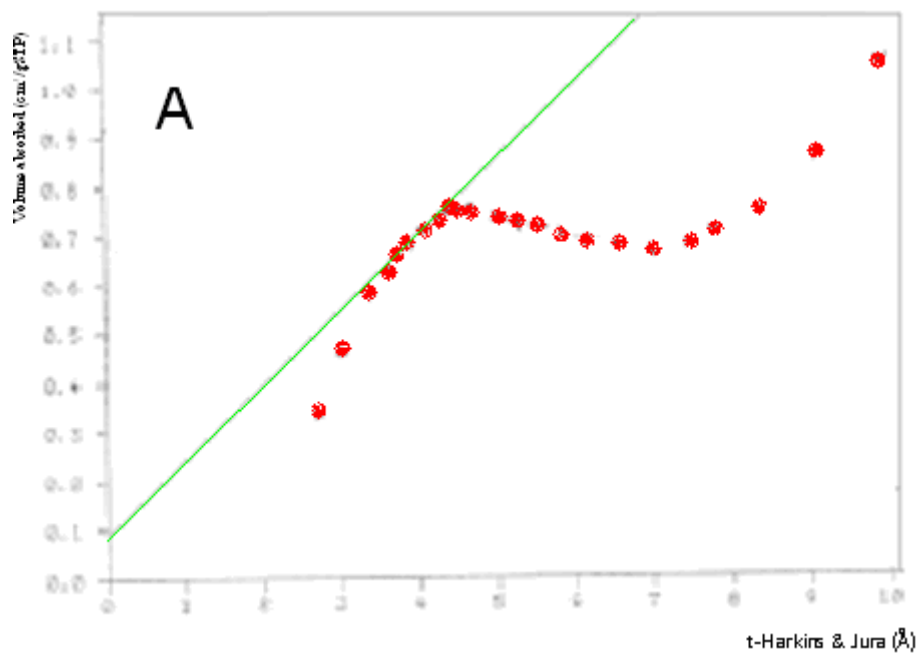


Figure 5.8-6 t-Plot of sample TS-A

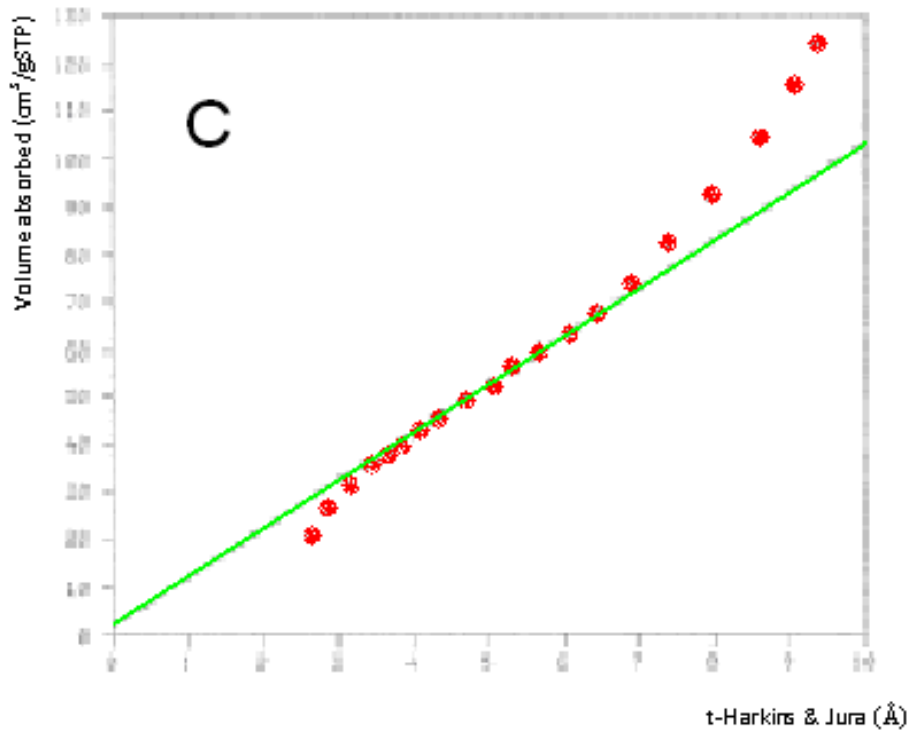
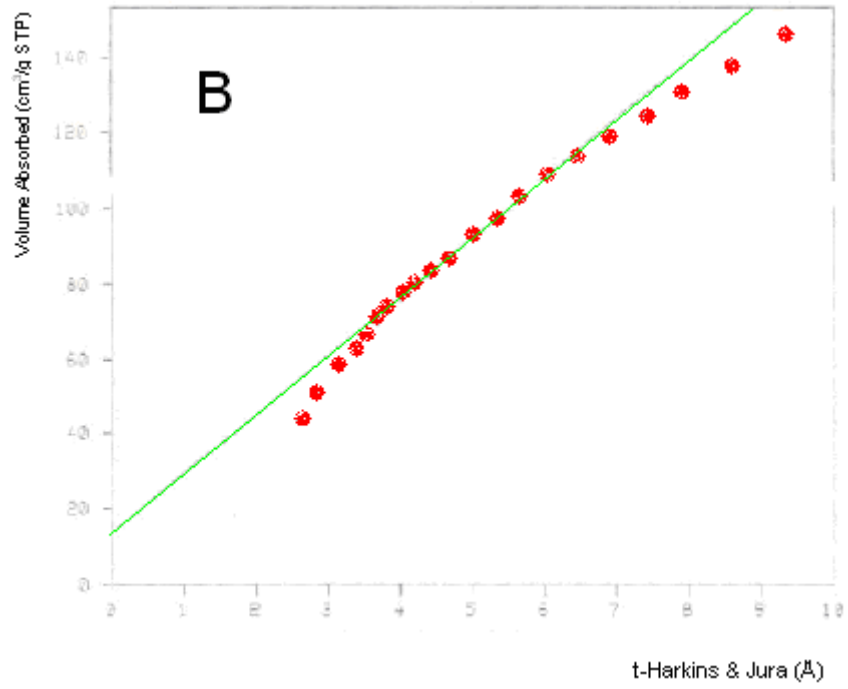


Figure 5.8-7 t-Plots of sample TS-B and TS-C

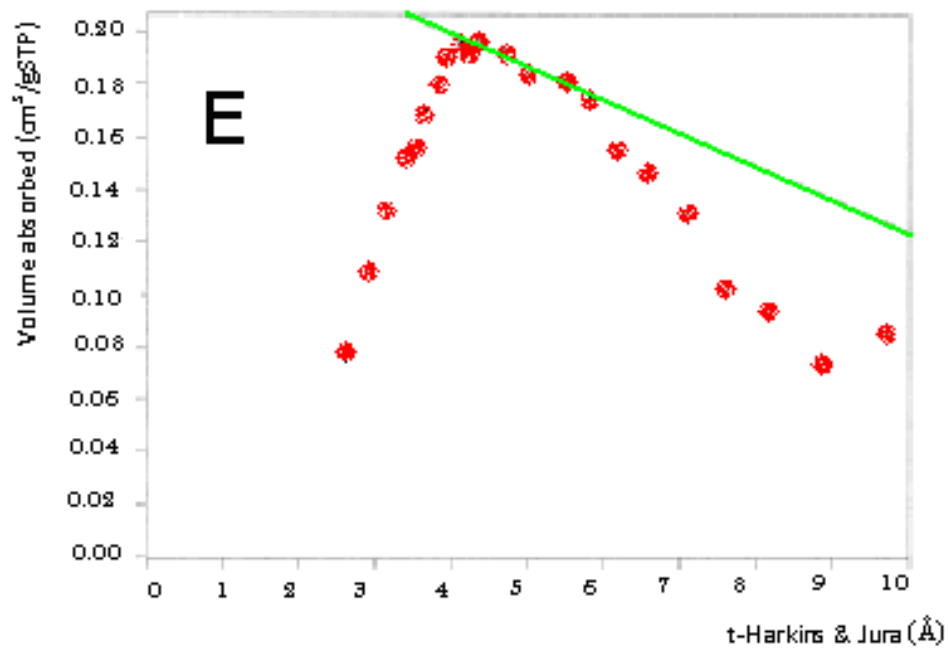
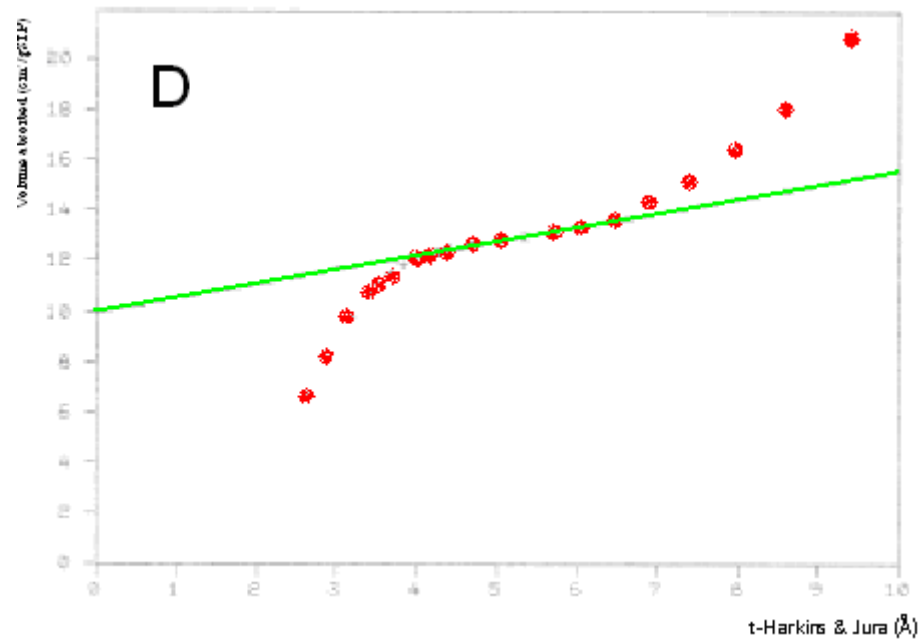


Figure 5.8-8 t-Plots of sample TS-D and TS-E

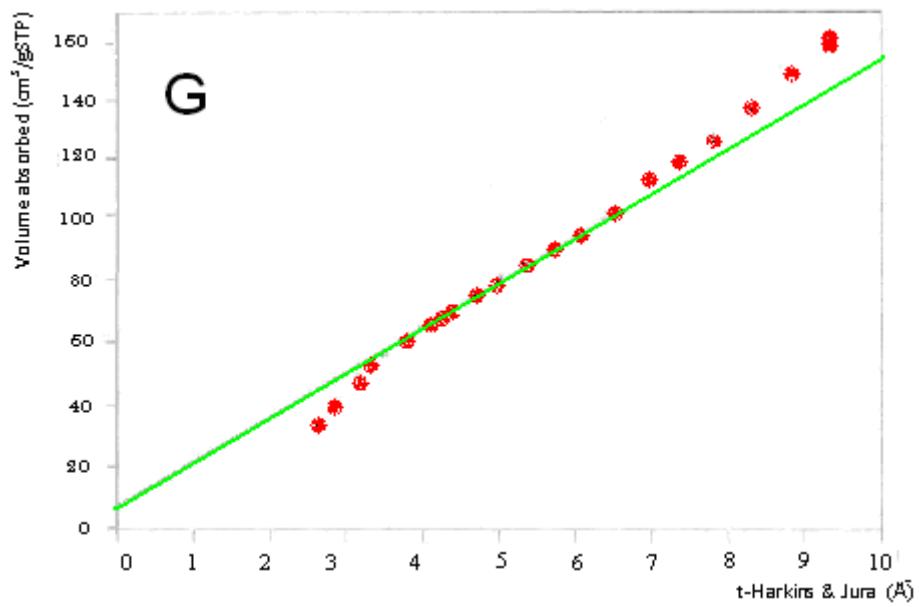
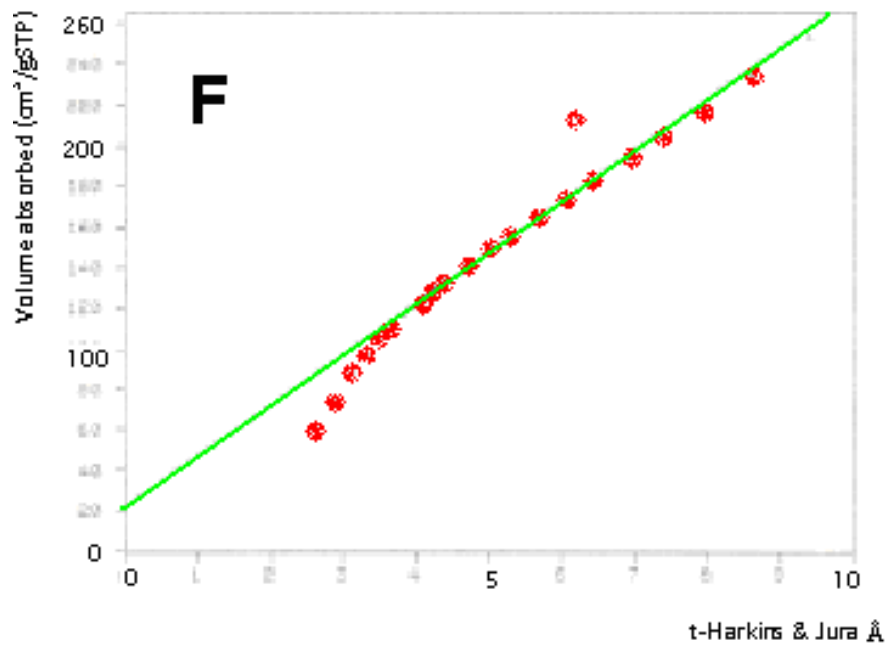


Figure 5.8-9 t-Plots of sample TS-F and TS-G

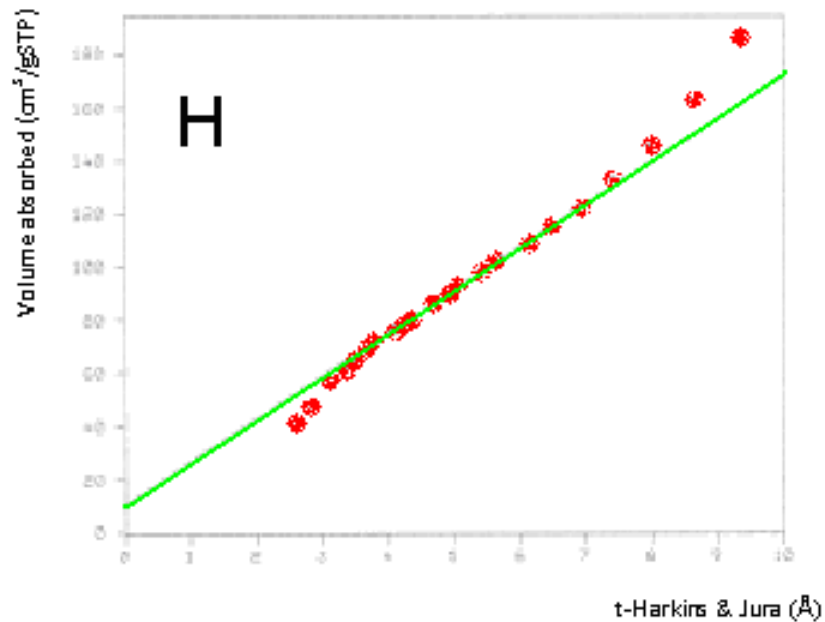


Figure 5.8-10 t-Plots of sample TS-H

The graph of abs vs. t is considered the t -plot [21,22]. If both reference and sample isotherms are identical, as is the case for nonporous solids, a straight line passing through or passing close to the origin, should be generated (**Figure 5.8-4**). The plot of the amount adsorbed versus ' t ' will be a straight line because of the adsorption is a layering process and the area for the adsorption does not change as the number of layers increases [179]. Horizontal departures from the straight line indicate the presence of micropores while vertical ones reveal mesopores. The micropore volume present is obtained from a straight line extrapolated to a positive intercept on the ordinate (**Figure 5.8-5**). [22].

If amount adsorbed versus t increases, then it indicates the presence of cylindrical pores, ink bottle pores or voids between closed packed spherical particles [179]. On the other hand, if it decreases this indicates slit shaped pores [179].

All adsorbents of TS- derived B,C,D,F,G and H show magnitude of the amount adsorbed increases which indicates the presence of cylindrical pores, ink bottle pores, or voids between closed packed spherical particles. On the other hand, adsorbent TS- derived A show the magnitude of the amount adsorbed have both increase and decreases which indicates apart from the presence of above forms mentioned, it also has slit-shaped pores.

Based on t-plots in **Figure 5.8-6**, **Figure 5.8-7**, **Figure 5.8-8**, **Figure 5.8-9** and **Figure 5.8-10**, it can be assumed that sample TS-A (**Figure 5.8-6**) and TS-D (**Figure 5.8-8**) are having both micro- and mesoporous solids (**Figure 5.8-5**). Generally, the t-plots of mesoporous materials pass through the origin implying the absence of micropores. However, all samples do not pass through the origin. The lowest micropore volume of $0.0003\text{cm}^3/\text{g}$ for adsorbent TS-E and the highest micropore volume of $0.045\text{ cm}^3/\text{g}$ for adsorbent TS-A recorded.

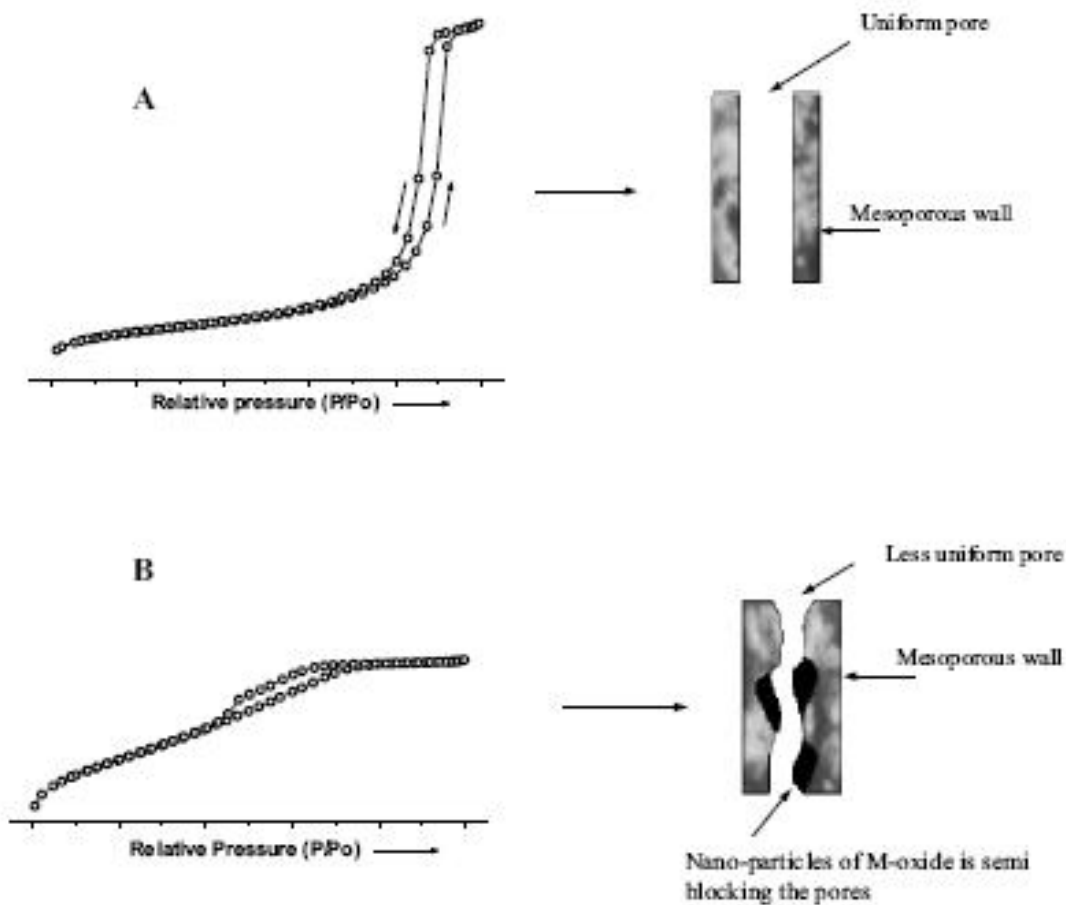


Figure 5.8-11 Illustrations for different type IV isotherms and their interpretation. The isotherm in A was observed for samples TS-E and TS-D, while the isotherm in B was observed for samples TS-A and TS-B. (Images copied from Ref. 62)

Roughly, we can distinguish two characteristic types of hysteresis loops. In the first case, (**Figure 5.8-11-A**), the loop is relatively narrow, the adsorption and desorption branches being almost vertical and nearly parallel (H1 hysteresis loop), which means that the isotherm is governed by delayed condensation, pores filling and emptying appear to occur in a narrow range on uniform near-cylindrical pores. While for isotherm in **Figure 5.8-11-B**, the hysteresis loop becomes broad, the desorption branch being much steeper than the adsorption, pores filling and emptying in a wide range on non-uniform pores (H2 hysteresis loop). This behavior can be explained by the formation of nano-particles of metal oxides inside the pores [62]. Micelles are known as effective templates to form nano-particles of metal oxides due to cage like behavior of the systems.

5.9 PRODUCT UTILIZATION STUDIES

5.9.1 Adsorption Characteristics of Adsorbents In Metal Solutions

The ability of adsorbents to remove a metal ion from aqueous solution can be expressed in terms of the amount of metal ions on the adsorbents (Q) and the distribution ratio (K_d). They can be calculated according to Eqs. (1) and (2):

$$Q = (C_0 - C_e) \times V/W \quad (1)$$

$$K_d = 10^3 Q/C_e \quad (2)$$

where Q is the amount of metal ion on the adsorbents (mmol/g), K_d is the distribution ratio of the metal (mL/g), V is the volume of the aqueous solution (L), W is the weight of the adsorbent (g), C_0 (mmol/L) and C_e (mmol/L) are the initial and final concentrations of the given ion in solution.

Table 5.9-1 Cu²⁺ Adsorption on all adsorbents

Adsorbent	Removal (%)	Uptake Q(mg/g)	K _d (mL/g)
A	56.19469	59.26667	1282.828
B	29.97788	31.61667	428.1201
C	19.13717	20.18333	236.6621
D	31.85841	33.6	467.5325
E	13.49558	14.23333	156.0102
F	15.48673	16.33333	183.2461
G	29.31416	30.91667	414.7105
H	30.64159	32.31667	441.7863

Table 5.9-2 Pb²⁺ Adsorption on three Adsorbents

Adsorbent	Removal (%)	Uptake Q(mg/g)	K _d (mL/g)
A	71.875	71.48333	2555.556
B	55.04261	54.74267	1224.329
C	48.08239	47.82037	926.1286
D	56.25	55.94347	1285.714
E	44.46023	44.21795	800.5115
F	45.73864	45.48939	842.9319
G	54.61648	54.31885	1203.443
H	55.46875	55.16648	1245.614

Table 5.9-1 and **Table 5.9-2** are the adsorption data of Cu²⁺ and Pb²⁺ respectively. It was found that adsorbent A possessed the highest loading capacity and distribution constant than the rest. The performance of the adsorbents decreases in the following order: A>D>H>B>G>C>F>E. The values of *Q* and *K_d* of adsorbent H are much smaller than

those of adsorbent A which use SDS as the surfactant and TPAOH as subsidiary structure-directing agent. The Q and K_d values of all adsorbents decreased in the order: $Pb^{2+} > Cu^{2+}$. This is in agreement with the sequence of hydrated radii (as shown in **Table 5.9-3**) which in turn determines the hydration energies.

The BET surface area and BET pore diameter of adsorbents are in the following order: $A > B > H > G > C > D > F > E$ and $F > E > H > G > A > B > D > C$ respectively (**Table 5.8-1**). It is not in agreement with the performance of the adsorbents. The uptake properties of the heavy metal ions on amorphous titanosilicate were considered complicated and not a simple relationship to pore diameter and surface area. Generally, the ionic and hydrated heavy metal ions both have a diameter smaller than the BET pore diameter size of all amorphous titanosilicate adsorbents. Sample TS-A (synthesized by hybrid surfactant) which show bimodal pore size distribution (as explained in section 5.8) and TS-H (synthesized by TPAOH only) have highest Q and K_d compared to the others adsorbents.

Table 5.9-3 Some Physical Parameters of Heavy Metal Ions in Solution (source from references 10 and references therein)

Metal	Ionic radius (Å)	Hydrated radius (Å)	Hydration energy (kJ/mol)	Solubility of hydroxides (pKs)
Lead	1.33	4.01	-1481	16.7
Copper	0.71	4.19	-2100	18.8

5.9.2 Equilibrium Time Study

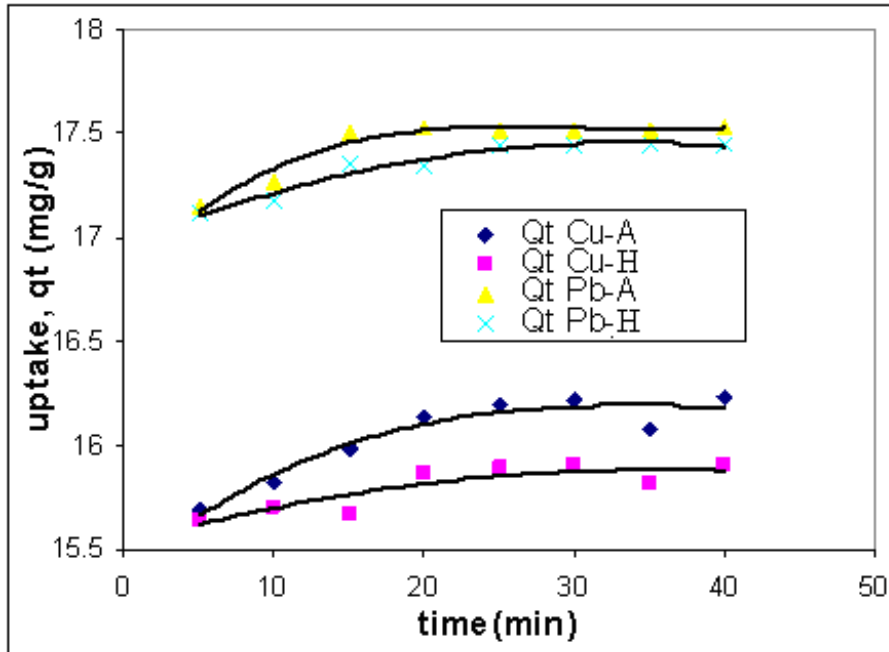


Figure 5.9-1 Contact Time Study for Metals Adsorption on Adsorbent A and Adsorbent H

Adsorption from a liquid is more difficult phenomenon to measure experimentally or described. When porous particle of adsorbent are immersed in a dilute solution, the pores is sufficiently larger in diameter than the ions diameter in the liquid, fill with liquid. The composition of the liquid in the pores differs from that of bulk liquid surrounding the adsorbent particles at equilibrium because of the differences in the extent physical adsorption among the the different molecules of the liquid mixtures.

Figure 5.9-1 shows the time profiles of adsorbent A and adsorbent H adsorption with Cu(II) and Pb(II) ions in aqueous solution respectively. The adsorption of Cu(II) and Pb(II) were rapid in the first 20 minutes and then followed by a slower rate of adsorption approaching an equilibrium after 35 minutes. The rate of heavy metals uptake and adsorption capacities of adsorbent A was higher than adsorbent H. The uptake and adsorption capacities of adsorbent TS derived A is higher than adsorbent TS derived H

for both ion metals possibly due to the adsorbent TS derived A has reasonably high surface area and micropore volume.

The author believed, based on nitrogen adsorption analysis (refer section 5.8), adsorbent TS-A have a combination of two pore range; the micropore range and macropore range which suggest it have small pore size with a reasonable porosity. Its bimodal pore size distribution provides good access of sorbate molecules to the interior network of adsorbent. High surface area provide large active site for either physical adsorption or chemisorption while slit shape of micropores provide space for storing most of adsorbed molecules due to their high dispersive force acting on adsorbate molecule. The mechanism of adsorption involve in micropores of adsorbent TS-A (which inavailable in adsorbent TS-H) is via the process of volume filling. Whereas for adsorbent TS derived H which have lower surface area compared TS-A, having pores in range macropores which only provide active site for physical sorption (van der waals adsorption) or chemisorption. The volume of macropore is so less which is negligible compared to the area contributed by the micropore, therefore, are of no significance in terms of adsorption capacity but they act as transport pores to allow adsorbate molecules to diffuse from the bulk into the particle interior of adsorbent. This is summarized graphically in **Figure 5.9-2**.

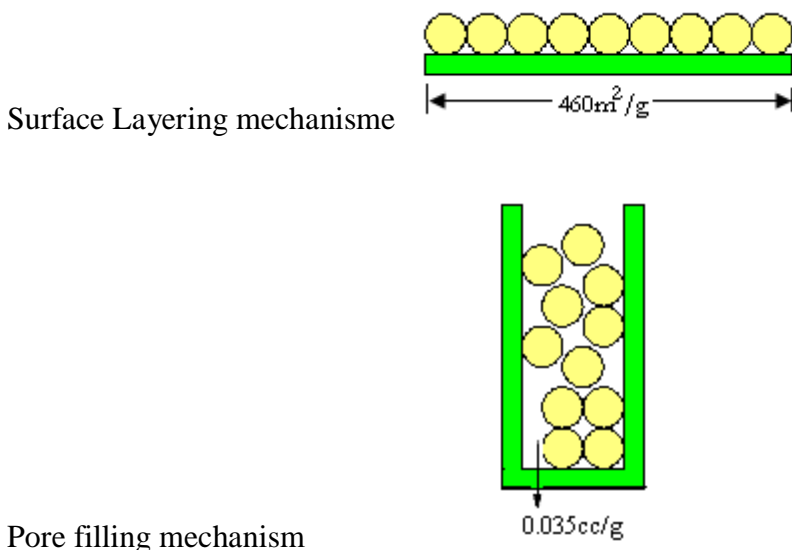


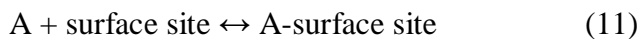
Figure 5.9-2 Possible adsorption mechanisms in adsorbent

From figure **Figure 5.9-1**, we note that residence time for Cu^{2+} solution is longer compared to Pb^{2+} which is in agreement with the hydrated radius of both metal ion (As shown in **Table 5.9-3**). Ions in aqueous solution tend to be hydrated radius especially copper which have higher pKs value than lead. Therefore, the author believe eventhough ion radii of Pb^{2+} is bigger than Cu^{2+} , hydrated Cu^{2+} which is inversely bigger than Pb^{2+} is regards as main factors of long residence time of copper uptake at equilibrium.

5.9.3 Adsorption Kinetics

In order to define the adsorption kinetics of heavy metal ions, the kinetic parameters for the adsorption process were studied for contact times ranging from 0 to 40 min by monitoring the percent removal of the heavy metals by the adsorbent. The kinetic of sorption describing the solute uptake rate which in turn governs the residence time of sorption reaction. Hence, kinetic sorption is important characteristic in order to define the efficiency of sorption. A solid with good capacity but slow kinetics is not a good choices as it means long residence time for adsorbates molecules to reach particle interior. On the other hand, a solid with fast kinetic but low capacity is not good either as it will required large amount of adsorbent for a given throughput

Generally, the adsorption of adsorbate (A) on the surface site can be represented by the following equation:



where A-surface site is the product. From this equation, the rate of adsorption is first order concerning the concentration of adsorbate in the solution, [A] and is also proportional to the amount of active surfaces on the sorbent [180,181]. If θ is the coverage fraction of the sorbent surface by the adsorbate, the rate of adsorption can be written as:

$$r_{ads} = K_{ad} [A](1-\theta) \quad (12)$$

where K_{ad} is the adsorption rate constant. The concentration of adsorbate, $[A]$ is usually used in large amount while the sorbent is in deficient amount in batch adsorption experiment so that the amount of sorbent can be negligible. Hence, the equation (12) is changed as follows:

$$r_{ads} = K_{ad} (1-\theta) \quad (13)$$

since the adsorption rate is independent towards the concentration of adsorbate $[A]$. If the adsorption keeps on up to the maximum monolayer coverage and reaches the equilibrium, the equation (13) can be written as:

$$r_{ads} = \frac{dq_t}{dt} K_{ad} (q_e - q_t) \quad (14)$$

where, q_t is the amount of adsorbate sorbed (mg/g) at any time, t and is equivalent to the coverage fraction, θ on the sorbent by the adsorbate and q_e is the amount of adsorbate sorbed at equilibrium which is equivalent to unit coverage. From this equation, since there is only one product $(q_e - q_t)$, the order of the adsorption is forced to one. Because of the order of the adsorption is approximated to the first order, it is called pseudo-first order with the pseudo- means apparently similar to. If the adsorption reaction is approximated to the second order with respect to $(q_e - q_t)^2$, it is called pseudo-second order and the equation is as follows:

$$\frac{dq_t}{dt} = K' (q_e - q_t) \quad (15)$$

where and K' is the adsorption rate constants for pseudo-first and pseudo second order, respectively. When equation (14) and (15) is integrated between the limits, $t = 0$ to $t = t$ and $q_t = 0$ to $q_t = q_t$, it becomes

$$\log (q_e - q_t) = \log q_e - K_{ad} t / 2.303 \quad (5)$$

$$1/(q_e - q_t) = 1/q_e - K' t \quad (6)$$

$$t/qt = 1/(K'q_e^2) + t/q_e \quad (7)$$

Equation (5) is for pseudo-first order (also known as Lagergren first-order model [141]), equation (6) is Lagergren second-order model and equation (7) is for pseudo-second order (also known as Ho's second-order model). If the adsorption follows the second order, a plot of t/q against t will yield straight lines. Hence, the rate constant and the amount of adsorbate sorbed on the sorbents at the equilibrium can be determined.

Linear plots of $\log (q_e - q_t)$ versus t , t/q_t versus t and $1/(q_e - q_t)$ versus t are shown in **Figure 5.9-3**. The values of the adsorption equilibrium, q_e , Lagergren rate constant, K_{ad} , pseudo second order rate constant K' , pseudo second order rate constant, K , calculated amount of adsorption equilibrium, q_e , and the correlation coefficient, R^2 which is derived from the pseudo second-order equation are shown in **Table 5.9-4**. It was found that the pseudo second-order provided the best description of the data obtained as shown having the highest values of correlation coefficients among the models used in the study. This indicate that the rate limiting step for both adsorbent may be a chemisorption involving forces through sharing or exchange of electron between both sorbate and adsorbent. In addition, the adsorption of both ions on both adsorbents is not only involves chemisorption but can also be adsorbed physically onto the surface of the adsorbents since the surface area of adsorbents is high. This explains the multilayer adsorption occurs during the adsorption, hence the sorption of uptake increase rapidly with time.

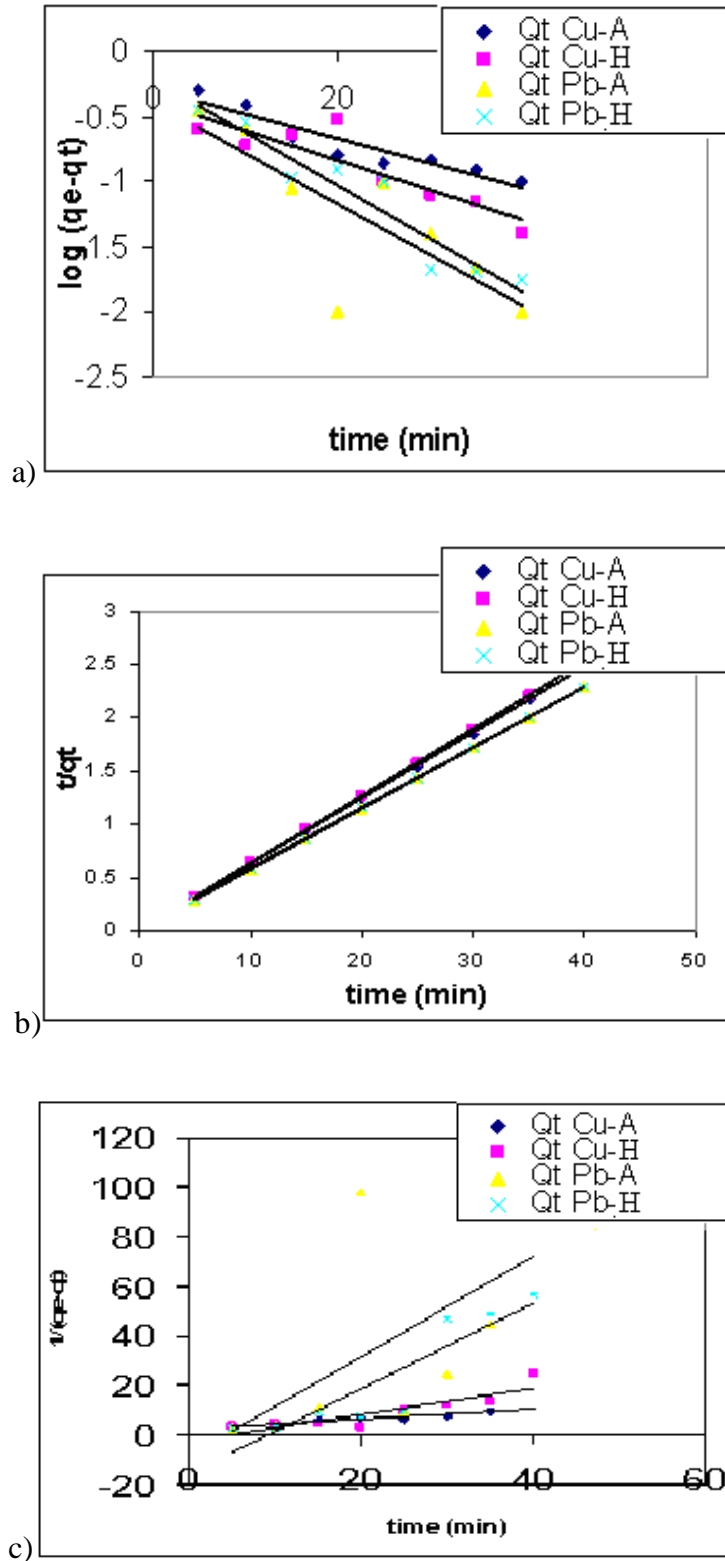


Figure 5.9-3 (A) First-Order Lagergren, (B) Pseudo Second-Order And (C) Lagergren Second Order Plots for Heavy Metals Adsorption on Adsorbent and Adsorbent D

Table 5.9-4 Langergren First-Order, Pseudo Second-Order and Langergren Second Order Constants and Correction Coefficient

Adsorption kinetics parameter	Adsorbent	TS-A		TS-H	
	Metal	Cu	Pb	Cu	Pb
Lagergen 1 st order	K _{ad}	0.1041	0.2333	0.1370	0.1723
	R ²	0.6346	0.945	0.6541	0.935
Pseudo second-order	K'	0.2599	0.4905	0.4467	0.5345
	R ²	0.9999	1.0000	1.0000	1.0000
Lagergen second-order	K	0.9578	0.1138	0.4688	1.7170
	R ²	0.3477	0.2551	0.3278	0.8207

5.10.4. Adsorption Isotherms

The adsorption data have been analyzed by fitting to the linearized form of the Langmuir and Freundlich isotherms. In comparative analysis of Langmuir Linear method, Kumar [38] have showed that Langmuir-2 best fitted for adsorption at room temperature. Hence, Langmuir-2 isotherm equation were tested within metal ion concentration ranging from 20–100 ppm. The linearized form of Langmuir-2 can be written as [8,11,13]

$$1/q_e = 1/(K_a q_m)(1/C_e) + 1/q_m \quad (6)$$

The Langmuir constants, q_m (maximum adsorption capacity corresponding to complete monolayer coverage) and K_a (values for Langmuir-2) are predicted from the plot between $1/q_e$ versus $1/C_e$ which are shown in **Figure 5.9-4** for adsorbent A and H.

The Freundlich adsorption isotherm assumes that different sites are involved with several adsorption energies, so it can be applied to nonideal adsorption on heterogeneous surfaces as well as multilayer adsorption. The Freundlich model is expressed as :

$$\ln q_e = \ln K_f + 1n(\ln C_e) \quad (7)$$

where q_e is the amount of metal ions adsorbed at equilibrium time,

C_e is equilibrium concentration of metal ion in solution.

K_f and n are isotherm constants which indicate the capacity and the intensity of the adsorption.

The intercept and slope of plot between $\ln q_e$ and $\ln C_e$ [11,146]. **Figure 5.9-5** gives results on Freundlich isotherm fittings for both adsorbent. The Langmuir-2 and Freundlich models parameter and statistical fits of the sorption data are given in **Table 5.9-5**. Both adsorption isotherm reasonably describe the adsorption isotherm for both Cu^{2+} and Pb^{2+} adsorption.

We can also evaluate whether the values of Langmuir constants indicate favorable condition for adsorption. According to Hall et al. [17] and others researchers [18,36], the essential features of the Langmuir isotherm can be expressed in terms of equilibrium parameter K_L which indicates the shape of the isotherm. It can be defined by the following relationship:

$$K_L = 1/(1 + K_a C_o) \quad (8)$$

Where K_L is a equilibrium parameter or dimensionless separation factor, C_o the initial concentration (mg/L), K_a the Langmuir constant (l/mg). The parameter K_L indicates the shape of the isotherm and nature of the adsorption process [$K_L > 1$: Unfavorable; $K_L = 1$: Linear; $0 < K_L < 1$: Favorable; $K_L = 0$: Irreversible]. The value of K_L obtained (shown in table 5.10.4.1) were in the between 0 and 1 indicating a highly favorable adsorption of Cu(II) and Pb(II) onto adsorbent TS-A and TS-H.

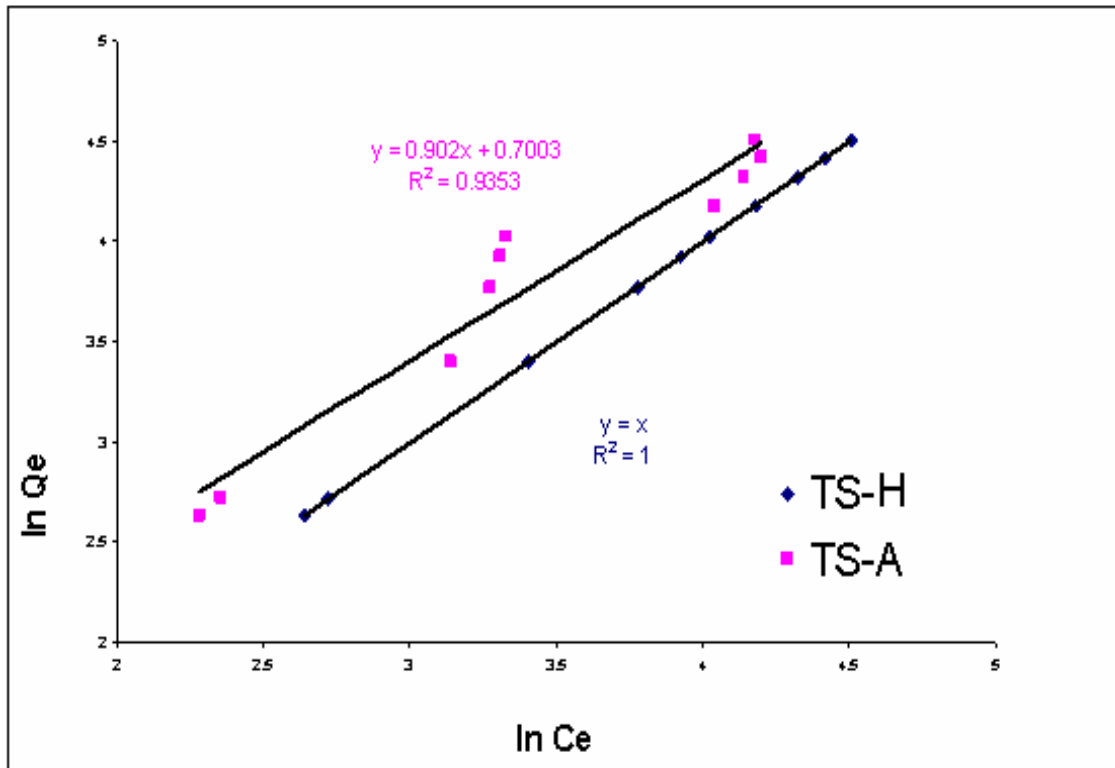
Based on R^2 values in table **Table 5.9-4**, almost all experimental data demonstrated are in general agreement with both Langmuir isotherm and Freundlich isotherm model. This is because the surface of adsorbent A is not uniform (based on SEM result, section 5.4) which creates the heterogeneity sites for both ions to be adsorbed onto adsorbent TS [182]. Thus, the adsorption behavior of both Pb and Cu ions onto both adsorbent TS-A

and TS-H mostly belong to a multilayer adsorption, hence, identical to the assumptions of the Freundlich isotherm [26]. These results in agreement with BET result which show appearance of hysteresis loop indicate heterogeneity sites adsorbents. These result also in concurrence with Kinetic studies. Based on Langmuir-2 parameter, adsorbent A give highest maximum adsorption capacity, q_m for both metal ions compared to adsorbent H. this in agreement with the fact that bigger pore sizes creates wider surface area hence giving more exchange sites and resulted in higher adsorption capacity. Although pore sizes of adsorbent TS-H is bigger than adsorbent H (based on nitrogen adsorption analysis results), the micropore volume and surface area of adsorbent A is higher which indicate micropore filling does have influence to adsorption capacity rather than depend on surface layer alone.

The reason that sorption capacity of Cu^{2+} is lower than Pb^{2+} is attributed to larger hydrated radius of Cu^{2+} which gives rise to weaker interaction between Cu^{2+} and negatively charged Ti. The Langmuir isotherm constant (K_a) can be used to indicate the affinity of adsorbent toward the heavy metal ions [10]. It is seen that from **Table 5.9-3**, the order of affinity $\text{Cu} > \text{Pb}$ for both adsorbents A & H are in agreement with the fact that Pb (II) have a lower hydration energy than Cu (II) (as shown in **Table 5.9-3**). It should also be noted that it might be the effect of the formation of copper hydroxide on the observed adsorption as Cu has the largest pKs values compare to Pb (II).

$1/n$ is the surface heterogeneity factor [26]. For Cu^{2+} adsorption through adsorbent H and Pb^{2+} adsorption through adsorbent A, both gives $1/n < 1$ which corresponds to a normal Langmuir isotherm and indicates only one mechanism is dominant during the reaction [146]. While Cu^{2+} adsorption through adsorbent A gives $1/n > 1$ which is indicative of a strong interaction between the molecules of adsorbate. Whereas Pb^{2+} adsorption through adsorbent H, give $1/n = 1$ show that the partition between two phases is independent on the concentration [146].

a)



b)

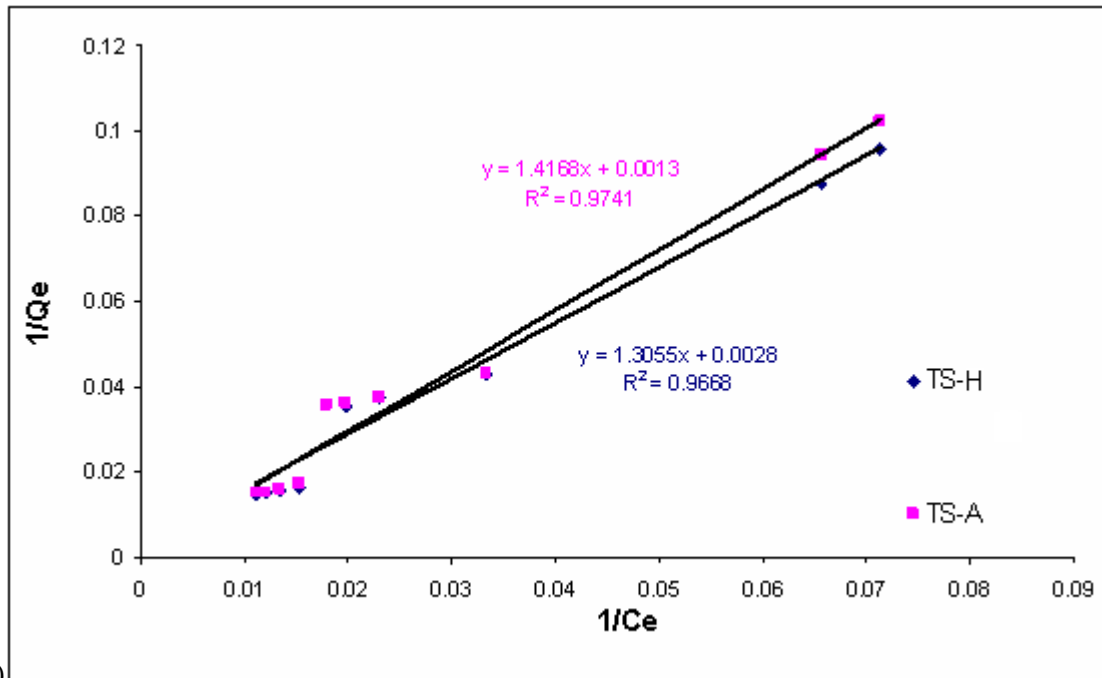


Figure 5.9-4 a) Langmuir-2 plots for Cu (II) adsorption on adsorbent A and H b) Langmuir-2 plots for Pb II adsorption on adsorbent A and H

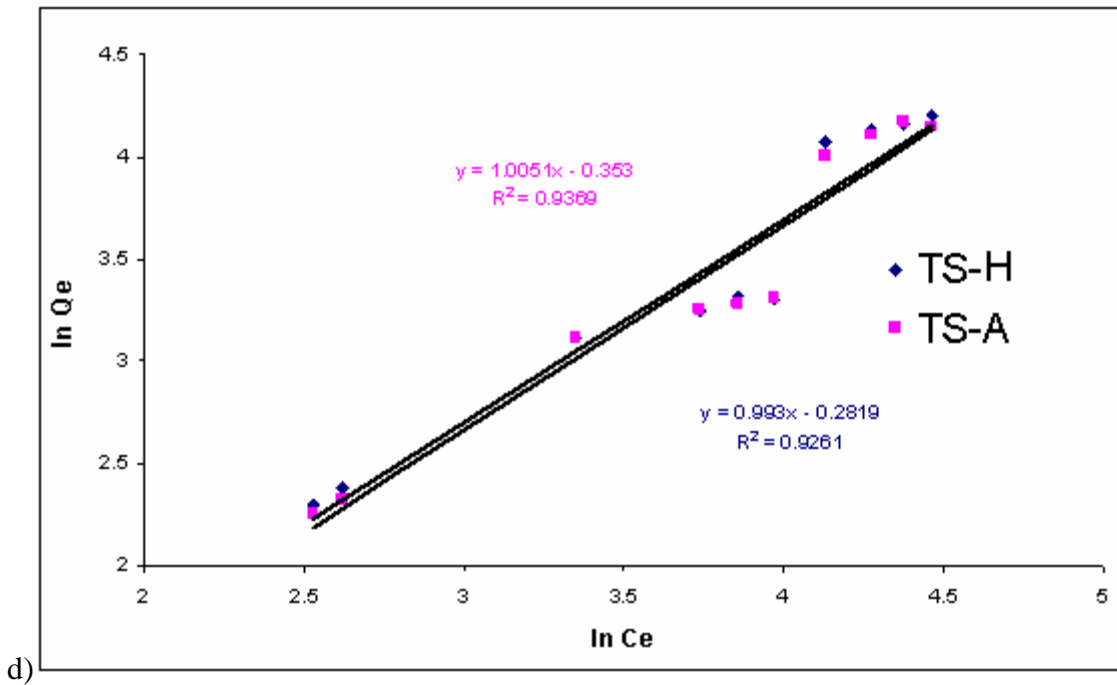
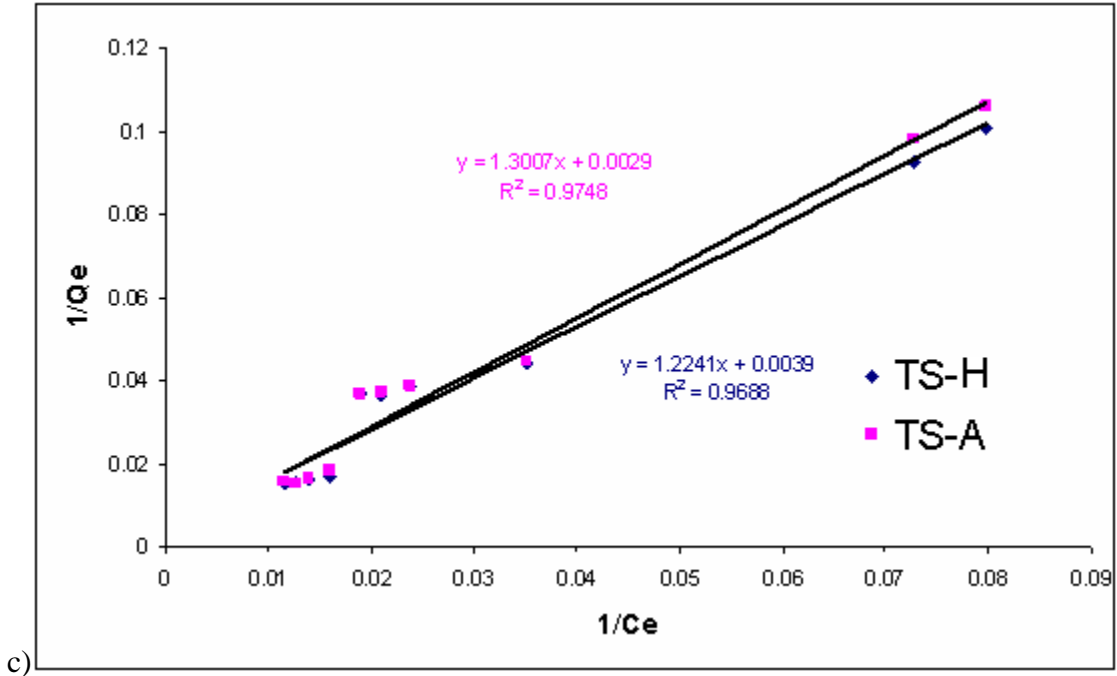


Figure 5.9-5 c) Freundlich plots for Cu (II) adsorption on adsorbent A and H, d) Freundlich plots for Pb (II) adsorption on adsorbent A and H

Table 5.9-5 Isotherm Parameters Obtained by Using Linear Method (q_m : mg/g; K_a : L/mg; K_F : mg/g)

Adsorbent	Langmuir-2				Freundlich		
	q_m	K_a	R^2	K_L	1/n	K_F	R^2
Cu^{2+} adsorption							
TS-A	344.8	0.0022	0.9750	0.9579	1.005	0.702	0.937
TS-H	256.4	0.0032	0.9690	0.9398	0.993	0.754	0.926
Pb^{2+} adsorption							
TS-A	769.2	0.0009	0.9740	0.9823	0.902	2.014	0.935
TS-H	357.1	0.0021	0.9670	0.8597	1	1	1

CHAPTER 6 CONCLUSION AND RECOMMENDATION

6.1 CONCLUSION

The following are the major findings:

- 1) An amorphous titanosilicates has been successfully produced.
- 2) In the presence of SDS only, the titanium is present as a tetrahedrally coordinated element in the zeolites framework and
- 3) without the presence of both SDS and TPAOH, the anatase TiO_2 was present as TiO_2 (anatase situated outside the zeolite framework).
- 4) In the presence of TPAOH only, the formation of anatase TiO_2 can be prevented for samples subjected to a protracted crystallization time (18h) but,
- 5) in hybrid surfactant (in which both SDS and TPAOH are present), titanium is tetrahedrally coordinated in the zeolite framework even at 0h crystallization.
- 6) Both samples at Si/Ti ratio 10:1 generate bands at higher intensity due to the amorphous structures of samples. Sample at Si/Ti ratio: 33 give stronger band and lower intensity.
- 7) SDS is a good template agent as it is completely removed from the product.
- 8) In the presence SDS, Ti-O-alkyl band is sharper and stronger in the SAM templated with hybrid surfactant (SDS and TPAOH). The band is broader and shallower for SAM not templated with any surfactant.
- 9) The FTIR spectra of all calcined samples prepared in hybrid surfactant and in the presence of TPAOH only show the splitting of the band at $\sim 550 \text{ cm}^{-1}$ (except for sample

TS-C and TS-G) and obvious band at $\sim 960 \text{ cm}^{-1}$ (except for TS-E), which are characteristic of nanocrystals and titanium framework, respectively

10) The size of SAM templated with SDS only is smaller and irregular. This sample gives mostly twin aggregate (spherical to oval shape morphology). However,

11) the size of SAM not templated with SDS, without TPAOH, is larger and more irregular. Whereas,

12) sample prepared in the presence of TPAOH give spherical to hexagonal morphology. Samples prepared in hybrid surfactant generated a more uniform structure with no aggregates due to cooperative behavior of SDS and TPAOH.

13) The product for SAM templated with SDS has an excellent thermal stability at 425-550°C and weight retention of up to 62.5 wt % whereas

14) for sample synthesized in hybrid surfactant and TPAOH only, there is slight changes in the temperature range between 650-800 °C which show unstability of titanosilicate.

15) Sample synthesized in hybrid surfactant exhibited higher BET surface area but small pore diameter and lower pore volume (from table 5.7.1). The micropore volume tend to decrease according to crystallization times. However,

16) sample synthesized in only TPAOH a higher crystallization time enhanced surface area.

17) TS-A, had the highest surface area despite its room temperature preservation compared to the other well known microporous titanium silicate. The latter requires elevated temperature preparation steps

18) In TS-A nitrogen sorption curve, two separate hysteresis are seen, one expressed as H2 hysteresis loop followed by a flat curve, corresponding to the filling of microporous belonging to zeolitic structure [89], and another hysteresis expressed as H1 hysteresis

loop as defined by IUPAC [45]. This leads support to the presence of a bimodal pore size distribution (BJH analysis of the adsorption branch of the isotherm).

19) The preliminary study showed that the adsorbent A and adsorbent D can be used effectively in the removal of Cu (II) and Pb (II) from aqueous solution through adsorption.

Synthesized TS-1 using SDS and combination of SDS and TPAOH as a template from TNBT and TEOS was successfully achieved. It was found that the synthesized product exhibited better adsorption properties compared to the counterpart using the TPAOH only as the surfactant.

The advantages of TS-hybrids produced are:

1. There was no requirement for the costlier TPAOH (the usual template for crystalline TS-1 production).
2. The preparation methods is simpler than that of TS-1 conventional preparation method
3. Products produced by hybrid surfactant, aged at room temperature, has a bimodal pore size distribution similar with MMATS [174]. Therefore it is considered accessible to bulkier molecules
4. It also leads to the production of amorphous titanosilicate with high surface area of up to $\sim 460 \text{ m}^2/\text{g}$ possessing small(8\AA) to large(up to 221\AA) pore diameters
5. A significant difference between the present amorphous titanosilicate and TS-1 is that TS-1 are crystalline after prolonged heating (crystallization in autoclave and calcinations) for more than 550°C while the amorphous titanosilicate produce does not undergo any phase transformation under similar conditions indicating its much higher structural stability.

6.2 CONCLUSION FOR PRODUCT UTILIZATION

TPAOH and SDS were used in combination as hybrid templates to produce mesoporous adsorbents. It was found that the synthesized product exhibited better adsorption properties than the counterpart using only TPAOH as the surfactant. It eliminates the tedious step of having to use special crystallization vessel to run samples at high temperatures and high pressures. This adsorbent has a high adsorption capacity mainly due to the large and well-proportioned pore size. The study shows that the adsorbent A and adsorbent H can be used effectively in the removal of Cu(II) and Pb(II) from aqueous solution through adsorption. The pseudo second-order model provided the best description for the experimental data obtained compared to first order Lagergren and second order kinetic models as shown in the correlation coefficients. Freundlich and Langmuir isotherm does well to represent the experimental adsorption data.

6.3 RECOMMENDATION

A few more characterization have to be done such as

- 1) utilize X-ray scattering techniques to obtain interatomic vectors in the radial electron density distribution. While peak in XRD pattern characterize crystalline material, peaks in the radial electron density distribution characterize and serve as a finger print for amorphous material which lack a long range order characteristic of crystalline materials
- 2) utilize the advantage of bimodal pores of the samples in application of oxidation of bulky hydrocarbons
- 3) support confirmation of a double pore system by TEM images
- 4) further complete studies on the material with additional research on different parameter such as effect of Si/Ti ratio, Si/OH⁻ ratio, SDS/Si/Ti ratio and calcinations temperature.
- 5) for FTIR characterization, do evacuation on sample in order to reconfirm that 960cm⁻¹ band in spectra indeed associated with tetrahedral Ti.
- 6) in addition to the adsorption mechanism, further studies on other mechanism such as ion exchanger or complexation that may be involved in the uptake process of the heavy metal ions in amorphous titanosilicate could be done
- 7) further experiment to studies the competitive ability on the heavy metal ions with proton and alkali metal cations for the adsorption sites on amorphous titanosilicate surface

PUBLICATIONS

SYMPOSIUM

1. A. Othman and I. M. Tan Zeolite growth in hybrid surfactant-templated and its application for heavy metal removal Accepted for National Postgraduate Conference, NPC Conference Publishing, Chemical Engineering Department, Universiti Teknologi Petronas, 31750 Tronoh, Perak, Malaysia

REFERENCES

- [1] Keane, M. A., Removal of Heavy Metals from Aqueous Media by Ion Exchange with Y Zeolites. U.S.A.: Marcel Dekker Inc. 2003.
- [2] Kirk, R. E. & Othmer, D. F., Kirk-Othmer *Encyclopedia of Chemical Technology*, USA : JohnWiley & Sons, Inc. 1979.
- [3] Ruiz-Manriquez, A., Magaña, P. I., Lopez, R., Guzman, R., Biosorption of Cu by *Thiobacillum ferrooxidans*, *Bioprocess Engineering*. Elsevier. **18**. pp. 113-118. 1998.
- [4] Eva Lotta Andersson, E.L., “Analysis Of Various Bioreactor Configurations For Heavy Metal Removal Using The Fungus *Penicillium Ochro-Chl*”. MSc Thesis. Worcester Polytechnic Insitute. 1999. unpublished.
- [5] online; www.water.gov.my/index.php Jabatan Pengairan dan Saliran Malaysia (JPS). 2008.
- [6] Xu, Y.M., Wang, R. S., Wu, F. Surface Characters and Adsorption Behavior of Pb (II) Onto a Mesoporous Titanosilicate Molecular Sieves, *Journal of Colloid and Interface Science*. Elsevier. **209**, pp. 380-385 .1999.
- [7] Bhattacharya, K. G., Gupta, S.S., Kaolinite, Montmorillonite and Their Modified Derivatives As Adsorbent for Removal of Cu(II) from Aqueous Solution, *Separation & Purification Technology* **50**, Elsevier, pp. 388-397. 2006.
- [8] Puangngam, M., Unob, F. Preparation and Use of Chemically Modified MCM-41 and Silica Gel As Selective Adsorbents for Hg (II) Ions, *Journal of Hazardous Materials*. Elsevier .2007.

- [9] Okieimen, F.E., Sogbaike, C.E., Ebhoaye, J.E. Removal of cadmium and copper ions from aqueous solution with cellulose graft copolymers, *Separation & Purification Technology* **44**, Elsevier, pp. 85-89.2005.
- [10] Lv, L., TSoi, G., Zhao, X.S. Uptake Equilibria and Mechanisms of Heavy Metal Ions on Microporous Titanosilicate ETS-10, *Ind. Eng. Chem. Res.* **43**, pp.7900-7906. 2004.
- [11] Sen, T.K., Sarzali, M., Removal of Cadmium Metal Ion (Cd^{2+}) From Its Aqueous Solution By Aluminium Oxide (Al_2O_3): A Kinetic and Equilibrium Study, *Chem. Eng. J.* Elsevier. pp. 1-7. 2008.
- [12] Karamanis, D., Assimakopoulos, P.A., Efficiency Of Aluminium-Pillared Montmorillonite On The Removal Of Cesium and Copper from Aqueous Solutions, *Water Research*. Academic Press Inc. **41**, pp. 1897-1906. 2007.
- [13] Tiwari, D., Kim, H. U., Lee, S.M, Removal Behavior Of Sericite For Cu(II) And Pb(II) From Aqueous Solutions: Batch And Column Studies. *Separation & Purification Technology*, **57**, Elsevier, pp. 11-16. 2007.
- [14] Choi, J.H., Kim, S.D., Noh, S.H., Oh, S.J., Kim, W.J., Ads. Behavior of Nano-Sized ETS-10 and Al Substituted-ETAS-10 In Removing Heavy Metal Ions, Pb^{2+} and Cd^{2+} , *Microporous & Mesoporous Materials*. **87**, Elsevier, pp. 163-169. 2006.
- [15] Foster, C., Wastewater Treatment and Technology. Thomas Telford publishing. 2nd edition. pp. 273-297. 2003
- [16] Tan, B., Lehmler, H., Vyas, S.M., Knutson, B.L., Rankin, S.E., Large- and Small-Nanopore Silica Prepared with a Short-chain Cationic fluorinated Surfactant. IOP Publishing Ltd. pp S502–S507. 2005.

- [17] Hall, K.R., Eagleton, L.C., Acrivos, A., Vermeulen, T., Pore- and Solid-Diffusion Kinetics in Fixed-Bed Adsorption under Constant-Pattern Conditions. *Ind. Eng. Chem. Fundam.* **5**(2). pp. 212–223. 1966.
- [18] Kundu, S. & Gupta, A.K., Adsorption Characteristics of As(III) from Aqueous Solution on Iron Oxide Coated Cement (IOCC). *Journal of Hazardous Materials.* **142**. pp. 97–104. 2001
- [19] Crompton, T. R., *Toxicants in the Aqueous Ecosystem*. New York: John Wiley & Sons, Inc. 1997.
- [20] Frederic, R. S., *Environmental Geochemistry of Potentially Toxic Metals*, Springer Verlag. 2002
- [21] Trunshke, A., *Modern Methods in Heterogeneous Catalysis Research; Surface Area and Pore Size Determination*. Presentation Slides. 2007. unpublished.
- [22] Rouquerol, F., Rouquerol, J., Sing, K., *Adsorption Powders and Porous Solids, Principles, Methodology and Applications*. Academic Press. 1999.
- [23] Sebastian Storck, S., Bretinger, H., Maier, W.F., Characterization of Micro- and Mesoporous Solids by Physisorption Methods and Pore-size Analysis. *Applied Catalysis A: General.* **174**. pp. 137-146. 1998.
- [24] Poots, V.J.P., McKay, G. Healy, J.J. Removal of Basic Dye from Effluent Using Wood As an Adsorbent, *Journal of Water Pollution Control*. Elsevier. **50**, pp. 926-935. 1978.

- [25] Zhao, G. X. S., Lee, J. L., Chia, P. A., Unusual Adsorption Properties of Microporous Titanosilicate ETS-10 Toward Heavy Metal Lead, *Langmuir*, **19**, pp. 1977-1979. 2003.
- [26] Yang, H., Xu, R., Xue, X., Li, F., Li, G., Hybrid Surfactant-Templated Mesoporous Silica Formed in Ethanol and Its Application for Heavy Metal Removal. *Journal of Hazardous Materials*. 2007.
- [27] Choi, J.H., Kim, S.D., Noh, S.H., Oh, S.J., Kim, W.J., Ads. behavior of ETS-10 and its variants, ETAS-10 on the removal of heavy metals, Cu^{2+} , Co^{2+} , Mn^{2+} and Zn^{2+} , *Microporous & Mesoporous Materials*. **96**, Elsevier, pp. 157-167. 2006.
- [28] Al-Asheh, S., Duvnjak, Z., Sorption of Cadmium and Other Heavy Metals By Pine Bark, *Journal of Hazardous Materials* **56**, Elsevier, pp. 35–51. 1997.
- [29] Low, K.S., Lee, C.K., Leo, A.C., Removal of Metals From Electroplating Wastes Using Banana Pith, *Bioresource Technology*. Elsevier. **51**, pp. 227–231. 1995.
- [30] Marshall, W.E., Johns, M.M., Agricultural By-products As Metal Adsorbents: Sorption Properties and Resistance to Mechanical Abrasion, *Journal of Chemical Technology and Biotechnology*, Academic Press Inc. **66**, pp.192–198.1996.
- [31] Wafwoyo, W., Seo, C.W., Marshall, W.E., Utilization of Peanut Shells As Adsorbents for Selected Metals, *Journal of Chemical Technology and Biotechnology*, Academic Press Inc. **74**, pp. 1117–1121.1999.
- [32] Barrer, R.M., in *Molecular Sieves:History and Nomenclature*, Szostak, R., Molecular Sieves Principles of Synthesis and Identification. Blackie Academic & Professional, 2nd ed.,vol. 1, pp.1-28. 1998.

- [33] Chen, S. & Rajagopalan, R. *Micellar Solutions and Microemulsions. Structure, dynamics and statistical thermodynamics*. New York: Springer-Verlag Inc. 1990.
- [34] Gennes, P.G., *The Physics of Liquid Crystal*. London: Oxford. 1975.
- [35] Nriagu, J.O., History of Global Metal Pollution. *Science*. **272**. pp. 223-224. 1996.
- [36] Ong, S., Seng, S., Lim, P., Kinetics of Adsorption of Cu(II) and Cd(II) from Aqueous Solution on Rice Husk and Modified Rice Husk. *Electronic Journal of Environmental, Agricultural and Food Chemistry*. 2003.
- [37] Forsters, T., Rybinski, W.V., Wadle, A., Influence of Microemulsion Phases On the Preparation of Fine-disperse Emulsions. *Advances in Colloid and Interface Science*, Elsevier. **58** . pp. 119-149. 1995.
- [38] Kumar, K.V., Comparative Analysis of Linear and Non-Linear Method of Estimating the Sorption Isotherm Parameters for Malachite Green onto Activated Carbon. *Journal of Hazardous Materials*. **B136**. pp. 197–202. 2006.
- [39] Livage, Sanchez, Babonneau, in “Chemistry of Advanced Materials”, edited by Interrante and Hampden-Smith, *Molecular Precursor Routes to Inorganic Solids*. Academic Press Inc, 1983
- [40] Hairston, D.W., Studies in surface Science and Catalysis. *Chemical Engineering J.*, New York, **103** (7) vol. 57. 1996.
- [41] D’ souza, L. and Richards, R., in Synthesis and Preparation of Nanostructured Oxides, edited by Rodriguez, J.A. and Fernandez-Garcia, M., *Synthesis Of Metal Oxide Nanoparticles: Liquid Solid Transformation. Synthesis, Properties, And Applications Of Oxide Nanomaterial*. John Wiley & Sons. pp. 81-119. 2007

- [42] Moscou, L., in *Introduction To Zeolite Science and Practice*, Bekkum H. V., Flanigen, E.M., Jansen, J.C., *Studies in surface Science and Catalysis*, **58**, Elsevier, vol. 1, 1991.
- [43] Slov, A.C., Logar, N.Z., Kaučič, V., Nanoporous Materials: From Catalysis and Hydrogen Storage to Wastewater Treatment. *Nanoporous Materials Catalysis Review Articl.* **53**. pp. 117-135. 2006
- [44] Kesharavaja, A., Ramaswamy, V., Soni, H.S., Ramaswamy, A.V., Ratnasamy, P., Synthesis, Characterization and Catalytic Properties of Micro-Mesoporous, Amorphous Titanosilicate Catalysts. *Journal of Catalysis*. Academic Press Inc. **157**. pp. 501-511. 1995.
- [45] Kosuge, K., Singh, P.S., *Titanium Containing Porous Silica and Process of Preparing Same*. United States Patent. 1999.
- [46] Shan, Z., Maschmeyer, T., Jansen, J.C., *Inorganic Oxides with Mesoporosity or Combined Meso- and Microporosity and Process for the Preparation Thereof*. United States Patent. 2004.
- [47] Su, L.L.F., Zhao, X.S., Synthesis and Characterisation of Microporous Titanosilicate ETS-10 with different titanium precursors. *Journal of Porous Materials*. Springer. **13**. pp. 263-267. 2006.
- [48] Cundy, C. S. and Cox, P. A. The Hydrothermal Synthesis of Zeolites: History and Development from the Earliest Days to the Present Time. *Chem.* **103**. pp. 663-701. 2003.
- [49] Behrens, E.A., Clearfield, A., Titanium Silicates, $M_3HTl_4O_4(SiO_4)_3 \cdot 4H_2O$ ($M=Na^+$, K^+), With Three Dimensional Structures For The Selective Removal of Strontium and Cesium for Wastewater Solutions. *Microporous Materials*. **11** Elsevier, pp. 65-75. 1997.

[50] Khomane, R. B, "Role Of Self-Organized Surfactant Systems In Organic Reactions, Nanoparticles And Molecular Sieves Synthesis". Ph. D Thesis, Chemical Engineering Division, University Of Pune, India, 2002. unpublished

[51] Lopes, C.B., Lito, P.F., Otero, M., Lin, Z., Rocha, J., Silva, C.M., Pereira, E. Duarte, A.C., Mercury Removal with Titanosilicate ETS-4: Batch Experiments and Modelling. *Microporous and Mesoporous Materials*. Elsevier. 2008.

[52] Mukherjee, P. "Solvent-free, Triphase Catalytic Oxidation Reactions Over TS-1/H₂O₂ System" Ph. D. Thesis, Catalysis Division, National Chemical Laboratory, Pune, India, 2000. unpublished.

[53] Payra, P., & Dutta, P. K., in Zeolites: A Primer, Aurbach, S.M., Carradp, K.A., Dutta, P.K., Handbook of Zeolites and Science Technology. Marcel Dekker Inc. 2003.

[54] Hamley, I.W. *Introduction To Soft Matter, Polymer, Colloids, Amphiphiles and Liquid Crystal*. New York: John Willey & Sons, 2003.

[55] Iler, R.K., in Metal Silicate *Molecular Sieves*, Szostak, R., Molecular Sieves Principles of Synthesis and Identification. Blackie Academic & Professional, 2nd ed., vol. 1, pp.208-250. 1998.

[56] Didik Prasetyoko. "Bifunctional Oxidative and Acidic Titanium Silicalite (TS-1) Catalysts for One Pot Synthesis of 1,2-Octanediol from 1-Octene Solvent-free, Triphase Catalytic Oxidation Reactions Over TS-1/H₂O₂ System" Ph.D. Thesis, Faculty of Science, Universiti Teknologi Malaysia, 2006. unpublished.

[57] Barrer, R.M., in *Fundamental of Synthesis*, Szostak, R., Molecular Sieves Principles of Synthesis and Identification. Blackie Academic & Professional, 2nd ed., vol. 1, pp.1-28. 1998.

- [58] Singh, R., & Dutta, P. K., in MFI: A A Case Study of Zeolite Synthesis, Aeurbach, S.M., Carradp, K.A., Dutta, P.K., Handbook of Zeolites and Science Technology. Marcel Dekker Inc. 2003.
- [59] Khiew, P.S., Huang, N.M., Radiman, M.S., Ahmad. Synthesis and characterization of conducting polyaniline coated cadmium sulphide nanocomposites in reverse microemulsion. *Colloids and Surfaces A: Physicochemistry and Engineering Aspects*, Elsevier. **58**, pp. 762-767. 2004.
- [60] Paul, B.K., Moulik, S.P., Uses and Applications of Microemulsions. *Special Section: Soft Condensed Matter*. Curent Science. **81**. pp. 990-1000. 2001
- [61] Hsieh W.C. & Shah, D.O., The Effect of Chain Length of Oil and Alcohol as well as Surfactant to Alcohol Ratio On The Solubilization, Phase Behavior and Interfacial Tension of Oil/Brine/Surfactant/Alcohol Systems. American Institute of Mining, Metallurgical and Petroleum Engineers, Inc. **6594**. pp. 44-100. 1976.
- [62] Hamdy, M.S., “Functionalized TUD-1: Synthesis, Characterization and (photo-) Catalytic Performance” MSc. Thesis, Universiti Van Helwan, Egypt, 2003. unpublished.
- [63] Demirbas, O., Karadag, A., Alkan, M., Dogan, M. Removal of Copper Ions from Aqueous Solutions by Hazelnut Shell, *Journal of Hazardous Materials*. Elsevier, 2007.
- [64] Genov, K.A., “Oxidation of Organic Compounds on TS-1 and Ti-Beta Zeolites Synthesized According to Wetness Impregnation Method” PhD. Thesis, Universiti of Bremen, 2004. unpublished.
- [65] Dantas T. N. C., Dantas Neto A. A. and Moura M. C. P. A. Use of Impregnated Natural Clay With Microemulsion In The Treatment of Effluents Containing Heavy Metals. Proceedings of International Conference of Urban Pollution Control Tecnology (ICUPCT), Hong Kong. pp. S1_S6. 1999.

[66] Wu, S. & Chen, J.P. Modification of A Commercial Activated Carbon for Metal Adsorption by Several Approaches. Department of Chemical and Environmental Engineering. 2000. unpublished.

[67] Dantas, T. N. C., Dantas Neto, A.A., Moura, M.C.P. A., Removal of Chromium from Aqueous Solutions by Diatomite Treated with Microemulsion. *Water Research*. Elsevier. 35(9). pp. 2219–2224. 2001.

[68] Sublet, R., Simonnot, M.O., Boireauc, A., Sardin, M., Selection of an Adsorbent for Lead Removal from Drinking Water by a Point-of-Use Treatment Device. *Water Research*. Elsevier. **37**. pp. 4904–4912. 2003.

[69] Qadeer, R., & Akhtar, S., Kinetics Study of Lead Ion Adsorption On Active Carbon. *Turk J Chem*. 29. pp. 95- 99. 2005.

[70] Sheng, P. X., Ting, Y.P., Chen, J. P., Hong, L., Sorption of Lead, Copper, Cadmium, Zinc, and Nickel by Marine Algal Biomass: Characterization of Biosorptive Capacity and Investigation of Mechanisms. *Journal of Colloid and Interface Science*. Elsevier. 275. pp. 131–141. 2004.

[71] Arunkumar Lagashetty, A. & Venkataraman, A., Adsorption Study Of Pb^{2+} Ions on Nanosized SnO_2 , Synthesized By Self-Propagating Combustion Reaction. *Bulletin Material Science*. Indian Academy Of Science. **27**(6). pp. 491–495. 2004.

[72] Erdem , E., Karapinar, N., Donat, R., The Removal of Heavy Metal Cations by Natural Zeolites. *Journal of Colloid and Interface Science*. Elsevier. **280**. pp. 309–314. 2004.

[73] Mustafa, M. H., Removal of Heavy Metal by Local Mineral Raw Material at different pH. Environmental and Pollution Control Research Centre, The University of Mosul, Mosul-Iraq. 2005. unpublished.

[74] Bhatti , H.N., Mumtaz, B., Hanif, M.A., Nadeem, R., Removal of Zn(II) ions from aqueous solution using *Moringa oleifera* Lam. (horseradish tree) biomass. *Process Biochemistry*. Elsevier. **42**. pp. 547–553. 2007.

[75] Venkatathri, N., Synthesis, Characterization and Catalytic Properties of Silicon Containing Anatase (TiO₂). *Buletin of the Catalysis Society of India*. Academic Press Inc. **3**. pp. 99-106. 2004.

[76] Wang, R., Hu, L., Chu, B., Zhao, L., Zhu, G., Qiu, S., Synthesis, Characterization, and Catalytic Activities of Mesostructured Titanosilicates Assembled from Quaternary Alkylammonium with Preformed Titanosilicate Precursors Under Alkaline Condition. *Catalysis Communications*. Elsevier. **6(7)**. pp.485–490. 2005.

[77] Ovejero, G., Grieken, R.V., Uguina, M.A., Serrano, D.P., Melero, J.A., Study on the Ti and Al Incorporation into the MFI Zeolitic Structure. *Journals of Materials Chemistry*. **8(10)**. pp. 2269-2276. 1998.

[78] Khomane, R.B., Kulkarni, B.D., Parasker, A., Sainkar, S.R., Synthesis, Characterization and Catalytic Performance of Titanium Silicalite-1 Prepared in Micellar Media. *Materials Chemistry and Physics*. Elsevier. **76(1)**. pp. 99-103.2002.

[79] Hui, C.X., Rong, C.L., Mei, W.K., Wei Ke-Mei., Effect of Tween on Synthesis and Catalytic Performance of TS-1. *Journal of Fuel Chemistry&Technology*. Elsevier. **33(01)**. pp. 112-116. 2005:

- [80] Liu, H., Lu & G., Hu, H., Synthesis, Characterization and Catalytic Performance of Titanium Silicalite-1 Prepared in The Presence of Nonionic Surfactants. *Materials Chemistry and Physics*. Elsevier. **100**(1). pp. 162-167.2006.
- [81] Nandi, M. & Bhaumik, A., Highly Active Ti-rich Ordered Mesoporous Titanium Silicate Synthesized under Strong Acidic Condition. *Chemical Engineering Science*. Elsevier. **61**. pp. 4373-4380. 2006.
- [82] Du, H., Zhou, F., Pang, W., Yue., Y., Synthesis and Characterization of Titanium Silicate Molecular Sieves with Zorite-Type Structure. *Microporous Materials*. Elsevier. **7**. pp. 73-80. 1996.
- [83] Tuel. A., & Taarit, Y.B., A New Template for the Synthesis Titanium Silicalites with the ZSM-48 structure. *Zeolites*. Elsevier. **15**. pp. 164-170, 1995.
- [84] Madhusudan Reddy, K., Kaliaguine,S., Sayari, A., Ramaswamy, A.V., Saraswathi Reddy, V., Vonnevot, L., Synthesis Titanium Silicalites ZSM-48 with Hexathonium ions. *Catalysis Letter*. Academic Press Inc. **23**. 1994.
- [85] Serrano, D.P., Hong-Xin, Li, Davis, Synthesis Titanium Silicalites with the ZSM-48 Mobodimensional Channel Structure. *Journal of Chemical Society, Chemical Communication*. Academic Press Inc. **745**. 1992.
- [86] Turta, N.A., Luca, P.D., Bilba, N., Nagy, J.B., Nastro. A., Synthesis of Titanosilicate ETS-10 in Presence Of Cetyltrimethyl Ammonium Bromide. *Microporous and Mesoporous Materials*. Elsevier. 2007.
- [87] Xia, Q.H. & Gao, Z., Crystallization Kinetic of pure TS-1 Zeolite using Quaternary Ammonium Halides as Templates. *Materials Chemistry and Physics*. Elsevier. **47**(2-3). pp. 225-230.1997.

- [88] Aikawa, K., Kaneko, K., Tamura, T., Fujitsu, M., Ohbu, K. Formation of Fractal porous Silica by Hydrolysis of TEOS In a Bicontinuous Microemulsion. *Journal of Colloids*. **150**. pp. 95–104. 1999.
- [89] Ungureanu A., On, D.T., Dumitriu, E., Kaliaguine S., Hydroxylation of 1-naphthol by hydrogen peroxide over UL-TS-1 and TS-1 coated MCF. *Applied Catalysis A: General*. Elsevier. **254**. pp. 203–223. 2003.
- [90] Chan, K.S. & Shah, D.O., *The Physico-Chemical Conditions Necessary to Produce Ultralow Interfacial Tension at The Oil / Brine Interface*. New York: Plenum Press. pp. 53-72. 1951.
- [91] Grieken, R.V., Sotelo, J.L., Martos, C., Fierro, J.L.G., Lopez-Granados, M., Mariscal, R., Surface Modified Amorphous Titanosilicate Catalysts for Liquid Phase Epoxidation. *Catalysis Today*. Elsevier. pp. 49-54. 2000.
- [92] Xiao, F, Lin, K., Sun,Z., Lin,S., Jiang, D. Ordered Mesoporous Titanosilicates with Better Catalytically Active Titanium Sites Assembled From Preformed Titanosilicate Precursors with Zeolite Building Units in Alkaline Media. *Journal of Microporous and Mesoporous Materials*. Elsevier. **72**. pp. 193-201. 2004.
- [93] Wang, Y., Lin, M., Tuel, A. Hollow TS-1 Crystal Formed Via a Dissolution-Recrystallization Process. *Journal of Microporous and Mesoporous Materials*. Elsevier. **102**. pp.80–85. 2006.
- [94] Yuan, Z. Blin, J., and Su, B., Design of bimodal mesoporous silicas with interconnected pore systems by ammonia post-hydrothermal treatment in the mild-temperature. *Chemistry Community*. Elsevier. pp. 504–505. 2002.

- [95] Mollet, H. Grubenmann, A. *Formulation Technology, Emulsions, Suspensions, Solid Forms*, translated by Payne, H.R., Weinheim. Federal Public of Germany, 2001
- [96] Wennerstrom, H., Soderman, O. Lindman, B., *Colloids and Surfaces A: Physicochemistry and Engineering Aspects*, **13-26**, pp. 123-124. 1997.
- [97] Safran, S.A., *Stastical Thermodynamics Of Surfaces, Interfaces and Membranes*. New York: Addison-Wesley Publications. 1994.
- [98] Meunier & Boccara, L.D. *Physics of Amphiphilic Bilayers*. Berlin: Springer-Verlag Inc.
- [99] Singhal, M., Chabra, V., Kang, P. & Shah, D.O. Synthesis of ZnO Nanoparticles For Various Application Using Zn-substituted Aerosol OT Microemulsion. *Surface Science*. **98**. Elsevier, pp. 427-436. 1996
- [100] Bauduin, P., Basse, A., Touraud, D., Kunz, W., Effect Of Short Non-Ionic Amphiphiles From Ethylene And Propylene Glycol Alkyl Ethers On The CMC of SDS. *Colloids and Surfaces A: Physicochemistry and Engineering Aspects*., Elsevier. **8-12**, pp. 270-271. 2005.
- [101] Hager, M., Currie, F., Holmberg, K., A Nucleophilic Substitution reaction in microemulsions based on either alcohol ethoxylate or a sugar surfactant. *Colloids and Surfaces A: Physicochemistry and Engineering Aspects*, Elsevier. **250**, pp. 163-170. 2004
- [102] Shah, D.O, & Sharma, M.K., *Macro and Microemulsions; Theory and Applications*. Washington; American Chemical Society. 1985
- [103] Luisi, P.L. & Straub, B.E. *Reverse Micelles. Biological and Technological Relevance of Amphiphilic Structures in Apolar Media*. New York: Plenum Press. 1982.

[104] Bansal, V.K. & Shah, D.O., in *Micellar Solutions for Improved Oil Recovery*, Shah, D.O., Micellization, Solubilization, and Microemulsion. New York: Plenum Press. Vol. 1. 1977.

[105] Hoffmann, H., Surfactant Systems for Various Fields of EOR: Drilling Fluids, Microemulsions, Control of Viscosity, Breaking Emulsions. *Technology Platform: Reservoir Engineering*. Plenum Press. Vol. 4 . 1. pp. 36-45. 2004.

[106] Chou, S.I. & Shah, D.O., The Optimal Salinity Concept for Oil Displacement by Oil-External Microemulsions and Graded Salinity Slugs. *The Canadian Mining and Metallurgical Bulletin*. Plenum Press. July/September, 1981.

[107] Somasundram, P., Celik, M., Goyal, A., *Precipitation and Redissolution of Sulfonates and Their Role in Adsorption of Minerals*. New York: Plenum Press. pp. 641-647. 1981.

[108] Bansal, V.K., Chan, K.S., McCallough, R., Shah, D.O., The Effect of Caustic Concentration on Interfacial Charge, Interfacial Tension and Droplet Size: A Simple Test for Optimum Caustic Concentration for Crude Oil. *Journal of Canadian Petroleum Technology*. Plenum Press. Vol. 17. **1**. pp. 1-4. 1978.

[109] Shah, D.O., & Hsieh, W.C, *Microemulsions, Liquid Crystals and Enhanced Oil Recovery*. American Institute of Mining, Metallurgical and Petroleum Engineers, Inc. pp. 137-154. 1976.

[110] Bansal, V.K., & Shah, D.O., *Microemulsion and Tertiary Oil Recovery*. American Institute of Mining, Metallurgical and Petroleum Engineers, Inc. pp. 149-173. 1976.

- [111] Hanna, S., Gayal, A., Somasundram, P., *Surface Active Properties of Certain Micellar Systems for Tertiary Oil Recovery*. VIIth International Congress on Surface Active Substances, Moscow. 12-18th September 1976.
- [112] Mittal, K.L., edited by Kumar, P., *Handbook of Microemulsion Science and Technology*, New York: Marcel Dekker Inc. pp 743-754. 1986.
- [113] Chan, K.S. & Shah, D.O., The Molecular Mechanism for Achieving Ultra Low Interfacial Tension in A Petroleum Sulfonate/Oil/Brine System. *Journal Dispersion Science & Technology*. Vol. 1. **1**. pp. 55-95. 1980.
- [114] Vijayan, S., Ramachandran, C., Doshi, H., Shah, D.O., *Porous Media of Emulsions in Tertiary Oil Recovery*. in *Surface Phenomena in Enhanced Oil Recovery*, New York: Plenum Press. pp. 327-375. 1981.
- [115] Rastogi, M.C., *Surface and Interfacial Science; Application to Engineering and Technology*. Naros Publishing House. 2003.
- [116] Salager, J.L., Marquez, L., Forgiavini, A., *Nanoemulsions: Where are They Going to*. Plenum Press. 2005.
- [117] Chen, H., Chang, X., Weng, T., Zhao, X., Gao, Z., Yang, Y., Xu, H., Yang, X., A Study of Microemulsion Systems for Transdermal Delivery of Triptolide. *Journal of Controlled Release*, Elsevier. **98**, pp. 427-436. 2004.
- [118] Guansheng, L., Jia, Z., Yujun, W., Adsorption of Diuretic Furosemide of Chitosan Nanoparticles With a Water-in-Oil Nanoemulsion System. *Reactive and Functional Polymers*, Elsevier. 2005.
- [119] Collings, P.J. & Hird, M., *Introduction To Liquid Crystals: Chemistry and Physics*. London: Taylor & Francis Ltd. 1997.

- [120] Lee, S., Carr, C.S., Shantz, D.F., Anionic Microemulsion-Mediated Low Temperature Synthesis of Anisotropic Silicalite-1 Nanocrystals. American Chemical Society. *Langmuir*. Plenum Press. 2005.
- [121] Boonamnuayvitaya, V., Tayamanon, C., Sae-ung, S., Tanthapanichakoon, W., Synthesis and Characterisation of Porous Media Produced by a Sol-Gel Method. *Chemical Engineering Science*. Elsevier. **61**. pp.1686–1691. 2006.
- [122] Jang, J., Bae, J., Fabrication of Mesoporous Polymer/Silica Hybrid Using Surfactant Mediated sol-gel Method. *Journal Of Non-Crystalline Solid*. Elsevier. **352**. pp. 3979-3984. 2006.
- [123] Sharma, S.C., Kunieda, H., Esquena, J., Abreu, C.R., Phase Behaviour and Preparation of Mesoporous Silica in Aqueous Mixtures of Fluorinated Surfactant and Hydrophobic Fluorinated Polymer. *Journal in Colloid and Interface Science*, Elsevier. 2005.
- [124] Corma, A. Di'az-Caban'as, M. J. Amorphous Microporous Molecular Sieves with Different Pore Dimensions and Topologies: Synthesis, Characterization And Catalytic Activity. *Microporous and Mesoporous Materials*. Elsevier. **89**. pp.39–46. 2005.
- [125] Lee, S. & Shantz, D.F., Zeolite Growth in Nonionic Microemulsions: Synthesis of Hierarchically Structured Zeolite Particles. American Chemical Society. *Chem. Mater.* Elsevier. **17**. pp. 409-417. 2005.
- [126] Ko, C.H, Kim, J. M., Ryoo, R., Mesocrystal Engineering Using Non-Bonded Interaction to Obtain Optically Transparent Mesoporous Silica Films and Plates With Uniform Orientation. *Microporous and Mesoporous Materials*. Elsevier. **21**. pp. 235-243.1998.

- [127] Tanev et al. Titanium containing Mesoporous Molecular Sieves for Catalytic Oxidation of Aromatic Compounds. *Nature*. Academic Press Inc. **368**. pp. 321-368. 1994.
- [128] Romano et al. Selective Oxidation with Ti-silicalite. *La Chimica and La industria*. **72**. pp. 610-616. 1990.
- [129] Saxton, R.J., Crystalline Microporous Titanium Silicates. *Topics in Catalysis*. Elsevier. **9**. pp. 43-57. 1999.
- [130] Kesharavaja, A., Ramaswamy, H.S., Ramaswamy, A.V., Ratnasamy,P., *Micro-Mesoporous, Amorphous Titanosilicate Catalysts and a Process for Preparing the Same*. United States Patent. **19**. 1998.
- [131] Kooyman, P.J., Titanium deposited from TiCl₄ on amorphous silica and silicalite-1 as catalyst in aromatic hydroxylation reactions. *Catalysis Letters*. **13**. pp. 229-238. 1992.
- [132] Shan, Z., Maschmeyer, T., Jansen, J.C., *Mesoporous Material and Use Thereof for the Selective Oxidation of organic Compounds*. United States Patent. 2005.
- [133] Figueras, F., Kochkar, H., Caldarelli, S., Crystallization of Hydrophobic Mesoporous Titano-Silicates Useful as Epoxidation Catalysts. *Microporous and Mesoporous Materials*. Elsevier. **39**. pp. 249-256. 2000.
- [134] Kumar, K. V., Subanandam, K., Ramamurthi, V., and Sivanesan, S., Solid Liquid Adsorption for Wastewater Treatment: Principle Design and Operation. ECO Services International. 2004.
- [135] Balasubramanian, N., Raja, R.E., Lalitha, K. Uma, R., Removal of Cr⁺ Ions Using Lignite. *Journal of Environmental Studies and Policy*. Elsevier. 1(1). pp. 21-24

- [136] El-Sikaily, A., Nemr, A.E., Khaled, A., Wehab, O.A., Removal of Toxic Chromium from Wastewater Using Green Alga *Ulva lactuca* and Its Activated Carbon. *Journal of Hazardous Materials*. Elsevier. **148**. pp. 216–228. 2007.
- [137] Gunay, A., Arslankaya, E., Tosun, I., Lead Removal from Aqueous Solution by Natural and Pretreated Clinoptilolite: Adsorption Equilibrium and Kinetics. *Journal of Hazardous Materials*. Elsevier. **146**. pp. 362–371. 2007.
- [138] M.N. Khan & M.F. Wahab, Characterization of Chemically Modified Corncobs and Its Application In The Removal of Metal Ions from Aqueous Solution. *Journal of Hazardous Materials*. Elsevier. **141**. pp. 237–244. 2007.
- [139] Akieh, M.N., Lahtinen, M., Vaisanen, A., Silanpaa, M., Preparation and Characterization of Sodium Iron Titanate Ion Exchanger and Its Application In Heavy Metal Removal from Waste Waters. *Journal of Hazardous Materials*. Elsevier. 2007.
- [140] Dias Filho, N.L., Marangoni, F., Costa, R.M., Preparation, Characterization, and CuX_2 and CoX_2 ($\text{X} = \text{Cl}^-$, Br^- , ClO_4^-) Adsorption Behavior of A Polyhedral Oligomer Silsesquioxane Functionalized with An Organic Base. *Journal of Hazardous Materials. Journal of Colloid and Interface Science*. Elsevier. **314**. pp.25–31.2007.
- [141] Wang, S. & Ariyanto, E., Competitive Adsorption of Malachalite Green and Pb Ions on Natural Zeolite. *Journal of Colloid and Interface Science*. Elsevier. **313**. pp.341–342.2007.
- [142] Su, L.F. & Zhao. X.S., Synthesis and Characterization of Microporous Titanosilicate ETS-10 with Different Titanium Precursors, *Journal of Porous Materials*. Elsevier, **13**, pp. 263-267. 2006.

- [143] Dodwell, G.W., Smith, B., Angerhald Corporation, Iselin, N.J., *Removal of Heavy Metals, Especially Lead, From Aqueous Systems Containing Competing Ions Utilizing Amorphous Tin and Titanium Silicates*. United States Patent. **19**. 2001.
- [144] Derouane, *Characterization of zeolites*. E.G. Collaborative Research Project between PRSS and Prof. E.G. Derouane. Petroliam Berhad. 1990.
- [145] Webb, P.A. & Orr, C., *Analytical Methods in Fine Particle Technology*. Micrometrics Instrument Corporation, USA. 1997.
- [146] Cooney, D. O., *Adsorption Design for Wastewater Treatment*, Lewis Publisher.1999.
- [147] Yonge, D.R. & Keinath, T.M., The effects of Non-Ideal Competition on Multi-component adsorption equilibria. *Journal WPCF*. **58**(77). 1986.
- [148] Al Duri, B., in Introduction to Adsorption, McKay, G., *Use of Adsorbents for the Removal of Pollutants from Wastewaters*. New York: CRC Press. 1995.
- [149] Freundlich, H.M.F. Über Die Adsorption in Llösungen. *Zeitschrift für Physikalische Chemie.*, **57**, pp. 385–470. 1906.
- [150] Langmuir, I. The Constitution and Fundamental Properties of Solids and Liquids. *Journal of American Chemical Society*. **38**. pp. 2221–2295. 1916
- [151] Hashim, M.A. & Chu, K.H., Biosorption of Cadmium by Brown, Green and Red Seaweeds. *Chemical Engineering Journal*. 97. pp. 249-255. 2004.
- [152] Ho, Y.S. and McKay, G., A Comparison of Chemisorption Kinetic Models Applied to Pollutant Removal on Various Sorbents. *Process Safety and Environmental Protection*, 76, No. B4, 332.1998.

- [153] Ho, Y., Selection of optimum sorption isotherm. *Letters to the Editor / Carbon*. **42**. pp. 2113-2130. 2004.
- [154] Kilic, M., Keskin, M.E., Terzi, O., Estimating Residual Concentration in Lead (II) Biosorption With Activated Sludge Using Artificial Neural Networks. *Journal of Science and Technology*. **2**. pp. 52-66. 2008
- [155] Ho, Y., Comment on 'An evaluation of Copper Biosorption by a Brown Seaweed Under Optimized Conditions' by Antunes, W.M., Luna, A.S., Henriques, C.A. and da Costa, A.C.A. *Electronic Journal of Biotechnology*. 2004.
- [156] Lagergren, S. . Zur Theorie der sogenannten Adsorption gelostn. Stoffe. Stcok. Ak. Handl. Bihay. **24**. 39. 1898.
- [157] Ho, Y.S. Adsorption of Heavy Metals from Waste Streams by Peat. Ph.D. Thesis, University of Birmingham, Birmingham, U.K. 1995.
- [158] Ho, Y.S. Wase, D.A.J. & Forster, C.F. Kinetic Studies of Competitive Heavy Metal Adsorption by Sphagnum Moss Peat. *Environmental Technology*. 17(1). pp. 71-77. 1996
- [159] Lv, L.. Su, F., Zhao, X.S., A Reinforced Study On Synthesis Of Microporous Titanosilicate ETS-10, *Microporous & Mesoporous Materials*. **76**, Elsevier, pp. 113-122. 2004.
- [160] Wang, X., Dou, T., Xiao, Y., Synthesis of Double-mesopore Silica using Aqueous Ammonia as Catalyst. *Chemistry Community*. pp. 1035-1036. 1998.
- [161] Eimer,G.A., Di'az, I., Sastre, E., Casuscelli,S.G., Crivello, M.E., Herrero, E.R. Joaqui'n Perez-Pariente,J., Mesoporous Titanosilicates Synthesized from TS-1 Precursors with Enhanced Catalytic Activity in The A-Pinene Selective Oxidation. *Applied Catalysis A: General*. Elsevier. 2008.

[162] Shan, Z., Jansen, J.C., Maschmeyer, T., Hamdy, M.S., *Inorganic Oxides with Mesoporosity or Combined Meso- and Microporosity and Process for the Preparation Thereof*. United States Patent. 2002.

[163] Shan, Z., Jansen, J.C., Yeh, C.J., Angevine, P.J., Maschmeyer, T., Hamdy, M.S., *Mesoporous Materials with Active Metals*. United States Patent. 2005.

[164] Caixia Qi, Q., Akita, T., Okumuraa, M., Kuraoka, K., Masatake Haruta, M., Effect of Surface Chemical Properties and Texture of Mesoporous Titanosilicates on Direct Vapor-Phase Epoxidation of Propylene over Au Catalysts at High Reaction Temperature. *Applied Catalysis A: General*. Elsevier. **253**. pp. 75-89. 2003.

[165] On, D.T., Litic, D., Kaliaguine, S., An Example of Mesostructured Zeolitic Material: UL-TS-1. *Journal of Microporous and Mesoporous Materials*. Elsevier. **44-45**. pp. 435-444. 2001.

[166] Rizzo, C., Carati, A., Millini R., Bellussi, G., Parker Jr, W.O., Zanardi S., Synthesis, Characterisation and Adsorption Capacities of Microporous titanosilicate EMS-3. *Journal of Microporous and Mesoporous Materials*. Elsevier. **90**. pp. 153-161. 2006.

[167] Chang, K. "Vanadium Incorporated MCM-41. PhD Thesis." Department of Chemical Engineering. 2003. unpublished

[168] Zhang, W., Mesoporous Titanosilicate Molecular Sieves Prepared at Ambient Temperature by Electrostatic (S^+T , S^+XT^+) and Neutral (S^0T^0) Assembly Pathways: A Comparison of Physical Properties and Catalytic Activity for Peroxide Oxidation. *J. Am. Soc.* Elsevier. **118**. pp.9164-9171. 2006.

[169] Li, G. & Zhao, X.S., Characterisation and Photocatalytic Properties Of Titanium Containing Mesoporous SBA-15. *Ind. Eng. Chem. Res.* Elsevier. **45**. pp.3569-3573. 2006.

[170] online: Koch, M. "Properties Of The Catalyst" *Mathias Homepage*, University of Bremen. 1998.

[171] Luan, Z. & Kevan, L., Electron Spin Resonance and Diffuse Reflectance Ultraviolet Visible Spectroscopies of Vanadium Immobilized at Surface Titanium Centers of Titanosilicate Mesoporous TiMCM-41 Molecular Sieves. *J. Phys. Chem.* Elsevier. **B. 101**. pp. 2020. 1997.

[172] Chang, T., Leu, F., Synthesis and Characterization of Vanado Titanium Silicate Molecular Sieves with MEL Structure. *Zeolites*. Elsevier. **15**. pp. 496-500. 1995.

[173] Bhaumik, A., Sujit Samanta, S., Mal, N.K., Highly Active Disordered Extra Large Pore Titanium Silicate. *Journal of Microporous and Mesoporous Materials*. Elsevier. **68**. pp.29–35. 2004.

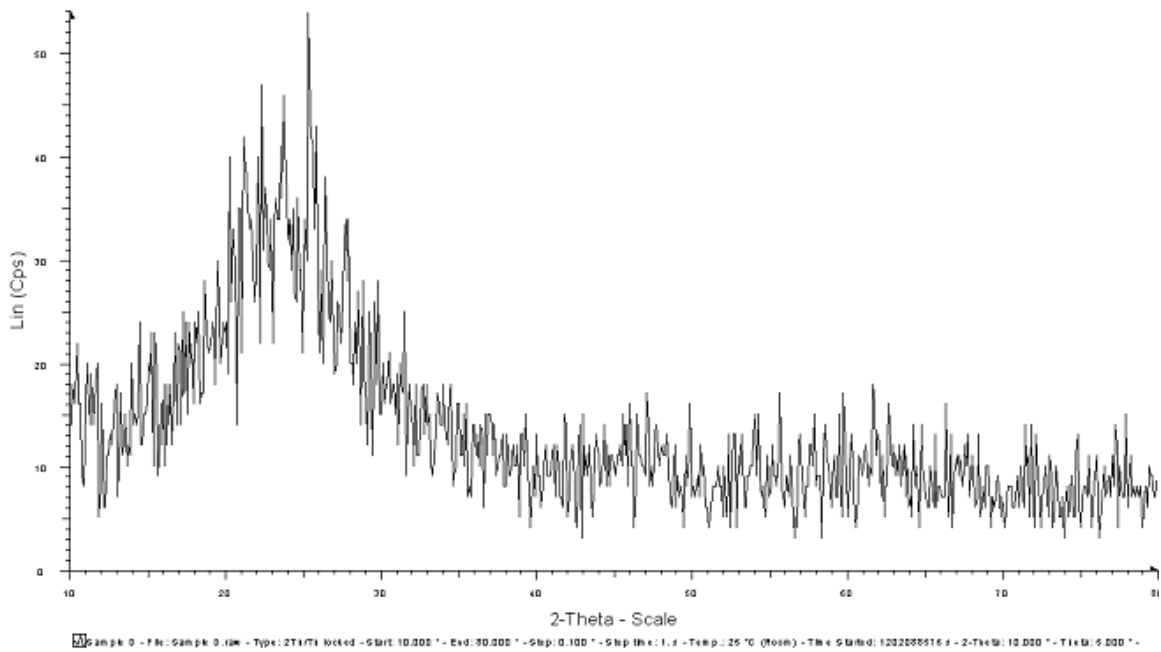
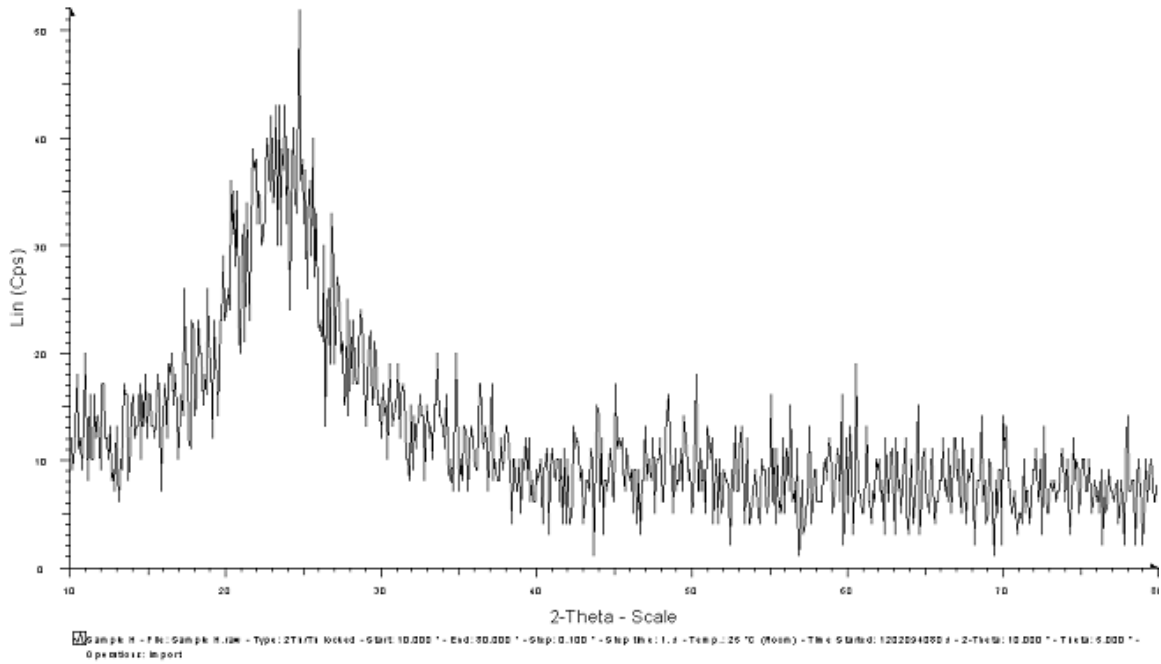
[174] Neumann, R., Levin-Elad, M., Metal Oxide (TiO₂, MoO₃, WO₃) Substituted Silicate Xerogels as Catalysts for the Oxidation of Hydrocarbons with Hydrogen Peroxide. *Journal Of Catalysis*. Academic Press. **166**. pp. 206–217. 1997

[175] Z.H. Luan, D.Y. Zhao, H.Y. He, J. Klinomski, L. Kevan, Characterization of aluminophosphate-based Tubular Mesoporous Molecular Sieves. *J. Phys. Chem.. B* 102 (7). pp. 1250–1259. 1998

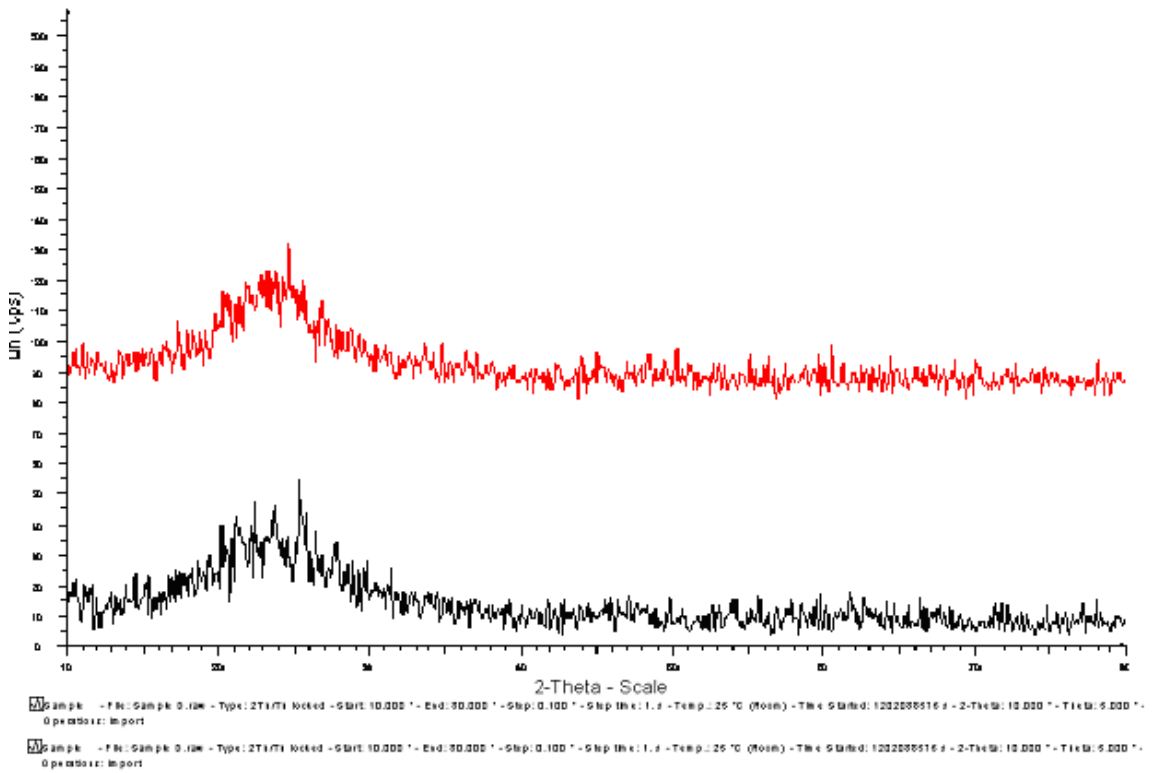
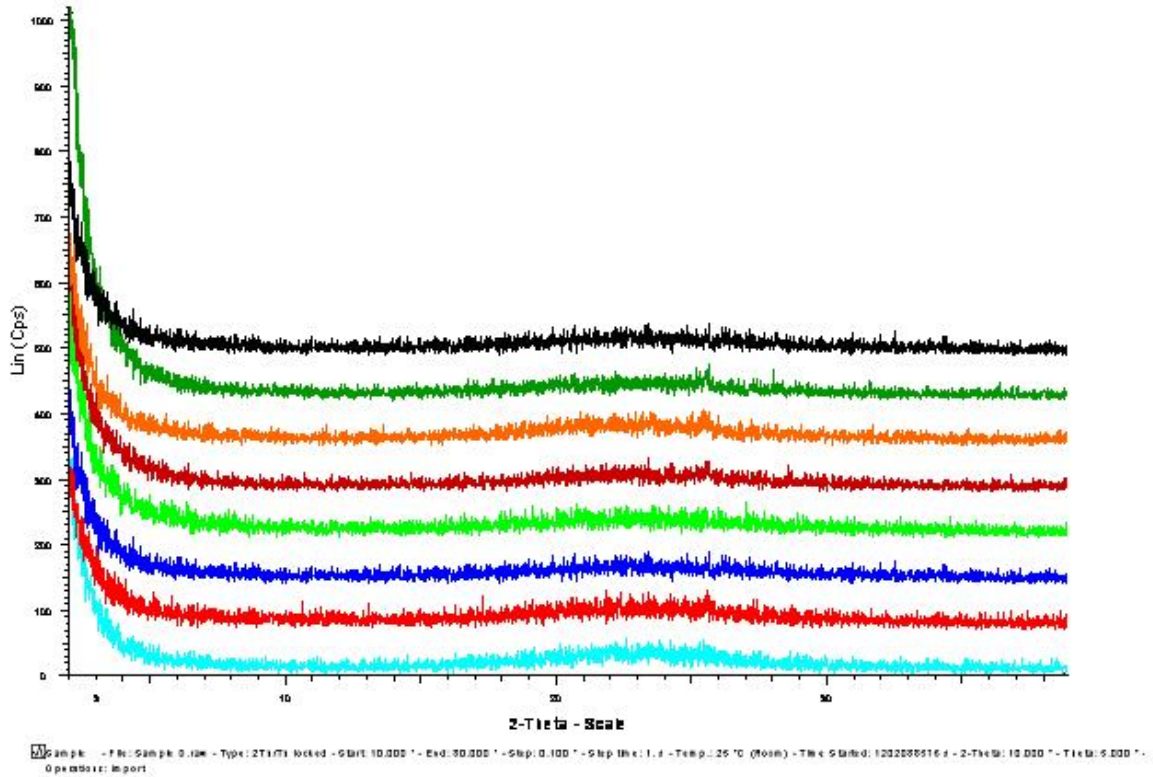
[176] Kim, S.D., Noh, S.H., Kim, W.J., Alkali Effect and Kinetic Studies on the Crystallization of a Small Pored Titanium Silicate Molecular Sieve, ETS-4 Using Different Sources of Silica and Titanium under Stirring Microporous and Mesoporous Materials 65 (2003) 165–175

- [177] Tan, B., Rankin, S.E., Effects of Progressive Changes in Organoalkoxysilane Structure on The Gelation and Pore Structure of Templated and Non-Templated Sol–Gel Materials. *Journal of Non-Crystalline Solids*. Elsevier. **352**. pp. 5453–5462. 2006.
- [178] Sotelo, J.L., Grieken, R.V., Martos, C., Catalytic Aerogel-Like Materials Dried at Ambient Pressure for Liquid –Phase Epoxidation. *Chem Comm.* pp. 549-550. 1999.
- [179] Mortimer, R. G. Physical Chemistry, The Benjamin/Cummings Publishing Company, California. 1993.
- [180] Andrews, J. E., brimblecombe, P., Juckells, T. D., Liss, P.S. Reid, B.J. An Introduction to Environmental Chemistry. Blackwell Publishing. 2005.
- [181] Ramalhp, R.S. Introduction to Wastewater Treatment Process, Academic Press Inc, 2nd edition, 1983.
- [182] Malek, N.A.N., “Surfactant Modified Zeolite Y as a Sorbent for Some Chromium and Arsenic Species in Water” MSc Thesis, Faculty of Science, UTM, 2007. unpublished

APPENDIX A

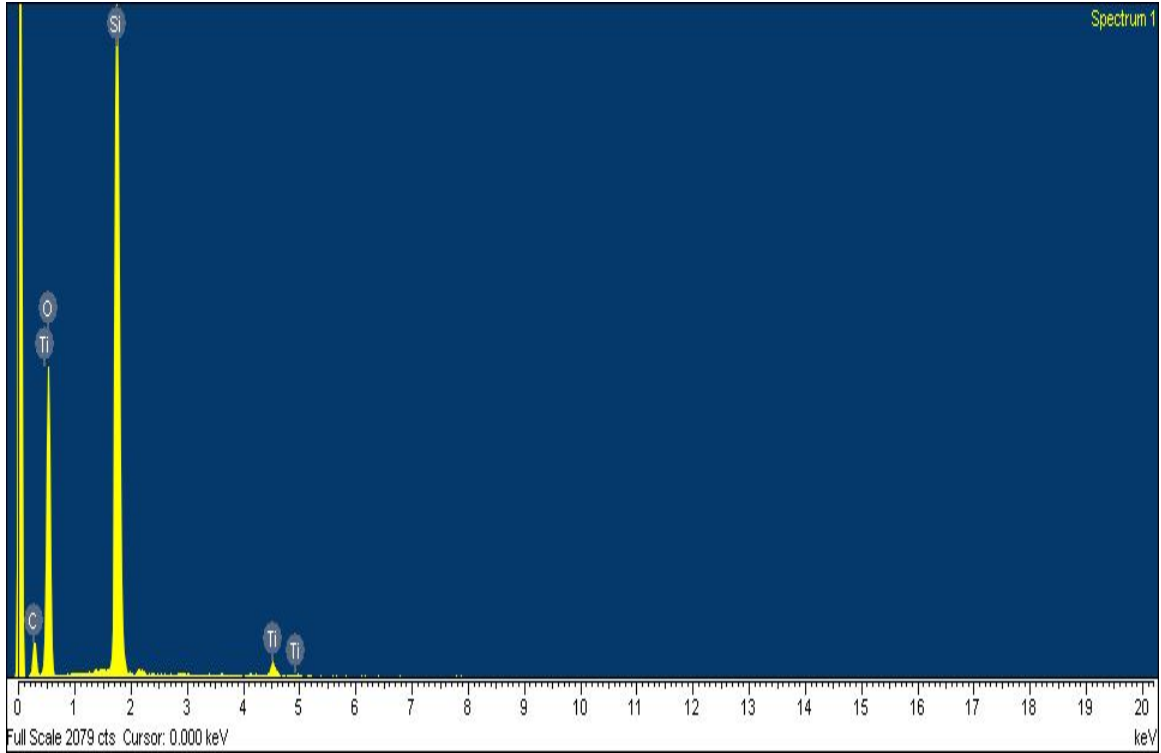


XRD of samples in short range order



XRD of samples in long range order

APPENDIX B



No peaks omitted

Processing option : All elements analyzed (Normalised)

Number of iterations = 6

Standard :

C CaCO₃ 1-Jun-1999 12:00 AM

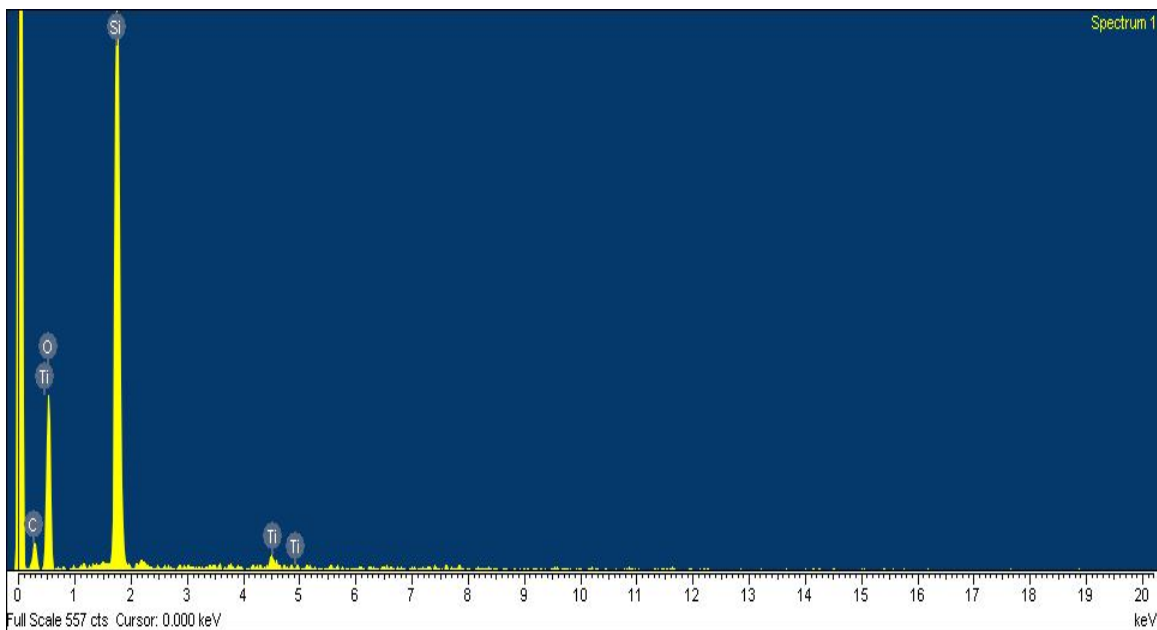
O SiO₂ 1-Jun-1999 12:00 AM

Si SiO₂ 1-Jun-1999 12:00 AM

Ti Ti 1-Jun-1999 12:00 AM

Element	Weight%	Atomic%
C K	17.94	24.89
O K	59.45	61.91
Si K	21.78	12.92
Ti K	0.82	0.29
Totals	100.00	

EDX Of Calcined TS-1



Spectrum processing :

No peaks omitted

Processing option : All elements analyzed (Normalised)

Number of iterations = 5

Standard :

C CaCO3 1-Jun-1999 12:00 AM

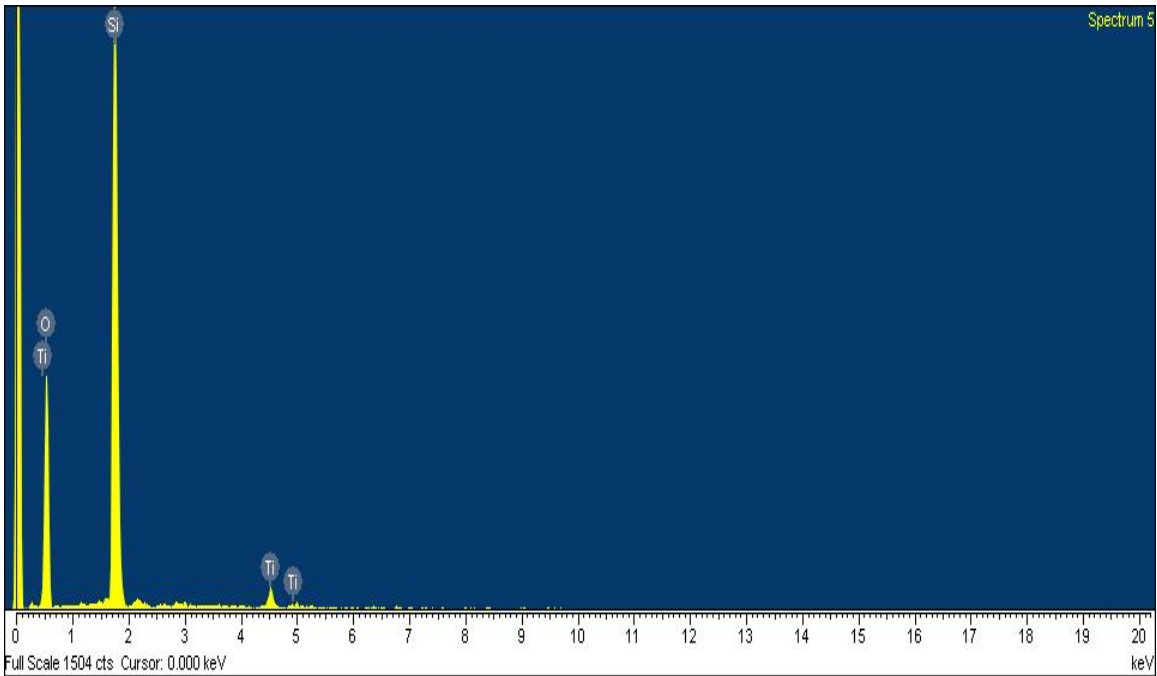
O SiO2 1-Jun-1999 12:00 AM

Si SiO2 1-Jun-1999 12:00 AM

Ti Ti 1-Jun-1999 12:00 AM

Element	Weight%	Atomic%
C K	21.42	29.73
O K	53.22	55.44
Si K	24.47	14.52
Ti K	0.89	0.31
Totals	100.00	

EDX Of Calcined TS-2



Spectrum processing :

No peaks omitted

Processing option : All elements analyzed (Normalised)

Number of iterations = 3

Standard :

C CaCO₃ 1-Jun-1999 12:00 AM

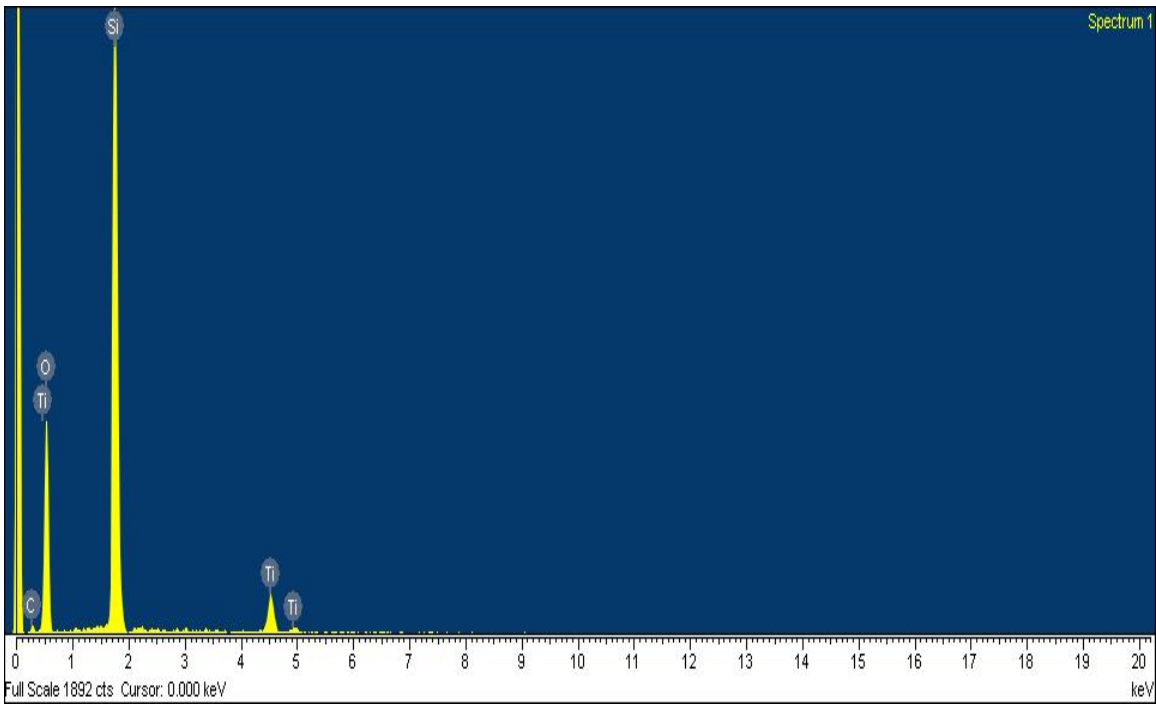
O SiO₂ 1-Jun-1999 12:00 AM

Si SiO₂ 1-Jun-1999 12:00 AM

Ti Ti 1-Jun-1999 12:00 AM

Element	Weight%	Atomic%
O K	51.51	66.01
Si K	43.81	31.98
Ti K	4.68	2.00
Totals	100.00	

EDX of calcined TS-3



Spectrum processing:

No peaks omitted

Processing option: All elements analyzed (Normalised)

Number of iterations = 5

Standard:

C CaCO₃ 1-Jun-1999 12:00 AM

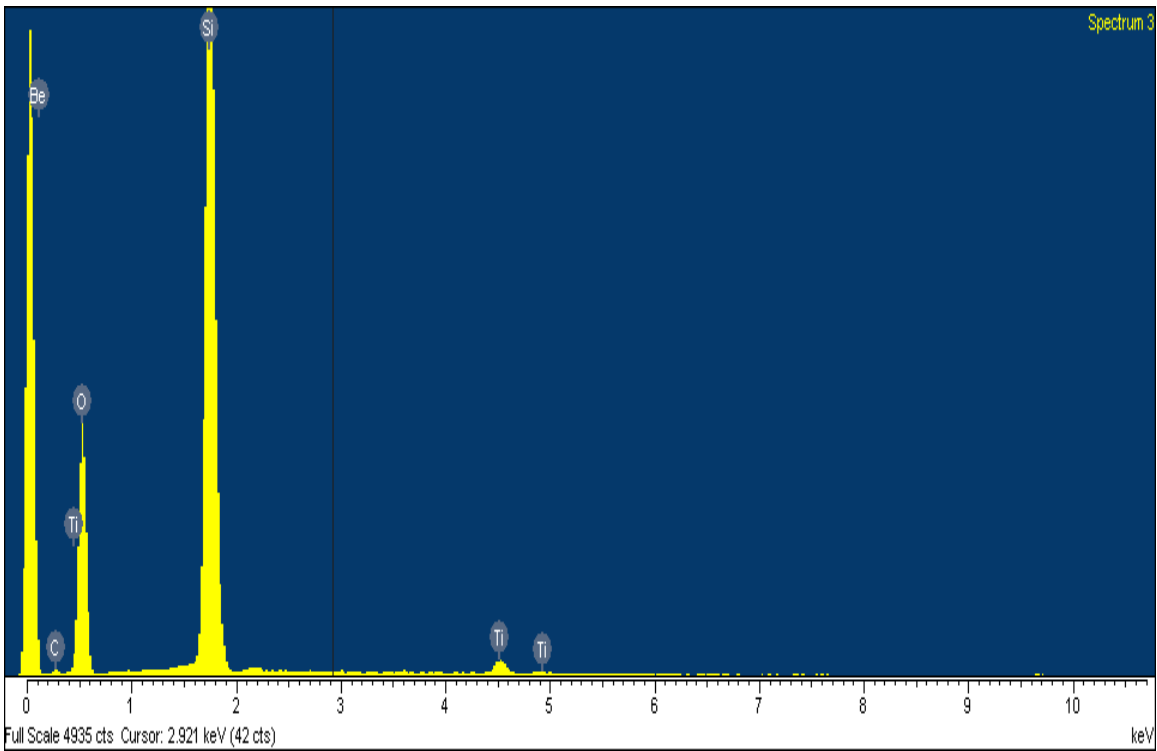
O SiO₂ 1-Jun-1999 12:00 AM

Si SiO₂ 1-Jun-1999 12:00 AM

Ti Ti 1-Jun-1999 12:00 AM

Element	Weight%	Atomic%
C K	6.56	10.08
O K	59.53	68.61
Si K	30.41	19.97
Ti K	3.50	1.35
Totals	100.00	

EDX of calcined TS-4



Spectrum processing:

Peak possibly omitted: 2.170 keV

Processing option: All elements analyzed (Normalised)

Number of iterations = 5

Standard:

C CaCO3 1-Jun-1999 12:00 AM

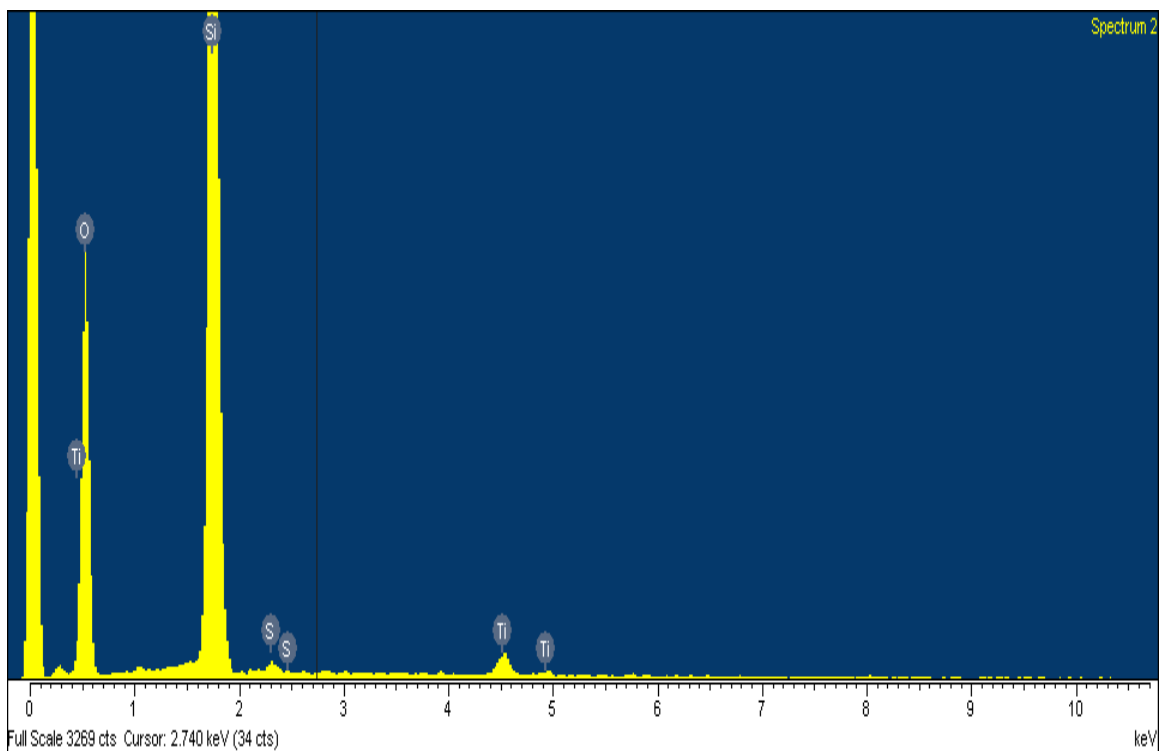
O SiO2 1-Jun-1999 12:00 AM

Si SiO2 1-Jun-1999 12:00 AM

Ti Ti 1-Jun-1999 12:00 AM

Element	Weight%	Atomic%
C K	6.36	9.71
O K	59.58	68.31
Si K	33.07	21.60
Ti K	0.99	0.38
Totals	100.00	

EDX of TS-A



Spectrum processing:

Peak possibly omitted: 11.880 keV

Processing option: All elements analyzed (Normalised)

Number of iterations = 5

Standard:

O SiO₂ 1-Jun-1999 12:00 AM

Si SiO₂ 1-Jun-1999 12:00 AM

S FeS₂ 1-Jun-1999 12:00 AM

Ti Ti 1-Jun-1999 12:00 AM

Element	Weight%	Atomic%
O K	63.14	75.33
Si K	35.24	23.95
S K	0.42	0.25
Ti K	1.19	0.48
Totals	100.00	

EDX of TS-E

APPENDIX C

Micromeritics Instrument Corporation		
MP 2000 V3.00	B	PAGE 10
SAMPLE DIRECTORY/NUMBER: DATA1 /71		START 14:33:06 12/09/06
SAMPLE ID: 6L		COMPL 18:04:23 12/09/06
SMITTER: TSOH_WITH SDS_S3C		REPR 07:58:37 12/10/06
ERATOR: ALINI		SAMPLE WT: 0.0328 g
IT NUMBER: 1		FREE SPACE: 54.1787 cc
ALYSIS GAS: Nitrogen		EQUIL INTRVL: 5 sec
SUMMARY REPORT		
AREA		
SURFACE AREA:	459.4782	sq. m/g
IGNIUR SURFACE AREA:	511.8917	sq. m/g
BLE POINT SURFACE AREA AT P/P ₀ 0.0777:	421.5352	sq. m/g
RDPORE AREA:	69.8479	sq. m/g
VOLUME		
BLE POINT TOTAL PORE VOLUME OF PORES LESS THAN 2753.5703 A DIAMETER AT P/P ₀ 0.9985:	0.524328	cc/g
RDPORE VOLUME:	0.034465	cc/g
PORE SIZE		
AVERAGE PORE DIAMETER (4V/A BY BET):	45.6455	A

BET Measurement Analysis Data of TS-A

Micromeritics Instrument Corporation

ASAP 2000 V3.00

B

PAGE 10

SAMPLE DIRECTORY/NUMBER: DATA1 172	START 08:12:22 12/10/06
SAMPLE ID: RA	COMPL 11:55:09 12/10/06
SUBMITTER: TS h_SIC	REPRT 12:10:06 12/10/06
OPERATOR: ALIMI	SAMPLE WT: 0.1287 g
UNIT NUMBER: 1	FREE SPACE: 56.7864 cc
ANALYSIS GAS: Nitrogen	EQUIL INTRVL: 5 sec

SUMMARY REPORT

AREA

BET SURFACE AREA:	282.5139	sq. m/g
LANGMUIR SURFACE AREA:	313.3360	sq. m/g
SINGLE POINT SURFACE AREA AT P/P ₀ 0.0775:	265.4973	sq. m/g
MICROPORE AREA:	39.7688	sq. m/g

PORE SIZE

AVERAGE PORE DIAMETER (4V/A BY BET):	38.1844	Å
SINGLE POINT TOTAL PORE VOLUME OF PORES LESS THAN MICROPORE VOLUME DIAMETER AT P/P ₀ 0.9903:	0.001688	cc/g

BET Measurement Analysis Data of TS-B

Micromeritics Instrument Corporation

ASAP 2000 V3.00

B

PAGE 10

SAMPLE DIRECTORY/NUMBER: DATA1 /68
 SAMPLE ID: R6
 SUBMITTER: S1A-24h
 OPERATOR: ALIM1
 UNIT NUMBER: 1
 ANALYSIS GAS: Nitrogen

START 08:26:39 12/06/06
 COMPL 14:15:33 12/06/06
 REPT 14:15:34 12/06/06
 SAMPLE WT: 0.1300 g
 FREE SPACE: 55.3663 cc
 EQUIL INTRVL: 5 sec

SUMMARY REPORT

AREA

BET SURFACE AREA:	158.6655	sq. m/g
LANGMUIR SURFACE AREA:	176.8934	sq. m/g
SINGLE POINT SURFACE AREA AT P/P ₀ 0.0780:	145.1345	sq. m/g
MICROPORE AREA:	2.2317	sq. m/g

VOLUME

SINGLE POINT TOTAL PORE VOLUME OF PORES LESS THAN 11.3945 A DIAMETER AT P/P ₀ 0.0099:	0.032182	cc/g
MICROPORE VOLUME:	0.003062	cc/g

PORE SIZE

AVERAGE PORE DIAMETER (4V/A BY BET):	8.1132	A
--------------------------------------	--------	---

BET Measurement Analysis Data of TS-C

```

ANALYSIS GAS: Nitrogen
EQUIL INTRVL: 5 sec

SUMMARY REPORT

AREA

BET SURFACE AREA: 47.8291 sq. m/g
LANGMUIR SURFACE AREA: 53.3341 sq. m/g
SINGLE POINT SURFACE AREA AT P/Po 0.0795: 44.2296 sq. m/g
MICROPORE AREA: 39.2164 sq. m/g

VOLUME

SINGLE POINT TOTAL PORE VOLUME OF PORES LESS THAN
11.4509 A DIAMETER AT P/Po 0.0103: 0.010422 cc/g
MICROPORE VOLUME: 0.015408 cc/g

PORE SIZE

AVERAGE PORE DIAMETER (4V/A BY BET): 8.7157 A

```

BET Measurement Analysis Data of TS-D

SUMMARY REPORT

AREA

BET SURFACE AREA:	0.7282	sq. m/g
LANGMUIR SURFACE AREA:	0.8244	sq. m/g
SINGLE POINT SURFACE AREA AT P/P ₀ 0.0798:	0.6280	sq. m/g
MICROPORE AREA:	0.9211	sq. m/g

VOLUME

SINGLE POINT TOTAL PORE VOLUME OF PORES LESS THAN 3281.2122 Å DIAMETER AT P/P ₀ 0.9941:	0.003396	cc/g
MICROPORE VOLUME:	0.000385	cc/g

PORE SIZE

AVERAGE PORE DIAMETER (4V/A BY BET):	186.5704	Å
--------------------------------------	----------	---

BET Measurement Analysis Data of TS-E

BET SURFACE AREA:	3.1220	sq. m/g
LANGMUIR SURFACE AREA:	3.4770	sq. m/g
SINGLE POINT SURFACE AREA AT P/P ₀ 0.0799:	2.9134	sq. m/g
MICROPORE AREA:	3.4940	sq. m/g
VOLUME		
SINGLE POINT TOTAL PORE VOLUME OF PORES LESS THAN 2800.1589 Å DIAMETER AT P/P ₀ 0.9931:	0.017292	cc/g
MICROPORE VOLUME:	0.001418	cc/g
PORE SIZE		
AVERAGE PORE DIAMETER (4V/A BY BET):	221.5442	Å

BET Measurement Analysis Data of TS-F

OPERATOR: ALIMI
UNIT NUMBER: 1
ANALYSIS GAS: Nitrogen

SAMPLE WT: 0.1134 g
FREE SPACE: 55.4630 cc
EQUIL INTRVL: 5 sec

SUMMARY REPORT

AREA

BET SURFACE AREA:	240.5179	sq. m/g
LANGMUIR SURFACE AREA:	267.2733	sq. m/g
SINGLE POINT SURFACE AREA AT P/P ₀ 0.0775:	223.2453	sq. m/g
MICROPORE AREA:	18.3715	sq. m/g

VOLUME

SINGLE POINT TOTAL PORE VOLUME OF PORES LESS THAN 2233.2532 Å DIAMETER AT P/P ₀ 0.9913:	0.726296	cc/g
MICROPORE VOLUME:	0.011077	cc/g

PORE SIZE

AVERAGE PORE DIAMETER (4V/A BY BET):	120.7886	Å
--------------------------------------	----------	---

BET Measurement Analysis Data of TS-G

UNIT NUMBER: 1
ANALYSIS GAS: Nitrogen

FREE SPACE: 54.3123 cc
EQUIL INTRVL: 5 sec

SUMMARY REPORT

AREA

BET SURFACE AREA:	277.5466	sq. m/g
LANGMUIR SURFACE AREA:	308.1315	sq. m/g
SINGLE POINT SURFACE AREA AT P/P ₀ 0.0768:	258.3148	sq. m/g
MICROPORE AREA:	27.8559	sq. m/g

VOLUME

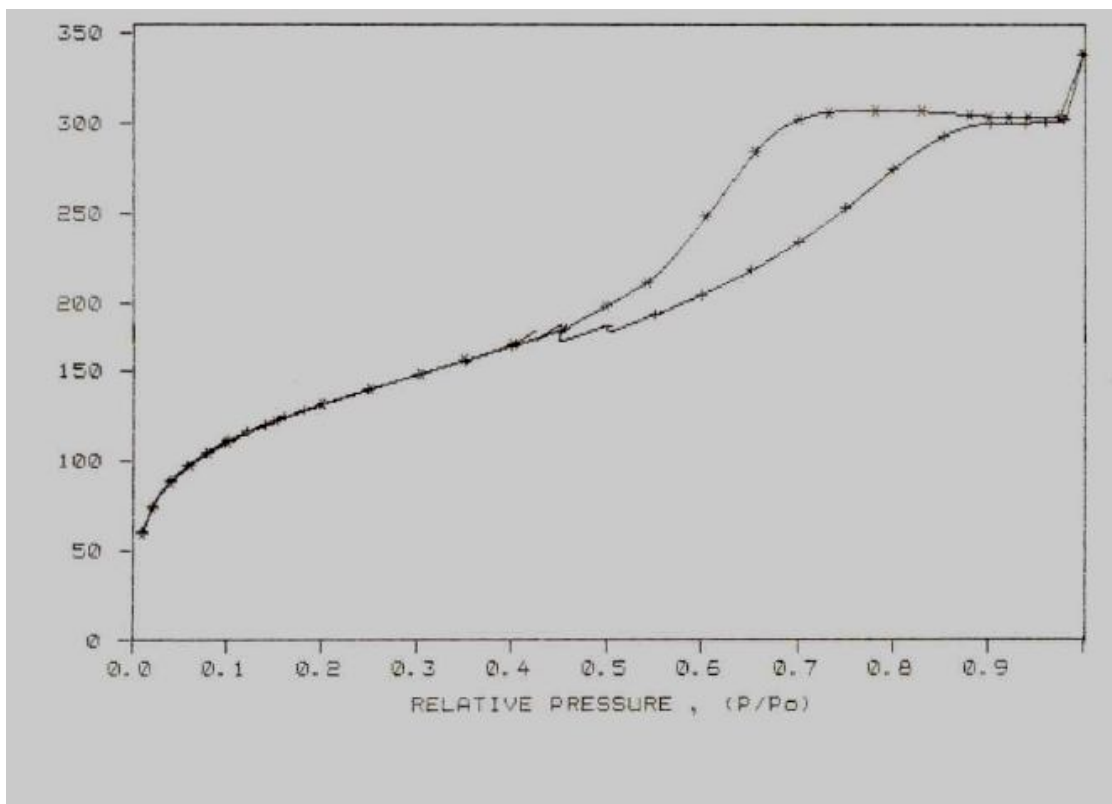
SINGLE POINT TOTAL PORE VOLUME OF PORES LESS THAN 6500.2803 Å DIAMETER AT P/P ₀ 0.9970:	1.270660	cc/g
MICROPORE VOLUME:	0.016319	cc/g

PORE SIZE

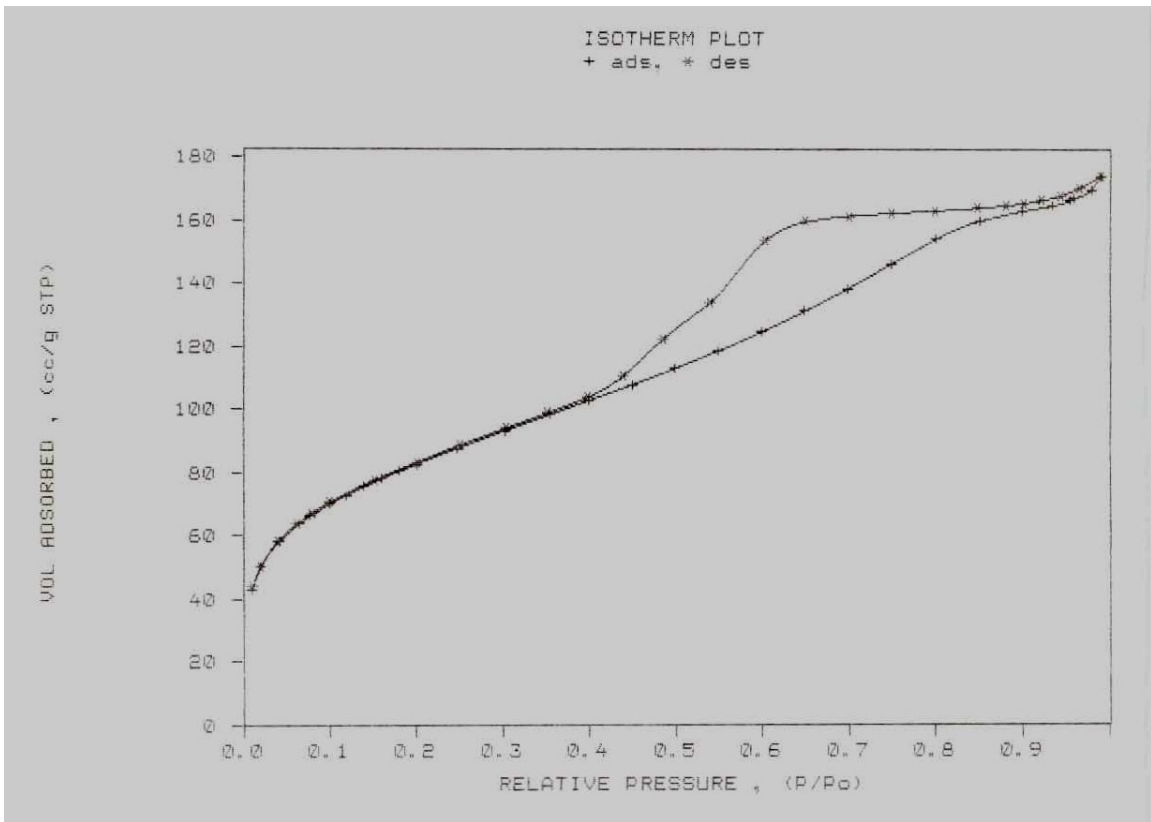
AVERAGE PORE DIAMETER (4V/A BY BET):	183.1275	Å
--------------------------------------	----------	---

BET Measurement Analysis Data of TS-H

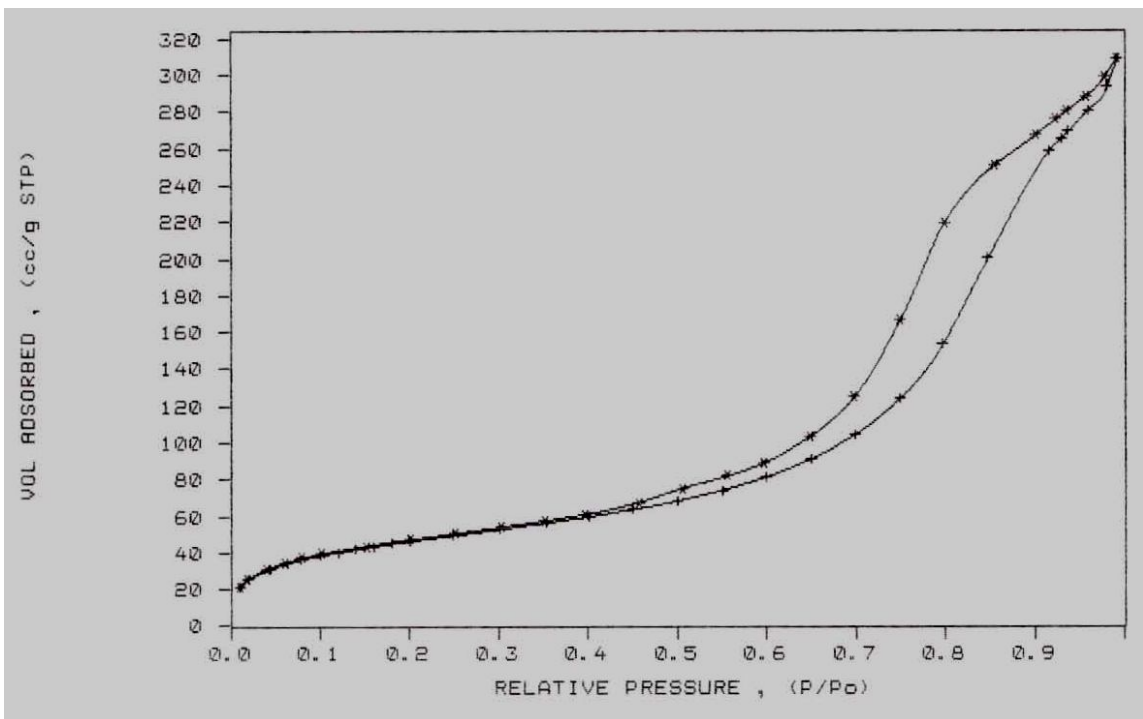
APPENDIX D



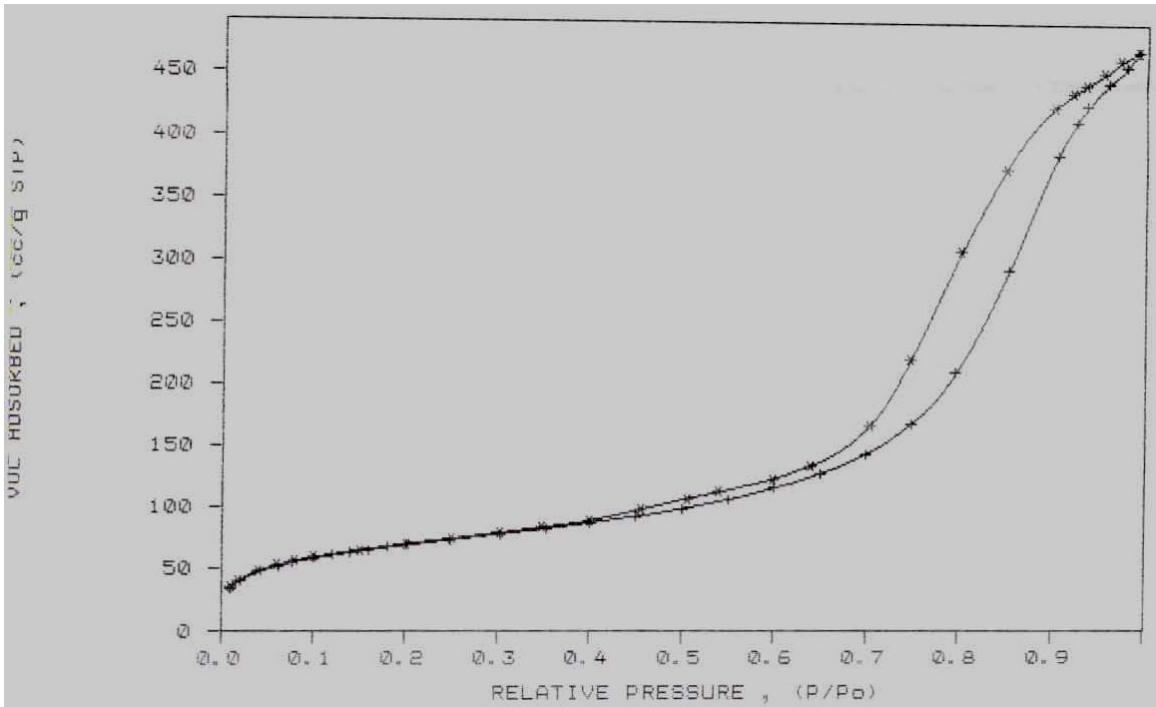
Isotherm plot of TS-A



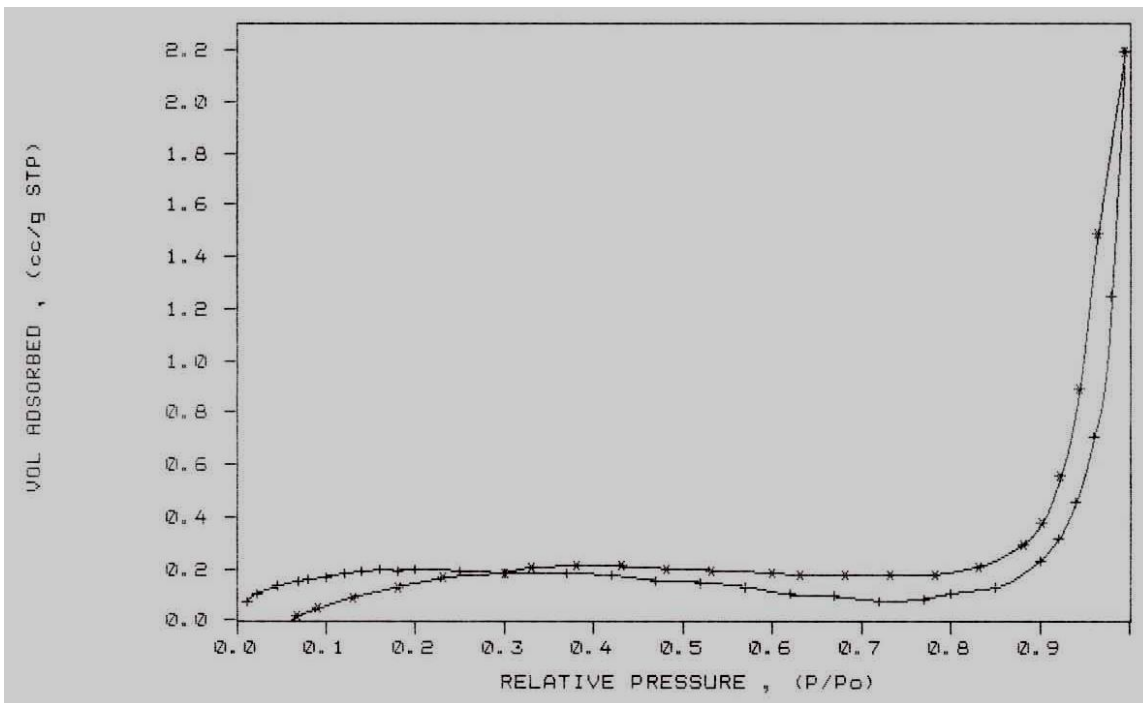
Isotherm plot of TS-B



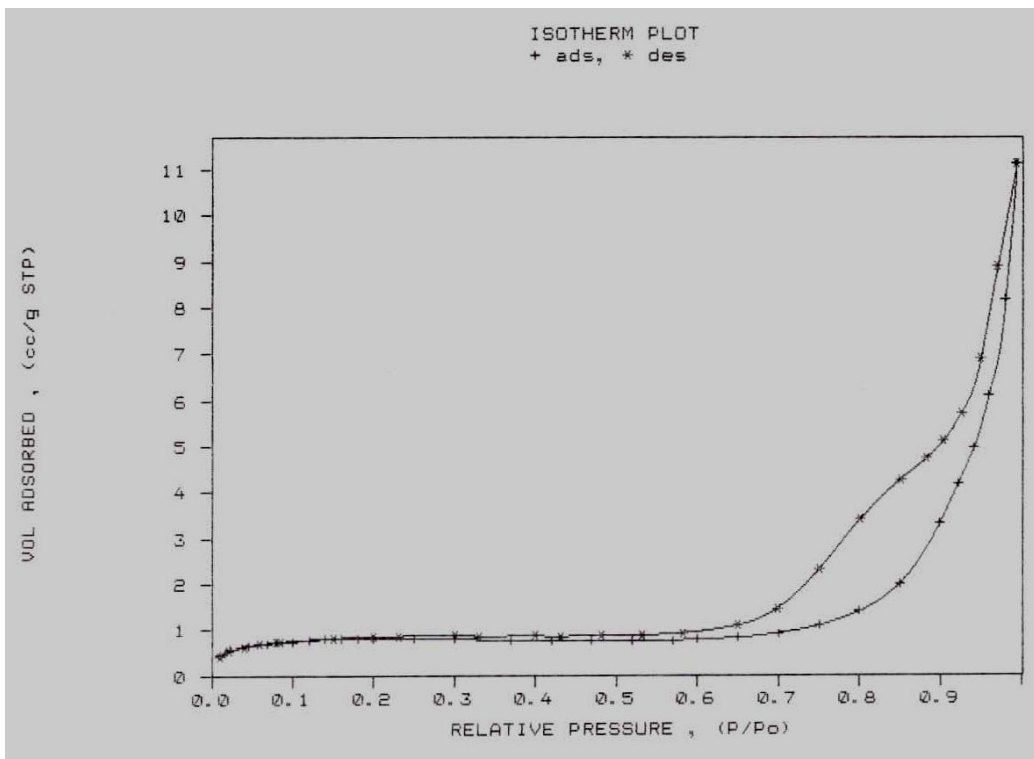
Isotherm Plot of TS-C



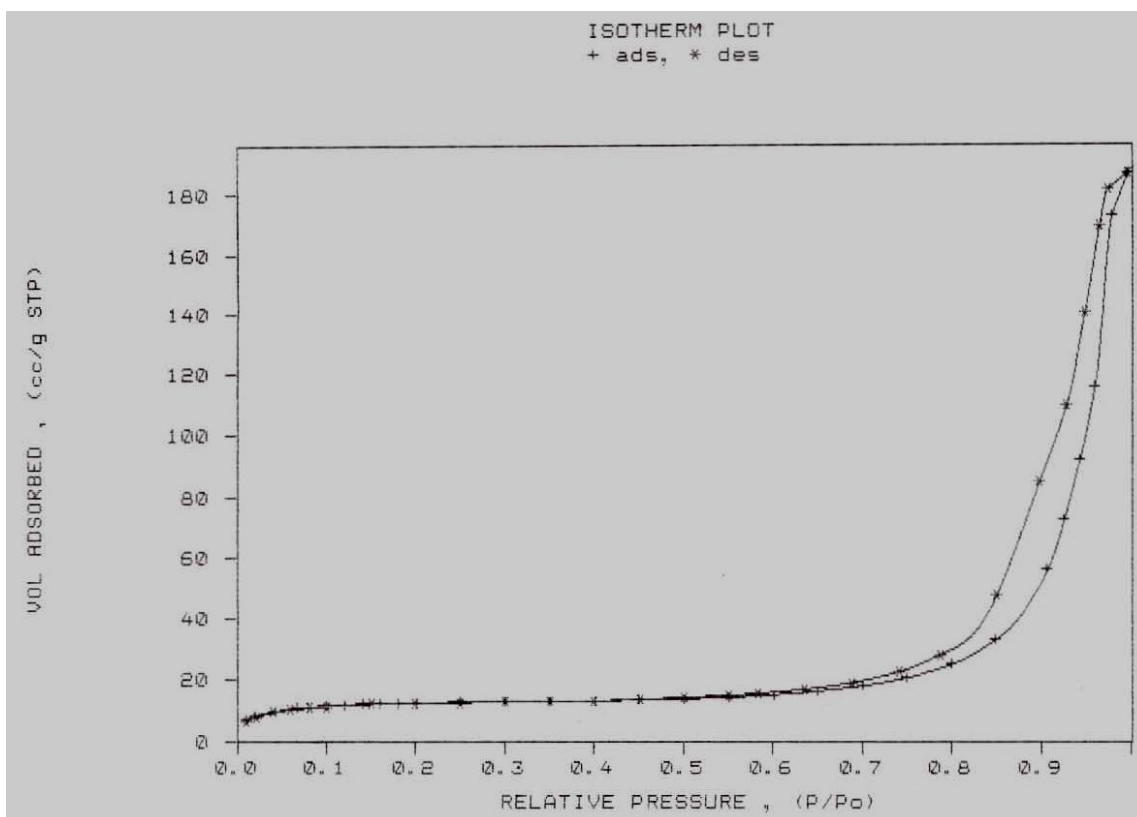
Isotherm Plot of TS-D



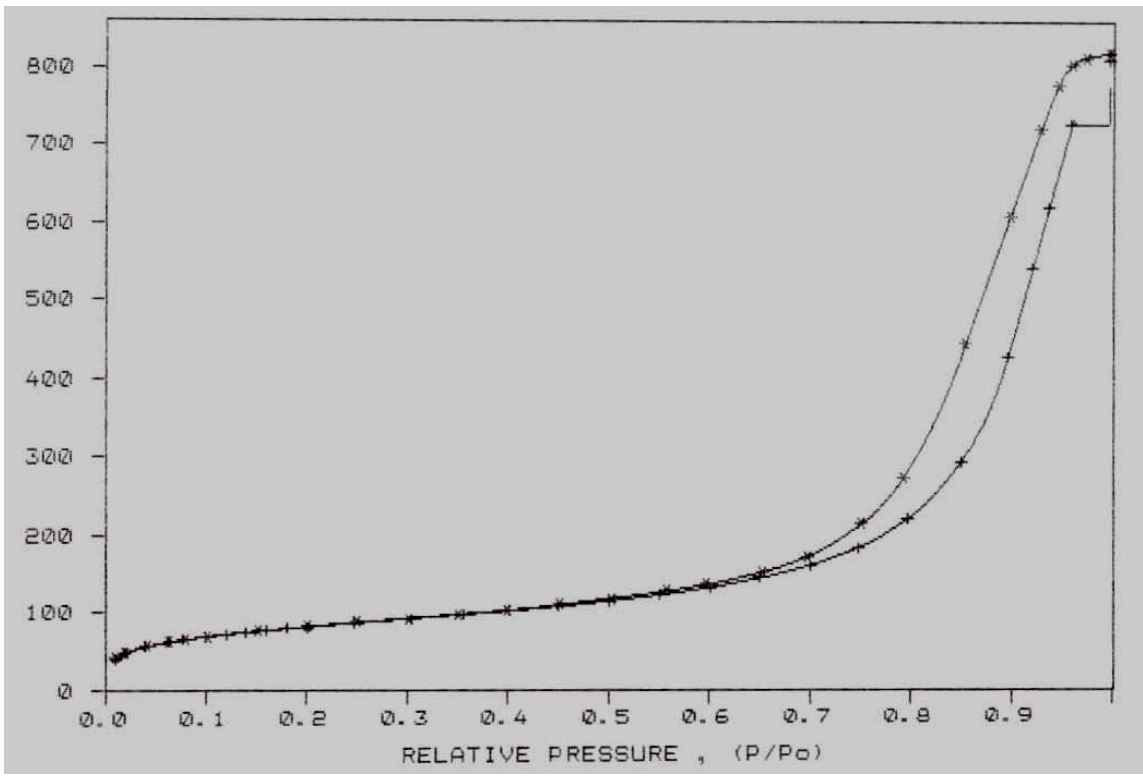
Isotherm Plot of TS-E



Isotherm Plot of TS-F



Isotherm Plot of TS-G



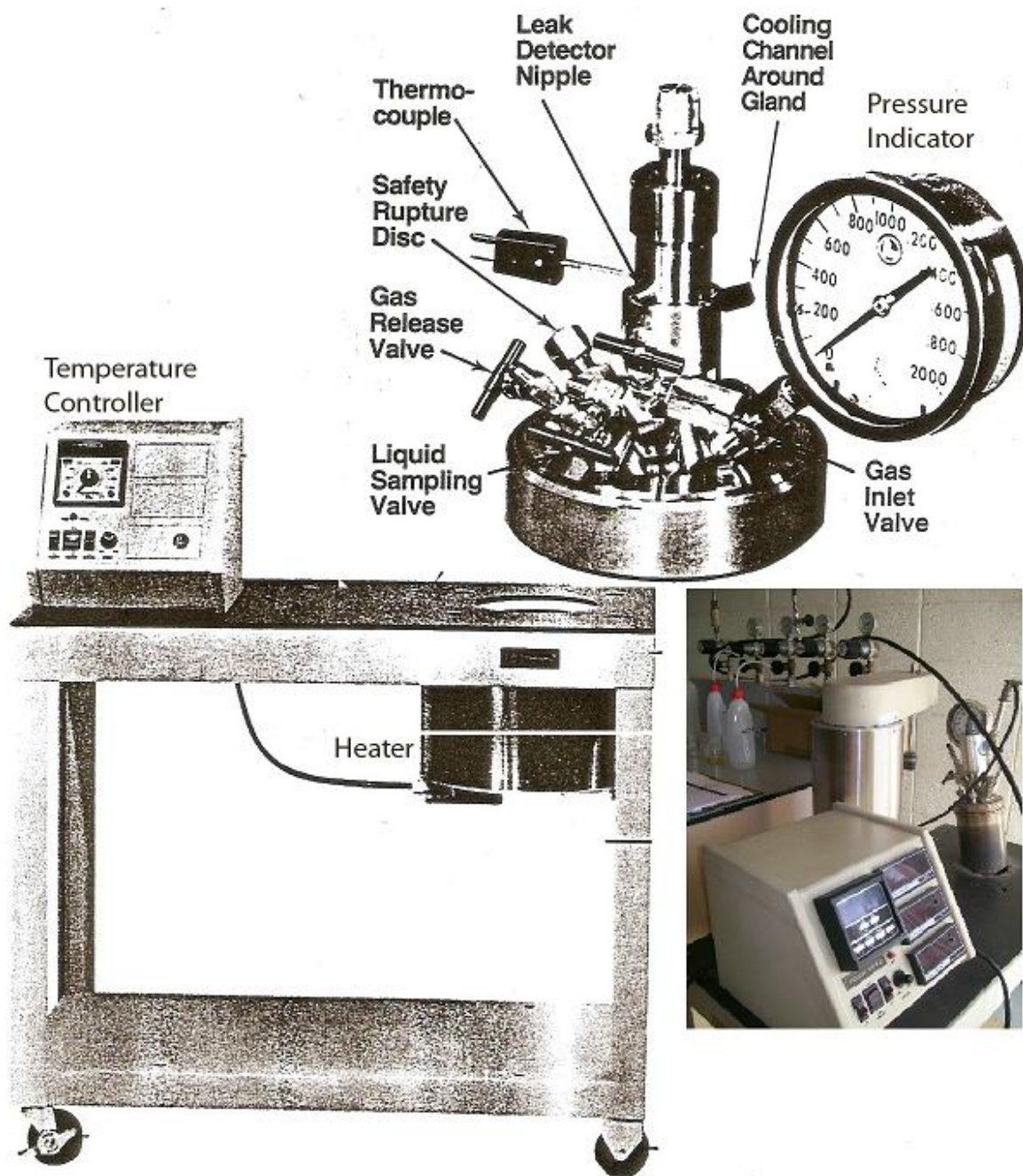
Isotherm Plot of TS-H

APPENDIX E

Effective Pore Diameter ΔD (Å)	Adsorption pore volume distribution				Desorption pore volume distribution	
	TS-A		TS-D		TS-H	
	Cumulative Pore Volume ΔV (cc/g)	Pore Distribution $\Delta V/\Delta D$ (cc/g)	Cumulative Pore Volume ΔV (cc/g)	Pore Distribution $\Delta V/\Delta D$ (cc/g)	Cumulative Pore Volume ΔV (cc/g)	Pore Distribution $\Delta V/\Delta D$ (cc/g)
2.5	0.0015	0.0006			0.008	0.0032
10.5	0.84	0.08			0.09	0.008571
16.5	4.95	0.3			0.6	0.036364
22.5	11.83129	0.525835	0.01518	0.02337	1.357742	0.060344
27.5	12.93509	0.470367	0.01518	0.017104	1.355715	0.049299
32.5	14.06148	0.432661	0.01518	0.013313	1.353566	0.041648
37.5	14.27666	0.380711	0.01518	0.010152	1.347624	0.035937
42.5	13.60531	0.320125	0.01518	0.007532	1.353566	0.031849
47.5	13.02911	0.274297	0.01518	0.005775	1.347624	0.028371
52.5	10.51334	0.200254	0.01518	0.003814	1.341334	0.025549
57.5	7.539515	0.131122	0.015088	0.00228	1.334577	0.02321
62.5	4.117063	0.065873	0.015028	0.001054	1.323485	0.021176
67.5	2.12355	0.03146	0.014613	0.000466	1.31246	0.019444
72.5	0.502425	0.00693	0.014259	9.56E-05	1.294377	0.017853
77.5	0.326895	0.004218	0.013476	5.44E-05	1.278417	0.016496
82.5	0.332393	0.004029	0.012791	4.88E-05	1.245619	0.015098
87.5	0.338275	0.003866	0.012183	4.42E-05	1.217843	0.013918
92.5	0.344378	0.003723	0.01148	4.02E-05	1.193739	0.012905
97.5	0.350708	0.003597	0.010861	3.69E-05	1.151706	0.011812
105	0.367395	0.003499	0.010357	3.33E-05	1.11495	0.010619
115	0.380305	0.003307	0.00948	2.88E-05	0.979018	0.008513
125	0.394	0.003152	0.008868	2.52E-05	0.881492	0.007052
135	0.40824	0.003024	0.008361	2.24E-05	0.800565	0.00593
145	0.422675	0.002915	0.007933	2.01E-05	0.731998	0.005048
155	0.437875	0.002825	0.007652	1.82E-05	0.659312	0.004254
170	0.46852	0.002756	0.0744	1.62E-05	0.594056	0.003494
190	0.49932	0.002628	0.007025	1.38E-05	0.481646	0.002535
210	0.53109	0.002529	0.006612	1.2E-05	0.393553	0.001874
230	0.56373	0.002451	0.006226	1.07E-05	0.323167	0.001405
250	0.59725	0.002389	0.005806	9.56E-06	0.265905	0.001064
270	63.099	0.2337	0.005454	0.000866	0.217736	0.000806
290	0.66526	0.002294	0.005096	7.91E-06	0.117023	0.000404
325	0.737425	0.002269	0.004644	6.98E-06	0.144165	0.000444
375	0.800625	0.002135	0.003716	5.69E-06	0.080302	0.000214
425	0.6307	0.001484	0.002975	3.49E-06	0.043716	0.000103
475	0.46455	0.000978	0.001962	2.06E-06	0.024237	5.1E-05
550	0.3212	0.000584	0.00117	1.06E-06	0.008954	1.63E-05

BJH Pore Size Distribution Analysis Data

APPENDIX F



Parr Autoclave in PRSB, Bangi